Some methods for estimating the effective properties of heterogeneous plates

Trung Kien Nguyen

▶ **To cite this version:**

Trung Kien Nguyen. Some methods for estimating the effective properties of heterogeneous plates. Other. Université Paris-Est, 2008. English. NNT : 2008PEST0270 . tel-00469274

HAL Id: tel-00469274
https://pastel.hal.science/tel-00469274

Submitted on 1 Apr 2010

HAL is a multi-disciplinary open access archive for the deposit and dissemination of scientific research documents, whether they are published or not. The documents may come from teaching and research institutions in France or abroad, or from public or private research centers.

L'archive ouverte pluridisciplinaire **HAL**, est destinée au dépôt et à la diffusion de documents scientifiques de niveau recherche, publiés ou non, émanant des établissements d'enseignement et de recherche français ou étrangers, des laboratoires publics ou privés.

UNIVERSITÉ PARIS-EST

THÈSE

présentée pour obtenir le grade de

DOCTEUR DE L'UNIVERSITÉ PARIS-EST

par

TRUNG-KIEN NGUYEN

Spécialité : Génie Civil

Titre:

Quelques méthodes pour l'estimation des propriétés effectives des plaques hétérogènes

Soutenue le 22 septembre 2008 devant le jury composé de :

M. Patrice CARTRAUD	Rapporteur	ECN
M. Jean-Claude MICHEL	Rapporteur	LMA/CNRS, Marseille
M. Pierre GILORMINI	Examinateur	ENSAM
Mme. Bernadette MIARA	Examinateur	ESIEE
M. Guy BONNET	Co-directeur de thèse	Université Paris-Est
M. Karam SAB	Directeur de thèse	ENPC

Université Paris-Est, UR Navier

Remerciements

Je tiens tout d'abord à remercier vivement mon directeur de thèse, Karam SAB. Il a suivi de près mon travail, m'a fait profiter de sa vaste connaissance et m'a souvent fasciné par sa rigueur, sa clarté d'esprit, son enthousiasme et sa curiosité intellectuelle. Son soutien m'a beaucoup aidé surtout pendant les moments de doute et d'incertitude. Qu'il trouve ici l'expression de ma profonde reconnaissance.

Je voudrais également remercier mon co-directeur de thèse, Guy BONNET, qui a participé à l'encadrement de ma thèse. Guy fût mon conseiller et interlocuteur. Je lui adresse ma sincère gratitude.

Je tiens à remercier Madame Bernadette MIARA qui m'a fait l'honneur de présider mon jury de thèse. Mes vifs remerciements sont également adressés à Messieurs Patrice CARTRAUD et Jean-Claude MICHEL pour avoir accepté la lourde tâche de rapporter mon mémoire et pour leur participation à mon jury. Je remercie aussi Monsieur Pierre GILORMINI pour l'intérêt qu'il a manifesté pour ce travail en acceptant d'être membre de mon jury.

Je voudrais adresser mes remerciements à tous les membres du LAMI, doctorants, permanents, stagiaires, avec qui les échanges scientifiques, techniques ou amicaux ont été très formateurs pour ma vie professionnelle et ont fait de ces trois années une belle étape de ma vie.

Mes vifs remerciements s'adressent aussi à tous mes amis pour leur soutien durant ces années de thèse. Mes pensées vont aussi à toute ma famille au Vietnam qui m'ont offert leur soutien et leur amour. Ma gratitude va aussi à ma femme, Huong-Nga, qui m'a beaucoup soutenu pour accomplir ce travail.

Enfin, je ne remercierais jamais assez mes parents pour leur soutien inconditionnel et leur amour. Je leur dédie ce travail.

Contents

List of Figures

List of Tables

Introduction Générale

Depuis le début du vingtième siècle, l'usage des matériaux sous la forme de plaques et de poutres s'est considérablement développé jusqu'à nos jours que ce soit dans l'industrie automobile, la construction, et plus récemment en aéronautique. Pourtant le comportement mécanique d'objets tels que du carton ondulé, des panneaux sandwich, du nid d'abeille, voire une simple dalle en béton fait l'objet de nombreuses recherches. Une des difficultés réside essentiellement dans le caractère hétérogène de ces structures. L'utilisation de méthodes numériques classiques pour estimer les constantes élastiques globales des structures multicouches et hétérogènes est très coûteuse en temps de calcul. C'est pourquoi de nombreuses méthodes simplifiées ont vu le jour, notamment quand la taille de l'hétérogénéité est petite devant les dimensions caractéristiques de la structure. Dans ce cas, cette dernière peut être perçue comme un milieu continu homogène et des méthodes d'homogénéisation peuvent donc être utilisées. En revanche, il existe des structures hétérogènes pour lesquelles la taille de l'hétérogénéité est du même ordre que l'épaisseur. Dans ce cas, l'utilisation des méthodes d'homogénéisation n'est plus appropriée. L'homogénéisation des plaques et des poutres élastiques périodiques a été largement étudiée par de nombreux auteurs en utilisant la technique d'homogénéisation asymptotique (Duvaut et Metellus, 1976; Caillerie, 1984; Kohn et Vogelius, 1984; Lewiński et Telega, 1999; Buannic et Cartraud, 2001; Cecchi et Sab, 2002a,b; Buannic et al., 2003; Cecchi et Sab, 2004). Certaines recherches se sont basées sur des calculs variationnels pour obtenir des bornes sur les propriétés élastiques effectives des plaques et des poutres hétérogènes (Kolpakov, 1998, 1999; Kolpakov et Sheremet, 1999).

L'objet de ce travail est de proposer quelques nouvelles méthodes pour l'estimation des propriétés effectives des plaques hétérogènes.

Dans les structures multicouches classiques, des couches homogènes sont collées les unes aux autres pour améliorer les performances (mécaniques, thermiques, acoustiques,...) de la structure (plaques sandwichs, structures renforcées par matériaux composites,...). L'inconvénient de cette démarche est de créer des concentrations des contraintes au niveau des interfaces entre les couches qui peuvent conduire à des délaminages, des fissures, et d'autres mécanismes d'endommagement en raison du changement brutal des propriétés mécaniques d'une couche à l'autre.
A la fin des années 80, une équipe de chercheurs japonais a proposé de surmonter ces difficultés en concevant de nouveaux matériaux dits fonctionnellement gradués (Functionally Graded Materials (FGMs)) dont les propriétés mécaniques varient lentement et continûment dans l'épaisseur de la structure. Ces structures pour lesquelles la notion d'interface n'a plus de sens nécessistent donc de

nouvelles méthodes de calcul. Les modèles de plaques et de poutres homogènes ont été largement étudiés depuis plusieurs années jusqu'à nos jours (Reissner, 1945; Mindlin, 1951; Timoshenko et Woinowsky-Krieger, 1959; Ciarlet, 1997; Reddy, 1997, 1999; Caron et Sab, 2001; Zenkour, 2003; Miara et Podio-Guidugli, 2006). Certains modèles ont été appliqués pour l'analyse des comportements thermomécaniques des plaques fonctionnellement graduées que ce soit le modèle de plaque classique de Love-Kirchhoff (He et al., 2001; Chi et Chung, 2006a,b), le modèle de plaque de Reissner-Mindlin (Praveen et Reddy, 1998; Croce et Venini, 2004), le modèle de plaque de déformation en cisaillement d'ordre 3 (Reddy, 2000) et le modèle de plaque de déformation en cisaillement sinusoïdal (Zenkour, 2003). L'effet du cissaillement dans les modèles de plaques fonctionnellement gradués a été beaucoup moins étudié.
Nous proposons donc dans la première partie un modèle de plaque basée sur la théorie de déformation en cisaillement de premier ordre. Les résultats de ce modèle seront comparés à ceux de la littérature.

Les matériaux fonctionnellement gradués sont des matériaux hétérogènes à l'échelle microscopique. L'un des objectifs de la mécanique des matériaux hétérogènes est d'établir des approches d'homogénéisation pour déterminer des propriétés effectives telles que le milieu homogénéisé équivalent puisse remplacer le milieu hétérogène, plus complexe, dans les calculs.
Les méthodes théoriques et numériques pour obtenir des propriétés effectives des matériaux hétérogènes ont fait l'objet de nombreuses études où les problèmes d'homogénéisation sont normalement associés à la résolution d'un problème élastique de localisation défini sur un volume élémentaire représentatif (VER), et à la détermination de la taille minimale de ce VER.
Pour les milieux périodiques, les propriétés effectives peuvent être obtenues par la résolution d'un problème d'élasticité sur le volume d'une période, appelé cellule de base, soumis à des conditions périodiques (Sanchez-Palencia, 1974; Bakhvalov, 1974; A. Bensoussan et Papanicolaou, 1978; Auriault et Bonnet, 1985; Bakhvalov et Panasenko, 1989). Numériquement, la méthode des éléments finis a été utilisée pour résoudre le problème de localisation avec une discrétisation à l'échelle de la cellule de base (Brockenbrough et al. (1991), Böhm et al. (1993), Gusev (1997), Michel et al. (1999), Moës et al. (2003), Sab et Nedjar (2005)). Les méthodes de Fourier ont été aussi utilisées par plusieurs auteurs (Iwakuma et Nemat-Nasser, 1983; Suquet, 1990; Luciano et Barbero, 1994; Moulinec et Suquet, 1994, 1998; Michel et al., 1999; Eyre et Milton, 1999; Michel et al., 2001; Cohen et Bergman, 2003; Bonnet, 2007). L'un des avantages de ces méthodes est dû à l'utilisation de Transformée de Fourier Rapide (FFT) permettant une réduction du temps de calcul.

Par ailleurs, profitant de la linéarité du système d'équations aux dérivées partielles issu d'un problème d'élasticité, il est possible d'utiliser des opérateurs de Green et des convolutions pour estimer des propriétés globales d'un milieu hétérogène. Jusqu'à présent, une telle stratégie était limitée à l'utilisation des opérateurs connus: l'opérateur $\mathbf{\Gamma}$ pour les milieux infinis (Willis, 1977, 1981; Drugan et Willis, 1996) et l'opérateur $\mathbf{\Gamma}$ pour les milieux périodiques (Suquet, 1990; Moulinec et Suquet, 1994, 1998; Michel et al., 1999). Dans certains cas, d'autres conditions aux limites spécifiques doivent être prises en compte: par exemple dans le cas des plaques ou des

poutres, les conditions aux limites de bord libre doivent être imposées. Dans ce cas, un nouvel opérateur $\mathbf{\Gamma}$ est donc nécessaire.

C'est pourquoi nous proposons dans la deuxième partie de contruire un nouvel opérateur $\mathbf{\Gamma}$ pour les milieux périodiques avec des conditions aux limites de bord libre.

Cet opérateur sera d'abord utilisé pour calculer numériquement des propriétés élastiques effectives des plaques périodiques. Puis, il sera utilisé pour estimer l'effet de taille de l'hétérogénéité des plaques aléatoires.

Certains auteurs ont utilisé les principes variationnels pour obtenir des bornes supérieure et inférieure des propriétés effectives des matériaux hétérogènes. Leurs applications pour des matériaux composites élastiques linéaires sont nombreuses (Hill, 1952; Hashin et Shtrikman, 1962a,b, 1963, 1965, 1967; Willis, 1977, 1981; Kolpakov, 1998, 1999; Kolpakov et Sheremet, 1999; Gilormini, 2001). L'utilisation des principes variationnels pour l'étude des milieux non linéaires peut être trouvée dans Tabot et Willis (1985); Castaneda (1991); Nebozhyn et al. (2001). Lorsque la taille caractéristique de l'échelle macroscopique n'est pas beaucoup plus grande que celle des hétérogénéités, les effets de taille nécessitent l'utilisation des méthodes plus efficaces pour saisir des réponses du matériau. La taille minimale du volume élémentaire représentatif (VER) a été analytiquement estimée par Drugan et Willis (1996); Drugan (2003) en utilisant le principe variationnel de Hashin-Shtrikman. Elle a été également étudiée numériquement par Sab (1992); Gusev (1997); Terada et al. (1998); Kanit et al. (2003); Sab et Nedjar (2005); Lachihab et Sab (2005, 2008).
En outre, pour certains matériaux comme les FGMs, l'hypothèse de l'homogénéité statistique ne s'applique pas. L'utilisation des méthodes développées pour des matériaux hétérogènes statistiquement uniformes n'est plus appropriée. Il existe des modèles micromécaniques dédiés à l'analyse des propriétés globales des FGMs (Reiter et Dvorak, 1997, 1998; Suresh et Mortensen, 1998; Luciano et Willis, 2004). Jusqu'à présent, l'utilisation des principes variationnels pour calculer des bornes des propriétés effectives des plaques hétérogènes a été peu étudiée.

Nous nous proposons donc de formuler un principe variationnel de Hashin-Shtrikman pour des plaques hétérogènes basé sur l'opérateur $\mathbf{\Gamma}$ pour les milieux périodiques avec des conditions aux limites de bord libre. Ce principe permettra d'estimer des bornes des propriétés effectives des plaques hétérogènes ainsi que l'effet de taille des hétérogénéités.

Cette thèse a été réalisée à l'Institut Navier, LAMI, et financée par l'Université de Marne-La-Vallée. Ce mémoire est divisé en deux parties indépendantes et cinq chapitres.

La première partie est dédiée à l'effet de cisaillement dans les plaques en matériaux FGMs.
Le premier chapitre présente les matériaux fonctionnellement gradués, leurs propriétés, l'histoire de leur développement, ainsi que leurs domaines d'application. Dans ce chapitre, nous rappelons ensuite les modèles de plaque utilisés pour l'analyse du comportement thermomécanique des FGMs et les méthodes d'homogénéisation utilisées pour le calcul de leurs propriétés effectives.
Le deuxième chapitre présente un modèle de plaque de Reissner-Mindlin pour les matériaux fonctionnellement gradués dans lequel l'effet du cisaillement transversal est identifié pour tenir

compte de la gradation du matériau dans l'épaisseur de la plaque. Le modèle proposé est comparé avec les modèles de la littérature.

La deuxième partie est dédiée à l'homogénéisation des plaques hétérogènes de type Love-Kirchhoff. L'objetif du troisième chapitre est de construire un nouvel opérateur $\mathbf{\Gamma}$ pour un milieu périodique avec des conditions aux limites de bord libre. Cet opérateur est utilisé pour calculer numériquement les propriétés élastiques effectives des plaques minces périodiques. La méthode est basée sur un procédé itératif ainsi que la Transformée de Fourier Rapide.
Le quatrième chapitre est consacré à la formulation d'un principe varationnel de Hashin-Shtrikman pour des plaques hétérogènes basé sur l'opérateur $\mathbf{\Gamma}$ construit dans le troisième chapitre.
Le cinquième chapitre présente des simulations numériques utilisant la méthode décrite dans le troisième chapitre pour estimer le VER minimal et les effets d'échelle dans les plaques aléatoires.

Enfin, les conclusions et les perspectives termineront cette thèse.

Part I

Shear Effects for Functionally Graded Material Plates

Chapter 1

Functionally Graded Materials

This chapter presents a family of composite materials known as Functionally Graded Materials (FGMs) whose properties vary continuously to improve the thermomechanical characteristics of multilayered composite materials. The properties of classical composite materials and weaknesses of multilayered structures are first reminded in section 1. Then, the definitions, the properties and the research activities of FGMs are provided in section 2, followed by a literature review of methods employed to determine the effective properties of FGMs. Finally, the last section contains a presentation of plate models used for the analysis of FGMs.

1.1 Composite Materials and Laminated Composites

Composite materials are engineered materials consisting of two or more phases on a macroscopic scale, whose mechanical performance and properties are designed to be superior to those of the constituent materials acting independently. One of the phases is usually discontinuous, stiffer, and stronger and is called reinforcement, whereas the less stiff and weaker phase is continuous and is called matrix. The matrix material surrounds and supports the reinforcement materials by maintaining their relative positions. The reinforcements impart their special mechanical and physical properties to enhance the matrix properties. The wide variety of matrix and strengthening materials allows the designer of the structure to choose an optimum combination. Sometimes, because of chemical interactions or other processing effects, an additional phase, called interphase, exists between the reinforcement and the matrix.

Composite materials are classified into two general categories depending on the type, geometry, and orientation of the reinforcement phase: particulate composites and fiber composites. Particulate composites consist of particles of various sizes and shapes randomly dispersed within the matrix. Because of the randomness of particle distribution, these composites can be regarded as quasi homogeneous on a scale larger than the particle size. Particulate composites may consist of metallic and nonmetallic particles in metallic and nonmetallic matrices. Fiber composites are composed of fibers as the reinforcing phase whose form is either discontinuous (short fibers or

whiskers), or continuous (long fibers). Fibers arrangement and their orientation can modulate the mechanical properties of composite materials. Figure 1.2 illustrates a cross section perpendicular to the axis of fibers of a fiber composite and figure 1.1 is an arbitrary cross section of a particulate composite.

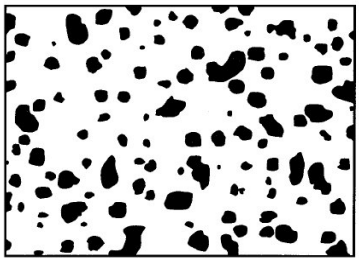

Figure 1.1: Illustration of a particulate composite.

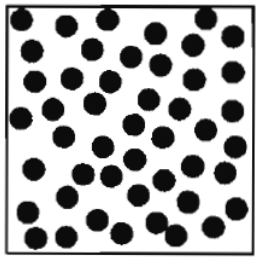

Figure 1.2: Illustration of a fiber composite.

The exploitation of basic material elements into various organic and inorganic compounds was made way for the development of advanced polymers and elastomers, alloys, glasses and ceramics, from which composite materials with processing methods can produce multilayered structures (figure 1.3). These consist of thin layers of different materials bonded together. The main disadvantages of such an assembly is to create a material discontinuity through the interfaces of layers along which stress concentrations may be high, more specifically when high temperatures are involved. These stress concentrations can yield damages, cracks and failures of the structure. The weaknesses at the interfaces of multilayered materials have raised important questions for the researchers and engineers. Many studies have been performed in recent years to predict exactly the effects of the stress concentration at the interfaces. Practically however, laminated composites encounter many difficulties when submitted to high temperatures.

1.2 Functionally Graded Materials

1.2.1 Definition and Characteristics

The development of the materials science aims to answer to service conditions and it requires that materials performance vary with location within the component. For example, the body of a gear must be tough, whereas its surface must be hard and wear-resistant. Likewise, a kitchen knife needs only be hard at its cutting edge, but elsewhere the material it is produced from must mainly be strong and tough. Many of most demanding current applications of materials enter into this category.

It is well known that abrupt transitions in materials composition and properties within a component often result in sharp local concentrations of stress. These stress concentrations can be greatly reduced if the transition from one material to the other is made gradual. These considerations form the essential elements of the logic underlying the conception of the majority of functionally graded materials.

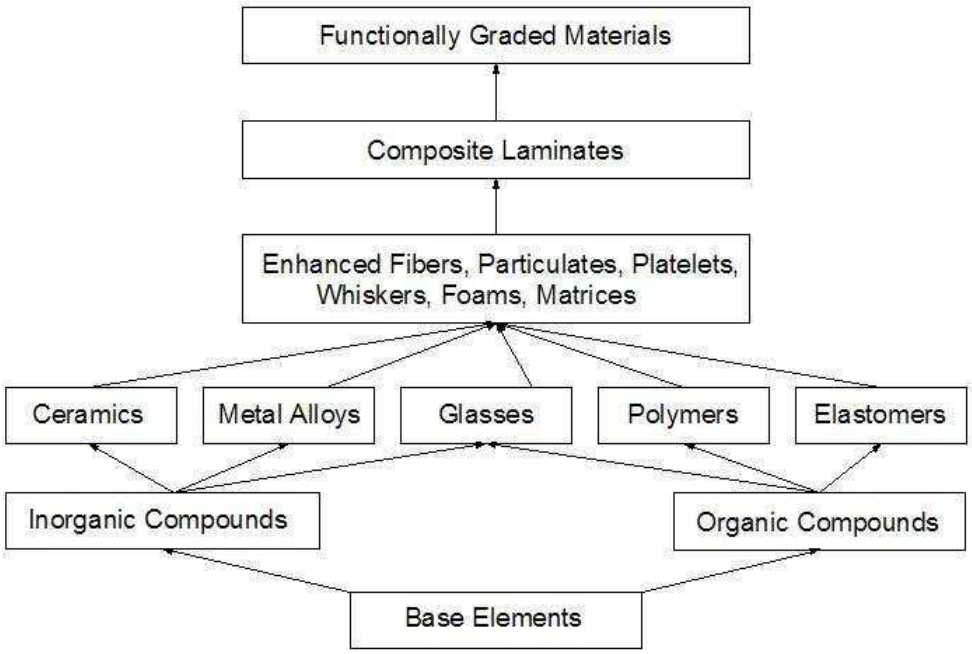

Figure 1.3: Illustration of a hierarchy of composite materials.

By definition, functionally graded materials (FGMs) are advanced composites, microscopically engineered to have a smooth spatial variation of material properties in order to improve and optimize the thermomechanical characteristics of structures. This is achieved by fabricating the composite material to have a gradual spatial variation in the volume fractions of constituent materials, thus tailoring its material composition based on functional performance requirements (Suresh and Mortensen, 1998). FGMs offer a great promise in applications where the operating conditions are severe such as spacecraft heat shields, biomedical implants, engine components, high power electrical contacts. For example, in a conventional thermal barrier coating for high temperature applications, a discrete layer of ceramic material is bonded to a metallic structure. However, the abrupt transition in material properties across the interface between distinct materials can cause large interlaminar stresses and lead to plastic deformations or crackings (Finot and Suresh, 1996). These destructive effects can be alleviated by grading the material to have a smooth spatial variation of material composition, where high concentrations of ceramic material are placed at corrosive, high temperature locations, while high concentrations of metal are placed at regions where mechanical properties, such as toughness, need to be high.

FGMs may consist of different materials. Most of FGMs are composed of ceramics and metals whose mechanical properties are compared in table 1.1. The voids are also considered as a component of FGMs. They can be distributed on the surface or inside the structure for ensuring a resistance to mechanical shock behind the thermal insulation.

High temperature face	Ceramic	Thermal resistance High resistance to oxidation Low thermal conductivity
Intermediary layers	Ceramic-metal	Elimination of the interface problems
Low temperature face	Metal	Mechanical resistance High thermal conductivity High fracture toughness

Table 1.1: Comparative properties of ceramic and metal

1.2.2 History of Development and Applications

Functionally graded materials are not new, the concept having been exploited for millennia in steel. The advent of composite materials with combinations of different phases made possible to create a gradient within such materials by varying the disposition of the two combined phases. This possibility was first suggested as a concept by Bever and Duwez (1972) and its exploitation in composite materials was sporadically tried in the 1950s, 1960s, 1970s and 1980s by several researchers in the United States (Goetzel and Lavendel, 1964). However those studies have had only a limited impact at that time because of the lack of a design, a manufacture method as well as an evaluation method of graded structures.

The term "Functionally Graded Materials" (FGMs) originated in the mid-1980s in Japan designating a new material against thermal effects in aerospace and the first research projects focused on the spaceplane came to the conclusion that many stringent demands of structural components in the high temperature medium require that compositional and microstructural gradients have to be introduced for best overall use of available materials, and for avoiding the stress concentrations at sharp interfaces separating different materials. These initial estimates on the advantage of FGMs were followed by a vast program, which attracted many research organizations (Koizumi, 1997; Suresh and Mortensen, 1998). They were focused on a structure subjected to cold conditions on one side and to very hot environment on the other. Ceramic materials were chosen for the hot surface with a temperature of 2000K in an oxidizing environment, while close to the cold surface with a temperature of 1000K, lower in temperature, strong, tough, and thermally conductive materials such as metal were selected. The transitional layer between the two surfaces was graded with a manufacturing technique such as power metallurgy, chemical or physical vapour deposition, plasma spraying, and self-propagating high temperature combustion synthesis (Suresh and Mortensen, 1998). Several research activities on FGMs can be found in Koizumi (1997).

Outside Japan, research on functionally graded materials rapidly became an active subject in materials research in the late 1980 in several countries including Germany, Switzerland, United States, China, Russia. Many applications of purposely introduced gradients have appeared over the recent years, including metal and ceramic joining such as: implants for humans, explosion device components, magnetic devices, cutting tools, resilient rocket. Functionally graded materials

have thus grown to become one of the major current themes in structural materials research.

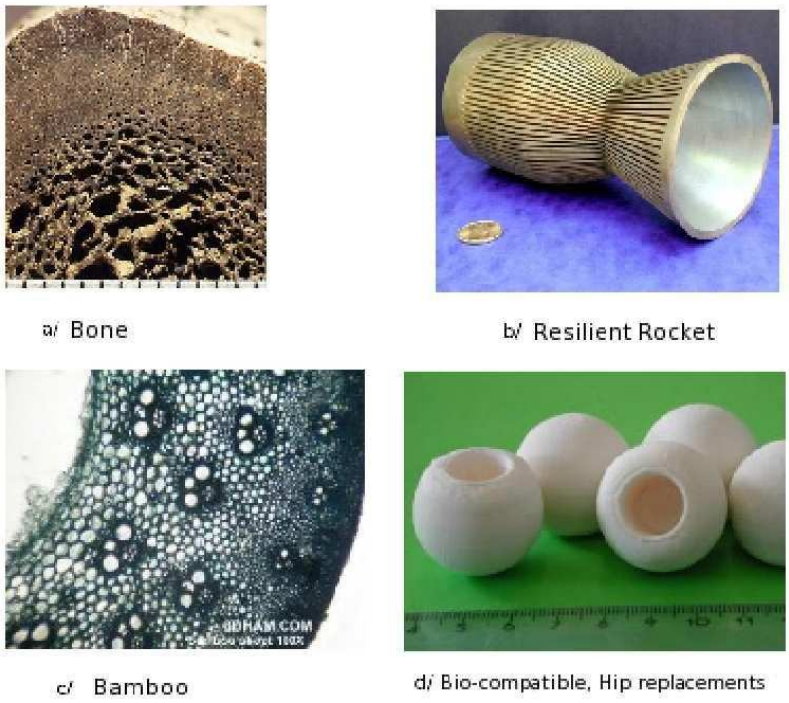

Figure 1.4: Examples of naturally occurring FGMs and FGMs engineered by humans.

a) *http* : *//www.geo.ucalgary.ca/* ∼ *macrae/t_origins/carbbones/dinobone.html*
b) *http* : *//science.nasa.gov/headlines/y*2004*//*13*apr_gradient.htm*
c) *http* : *//www.*3*dham.com/microgallery/bamboo.html*
d) *http* : *//www.mtm.kuleuven.be/Research/C*2*/EPD.htm*

Figure 1.4 presents examples of structures made of FGMs in nature or manufactured. Bamboo is an excellent natural example where the microstructure consists of a spatially varying concentration of voids in order to maximize bending rigidity, while minimizing mass. Likewise, bones have similar functional gradings, while human skin is graded to provide certain toughness, tactile and elastic qualities as a function of skin depth and location on the body.

In the case of components engineered by humans, FGMs most commonly involve two isotropic material phases: ceramic materials (zirconia, alumina, silicon carbide, tungsten-carbide) and metal materials (magnesium alloy, aluminium, copper, titanium, tungsten, steel). Although more difficult to manufacture, orthotropic FGMs have been produced with a spatial variation of fiber volume fractions, as well as their orientations for certain applications.

Some examples of human engineered FGMs components under development are also shown in figure 1.4: the resilient rocket and the product using bio-compatible in the Hip replacement. In comparison with natural FGMs, there exist strong differences between living graded structures and those produced artificially. Living organisms have the added capacity to dynamically build and adapt the structures they produce: living "FGMs" are also intelligent in that they can sense their environment by compositional internal divisions in the life of the structures, while the

creation of current FGMs lacks such a capability at the present time.

1.3 Material Gradient of Functionally Graded Material Plates

Functionally graded materials (FGMs) can be produced by continuously varying the constituents of multi-phase materials in a predetermined profile. The most distinct features of a FGM are the non-uniform microstructures with continuously graded macroproperties. A FGM can be defined by the variation in the volume fractions. Most researchers use the power-law function, exponential function, or sigmoid function to describe the volume fractions (see Delale and Erdogan (1983); Yung and Munz (1996); Jin and Batra (1996); Jin and Paulino (2001); Chi and Chung (2002) and references therein). Therefore, FGM plates with a grading in the thickness according to the power-law function (P-FGM), to the exponential function (E-FGM), and to the sigmoid function (S-FGM) will be considered in this section.

Consider a plate having a thickness h. The z-axis originated at the middle surface is in the thickness direction. The lower and upper surfaces of the plate is at the location $z = -h/2$ and at the location $z = h/2$, respectively. The material properties vary in the thickness direction to create functionally graded material plates.

1.3.1 Material Distribution in Power-Law Function

The volume fraction function of functionally graded materials can be expressed by a power law as follows:

$$f(z) = \left(\frac{2z+h}{2h}\right)^p, \tag{1.1}$$

where p is a material parameter that represents the order of polynomial. The variation of the volume fraction of phases in terms of p is shown in figure 1.5. It is noted that the material compositions change rapidly near the upper surface ($z = h/2$) for $p > 1$ and near the lower surface ($z = -h/2$) for $p < 1$. This profile is widely used in the analysis of FGM plates (see Reddy (2000); Cheng and Batra (2000b); Croce and Venini (2004); Chi and Chung (2006a,b)).

1.3.2 Material Distribution in Sigmoid Function

To reduce the rapid variation of the material near the upper and lower surfaces, materials distribution using two power-law functions was defined (Chi and Chung, 2002, 2006a,b). This distribution is called the sigmoid function. The material volume fraction is therefore given by the following form:

$$\begin{cases} f_1(z) = 1 - \frac{1}{2}\left(\frac{h-2z}{h}\right)^p & \text{for} \quad 0 \le z \le \frac{h}{2} \\ \\ f_2(z) = \frac{1}{2}\left(\frac{h+2z}{h}\right)^p & \text{for} \quad -\frac{h}{2} \le z \le 0. \end{cases} \tag{1.2}$$

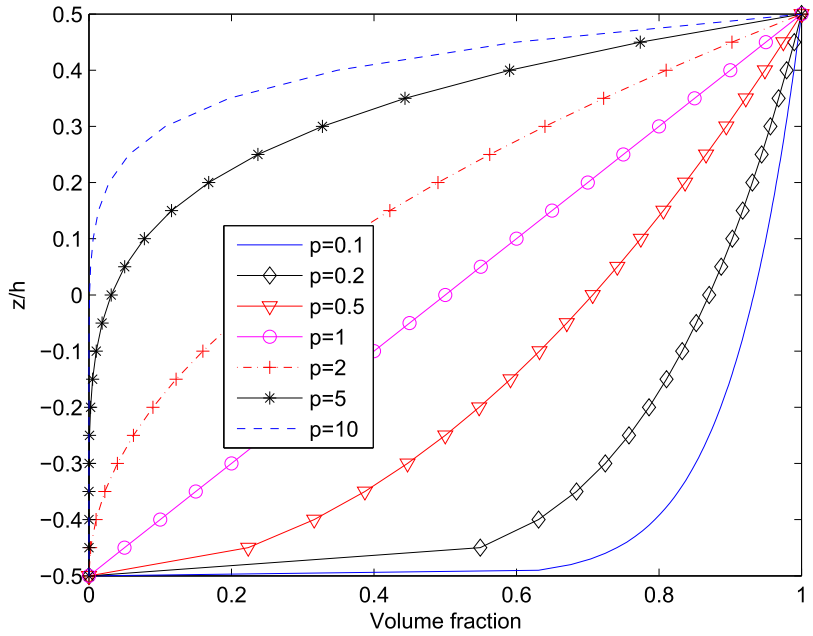

Figure 1.5: Variation of the volume fraction in a P-FGM plate

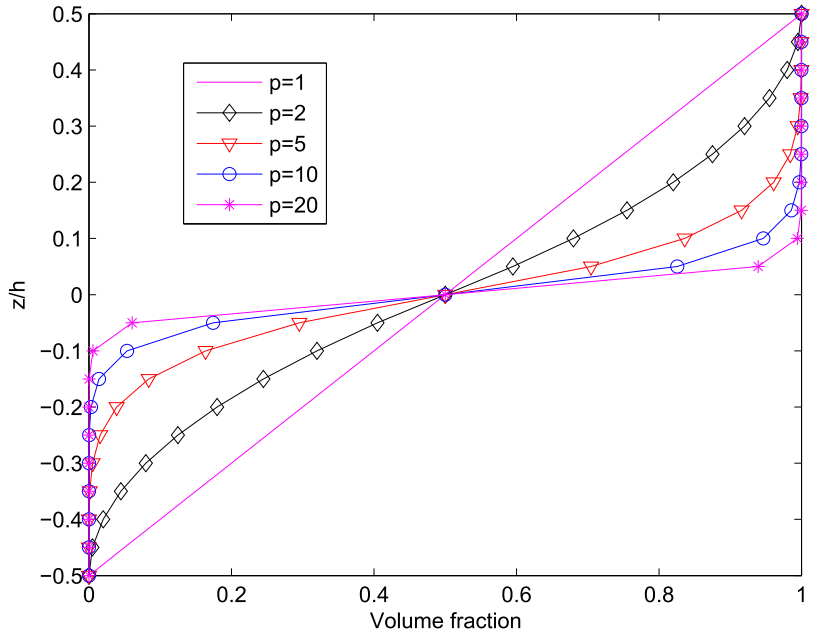

Figure 1.6: Variation of the volume fraction in a S-FGM plate

Figure 1.6 displays the variation of the volume fraction function for $p > 1$. Since this distribution represents the power-law function in a half thickness, the material compositions in grading vary slower than the distribution of the power-law function.

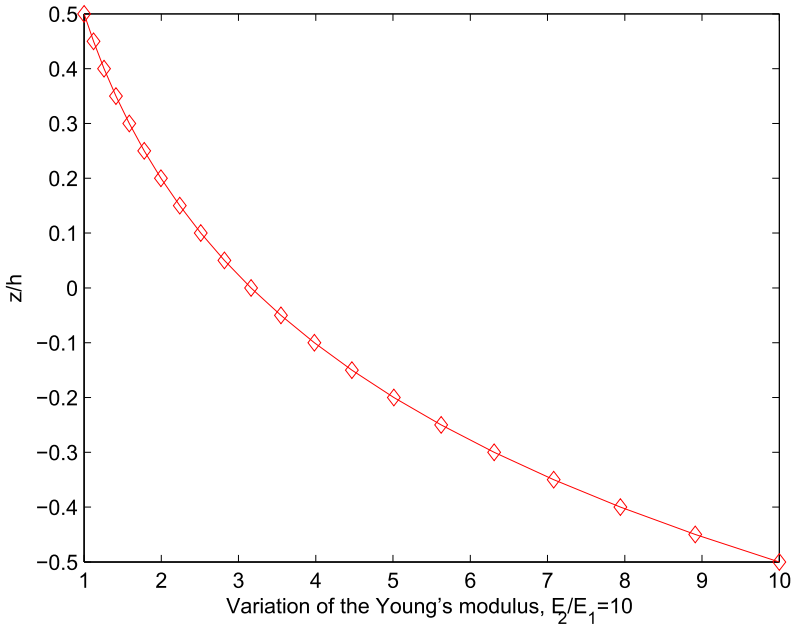

Figure 1.7: Variation of the Young's modulus in an E-FGM plate.

1.3.3 Material Distribution in Exponential Function

Several researchers have used a material distribution in exponential law (Delale and Erdogan, 1983; Long and Delale, 2005; Chi and Chung, 2006a,b) to describe the material properties of FGM plates. This method defines a direct variation of Young's modulus in the thickness of the plate as a function of constituent modules without a material parameter. The effective Young's modulus is expressed in terms of the contrast of constituents as:

$$E(z) = E_2 \left(\frac{E_1}{E_2} \right)^{\frac{2z+h}{2h}} . \tag{1.3}$$

The material distribution in the thickness direction of E-FGM plates is plotted in figure 1.7.

Three volume fraction functions for FGM plates (P-FGM, S-FGM and E-FGM) have been presented in the above paragraphs. Following section will present several micromechanical models used to estimate the effective properties of FGM plates.

1.4 Effective Properties of Functionally Graded Material Plates

Despite the continuity of material compositions on a macroscopic scale, the microstructure of functionally graded materials is heterogeneous. Therefore, to analyze functionally graded materials in an efficient manner, homogenization schemes are necessary to simplify computations of heterogeneous complex microstructures. The purpose of this section is thus to review the main methods used to estimate the effective properties of FGMs.

The analysis and optimal design of functionally graded materials have indeed attracted a growing interest of scientific community in last decades (see Markworth et al. (1995), Obata and Noda (1996), Nadeau and Ferrari (1999), Cho and Ha (2002), Huang et al. (2002) and references therein). To estimate the effective properties of functionally graded material plates, one can distinguish two main computational models: continuous model and discrete model (an illustration of both models is given in figure 1.8). The first model assumes a continuous material distribution in the thickness direction of the plate without taking into account the microstructure, and then the effective moduli will be analytically calculated based on the classical average methods, whereas the discrete models take into account the microstructure with idealized geometries and the conventional analytical and numerical methods are then implemented. In both methods, FGM plates are first homogenized with their effective moduli such as Young's modulus, Poisson's coefficient and thermal conductivity. The effective properties of FGM plates are then obtained from homogeneous plate theories.

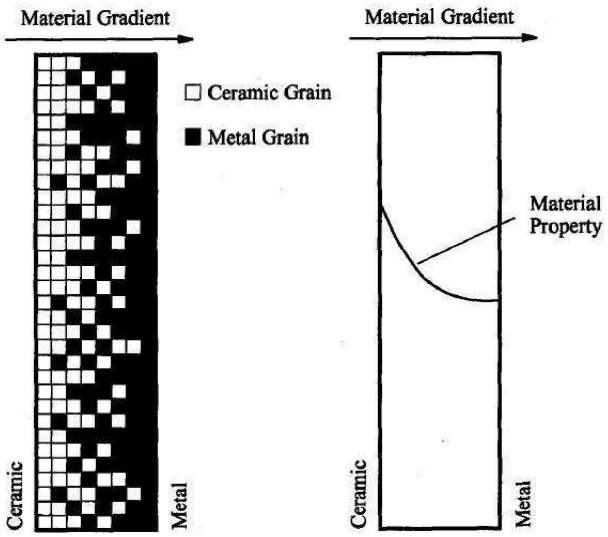

Figure 1.8: Illustration of a discrete model and a continuous model (Dao et al., 1997).

For the continuous model, based on volume fraction functions, most of approaches were based on the classical averaging homogenization methods. The effective moduli of FGMs are analytically expressed in terms of the properties of constituent materials and their volume fractions. In fact, the approximations of Voigt (1889) and Reuss (1929) are widely used to estimate the

effective properties of FGMs such as Young's modulus, the Poisson's coefficient, thermal conductivity (Reddy, 2000; Croce and Venini, 2004; Chi and Chung, 2006a,b; Zenkour, 2006). Another analytical expression applied to isotropic composite, which has been used for FGMs is the self-consistent scheme (Hill, 1965). This approach traditionally consists in solving an elastic problem in which an ellipsoid inclusion is plunged into a matrix with effective properties of the composite. This method does not distinguish the matrix phase and the reinforcement phase since the role of the phases is interchangeable. The self-consistence scheme was applied to calculate the thermoelastic properties of FGMs in the area having interconnected phases (Reiter and Dvorak, 1997, 1998; Vel and Batra, 2002). Vel and Batra (2002) have also used the scheme of Mori and Tanaka (1973) to estimate the effective properties of FGMs. Indeed, the Mori-Tanaka estimate based on the mean-field method implies that a spherical particle is surrounded by a matrix medium. This analytical formula is appropriate for estimating the effective properties of FGMs in the matrix-inclusion region. Other mean-field micromechanic models used for FGMs can be found in Suresh and Mortensen (1998); Gasik (1998); Aboudi et al. (1999); Cho and Ha (2001).

A literature review on homogenization methods applied for FGMs showed that most of studies were based on continuous models where authors assumed that the volume fraction functions of the constituent materials, from which the effective moduli of the material are calculated, vary continuously. In reality, the microstructure of FGMs is discreetly and randomly arranged as illustrated in figures 1.9 and 1.10. The microstructure of FGMs is distinguished by three different zones: two zones with a low concentration of phases represent particle-matrix areas, while the intermediate zone is a transition in which there is an interconnection of phases.

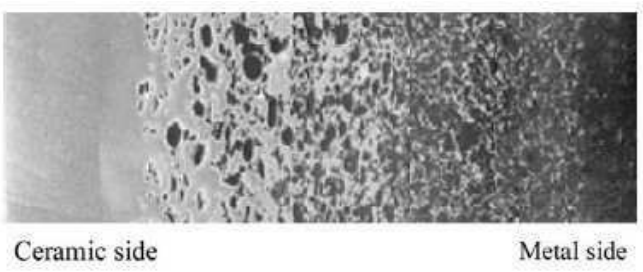

Figure 1.9: Microstructure of a ceramic-metal FGM (Tohgo et al., 2006).

The classical averaging approximations have been applied for the calculation of the effective properties of such a microstructure. The Mori-Tanaka scheme has been used for the matrix-particle region, while the self-consistent method has been used for the transition region having interconnected phases (Zuiker and Dvorak, 1994; Reiter and Dvorak, 1997, 1998; Vel and Batra, 2002). Another approach is to break the grading domain into homogenized discrete layers where the effective properties of the layer are determined by Mori-Tanaka and self-consistent schemes as illustrated in figure 1.11 (Weissenbek et al., 1997; Reiter and Dvorak, 1997, 1998; Sill et al., 2002; Vemaganti and Deshmukh, 2006). Yin et al. (2004) developed an elastic micromechanical model taking into account the interactions between particles using an infinite Green's operator

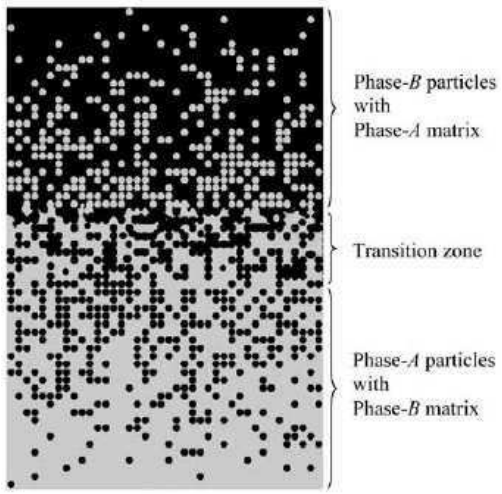

Figure 1.10: Schematic illustration of two-phase FGM (Yin et al., 2004).

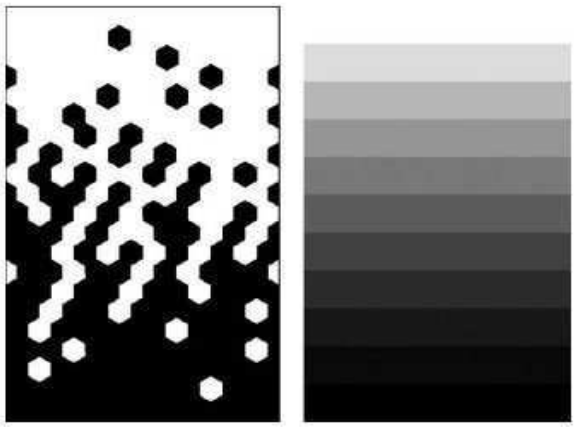

Figure 1.11: Idealized microstructure and homogenized multilayered model (Reiter and Dvorak, 1997, 1998).

and the Eshelby's equivalent inclusion method. Luciano and Willis (2004) proposed a non-local constitutive equation for FGMs based on a Green's operator of an infinite medium and an approximation of Hashin-Strikman type (Willis, 1977, 1981; Drugan and Willis, 1996). Numerous other studies on graded materials can also be found in the review article of Buryachenko (2001).

The finite element method with a discretization at the microscopic scale has meshing difficulties when the complex microstructures are in view. Practically however, this problem can be alleviated if the microstructure is idealized. Reiter and Dvorak (1997, 1998) have developed a micromechanical model for a functionally graded material manufactured from C/SiC where the particles are idealized by hexagons (see figure 1.11). Elastic response of plane arrangements with a linear fraction volume of phases is considered under both uniform and linear varying boundary tractions and displacements. The finite element method has been used with large domains

containing up to several thousand inclusions. In comparison, the method has numerically confirmed that the average method can be used to characterize functionally graded materials and compares well with the results of the Mori Tanaka scheme for the matrix-inclusion zone and to the self-consistent approach for the transition zone with interconnected phases.

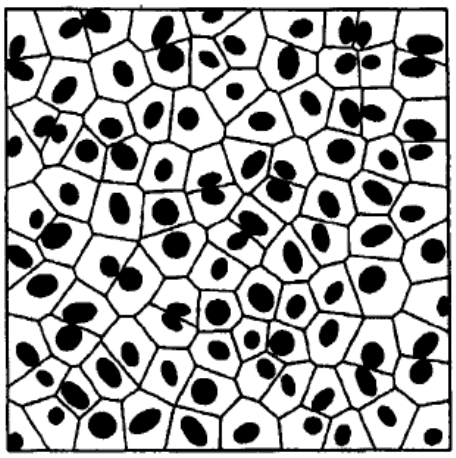

Figure 1.12: Meshing of the Voronoi cell in the matrix-particle zone (Grujicic and Zhang, 1998b).

Grujicic and Zhang (1998b) applied the finite element method with Voronoi cells and the Dirichlet tessellation scheme describing the representative material elements in a network with the elements of convex Voronoi polynomial (VCFEM) (Ghosh et al., 1995) and calculated the effective properties of FGMs. The microstructure is also idealized with the three zones: two matrix-particle zones (figure 1.12) and a transition zone with interconnected phases. The particles are placed in the Voronoi elements. This method has been reported to provide more reliable local responses, for randomly dispersed composite materials, when compared to the results predicted by averaging approaches.

For micromechanical models, several researchers (Dao et al., 1997; Cho and Ha, 2001) divided the FGM domain into uniform rectangular cells and the particles are randomly and discreetly arranged according to a specified fraction volume (figure 1.8). Mishnaevsky (2005) has numerically studied the artificial graded microstructures. The microstructure effects on the shape, size, orientation, the dispersal of the constituents, the loading and the boundary conditions to the mechanical behavior and damage resistance have been reported. The different geometries were randomly generated with different shapes, sizes and orientations of inclusions, and the calculations were done by the finite element method. There exist other numerical micromechanical models for FGMs using the FEM (see Pindera and Dunn (1997); Buryachenko and Rammerstorfer (1998); Becker et al. (2002)).

1.5 Plate Models for Functionally Graded Materials

A plate is a structural element with in-plane dimensions that are large compared to its thickness and is subjected to loads that cause bending deformation in addition to stretching. The theories of plate are developed assuming the shape of the displacement field or the stress field as a linear combination of unknown functions and thickness coordinates expressed generally in the form:

$$\varphi_i(x, y, z, t) = \sum_{j=0}^{N} z^j \varphi_i^j(x, y, t), \tag{1.4}$$

where φ_i is the ith component of displacement or of stress, (x, y) are the in-plane coordinates, z is the thickness coordinate, t denotes the time and φ_i^j are the functions to be determined. The time factor will be not considered here. There exist many plate theories with different forms of (1.4) seeking an expression of φ_i^j. A review on plate models can be found in Ghugal and Shimpi (2002), and Tung (2004).

In order to study the behavior of plates made of functionally graded materials, four plate models used for this material are briefly introduced: the classical plate model of Kirchhoff-Love (CPT), the plate model based on the first-order shear deformation theory (FSDT), the plate model of third-order shear deformation theory (TSDT) and the plate model of sinusoidal shear deformation theory (SSDT).

1.5.1 Love-Kirchhoff Plate Model

The plate model based on the classical plate theory (CPT) satisfies the assumption of Love-Kirchhoff with a linear distribution of the displacements in the thickness. Straight line perpendicular to the mid-surface before deformation, remains straight after deformation. The assumption of Kirchhoff neglects the effect of transverse shear and the deformation is entirely due to bending and membrane deformation. A detailed description of the plate models, including the present model can be referred in Timoshenko and Woinowsky-Krieger (1959), Reddy (1997, 1999).

Based on the above assumptions, the displacement field of the plate model developed in the form (1.4) is then given by the following equation:

$$\begin{aligned} u(x, y, z) &= u_o(x, y) - z\tfrac{\partial w_o}{\partial x}, \\ v(x, y, z) &= v_o(x, y) - z\tfrac{\partial w_o}{\partial y}, \\ w(x, y, z) &= w_o(x, y), \end{aligned} \tag{1.5}$$

where (u_o, v_o, w_o) are the components of the displacement field at the mid-surface (z=0).

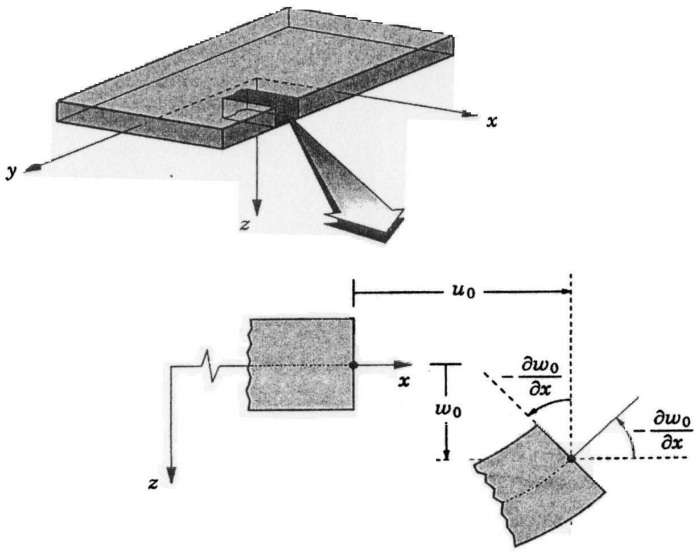

Figure 1.13: Illustration of the Love-Kirchhoff plate (Reddy, 1997).

Since this model does not take the shear energy into account, it gives inaccurate result for thick plates. However because of its simplicity with only three translation degrees of freedom, this classical model remains a good first approach. The analyses of the behavior of functionally graded (FG) plates using the classical plate model of Love-Kirchhoff have been studied by He et al. (2001); Chi and Chung (2006a,b).

1.5.2 First-Order Shear Deformation Plate Model

Unlike the classical model, this model takes into account transverse shear deformations, which are assumed constant in the thickness of the plate. The model requires hence a correction factor to calculate the transverse shear effort. Initial studies on the theory of first-order shear deformation plate (FSDT) can be found in (Reissner, 1945, 1975; Mindlin, 1951) which led to the Reissner-Mindlin plate model. The studies on this model can be referred in Timoshenko and Woinowsky-Krieger (1959); Reddy (1997, 1999); Miara and Podio-Guidugli (2006).

The first-order theory is based on the displacement field under the same assumptions and restrictions as the classical plate theory but with relaxed normality state,

$$\begin{aligned} u(x,y,z) &= u_o(x,y) + z\phi_x(x,y), \\ v(x,y,z) &= v_o(x,y) + z\phi_y(x,y)), \\ w(x,y,z) &= w_o(x,y), \end{aligned} \tag{1.6}$$

where (u_o, v_o, w_o) and (ϕ_x, ϕ_y) are the displacements in the middle surface and the rotations around the y and x axis, respectively. The displacement field defined in the above expression enables to resume the classical plate theory described in the last section by replacing $\phi_x = -\partial w_o/\partial x$, $\phi_y = -\partial w_o/\partial y$. The FSDT is hence an extension of the kinematics of the CPT by a transverse shear deformation in their kinematic hypothesis.

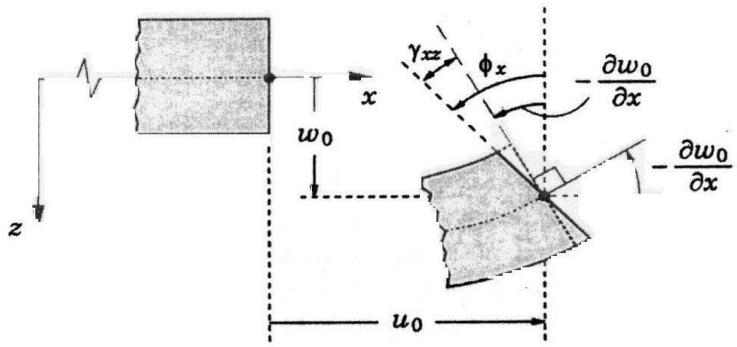

Figure 1.14: Illustration of the Reissner-Mindlin plate (Reddy, 1997)

The FSDT model has been widely used for the analysis of functionally graded materials because of its simplicity of the analysis and programming (Praveen and Reddy, 1998; Croce and Venini, 2004). However, the fact that the transverse shear deformation is constant in the thickness, it thus requires a correction when calculating the transverse shear stresses and efforts. Practically, a transverse shear correction of homogeneous plate model has been taken.

Moreover, to avoid the difficulties with the shear correction, plate theories of higher-order shear deformation have been developed. Several authors have applied high-order plate theories for FGMs. In next section, we will recall two plate models based on high-order shear deformation theories used for the analysis of FGMs: a plate model based on the third-order shear deformation theory (TSDT) proposed by Reddy (1997, 1999) and a plate model based on the sinusoidal shear deformation theory (SSDT) studied by Zenkour (2003, 2004a,b).

1.5.3 High-Order Shear Deformation Plate Model

The high-order shear deformation plate theories have been developed in recent years, initially for analysis of several isothermal plate problems and then deployed to understand physical phenomena induced within the plate. Unlike the CPT and FSDT with the assumptions of linear distribution of displacement through the thickness, the high-order theory is based on a non-linear distribution of the fields in the section. Therefore, the effects of transverse shear deformation and transverse normal deformation are taken into account. These models do not require correction factors. The references on such models can be found in (Hildebrand et al., 1949; Naghdi, 1957; Liberscu, 1967; Nelson and Lorch, 1974; Reissner, 1975; Lo et al., 1977a,b; Reddy, 1997; Kant and

Swaminathan, 2002; Zenkour, 2003). We introduce here two plate models used for analyzing the behavior of functionally graded materials. The displacement field is generally written as follows:

$$\begin{aligned} u(x,y,z) &= u_o(x,y) - z\frac{\partial w_o(x,y)}{\partial x} + \Psi(z)\varphi_x(x,y), \\ v(x,y,z) &= v_o(x,y) - z\frac{\partial w_o(x,y)}{\partial y} + \Psi(z)\varphi_y(x,y), \\ w(x,y,z) &= w_o(x,y), \end{aligned} \tag{1.7}$$

where (u_o, v_o, w_o) et (φ_x, φ_y) are the membrane displacements and the shear rotations around of the axis y and x, respectively ($\varphi_x = \partial w_o/\partial x + \phi_x$, $\varphi_y = \partial w_o/\partial y + \phi_y$), $\Psi(z)$ is a general function in z characterizing the corresponding theories. Indeed, the displacements of the classic plate theory (CPT) is obtained by an arrangement $\Psi(z)$=0, while the first-order theory (FSDT) can be resumed by taking $\Psi(z) = z$.

The displacements of the third-order shear deformation theory of Reddy (TSDT) (Reddy, 1997, 1999) are obtained by:

$$\Psi(z) = z(1 - \frac{4}{3h^2}z^2). \tag{1.8}$$

The third order shear deformation theory (TSDT), which assumes that the transverse shear stress is approximated with a quadratic form in the thickness of the plate, was proposed by Reddy (see Reddy (1997, 1999)). It does not require any shear correction factors. The third-order theory has been widely used to analyze behaviors of FG plates (see Reddy (2000); Cheng and Batra (2000a); Ferreira et al. (2004)).

The sinusoidal shear deformation plate theory (SSDT) of Zenkour (2003, 2004a,b) is obtained by the assumption:

$$\Psi(z) = \frac{h}{\pi}sin(\frac{\pi z}{h}), \tag{1.9}$$

where the resulting displacement field is based on that of the classical plate theory by adding the term $\frac{h}{\pi}sin(\frac{\pi z}{h})\varphi_\alpha$ into the in-plane displacement components, u_α. This plate model has been also used to study the behavior of FG plates by (Zenkour, 2005b,a, 2006). As for the TSDT, no transverse shear correction factors are used in this theory.

1.6 Conclusion of the Chapter

This chapter presented briefly definitions, properties and calculation models for functionally graded materials (FGMs). The gradual spatial variation in material properties of FGMs allows to create innovative structures in numerous application domains. Since the smooth material distribution in the thickness of functionally graded plates has caused changes on behaviors at the

interior of the plate, the application of homogeneous plate models for analysis of FGMs needs to be clarified. More especially, the plate model based on the first-order shear deformation theory (FSDT) used a transverse shear correction of homogeneous plates, however this correction is no longer appropriate for FGMs.
For this reason, a functionally graded plate model based on the FSDT will be studied in next chapter in which the transverse shear correction coefficient will be identified. The static responses of the model will be compared with those obtained from other functionally graded plate models.

Moreover, a literature review on analytical and numerical homogenization methods for estimating the effective properties of FGM plates showed that most of approaches considered plates as a material medium, from which the mean-field homogenization methods have been used to derive the effective moduli such as Young's modulus, Poisson's coefficient and thermal conductivity. The effective properties of the plate were then obtained from homogeneous plate theories. Such a strategy is appropriate when the size of heterogeneity is much smaller than that of in-plane sizes of the plate and its thickness. There exist in reality many plate and beam structures (in civil engineering for example) whose thickness and characteristic size of the heterogeneity are the same order.
The second objective of this thesis is thus to build a homogenization method for general heterogeneous plates from which the calculation of the effective properties of functionally graded plates will be considered as a special case. To do so, a new $\mathbf{\Gamma}$-operator for periodic media with traction-free boundary conditions will be constructed in the second part of this thesis. This operator will be used to compute the effective elastic properties of periodic plates and to formulate a Hashin-Shtrikman variational principle for heterogeneous plates. It is also used to estimate the effect of the size of the heterogeneity for random plates.

Chapter 2

First-Order Shear Deformation Plate Models for Functionally Graded Materials

In this chapter, first-order shear deformation plate models for modelling structures made of functionally graded materials are proposed. Identification of transverse shear factors is investigated through these models by energy equivalence. The transverse shear stresses are derived from the expression of membrane stresses and equilibrium equations. Using the obtained transverse shear factor, a numerical analysis is performed on the examples of a simply supported square plate and of a cylindrical bending sandwich plate clamped at both ends. The material properties are assumed to be isotropic at each point and vary through the thickness according to a power law distribution. The numerical results of the static analysis are compared to available solutions from previous studies.

2.1 Introduction

The concept of functionally graded material (FGM) was proposed in 1984 by the material scientists in the Sendai area of Japan (Koizumi, 1997). The FGM is a composite material whose composition varies according to the required performance. It can be produced with a continuously graded variation of the volume fractions of the constituents. That leads to a continuity of the material properties of FGM: this is the main difference between such a material and an usual composite material. The FGM is suitable for various applications, such as thermal coatings of barrier for ceramic engines, gas turbines, nuclear fusions, optical thin layers, biomaterial electronics, etc.

The composite plates are studied widely in the literature (a review of the plate theories can be found in Ghugal and Shimpi (2002)). Plate models for the functionally graded materials have been studied with analytical and numerical methods. Various approaches have been developed

to establish the appropriate analysis of the functionally graded (FG) plates. The model based on classical plate theory (CPT) of Love-Kirchhoff was applied by Chi and Chung (2006a,b) for the FGM. They developed the analytical solution for simply supported FG plates subjected to mechanical loads. A finite element formulation based on the CPT was studied by He et al. (2001) to control the shape and vibration of the FG plate with integrated piezoelectric sensors and actuators. In practice, this model is not used for thick plates which have an important contribution of the shear deformation energy. Several authors studied the behavior of thick FG plates. They suggested models that take into account the transversal shear effect, by using the First-order Shear Deformation Theory (FSDT) (Reissner, 1945; Mindlin, 1951) and higher-order shear deformation theories (Reddy, 1997, 1999). Praveen and Reddy (1998) examined the nonlinear static and dynamic responses of functionally graded ceramic-metal plates using the first-order shear deformation theory (FSDT) and the von Karman strain (see Reddy (1997, 1999)). Croce and Venini (2004) formulated a hierarchic family of finite elements according to the Reissner-Mindlin theory. The model of FSDT plate is the simplest model that accounts for the transverse shear strains. It requires shear correction coefficients to compute transverse shear forces. To avoid this difficulty, several authors proposed the higher-order shear deformation theory and applied it to FGM. Reddy (2000) developed the Navier's solutions for functionally graded plates using the Third-order Shear Deformation plate Theory (TSDT) and an associated finite element model. Cheng and Batra (2000a) used also the theory of Reddy (TSDT) for studying the buckling and steady state vibrations of a simply supported functionally graded polygonal plate. Moreover, the Sinusoidal Shear Deformation Theory (SSDT) of Zenkour (Zenkour, 2003, 2004a,b) was used for FG plates. By using the theory himself, Zenkour (2006) presented Navier's analytical solution of FG plates. Furthermore, he presented the analysis of FG sandwich plates for the deflection, stresses, buckling and free vibration in Zenkour (2005b,a). In the higher-order shear deformation theory, the transverse shear stresses are taken into account throughout the thickness and consequently no transversal shear correction factors are needed. For the thick FG plates whose thickness is not negligible, when compared to the side length, the three-dimensional models for static and dynamic problems can be used. Cheng and Batra (2000b) studied thermomechanical deformations of the FG plates. Elishakoff et al. (2005) used the Ritz's method to derive the three-dimensional governing equation for the all-round clamped FG plates. A discrete layer approach was proposed by Ramirez et al. (2006) for the static analysis of three-dimensional FG plates. For analysis of functionally graded beams, Reddy (2003) also presented a FG finite element beam model by using the FSDT (Timoshenko beam) and the TSDT. Satchi and Bhavani (2001) analyzed the sandwich beam with a functionally graded core for which they proposed an elasticity solution.

The models based on the first-order shear deformation theory (FSDT) are very often used owing to their simplicity in analysis and programming. It requires however a convenient value of the shear correction factor. In practice, this coefficient has been assumed to be given by 5/6 as for homogeneous plates. This value is a priori no longer appropriate for functionally graded material analysis due to the position dependence of elastic properties.

The primary objective of this chapter is thus to identify the shear correction coefficients for the FSDT models made of functionally graded materials. Applications are presented for a simply supported plate and for a sandwich panel which is clamped at both ends. The influence of this factor on the static response is then presented. The material elastic properties are supposed to be isotropic and varying through the thickness according to a power-law function of the position.

2.2 Theoretical Formulation

Consider a FSDT plate model (figure 2.1) having a thickness h which is located within a domain $\Psi = \Omega \times]-\frac{h}{2}, \frac{h}{2}[$, $h \in R^+$. $\Omega \in R^2$ is a area possessing a boundary with a suitable regularity $\partial\Omega$. The top and bottom surfaces of the plate are denoted by $\Psi^{\pm} = \Omega \times \{\pm\frac{h}{2}\} = \{x, y \in \Psi,\, z = \pm\frac{h}{2}\}$. The plate is made of a functionally graded material which is constituted by a mixture of ceramic and metallic components. The material properties vary through the plate thickness according to the volume fractions of the constituents. All formulations are performed under the assumption of a linear elastic behavior and small deformations of materials. The gravity is not taken into account.

This section presents the steps used in order to compute the shear stiffnesses of the FG plates based on the FSDT. To do so, the shear strain energy is obtained from the expression of the transverse shear stresses obtained from the membrane stresses and equilibrium equations. The appropriate shear correction factors will then be obtained. The sandwich panel model will be studied as a special case. In this section, the Greek indices are assumed to range within {1,2} while the Latin indices take values {1,2,3}.

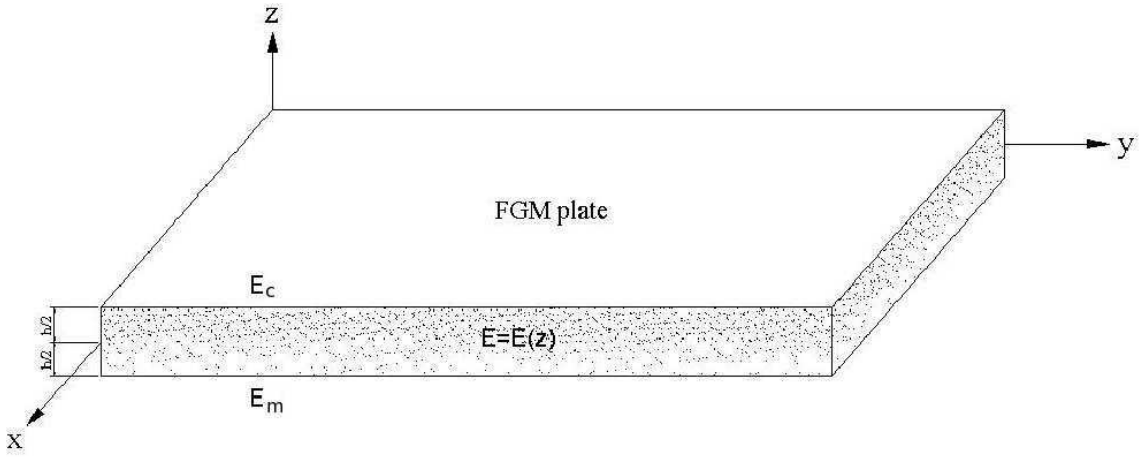

Figure 2.1: Geometry of the functionally graded plate.

2.2.1 Stress Fields

The displacement field of the first-order shear deformation theory (FSDT) has been defined in Eqs. (1.6) of the first chapter and the basic equations of the plate model can be found in Timoshenko and Woinowsky-Krieger (1959); Reddy (1997, 1999).

2.2.1.1 In-Plane Stresses

The generalized stresses associated to the in-plane stress field $\sigma_{\alpha\beta}(N, M)$ can be defined as follows:

$$\begin{aligned} N_{\alpha\beta}(x,y) &= \textstyle\int_{-h/2}^{h/2} \sigma_{\alpha\beta}(x,y,z)\, dz, \\ M_{\alpha\beta}(x,y) &= \textstyle\int_{-h/2}^{h/2} z\sigma_{\alpha\beta}(x,y,z)\, dz. \end{aligned} \tag{2.1}$$

The generalized strains are given by,

$$\begin{aligned} \epsilon^o_{\alpha\beta}(x,y) &= \tfrac{1}{2}(u_{\alpha,\beta} + u_{\beta,\alpha})(x,y), \\ \chi_{\alpha\beta}(x,y) &= \tfrac{1}{2}(\theta_{\alpha,\beta} + \theta_{\beta,\alpha})(x,y), \end{aligned} \tag{2.2}$$

where the comma indicates partial differentiation with respect to the coordinate subscript that follows, u and θ the displacement and rotation of the FSDT. The strain is assumed to be linear through the thickness of the FG plate,

$$\epsilon_{\alpha\beta}(x,y,z) = \epsilon^o_{\alpha\beta}(x,y) + z\chi_{\alpha\beta}(x,y). \tag{2.3}$$

The membrane strains and in-plane stresses are related by the constitutive equation,

$$\sigma_{\alpha\beta}(x,y,z) = C_{\alpha\beta\gamma\delta}(z)(\epsilon^o_{\gamma\delta}(x,y) + z\chi_{\gamma\delta}(x,y)), \tag{2.4}$$

where $C_{\alpha\beta\gamma\delta}(z)$ are the components of the reduced elasticity tensor at location z. Substituting (2.4) into (2.1) leads to:

$$\begin{aligned} N_{\alpha\beta}(x,y) &= A_{\alpha\beta\gamma\delta}\, \epsilon^o_{\gamma\delta}(x,y) + B_{\alpha\beta\gamma\delta}\, \chi_{\gamma\delta}(x,y), \\ M_{\alpha\beta}(x,y) &= B_{\alpha\beta\gamma\delta}\, \epsilon^o_{\gamma\delta}(x,y) + D_{\alpha\beta\gamma\delta}\, \chi_{\gamma\delta}(x,y), \end{aligned} \tag{2.5}$$

where $A_{\alpha\beta\gamma\delta}$, $B_{\alpha\beta\gamma\delta}$, $D_{\alpha\beta\gamma\delta}$ are the stiffnesses of the plate which are given by,

$$(A_{\alpha\beta\gamma\delta}, B_{\alpha\beta\gamma\delta}, D_{\alpha\beta\gamma\delta}) = \int_{-h/2}^{h/2} (1, z, z^2) C_{\alpha\beta\gamma\delta}(z) dz. \tag{2.6}$$

It can be noticed that, unlike for a homogeneous symmetrical isotropic plate where the coupling stiffnesses $B_{\alpha\beta\gamma\delta}$ are null, the $B_{\alpha\beta\gamma\delta}$ are present in the constitutive equation for the non-symmetrical functionally graded plates. The membrane strains are finally:

$$\begin{aligned} \epsilon^{o}_{\alpha\beta}(x,y) &= a_{\alpha\beta\gamma\delta}N_{\gamma\delta}(x,y) + b_{\alpha\beta\gamma\delta}M_{\gamma\delta}(x,y), \\ \chi_{\alpha\beta}(x,y) &= b_{\alpha\beta\gamma\delta}N_{\gamma\delta}(x,y) + d_{\alpha\beta\gamma\delta}M_{\gamma\delta}(x,y), \end{aligned} \tag{2.7}$$

where $(a_{\alpha\beta\gamma\delta}, b_{\alpha\beta\gamma\delta}, d_{\alpha\beta\gamma\delta})$ are the components of the compliance matrix. The matrices C, A, B, D, a, b and d can be explicitly expressed in terms of the functions $E(z)$ and $\nu(z)$ describing the Young modulus and the Poisson's ratio at z, respectively. Moreover, it appears that the matrix b is symmetric owing to the fact that the material elastic properties are isotropic. Substituting (2.7) in (2.4) leads to:

$$\sigma_{\alpha\beta}(x,y,z) = n_{\alpha\beta\gamma\delta}(z)N_{\gamma\delta}(x,y) + m_{\alpha\beta\gamma\delta}(z)M_{\gamma\delta}(x,y), \tag{2.8}$$

where $n_{\alpha\beta\gamma\delta}(z), m_{\alpha\beta\gamma\delta}(z)$ are the components of the localization tensors that are expressed as:

$$\begin{aligned} n_{\alpha\beta\gamma\delta}(z) &= C_{\alpha\beta\varepsilon\varphi}(z)(a_{\varepsilon\varphi\gamma\delta} + zb_{\varepsilon\varphi\gamma\delta}), \\ m_{\alpha\beta\gamma\delta}(z) &= C_{\alpha\beta\varepsilon\varphi}(z)(b_{\varepsilon\varphi\gamma\delta} + zd_{\varepsilon\varphi\gamma\delta}). \end{aligned} \tag{2.9}$$

2.2.1.2 Transverse Shear Stresses

The calculation of the transverse shear stresses from the constitutive equation is not realistic because of the assumption of a constant shear strain through the thickness of the plate. The transverse shear stresses are derived classically from the equilibrium equation. The equilibrium equation in Ω allows to determine the shear stresses $\sigma_{\alpha 3}$ which are given by:

$$\sigma_{\alpha 3} = -\int_{-h/2}^{z} \sigma_{\alpha\beta,\beta}\, d\xi, \tag{2.10}$$

where the integration coefficients have been selected to satisfy the boundary condition for shear stresses at the upper and lower faces of the plate. By substituting (2.8) into (2.10), the following relationship is obtained:

$$\sigma_{\alpha 3} = \tilde{n}_{\alpha\beta\gamma\delta}(z)N_{\gamma\delta,\beta}(x,y) + \tilde{m}_{\alpha\beta\gamma\delta}(z)M_{\gamma\delta,\beta}(x,y), \tag{2.11}$$

where,

$$\begin{aligned} \tilde{n}_{\alpha\beta\gamma\delta}(z) &= -\textstyle\int_{-h/2}^{z} C_{\alpha\beta\varepsilon\varphi}(\xi)\,[a_{\varepsilon\varphi\gamma\delta} + \xi b_{\varepsilon\varphi\gamma\delta}]\, d\xi, \\ \tilde{m}_{\alpha\beta\gamma\delta}(z) &= -\textstyle\int_{-h/2}^{z} C_{\alpha\beta\varepsilon\varphi}(\xi)\,[b_{\varepsilon\varphi\gamma\delta} + \xi d_{\varepsilon\varphi\gamma\delta}]\, d\xi, \\ \tilde{n}_{\alpha\beta\gamma\delta} &= \tilde{n}_{\gamma\delta\alpha\beta} = \tilde{n}_{\beta\alpha\gamma\delta}, \quad \tilde{m}_{\alpha\beta\gamma\delta} = \tilde{m}_{\gamma\delta\alpha\beta} = \tilde{m}_{\beta\alpha\gamma\delta}. \end{aligned} \tag{2.12}$$

It is noted that the expression (2.12) is obtained due to the uniform properties of the material in the plane of the laminate ($n_{\alpha\beta\gamma\delta,\beta} = 0, m_{\alpha\beta\gamma\delta,\beta} = 0$).

A direct computation of the shear stresses within equation (2.10) will require the second order derivatives of the displacement. For finite element methods, several authors (Lee and Lee, 2003; Sze, 2000; Zienkiewicz and Zhu, 1992; Rolfes and Rohwer, 1997; Rolfes et al., 1998) used a method of postprocessing based on the three-dimensional equilibrium equations or a predictor-corrector approach or simplified assumptions. A simplifying assumption (Rolfes and Rohwer, 1997; Rolfes et al., 1998) which is used thereafter, enables the computation of shear stresses from transverse shear forces. This process allows to comply to boundary conditions on the transverse shear stresses and to save an order of derivation. A last simplification is achieved by using a cylindrical bending assumption. Assuming cylindrical bending around the axis y, using the equilibrium equations of the plate ($N_{\alpha\beta,\beta} = 0$, $M_{\alpha\beta,\beta} - Q_\alpha = 0$) and omitting the weak terms ($N_{22,1}$ and $M_{22,1}$), leads to:

$$\sigma_{xz}(x,z) = \tilde{m}_{1111}(z) Q_x(x), \tag{2.13}$$

with $\tilde{m}_{1111}(z)$ given in (2.12). Practically, this relation is very often used to compute the shear stress of the homogeneous model with a quadratic form of $\tilde{m}_{1111}(z)$, especially when commercial finite element packages are used.

2.2.2 Shear Correction Factors

It is well-known that the models based on the first-order shear deformation theory require a correct value of the shear correction factors to compute the shear force. Several authors made contributions in order to improve the models used for the FSDT. Hutchinson (2001), Gruttmann and Wagner (2001) presented a new formula in order to compute the shear coefficients of different cross-sections of a Timoshenko's beam. The discussion of this topic for the plate and shell problems can be found in (Berthelot, 1992; Caron and Sab, 2001; Rolfes and Rohwer, 1997; Vlachoutsis, 1992; Nguyen et al., 2005). In this chapter, the shear coefficients are studied by considering the shear deformation energy.

The shear forces (Q_x, Q_y) are related to the average shear strains $(\gamma_{xz}, \gamma_{yz})$ by,

$$\left\{ \begin{array}{c} Q_y \\ Q_x \end{array} \right\} = \left[\begin{array}{cc} H_{44} & H_{45} \\ H_{45} & H_{55} \end{array} \right] \left\{ \begin{array}{c} \gamma^o_{yz} \\ \gamma^o_{xz} \end{array} \right\}, \tag{2.14}$$

where H_{ij} $(i,j = 4,5)$ are the shear stiffnesses. For isotropic materials, there is no coupling between the shear deformations in two directions, i.e., H_{45}=0 and $H_{44} = H_{55}$. Therefore, it is sufficient to identify only one of the components H_{55} or H_{44}.

By using the shear stress defined in (2.13), the shear deformation energy per unit middle surface area is then given by the following expression:

$$\Pi_s = \frac{1}{2} Q_x^2 \int_{-h/2}^{h/2} \frac{[\tilde{m}_{1111}(z)]^2}{G(z)}\, dz, \tag{2.15}$$

where $G(z) = E(z)/(2(1+\nu(z)))$ is the transverse shear modulus at location z. Furthermore, the shear deformation energy per unit middle surface area is expressed by using the average shear deformation,

$$\Pi_{sm} = \frac{1}{2} Q_x \gamma_{xz}^o = \frac{1}{2} \frac{Q_x^2}{H_{55}}. \tag{2.16}$$

The balance of the shear energy enables us to deduce,

$$H_{55} = \left(\int_{-h/2}^{h/2} \frac{[\tilde{m}_{1111}(z)]^2}{G(z)}\, dz \right)^{-1}, \tag{2.17}$$

where H_{55} is the improved shear stiffness for FG plates. The shear correction coefficients are finally obtained from:

$$k_{55} = \frac{H_{55}}{\int_{-h/2}^{h/2} G(z)\, dz}. \tag{2.18}$$

The shear correction factor is equal to 5/6 for homogeneous plates assuming a parabolic variation of the shear stress and a priori relations (2.18), (2.17) and (2.12) will lead to different values for the FGM. Moreover, the use of the improved shear stiffnesses in equation (2.17) will provide a better evaluation of transverse shear forces in (2.14).

2.3 Applications

The numerical applications in the case of the FSDT model are performed with two examples. The first test is the study of the cylindrical bending of a clamped-clamped sandwich panel. A comparison is performed with solutions obtained from discrete finite element model and other cylindrical bending plate models. In the second example, a simply supported plate is studied. Navier's analytical solution is achieved and compared to the FSDT, TSDT, SSDT solutions and to a three-dimensional discrete finite element solution.

2.3.1 Sandwich Panel with Functionally Graded Faces

2.3.1.1 Material Distribution

Consider the 3-layers sandwich strip shown in figure 2.2. The face layers are made of a ceramic-metal isotropic material whose properties vary smoothly through the thickness according to the volume fractions of the constituents. The core layer is constituted by the metal isotropic

homogeneous material. The vertical positions of the bottom and top faces, and of two interfaces between the layers are respectively denoted by $h_o = -h/2$, h_1, h_2, $h_3 = h/2$, which are directly related to e_c, e_{fb}, e_{ft} being the thicknesses of the core, of the bottom and top faces respectively.

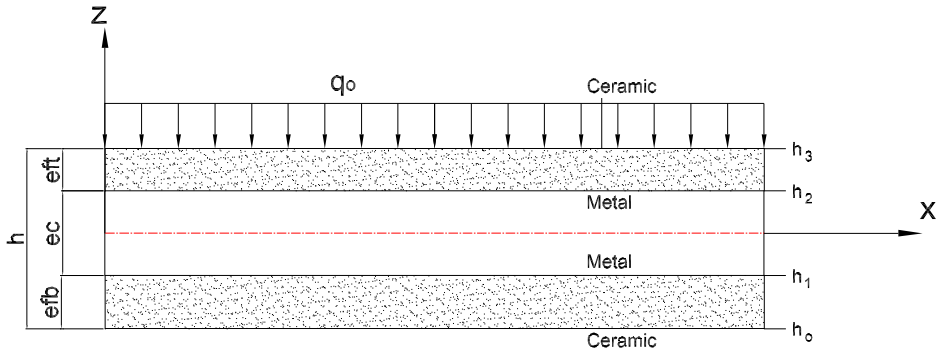

Figure 2.2: Geometry of the sandwich panel with the functionally graded faces.

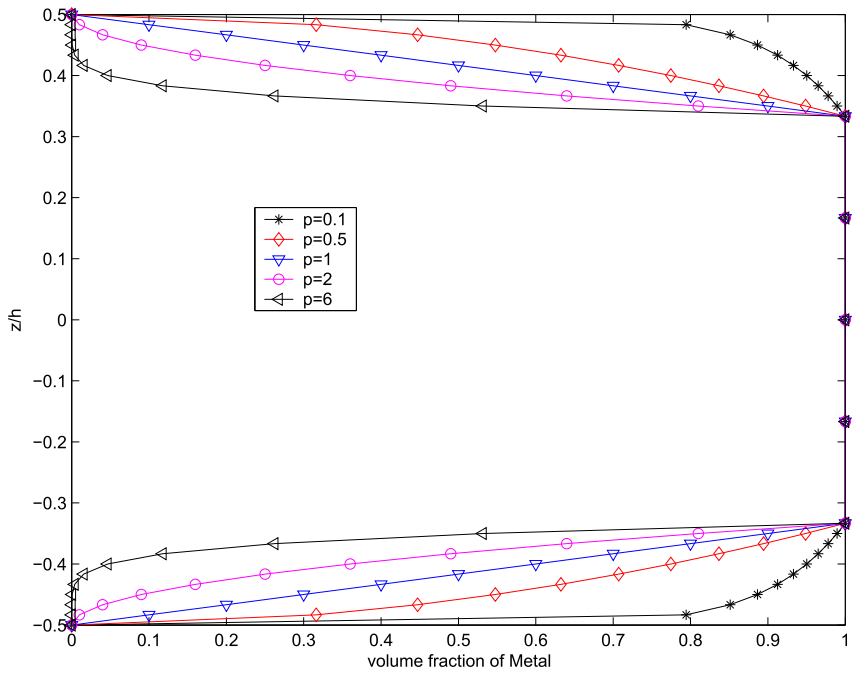

Figure 2.3: Variation of V_m through the thickness of the plate according to p.

The distribution of elastic properties through the thickness of the sandwich plate is assumed to be a power-law relation:

$$E^{(k)}(z) = (E_m - E_c)V_m^{(k)}(z) + E_c, \tag{2.19}$$

where E_c and E_m are the Young's moduli of ceramic and metal, $V_m^{(k)}$ being given by:

$$\begin{cases} V_m^{(1)}(z) = \left(\frac{z-h_o}{h_1-h_o}\right)^p & for \quad z \in [h_o, h_1] \\ V_m^{(2)}(z) = 1 & for \quad z \in [h_1, h_2] \\ V_m^{(3)}(z) = \left(\frac{z-h_3}{h_2-h_3}\right)^p & for \quad z \in [h_2, h_3] \end{cases} \tag{2.20}$$

where p is a material parameter which is positive, h is the thickness of the plate and $z \in [-h/2, h/2]$. The implicit assumption within (2.19) is that the mixture of the two materials is taken into account by the "Voigt model". It can be shown that this assumption is convenient if the contrast between the phases is not too large. Many more approximations of the effective elastic properties can be found within the literature (Gasik, 1998; Vel and Batra, 2002; Grujicic and Zhang, 1998a). The material variation profiles under consideration are shown in figure 2.3 for different values of p.

2.3.1.2 Numerical Results

A sandwich panel that is clamped at two opposite ends and subjected to the uniformly distributed load acting downward q_o (figure 2.2) is now considered. The closed-form expression of the displacement field within a FG sandwich panel is given in appendix. In this section, the effect on the deflection of the plate due to changing the shear correction factors is shown. In the following, the Poisson's ratio is assumed to be constant. The study of its effect on the static response of the plate can be found in Chi and Chung (2006a,b). The following parameters are used for numerical computations, $\nu = 0.3$, $q_o = 10^4, e_{ft} = 0.01, e_{fb} = 0.01$.

Table 2.1: Shear correction factors, $e_c/e_{ft} = 4$.

p	E_c/E_m									
	1	2	3	4	5	6	8	10	15	20
0	5/6	5/6	5/6	5/6	5/6	5/6	5/6	5/6	5/6	5/6
0.2	5/6	0.8137	0.7921	0.7699	0.7478	0.7262	0.6851	0.6474	0.5672	0.5037
0.4	5/6	0.7973	0.7589	0.7214	0.6860	0.6532	0.5949	0.5454	0.4505	0.3832
0.6	5/6	0.7843	0.7338	0.6865	0.6437	0.6051	0.5393	0.4859	0.3887	0.3237
1.0	5/6	0.7654	0.6993	0.6409	0.5902	0.5464	0.4749	0.4196	0.3245	0.2645
2.0	5/6	0.7395	0.6552	0.5855	0.5281	0.4805	0.4065	0.3520	0.2633	0.2102
4.0	5/6	0.7184	0.6215	0.5450	0.4843	0.4353	0.3616	0.3080	0.2263	0.1784
6.0	5/6	0.7093	0.6074	0.5284	0.4667	0.4175	0.3443	0.2926	0.2126	0.1669
8.0	5/6	0.7043	0.5996	0.5194	0.4572	0.4078	0.3350	0.2840	0.2055	0.1609
10.0	5/6	0.7011	0.5947	0.5137	0.4512	0.4018	0.3292	0.2786	0.2011	0.1572
15.0	5/6	0.6966	0.5877	0.5057	0.4428	0.3934	0.3212	0.2712	0.1950	0.1522
20.0	5/6	0.6942	0.5840	0.5014	0.4384	0.3890	0.3171	0.2674	0.1919	0.1496

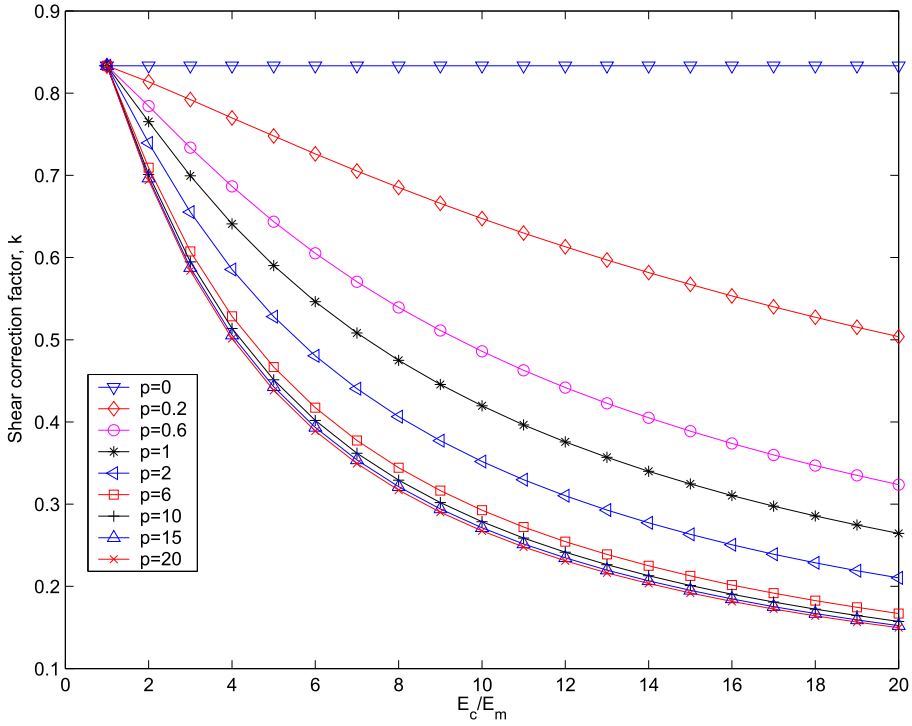

Figure 2.4: Variation of the shear factors according to the ratio of E_c/E_m, $e_c/e_{ft} = 4$.

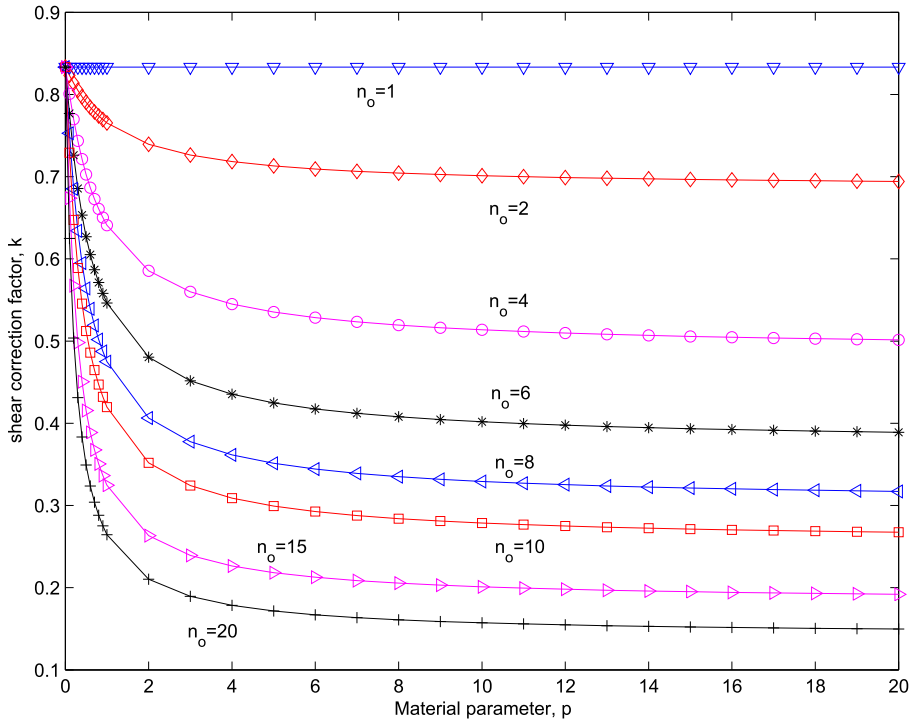

Figure 2.5: Variation of the shear factor according to p, $e_c/e_{ft} = 4$.

Table 2.2: Shear correction factors, $E_c/E_m = 6$.

p	e_c/e_{ft}									
	1	2	4	6	8	10	15	20	30	40
0	5/6	5/6	5/6	5/6	5/6	5/6	5/6	5/6	5/6	5/6
1	0.4591	0.4819	0.5464	0.5990	0.6392	0.6701	0.7215	0.7520	0.7848	0.8012
2	0.3981	0.4158	0.4805	0.5368	0.5815	0.6171	0.6790	0.7177	0.7615	0.7844
4	0.3583	0.3719	0.4353	0.4929	0.5399	0.5780	0.6462	0.6903	0.7420	0.7700
6	0.3429	**0.3547**	0.4175	0.4754	0.5231	0.5620	0.6326	0.6787	0.7335	0.7635
8	0.3347	0.3454	0.4078	0.4659	0.5139	0.5533	0.6250	0.6723	0.7287	0.7599
10	0.3294	0.3397	0.4018	0.4599	0.5081	0.5478	0.6203	0.6682	0.7257	0.7576

Table 2.3: Deflection and relative error in a clamped sandwich strip, $E_c/E_m = 6$, $p = 6$, $e_c/e_{ft} = 2$

a/h	FEM	FSDT		
		$k = 1$	$k = 5/6$	$k = 0.3547$
5	6.023e-8	3.495e-08 (-41.97 %)	3.791e-8 (-37.06 %)	6.183e-8 (2.66 %)
10	4.822e-7	3.820e-07 (-20.78 %)	3.938e-7 (-18.33 %)	4.895e-7 (1.51 %)
20	5.868e-6	5.403e-06 (-7.92 %)	5.450e-6 (-7.12 %)	5.833e-6 (-0.60 %)
30	2.794e-5	2.669e-05 (-4.47 %)	2.679e-5 (-4.12 %)	2.765e-5 (-1.04 %)
40	8.636e-5	8.360e-05 (-3.20 %)	8.379e-5 (-2.98 %)	8.532e-5 (-1.20 %)
50	2.086e-4	2.033e-04 (-2.54 %)	2.036e-4 (-2.40 %)	2.060e-4 (-1.25 %)

Figures 2.4 and 2.5 present the variation of the shear correction factors according to the ratio of elastic moduli $n_o = E_c/E_m$ and to the power-law parameter p, where p is within the range [0-20], while n_o is within the range [1-20]. The ratio e_c/e_{ft} is within the range [1-40]. The values of the shear correction factors for every couple (p, n_o) and $(p, e_c/e_{ft})$ are given in tables 2.1 and 2.2. It is important to notice that the shear correction factor k depends strongly on the values of p and on the ratio of E_c/E_m and e_c/e_{ft}. It can be seen that the shear correction factors decrease when the ratio of the elastic moduli increases (figures 2.4 and 2.5). On the other hand, the shear correction factor increases when the ratio of thickness between the core and face increases (figure 2.6). The shear correction factor is equal to 5/6 as for a homogeneous plate for p=0 and n_o=1 and is smaller than 5/6 in other cases. Table 2.2 and figure 2.6 represent the variation of the shear correction factor in terms of the ratio of the thickness of the homogeneous core and of the thickness of the functionally graded faces. When the ratio e_c/e_{ft} is very large, the shear factor tends to the value obtained for homogenous plates (figure 2.6).

To consider the effect on the deflection of the sandwich panel induced by changing the shear correction factor, the value k=0.3547 is taken (table 2.2). This value corresponds to p=6,

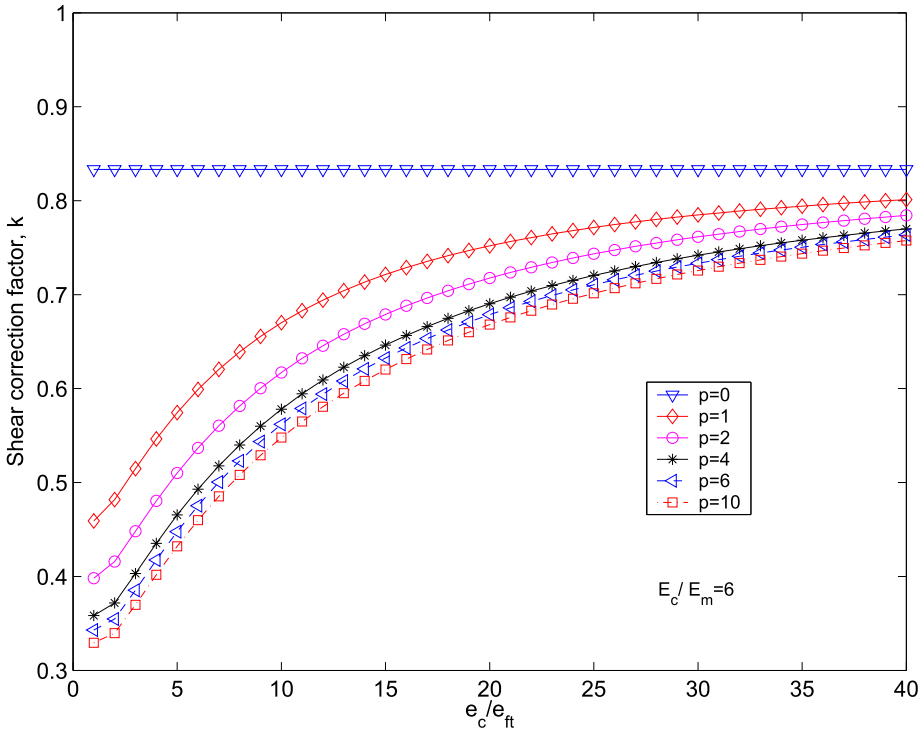

Figure 2.6: Variation of the transverse shear correction factors in terms of the ratio of e_c/e_{ft}, $E_c/E_m = 6$.

E_c/E_m=6 (SiC, E_c=420GPa and Aluminum, E_m=70GPa) and $e_c/e_{ft} = 2$. The obtained deflection is compared in a first step to that of the model using the correction factor $k = 5/6$. The measurement of a "relative error" is defined by the relationship:

$$error(\%) = \frac{M_c - M_m}{M_m} \times 100\% \tag{2.21}$$

where M_m is the value of the maximum deflection obtained from the present model, and M_c is that of other models.

Figures 2.7 and 2.8 show the variation profile of the relative error of the maximal deflection at the center of the plate for the corrected shear coefficient using the five-sixth factor. It can be observed that the difference increases with the value n_o and the plate thickness. That is explained by the fact that the correction factor decreases strongly in those cases. The difference between the maximal deflection for the case of the five-sixth factor compared to the present model is 37.5% for n_o=6 (SiC-Al) and p=6. This deviation is higher for a larger value of n_o.

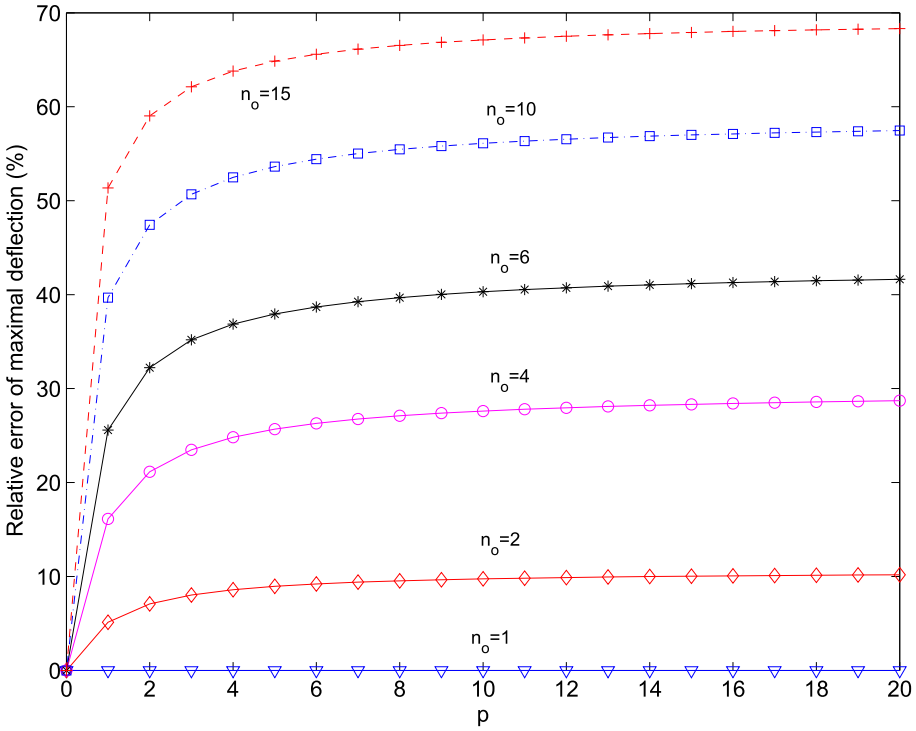

Figure 2.7: Relative error of maximal deflection in terms of p, $e_c/e_{ft} = 2$, a/h=5.

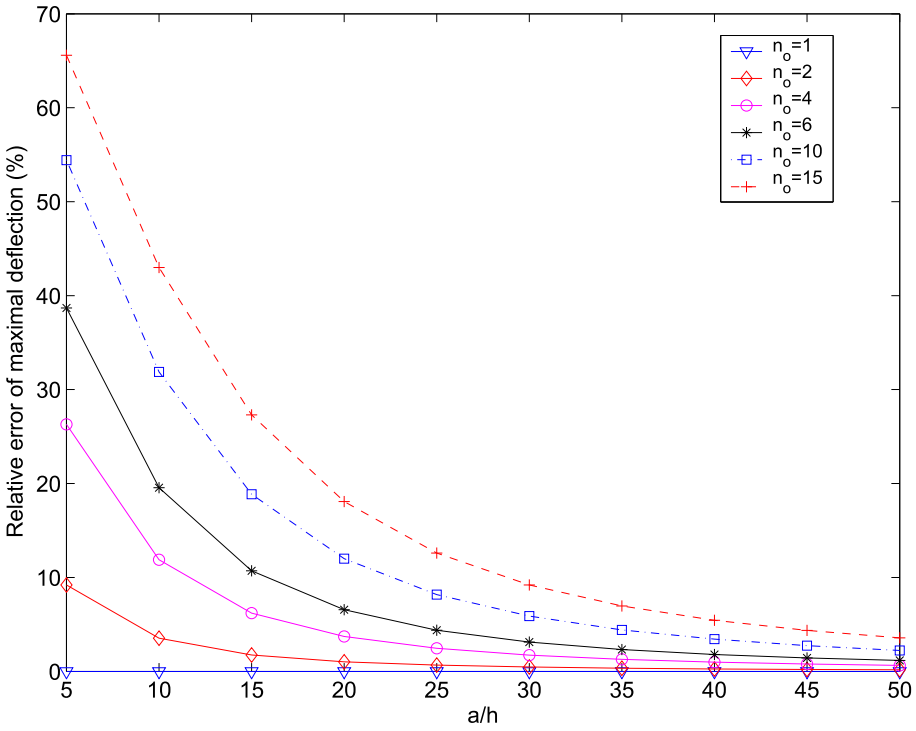

Figure 2.8: Relative error of maximal deflection according to the ratio of length-thickness, $e_c/e_{ft} = 2$, p=6.

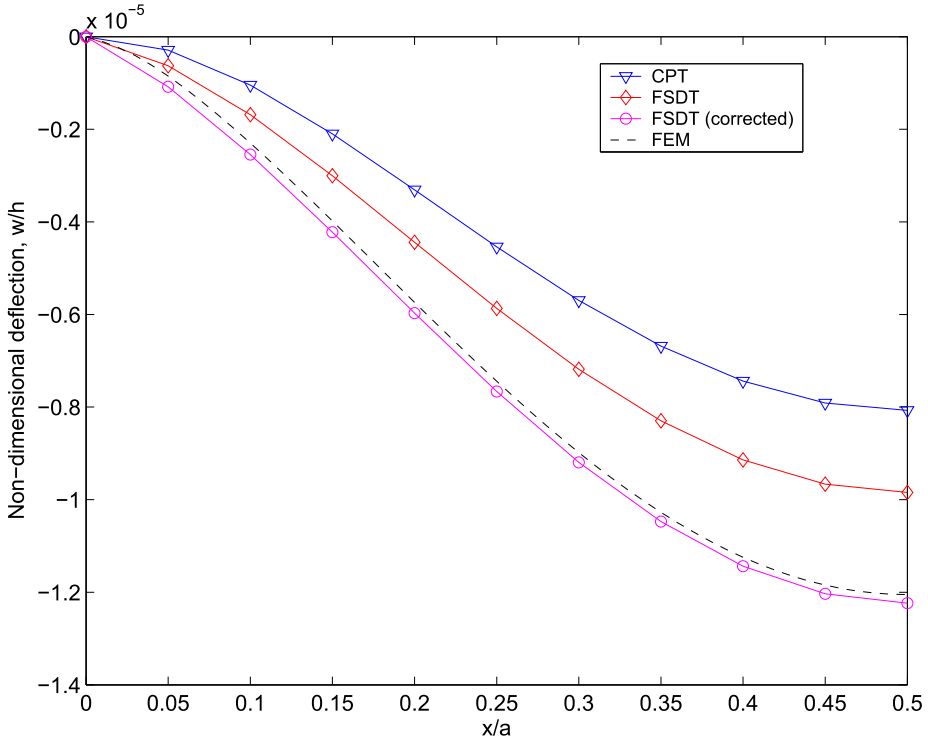

Figure 2.9: Variation profile of deflection for various model, $E_c/E_m = 6$, $p = 6$, a/h=10, $e_c/e_{ft} = 2$.

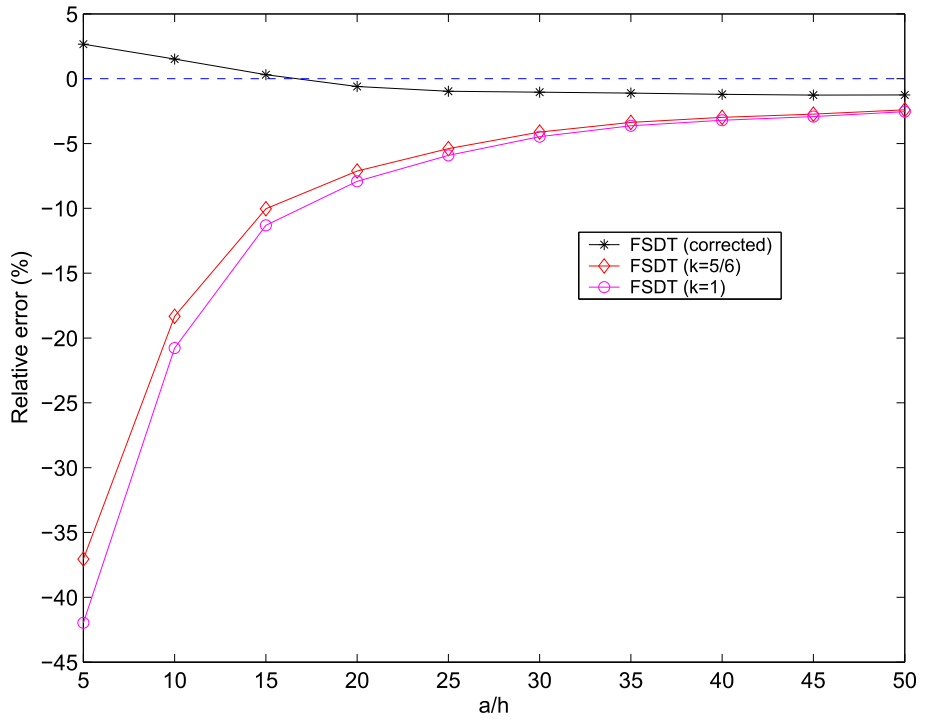

Figure 2.10: Relative error of the maximal deflection, $E_c/E_m = 6$, p=6, $e_c/e_{ft} = 2$.

The validation of the solution of the present model is performed by comparison with that of a finite element model. The finite element computation is performed with five discrete layers through the layer-thickness of the plate. The 3D solution is obtained by using Abaqus software and linear quadrilateral elements CPE4R (plane strain). In comparison, the deflection obtained by the finite element model is approximately equal to that of the model using the corrected shear factor (figure 2.9). The relative error in comparison with the finite element solution is determined by using (2.21) (where M_m is the magnitude given by the discrete finite element model, and M_c that of the other models). The errors can be seen in table 2.3 and are shown in figure 2.10. It is seen that the corrected FSDT solution is in a good agreement with the finite element solution, whereas the results obtained by the FSDT model taking the factor of correction k=5/6 are different even for a thin plate.

2.3.2 Functionally Graded Simply Supported Plate

2.3.2.1 Material Distribution

The distribution of a functionally graded material within a non-symmetrical plate is now considered. The plate is made of a mixture of ceramic and metallic components (figure 2.1).

The effective modulus through the plate is defined in (2.19) where $V_m(z) = 1 - V_c(z)$.

$$V_c(z) = \left(\frac{z + \frac{h}{2}}{h} \right)^p . \tag{2.22}$$

The distribution of the materials under consideration (2.22) is presented in figure 2.11. It can be seen that the V_c varies quickly near the lowest surface for p <1 and increases quickly near the top surface for p >1.

2.3.2.2 Numerical Results

In this part, the effect on the deflection of the plate due to changing the shear correction factors will be shown. Moreover, some results for the static analysis of a squared, simply supported FG plate under uniformly distributed load of intensity q_o, are presented. They are compared to the third-order shear deformation plate model (TSDT) of Reddy (Reddy, 2000), the sinusoidal shear deformation plate model (SSDT) of Zenkour (Zenkour, 2006) and a discrete three-dimensional finite element model. The following parameters are used for numerical computations, $\nu = 0.3, a = b = 1, q_o = 10^4$. The deflection and stress fields within the plate are obtained by the Navier's solution given in the appendix. The following non-dimensional parameters are used: $\overline{w} = w/h, \overline{\sigma} = \sigma h^2/(q_o a^2)$.

Figures 2.12 and 2.13 present the variation of the shear correction factors according to n_o and p, where the parameters p and n_o are changed as for the previously studied sandwich panel.

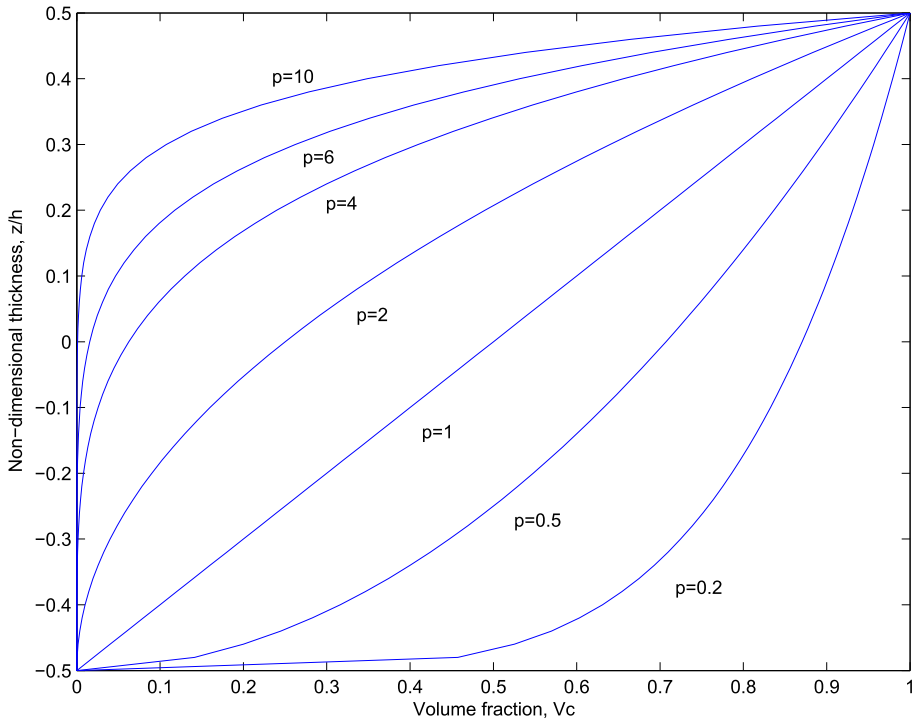

Figure 2.11: Variation of V_c through plate thickness for various values of p.

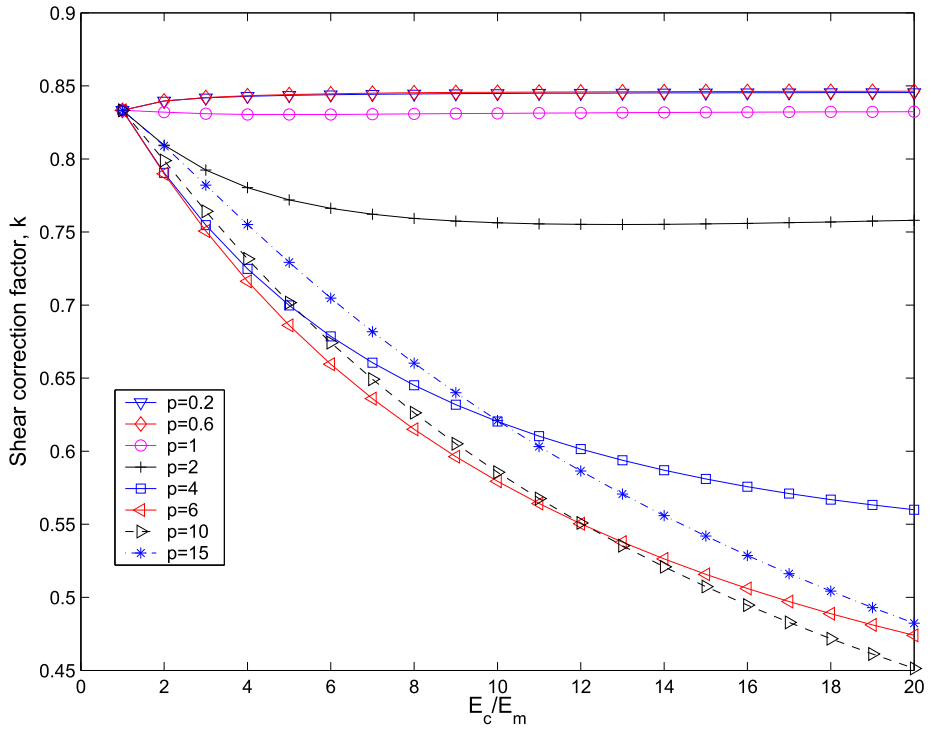

Figure 2.12: Variation of the shear correction factor according to $n_o = E_c/E_m$.

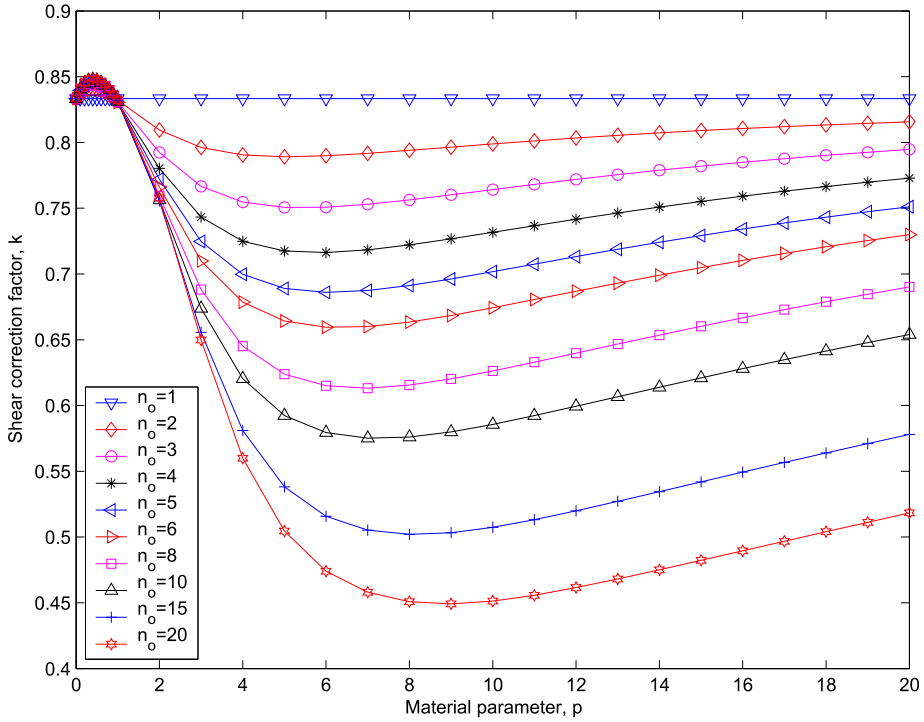

Figure 2.13: Variation of the shear correction factor according to p.

The shear correction factors are equal to 5/6 as for a homogeneous plate for p=0 or n_o=1 and approximately this usual value for p=1. They are higher than 5/6 for p <1.

Table 2.4 gives the values of shear correction factors related to every couple (p, n_o). It can be seen that, with the same material distribution of FGM (SiC-Al), the shear factor of the plate (k=0.6595) is larger than for the case of a symmetric sandwich plate (k=0.3547, see table 2.2).

The relative error is obtained by formula (2.21) where M_m is the magnitude obtained by the corrected FSDT model and M_c the value taken from FSDT model. Figure 2.14 presents the variation of the relative error on the maximal deflection in terms of the parameters (p, n_o). This difference is shown in figure 2.15 as a function of the ratio length/thickness of the plate. It can be seen in this case that the variation of the shear correction factor does not affect the deflection of the thin and medium-thick plates. This is due to the fact that the contribution of the shear deformation energy is negligible compared to the bending deformation energy. The effect of the shear correction factor is non-negligible only for the thick plate ($a/h \leq$10). However, the effect of the shear correction factor becomes more significant when the ratio of elastic moduli increases (see figure 2.15).

In order to validate the results of the model, a comparison is made with previous results of the literature and with a finite element solution. To do this, a three-dimensional finite element computation with element C3D8R is performed as explained in the previous section. An appropriate meshing comprising 8 discrete layers in the thickness direction is used.

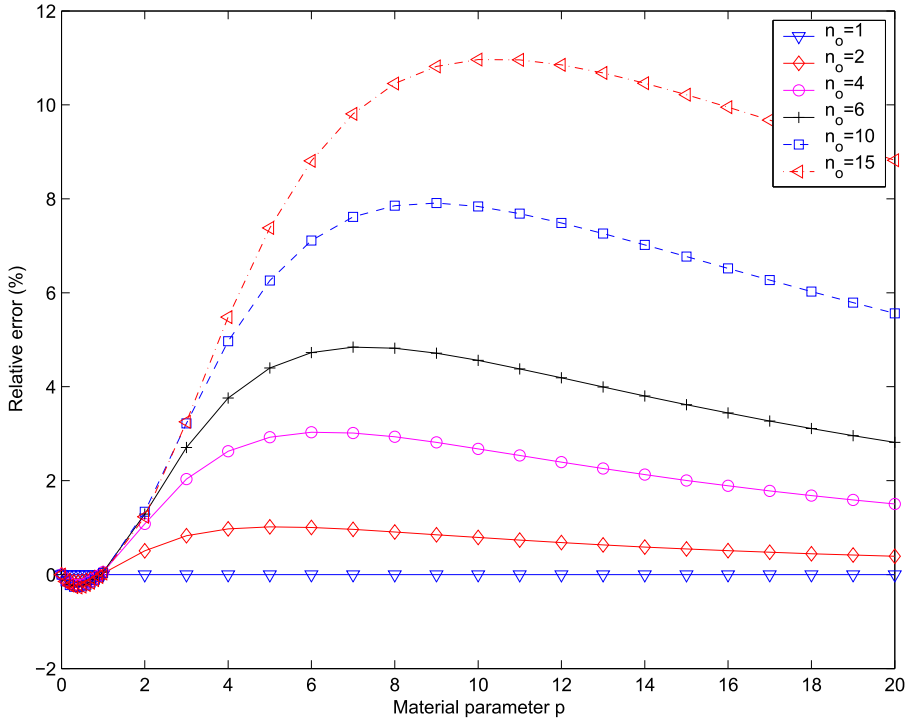

Figure 2.14: Relative error of maximal deflection, a/h=5

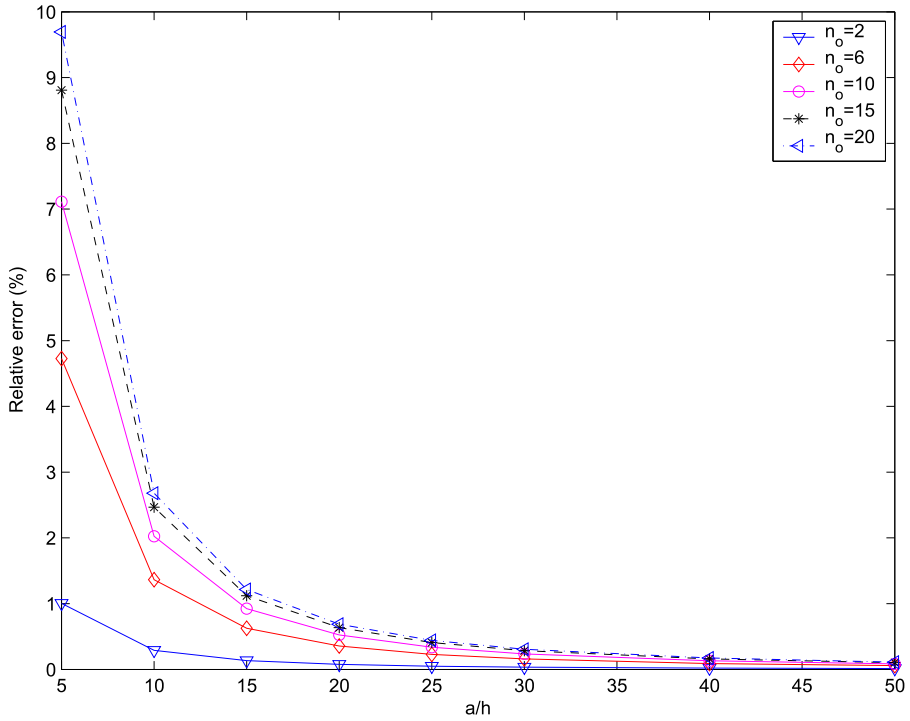

Figure 2.15: Relative error of maximal deflection, p=6

Table 2.4: Shear correction factors for the FG plate

p	E_c/E_m									
	1	2	3	4	5	6	8	10	15	20
0	5/6	5/6	5/6	5/6	5/6	5/6	5/6	5/6	5/6	5/6
0.2	5/6	0.8396	0.8418	0.8429	0.8435	0.8440	0.8445	0.8448	0.8453	0.8455
0.4	5/6	0.8411	0.8439	0.8453	0.8462	0.8467	0.8474	0.8478	0.8483	0.8486
0.6	5/6	0.8396	0.8420	0.8433	0.8441	0.8446	0.8453	0.8457	0.8461	0.8463
0.8	5/6	0.8364	0.8374	0.8381	0.8386	0.8389	0.8395	0.8399	0.8404	0.8406
1.0	5/6	0.8320	0.8309	0.8305	0.8304	0.8305	0.8308	0.8312	0.8319	0.8323
2.0	5/6	0.8095	0.7924	0.7804	0.7720	0.7662	0.7593	0.7563	0.7555	0.7580
3.0	5/6	0.7961	0.7666	0.7433	0.7247	0.7099	0.6882	0.6738	0.6556	0.6498
4.0	5/6	0.7905	0.7547	0.7248	0.6997	0.6786	0.6451	0.6203	0.5810	0.5599
5.0	5/6	0.7891	0.7506	0.7175	0.6890	0.6643	0.6238	0.5923	0.5381	0.5046
6.0	5/6	0.7899	0.7507	0.7163	0.6861	**0.6595**	0.6150	0.5794	0.5158	0.4741
7.0	5/6	0.7917	0.7530	0.7183	0.6875	0.6600	0.6132	0.5751	0.5053	0.4581
8.0	5/6	0.7940	0.7563	0.7221	0.6912	0.6634	0.6155	0.5759	0.5020	0.4508
9.0	5/6	0.7964	0.7602	0.7267	0.6962	0.6685	0.6202	0.5799	0.5032	0.4492
10.0	5/6	0.7989	0.7642	0.7316	0.7017	0.6743	0.6262	0.5856	0.5073	0.4513
15.0	5/6	0.8090	0.7820	0.7551	0.7293	0.7048	0.6602	0.6210	0.5419	0.4823
20.0	5/6	0.8157	0.7947	0.7729	0.7511	0.7300	0.6902	0.6540	0.5780	0.5183

It can be seen in figure 2.16 that the deflection obtained from the present study is identical to that of the discrete three-dimensional finite element model and to the higher-order shear deformation models (TSDT, SSDT). The difference between these results and the result received from the model using the five-sixth shear correction factor is approximately 5% for the SiC-Al FGM, 7% for WC-Al FGM and this percentage continue to increase in terms of the augmentation of n_o. Furthermore, the models taking into accounts the shear deformation are also compared to the model of Love-Kirchhoff in figure 2.16. That comparison allows us to remark that there is an important difference between the CPT model and the others. That is logical because the contribution of shear deformation energy is significant for the actual thickness of plate (a/h=5).

The variation of the plane stress σ_{xx} at the center of the FG plate along the thickness direction is depicted in figure 2.17. It can be seen that the maximum compressive stress is at the top surface and increases with p. In comparison, the maximum tensile stress is located inside the plate for p <1. This is a significant difference compared with usual homogeneous composite laminate. There is not important difference of the membrane stresses between the models, the prediction of the their distribution is thus not represented.

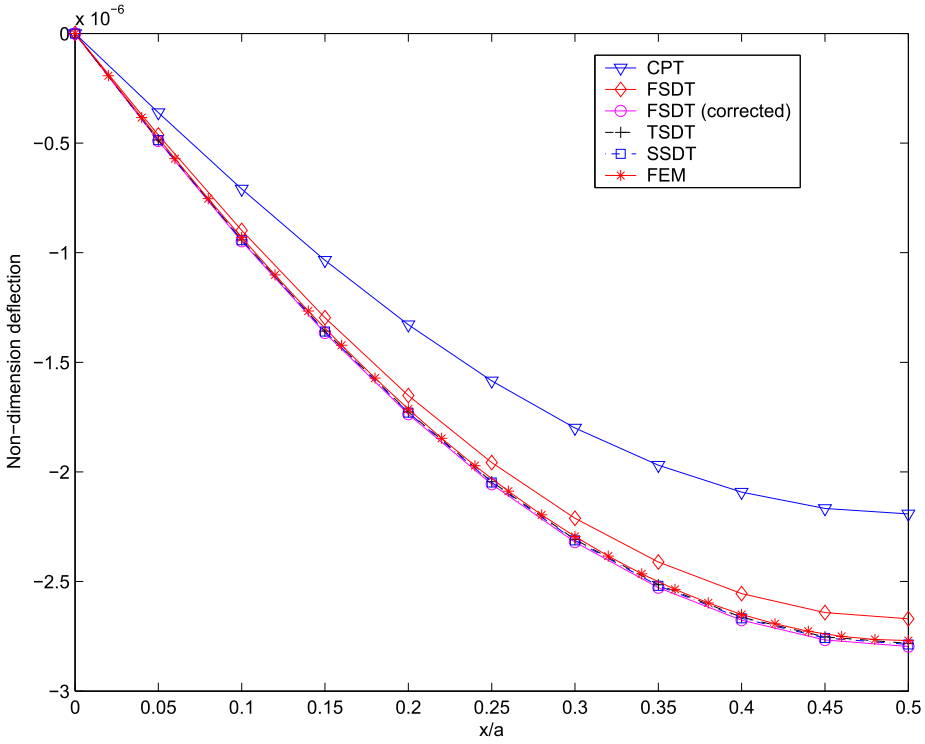

Figure 2.16: Non-dimensional deflection for various models, a/h=5, p=6, SiC-Al.

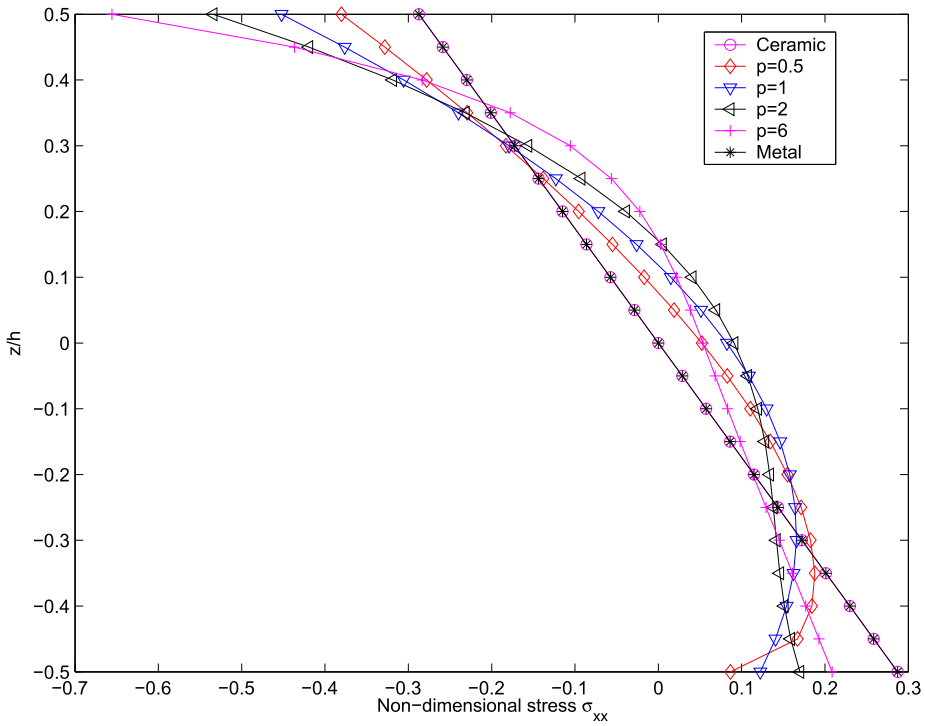

Figure 2.17: Non-dimensional stress $\overline{\sigma}_{xx}$, a/h=5, Si-Al

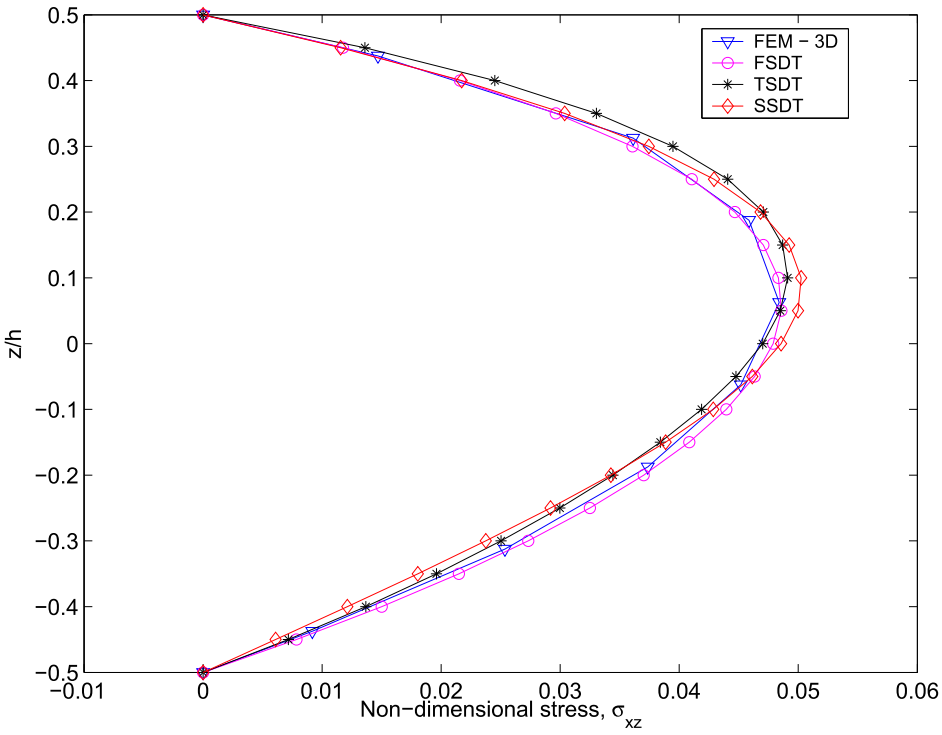

Figure 2.18: Non-dimensional stress $\overline{\sigma}_{xz}$, E_c/E_m=2, p=2, a/h=10.

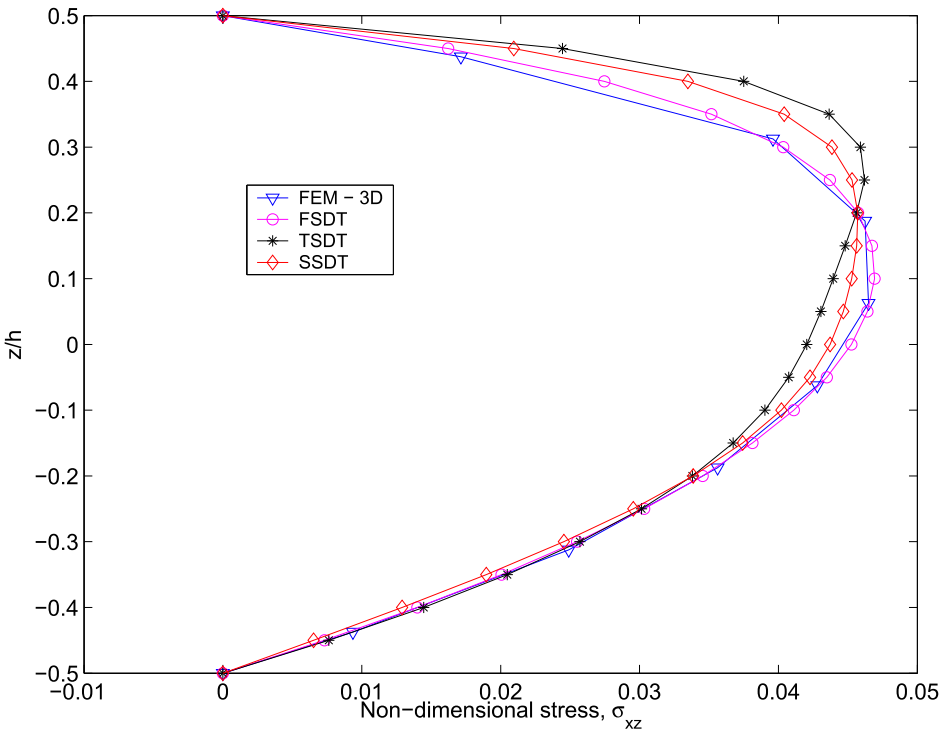

Figure 2.19: Non-dimensional stress $\overline{\sigma}_{xz}$, E_c/E_m=4, p=6, a/h=10.

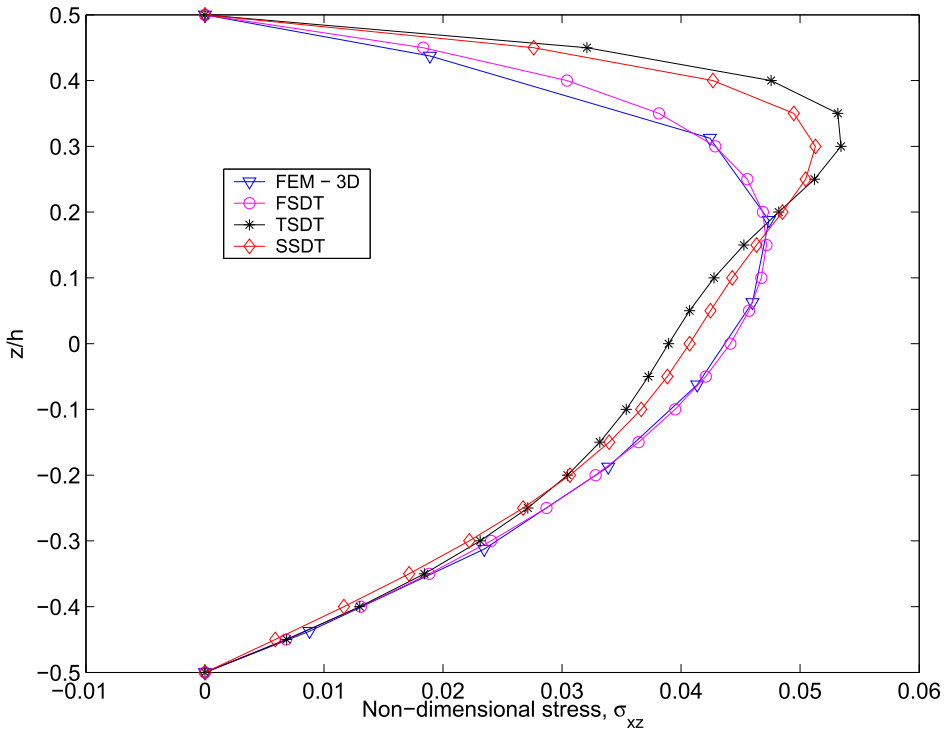

Figure 2.20: Non-dimensional stress $\overline{\sigma}_{xz}$, E_c/E_m=6, p=6, a/h=10.

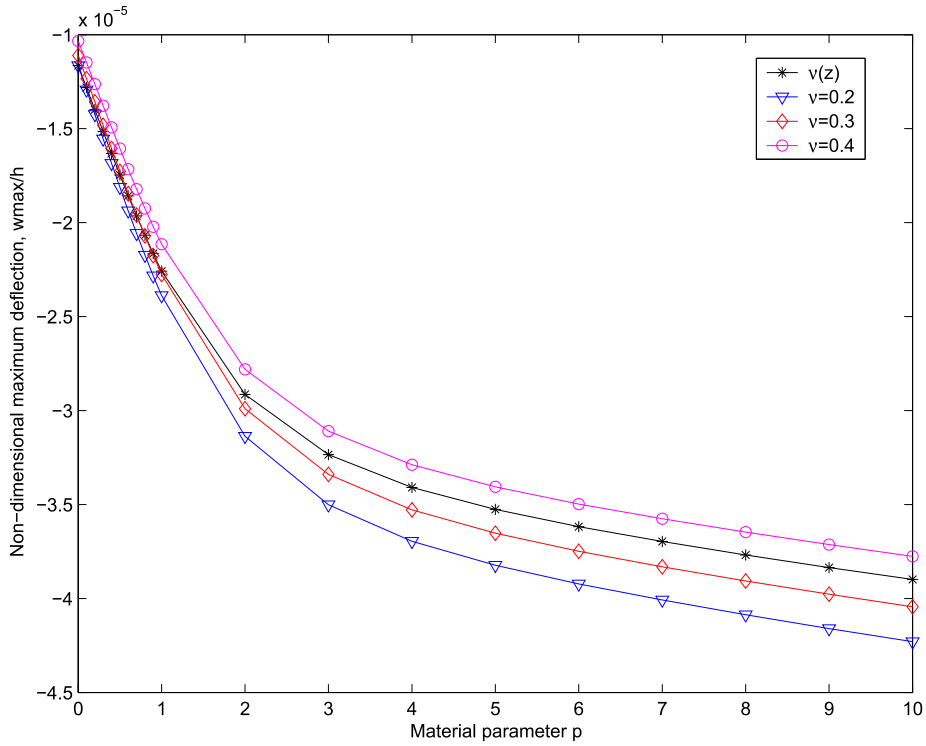

Figure 2.21: Effect of the Poisson's ratio on the maximal deflection, a/h=10, E_c/E_m=6.

The transverse shear stress defined in (2.13) near the boundary edge ($x = 99a/100, y = 49b/100$) is shown in figures 2.18, 2.19 and 2.20. It is compared to the shear stress given by higher-order models and to the results obtained from a three-dimensional finite element model. In comparison, the shear stresses of the corrected FSDT model and those of the three-dimensional element finite model are nearly the same. It can be seen that, for higher-order models, the curves are clearly different for the three models (FSDT, TSDT, SSDT) (see figures 2.19 and 2.20). The relative difference between the values of shear stresses can reach 25% (figure 2.20) at some locations within the plate for (n_o=6, p=6). Clearly, this distinction depends on the parameters n_o and p. The difference between the FSDT model and the higher-order models (TSDT, SSDT) is indeed small for the smaller values of (n_o, p) (see figure 2.18).

The results of the FG plate based on the FSDT in the previous part is based under the assumption that the Poisson's ratio is constant. To investigate the effect due to this coefficient, a continuously graded Poisson's ratio through the thickness of the plate is considered, as given by relationship (2.19) and (2.22), with ν_c=0.2 et ν_m=0.4. The maximum deflection according to the variation of the material parameter thus obtained is shown in figure 2.21. The results can be compared with those related to constant values of the Poisson's ratio and show that the deflection of the FG plate is affected by the variation of Poisson's ratio through the thickness of the plate for p>2.

2.4 Conclusion of the Chapter

The improved shear stiffnesses and shear correction coefficients for the functionally graded plate models using FSDT were presented. The closed-form solutions for the simply supported square functionally graded plate and for the cylindrically bended sandwich plate with functionally graded faces based on the first-order shear deformation (FSDT) were obtained. The obtained results show that the shear correction factor is not the same as the one of the homogeneous FSDT models, and is a function of the ratio between elastic moduli of constituents and of the distribution of materials through the models. Its effect is the most significant for the sandwich plate. For a classical, non-symmetrical FGM plate, the maximum tensile stress is located within the plate, contrarily to the case of a homogenous plate. The variation of the shear stress through the thickness of the FG plate given by the FSDT model is identical to the one given by the finite element model.

Part II

Green's Operator for a Periodic Medium with Traction-Free Boundary Conditions and Computation of the Effective Elastic Properties of Heterogeneous Plates

Chapter 3

Green's operator for a periodic medium with traction-free boundary conditions

The purpose of this chapter is to present a new theory for the computation of the effective elastic properties of periodic media with stress-free boundary conditions. The method is based on a new Green's operator ($\boldsymbol{\Gamma}$-operator), projection of the polarization stress field onto the strain field, which is necessary for resolution of the localization elastic problem on a period. To do this, the solution field of the problem is split into a classical periodic solution and a complementary solution to account for stress-free boundary conditions. Based on the Fast Fourier Transform (FFT) and an iterative procedure, this operator is used to calculate the effective elastic properties of thin heterogeneous plates made of periodic cells. Numerical applications are provided, including comparisons with closed-form solutions and finite element solutions.

The chapter is organized as follows. Before presentation of the theoretical formulation and the above mentioned numerical computations, section 1 is devoted to recall briefly the basic steps of homogenization of periodic media including the definition of the periodic unit cell, the localization elastic problem as well as the homogenization step leading to the effective properties. This section will also summarize the homogenization methods used for periodic media, including $\boldsymbol{\Gamma}$-operators and FFT-based numerical methods. Section 2 presents homogenization of periodic plates. To do so, the homogenization methods for periodic heterogeneous plates and the homogenization problem of thin periodic plates will be first recalled, and followed by the formulation of a new $\boldsymbol{\Gamma}$-operator for periodic media with traction-free boundary conditions. The application of this operator for the computation of the effective elastic properties of thin periodic plates is then introduced using a basic iterative method and the Fast Fourier Transform. Two numerical applications will be presented in section 3.

3.1 Homogenization of Periodic Media

Modelling structures with heterogeneous microstructures requires information about the mechanical properties of the constituents at the heterogeneity scale. It asks thus a great computing power due to discretization at the microscopic scale. To overcome this problem, an equivalent homogeneous medium is introduced and the problem is to find the relationship between the two media, as well as the constitutive law of the effective medium. Actually, there exist two main methods to achieve this goal: the phenomenological approach and the homogenization method.

The first approach is based on experimental identifications. This requires numerous tests to determine the constitutive laws of the effective medium. In contrast, the homogenization method is a technique of good performance which enables to evaluate the overall behavior of heterogeneous media with high heterogeneity. It takes into account the mechanical phenomena involved in the heterogeneity scales so that it has been used as a main numerical technique for construction of the equivalent homogeneous media.

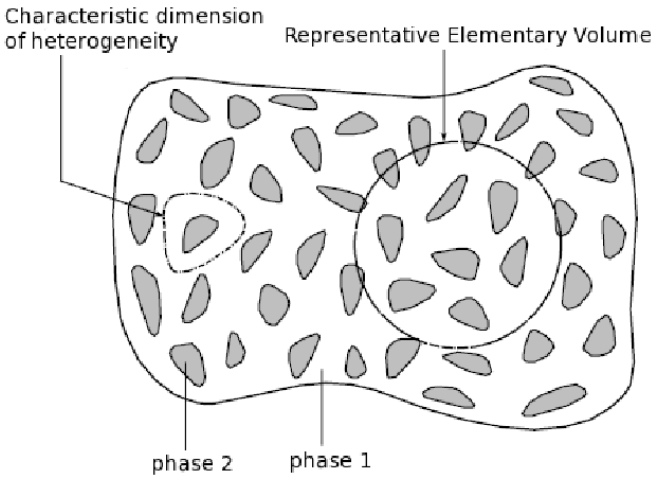

Figure 3.1: Illustration of a heterogeneous body and elementary concepts.

Generally, to determine the effective properties of the equivalent homogeneous medium, it is necessary to distinguish the three following main stages in the homogenization: The identification of the size of the Representative Volume Element (RVE), the localization problem and the homogenization. The definition of the representative volume element is indeed required, it helps to describe at the microscopic scale the type of constituent materials, their spatial distribution and mechanical behavior. The dimension of the RVE has to be large enough comparing to the heterogeneity scale. This is the representation stage that the structure is represented by a representative cell. After definition of the RVE, it is necessary then to connect the microscopic quantities to the macroscopic quantities owing to a localization problem, and it establishes finally the constitutive law of the effective media by the average operations on the representative cell. The homogenization methods differ mainly at the step of the localization and they are also associated with problems of choice of the RVE size.

In reality, there exist many structures with periodic microstructures where the computation methods can be simplified. Indeed, the effective properties of such a medium can be obtained by studying only the response of a periodic unit cell. The important question is thus to find the solution of the localization problem defined on the period of the structure. As a consequence, these local calculations enable to determine the overall properties of the medium when the dimension of the structure is much greater than that of the unit cell. The determination of the effective properties of the periodic medium has been an interesting subject concerning numerous researches and it will also be studied in this chapter.

3.1.1 Composites with Periodic Microstructure

One of the difficulties in the determination of the effective properties of heterogeneous media is due to the lack of the information on the microstructure. For periodic media, these data are perfectly specified from the geometrical and material properties of a unit cell which generates by periodic repetition the whole microstructure.

3.1.1.1 Unit Cell

A periodic medium is defined by a unit cell and three vectors (3D dimensions) of translation invariance. To describe in details this medium, we consider a linear elastic heterogeneous material medium which is periodic in the space and whose constituent materials are described by a elastic tensor $\mathbf{L}(\mathbf{x})$ at the location $\mathbf{x}$, that verifies:

$$\mathbf{L}(\mathbf{x}) = \mathbf{L}(\mathbf{x} + c_1\, l_1\, \boldsymbol{e}_1 + + c_2\, l_2\, \boldsymbol{e}_2 + + c_3\, l_3\, \boldsymbol{e}_3) \quad \forall \mathbf{x},\, \forall \mathbf{c}, \tag{3.1}$$

where $\boldsymbol{e} = (\boldsymbol{e}_1, \boldsymbol{e}_2, \boldsymbol{e}_3)$ are the basic vectors, $\mathbf{c} = (c_1, c_2, c_3)$ any integer numbers and l_i the lengths of the basic cell Y occupied by domain:

$$Y = \left]-\frac{l_1}{2}, \frac{l_1}{2}\right[\times \left]-\frac{l_2}{2}, \frac{l_2}{2}\right[\times \left]-\frac{l_3}{2}, \frac{l_3}{2}\right[, \tag{3.2}$$

with the boundary ∂Y. If we impose a field $\mathbf{L}(\mathbf{x})$ on Y, it is given on the whole space by periodic repetition of the cell with 3 vectors of translation invariance. Figure 3.2 presents a two-phase composite material consisting of spherical inclusions periodically distributed in a matrix. Figure 3.2 shows that a same periodic material can be described with different unit cells. Although this definition is not unique, the effective behavior of the periodic medium made of different unit cells generating the same microstructure should coincide since the physical effective properties of periodic media are well defined independently of the choice of the unit cell. This choice is often motivated by the differences in geometrical symmetries which can be used to simplify the numerical solutions of the localization elastic problem.

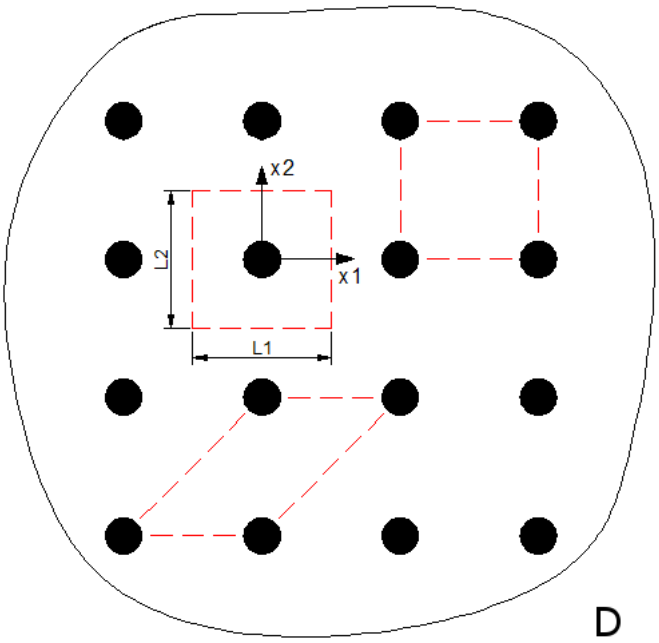

Figure 3.2: Domain D and different possible choices of the unit cell.

3.1.1.2 Periodic Strain Fields

Let us consider a domain D which contains a large number of periodic cells. Assume first that this medium has been homogenized and behaves as a homogeneous body. Then, if an affine displacement is imposed on the boundary of the domain D as:

$$\mathbf{u}(\mathbf{x}) = \mathbf{E}\,.\,\mathbf{x} \quad \forall \mathbf{x} \in \partial D, \tag{3.3}$$

the displacement and strain fields produce in D are $\mathbf{E}\,.\,\mathbf{x}$ and $\mathbf{E}$, respectively. This homogeneous strain generates a homogeneous stress $\mathbf{\Sigma}$ and the effective constitutive relations express the relations between $\mathbf{E}$ and $\mathbf{\Sigma}$. In contrast, if the heterogeneous medium is considered, the displacement field is equal to $\mathbf{E}\,.\,\mathbf{x}$ added to perturbation field $\mathbf{u}^p(\mathbf{x})$:

$$\mathbf{u}(\mathbf{x}) = \mathbf{E}.\mathbf{x} + \mathbf{u}^p(\mathbf{x}). \tag{3.4}$$

It is reasonable to assume that if the domain D is much greater than the size of the unit cell, the displacement field $\mathbf{u}^p(\mathbf{x})$ is periodic anywhere in D excepted near its boundary. Therefore, the periodic displacement field is completely known if it is specified on the unit cell. This field has to be continuous in order to be kinematically admissible such that it takes the same values at the points which are situated on the opposite faces of the unit cell Y. In other terms, the following relation has to be verified: $\mathbf{u}^p(\mathbf{x}) = \mathbf{u}^p(\mathbf{x}')$ for any point couples $(\mathbf{x}, \mathbf{x}')$ in the basic $\boldsymbol{e} = (\boldsymbol{e}_1, \boldsymbol{e}_2, \boldsymbol{e}_3)$ with:

$$\begin{cases} \mathbf{x} = (x_1, x_2, l_3/2) \quad \text{and} \quad \mathbf{x}' = (x_1, x_2, -l_3/2), \\ \mathbf{x} = (x_1, l_2/2, x_3) \quad \text{and} \quad \mathbf{x}' = (x_1, -l_2/2, x_3), \\ \mathbf{x} = (l_1/2, x_2, x_3) \quad \text{and} \quad \mathbf{x}' = (-l_1/2, x_2, x_3). \end{cases} \tag{3.5}$$

We define thus a field $\mathscr{U}_p$ that is the ensemble of displacement fields given by the following form:

$$\mathscr{U}_p = \left\{ \mathbf{u}(\mathbf{x}) \,\middle|\, \mathbf{u}(\mathbf{x}) = \mathbf{E} \,.\, \mathbf{x} + \mathbf{u}^p(\mathbf{x}),\ \mathbf{u}^p(\mathbf{x}) \text{ periodic on } \partial Y \right\}, \tag{3.6}$$

The local strain field $\boldsymbol{\epsilon}(\mathbf{u}(\mathbf{x}))$ conforms to the periodic arrangement of the cells. It can be determined on a single unit cell Y. This strain field can be split into the overall strain $\mathbf{E}$ which would be the actual strain field in the unit cell if it were homogeneous, and a correction $\mathbf{e}^p(\mathbf{u}^p(\mathbf{x}))$ (the symmetrical part $\mathbf{u}^p(\mathbf{x}) \otimes^s \boldsymbol{\nabla}$ of $\mathbf{u}^p(\mathbf{x}) \otimes \boldsymbol{\nabla}$) which accounts for the presence of heterogeneities. This correction derived from a displacement field $\mathbf{u}^p(\mathbf{x})$ is therefore a fluctuation about this mean deformation. Note that the nabla operator $\boldsymbol{\nabla}$ is used to express the gradient and divergence operators ($\mathbf{u}^p \otimes \boldsymbol{\nabla} = u^p_{i,j}\, \boldsymbol{e}_i \otimes \boldsymbol{e}_j$, $\boldsymbol{\sigma} \,.\, \boldsymbol{\nabla} = \sigma_{ij,j}\, \boldsymbol{e}_i$). The Greek indices are assumed to range within $\{1, 2\}$ while the Latin indices take values $\{1, 2, 3\}$.

The total strain field in the unit cell Y admits thus the following decomposition:

$$\boldsymbol{\epsilon}(\mathbf{u}(\mathbf{x})) = \mathbf{E} + \mathbf{e}^p(\mathbf{u}^p(\mathbf{x})), \quad \text{with} \quad \mathbf{u}^p(\mathbf{x}) \text{ periodic on } \partial Y. \tag{3.7}$$

Note that the periodicity of $\mathbf{u}^p$ implies that the average of the corresponding strain on the unit cell vanishes and that therefore the average of the total strain field $\boldsymbol{\epsilon}(\mathbf{u})$ is $\mathbf{E}$:

$$< \mathbf{e}^p(\mathbf{u}^p(\mathbf{x})) >_Y = 0, \quad < \boldsymbol{\epsilon} >_Y = \mathbf{E}, \tag{3.8}$$

where the brackets $< \,.\, >_Y$ is the average of a field on the unit cell Y:

$$< f >_Y = \frac{1}{|Y|} \int_Y f(\mathbf{x})\, d\mathbf{x}. \tag{3.9}$$

To prove (3.8), the integration by parts of the first term of (3.8) yields:

$$< \mathbf{e}^p(\mathbf{u}^p) >_Y = \frac{1}{|Y|} \int_{\partial Y} \mathbf{u}^p \otimes^s \mathbf{n}\, dS, \tag{3.10}$$

where $(\mathbf{a} \otimes^s \mathbf{b})_{ij} = \frac{1}{2}(a_i b_j + a_j b_i)$ and $\mathbf{n}$ is the normal vector. The boundary integral vanishes since $\mathbf{u}^p$ takes identical values on opposite sides of ∂Y whereas $\mathbf{n}$ takes opposite values on these opposite sides.

3.1.1.3 Periodic Stress Fields

The local stress field $\boldsymbol{\sigma}$ is also periodic and is in equilibrium throughout the entire periodic medium. Thus, the stress field satisfies an equilibrium equation inside Y and an equilibrium equation on the boundary of Y to express that the boundaries between neighbouring unit cells are equilibrated. It follows from the first condition that $\boldsymbol{\sigma}$ is a divergence-free field in Y. The second equilibrium conditions show that the tractions on opposite sides on ∂Y are opposite vectors. That can be deduced from the periodicity of $\boldsymbol{\sigma}$ and from the fact that the normal vectors $\mathbf{n}$ at opposite points of ∂Y are opposite. These equilibrium conditions of the stress field enable to define a statically admissible field $\mathscr{S}_p$ as:

$$\mathscr{S}_p = \left\{ \boldsymbol{\sigma}(\mathbf{x}) \,\middle|\, \boldsymbol{\sigma}(\mathbf{x}) \,.\, \boldsymbol{\nabla} = 0,\ \boldsymbol{\sigma}(\mathbf{x}) \,.\, \mathbf{n} \text{ anti-periodic on } \partial Y \right\}, \tag{3.11}$$

which is an ensemble of statically admissible stress fields that satisfy the equilibrium conditions in the unit cell Y and the antiperiodic conditions on opposite sides of ∂Y.

The effective stress tensor $\boldsymbol{\Sigma}$ is defined as the average of the microscopic stress tensor:

$$\boldsymbol{\Sigma} = < \boldsymbol{\sigma} >_Y \,. \tag{3.12}$$

Moreover, for $\mathbf{u} \in \mathscr{U}_p$ and $\boldsymbol{\sigma} \in \mathscr{S}_p$, the following relation is verified:

$$< \boldsymbol{\sigma}\, \boldsymbol{\epsilon}(\mathbf{u}) >_Y = < \boldsymbol{\sigma} >_Y < \boldsymbol{\epsilon}(\mathbf{u}) >_Y, \tag{3.13}$$

The above equality is known as Hill's lemma that plays a fundamental role in the computation of effective properties of heterogeneous materials. The Hill's theorem presents the fact that the average of the microscopic strain energy is precisely the macroscopic strain energy. To prove (3.13), it is sufficient to prove $< \boldsymbol{\sigma}\, \mathbf{e}^p(\mathbf{u}^p(\mathbf{x})) >_Y = 0$ for every periodic displacement field $\mathbf{u}^p$. This condition is indeed satisfied by using Green's theorem:

$$< \boldsymbol{\sigma}\, \mathbf{e}^p(\mathbf{u}^p(\mathbf{x})) >_Y = \frac{1}{|Y|} \int_{\partial Y} (\boldsymbol{\sigma} \,.\, \mathbf{n}) \,.\, \mathbf{u}^p \, dS = 0. \tag{3.14}$$

This boundary integral vanishes since the stresses take opposite values on opposite sides of ∂Y whereas the displacements take identical values on opposite sides of ∂Y.

3.1.2 Localization Problem

Section 3.1.1 presented the unit cell and the periodicity properties of the displacement, strain and stress fields of composites with periodic microstructure. This section introduces an elastic problem described on the unit cell whose resulting solution field will enable to calculate the effective properties of composite materials. To do so, let us consider a linear elastic periodic medium with stiffness $\mathbf{L}(\mathbf{x})$. This additional information is sufficient to determine the local stress

and strain fields induced at the microscopic scale with an overall strain $\mathbf{E}$ or an overall stress $\mathbf{\Sigma}$ by solving the localization problem which consists of the constitutive law of each constituent, the equilibrium equations and periodicity boundary conditions:

$$\begin{cases} \boldsymbol{\sigma}(\mathbf{x}) \,.\, \boldsymbol{\nabla} = 0,\ \boldsymbol{\sigma}(\mathbf{x}) = \mathbf{L}(\mathbf{x})\, \boldsymbol{\epsilon}(\mathbf{u}(\mathbf{x})),\ \boldsymbol{\epsilon}(\mathbf{u}(\mathbf{x})) = \mathbf{E} + \mathbf{e}^p(\mathbf{u}^p(\mathbf{x})), \\ \\ \mathbf{e}^p(\mathbf{u}^p(\mathbf{x})) = \mathbf{u}^p(\mathbf{x}) \otimes^s \boldsymbol{\nabla}, \\ \\ \mathbf{u}^p(\mathbf{x}) \text{ periodic on } \partial Y, \quad \boldsymbol{\sigma}(\mathbf{x}) \,.\, \mathbf{n} \text{ anti-periodic on } \partial Y, \end{cases} \tag{3.15}$$

Under the usual assumptions of symmetry, boundedness on the elasticity tensor $\mathbf{L}(\mathbf{x})$, the problem (3.15) admits a unique solution field $(\mathbf{u}^p, \boldsymbol{\epsilon}, \boldsymbol{\sigma})$. Once the local problem (3.15) is solved, a relationship between the microscopic quantities and the macroscopic quantities as well as the macroscopic behavior law are then required. The overall stress $\mathbf{\Sigma}$ is computed by means of Eq. (3.12) and the effective stiffness $\mathbf{A}^p$ of the composite is determined through the relation:

$$\mathbf{A}^p\, \mathbf{E} = \mathbf{\Sigma} = < \boldsymbol{\sigma} >_Y = < \mathbf{L}(\mathbf{x})\, \boldsymbol{\epsilon}(\mathbf{u}) >_Y, \tag{3.16}$$

where $\boldsymbol{\epsilon}(\mathbf{u}) = \mathbf{E} + \mathbf{e}^p(\mathbf{u}^p(\mathbf{x}))$. The overall strain $\mathbf{E}$ is the generalized loading in (3.15). It can be considered as an eigenstrain (similar to a thermal strain). The effective stiffness $\mathbf{A}^p$ can thus be computed from the average of the local stress field on the unit cell. These effective properties can also be derived from consideration of the elastic deformation energy:

$$\mathbf{E}\, \mathbf{A}^p\, \mathbf{E} = W(\mathbf{E}) = \mathrm{Min}_{\mathbf{u} \in \mathscr{U}_p} < \boldsymbol{\epsilon}(\mathbf{u})\, \mathbf{L}(\mathbf{x})\, \boldsymbol{\epsilon}(\mathbf{u}) >_Y \quad \forall \mathbf{E}. \tag{3.17}$$

This property expresses the fact that the effective strain energy is the minimum of the average potential energy among all the displacement fields $\mathbf{u} \in \mathscr{U}_p$, and that the stationary condition of the functional leads to the macroscopic constitutive relation (3.16). Moreover, a variational formulation based on the complementary energy with a statically admissible stress field $\boldsymbol{\sigma} \in \mathscr{S}_p$ also enables to calculate the effective stiffness $\mathbf{A}^p$:

$$\mathbf{E}\, \mathbf{A}^p\, \mathbf{E} = W(\mathbf{E}) = \mathrm{Max}_{\boldsymbol{\sigma} \in \mathscr{S}_p} [2\mathbf{E} \, < \boldsymbol{\sigma} >_Y - < \boldsymbol{\sigma}\, \mathbf{S}(\mathbf{x})\, \boldsymbol{\sigma} >_Y], \tag{3.18}$$

where $\mathbf{S}(\mathbf{x})$ is the compliance tensor at the location $\mathbf{x}$, $\mathbf{S}(\mathbf{x}) = (\mathbf{L}(\mathbf{x}))^{-1}$.

Several problems are practically requiring that the overall stress field $\mathbf{\Sigma}$ is prescribed in place of the overall strain field $\mathbf{E}$. The use of the stress approach for estimating the effective flexibility tensor $\mathbf{S}^{per}$ therefore yields:

$$\mathbf{\Sigma}\, \mathbf{S}^p\, \mathbf{\Sigma} = \mathrm{Max}_{\mathbf{u} \in \mathscr{U}_p} \left[2\mathbf{\Sigma} \, < \boldsymbol{\epsilon}(\mathbf{u}) >_Y - < \boldsymbol{\epsilon}(\mathbf{u})\, \mathbf{L}(\mathbf{x})\, \boldsymbol{\epsilon}(\mathbf{u}) >_Y \right], \tag{3.19}$$

$$\boldsymbol{\Sigma}\,\mathbf{S}^{p}\,\boldsymbol{\Sigma} = \mathrm{Min}_{\boldsymbol{\sigma}\in\mathscr{S}_p,\,<\boldsymbol{\sigma}>_Y=\boldsymbol{\Sigma}} < \boldsymbol{\sigma}\,\mathbf{S}(\mathbf{x})\,\boldsymbol{\sigma} >_Y \,. \tag{3.20}$$

The variational expressions (3.17), (3.18), (3.19) and (3.20) will thus supply upper and lower bounds for the effective elastic properties of the periodic medium in which the quality of the bounds depends on the hypothesis imposed on the kinematically admissible displacement field and the statically admissible stress field. Moreover, note that the variational characterization based on the displacement field is often more appropriate for numerical purposes, since it can be used with a displacement-based finite element method code.

3.1.3 Resolution Methods of the Localization Problem

As explained previously, a rigorous procedure can be described to obtain the effective properties of periodic media if a localization problem is solved on a period.

Finite Element Method (FEM) has been used for the analysis of periodic materials. Most of the analyses are limited to simple microstructures. Recently, several authors studied more complex microstructures with inclusions of varying numbers and shapes (see Brockenbrough et al. (1991), Böhm et al. (1993), Gusev (1997), Michel et al. (1999), Moës et al. (2003), Sab and Nedjar (2005)). The method needs however finite element meshings which are obviously tedious to implement, especially as soon as 3D computations are in view.

Several authors (Iwakuma and Nemat-Nasser, 1983; Luciano and Barbero, 1994; Cohen and Bergman, 2003) applied the method of Fourier series for calculating the effective properties of composites with a periodic microstructure. Kaßbohm et al. (2005, 2006) proposed an approximate method of Fourier coefficients for computing the properties of periodic structures with an arbitrary stiffness distribution. By using the Fast Fourier Transform (FFT), Suquet (1990), Moulinec and Suquet (1994, 1998), and Michel et al. (1999) proposed an iterative numerical method to investigate the effective properties of linear and non-linear composites. The method was afterwards extended by Eyre and Milton (1999), and by Michel et al. (2001), Moulinec and Suquet (2003). This method makes direct use of digital images of the microstructure of the composites. It is based on the exact expression of the $\boldsymbol{\Gamma}$-operator for a linear isotropic elastic homogeneous material and periodic boundary conditions. A part of the efficiency of this method is due to the use of FFT packages, which allows to reduce the calculation times and to analyze the plane (2D) or volumic (3D) periodic complex microstructures without FEM meshing. Using discrete Fourier transforms, Neumann et al. (2001, 2002) presented also a method for the analysis of heterogeneous bodies. Bonnet (2007) proposed an explicit series solution for the calculation of the effective properties of composites having periodically positioned heterogeneities by using Neuman series and exact expressions of the shape factors in Fourier space. Recent studies using the Fourier method and FFT algorithms showed their efficiency when used for obtaining the effective properties of periodic media.

3.1.4 Γ-Operators and FFT-based Numerical Method

3.1.4.1 Γ-Operators and Effective Properties

Theoretical and numerical methods which aim at obtaining the effective elastic properties of multiphase composite materials have been the subject of numerous studies. If one considers the case of periodic media, it is possible to show that the effective properties of heterogeneous materials can be obtained if the solution of an elasticity problem (localization problem) on the volume of a period subjected to periodicity boundary conditions and to "body forces" is solved. These body forces are computed from the heterogeneous elastic properties and from given macroscopic strains (see Sanchez-Palencia (1974), Bakhvalov (1974), A. Bensoussan and Papanicolaou (1978), Auriault and Bonnet (1985), Bakhvalov and Panasenko (1989), and further references therein).

Similarly, if a representative volume element (RVE) is considered, the effective properties can be obtained if the solution of an elasticity problem on the RVE subjected to homogeneous boundary conditions (displacement null on the boundary for example) and to body forces is solved (see e.g. Kröner (1971); Milton (2002)).

In both cases, it is possible to replace the problem on a volume containing heterogeneities by a sequence of problems characterized by body forces applied to a "homogeneous reference medium" and by homogeneous (or periodic) boundary conditions similar to those previously defined.

From another point of view, it is well known that the displacement which is solution of an elasticity problem characterized by homogeneous (or periodic) boundary conditions and by body forces can be expressed by using a Green's function. From the Green's function, an operator can be derived, allowing the computation of the strain field induced by a polarization tensor, the so-called $\boldsymbol{\Gamma}$-operator (see e.g. Milton (2002)) from the notation of the first authors using this operator (see e.g. Kröner (1971); Willis (1977)), which is also named Green's operator by (Suquet, 1990; Moulinec and Suquet, 1994, 1998). In the following, the name $\boldsymbol{\Gamma}$-operator will be used. There is a close relation between the search of effective properties and the use of $\boldsymbol{\Gamma}$-operators.

Up to now such a strategy was restricted to the use of known $\boldsymbol{\Gamma}$-operators: $\boldsymbol{\Gamma}$-operator for an infinite domain and $\boldsymbol{\Gamma}$-operator for periodic boundary conditions in the case of solutions related to a periodic cell. The main reason of such a situation is that $\boldsymbol{\Gamma}$-operators for specific boundary conditions are known only for some special situations: infinite and semi-infinite domains, periodicity conditions, mixed boundary conditions ... (see e.g. Seremet (1991); Mura (1991)).
In the first step, the two following subsections will summarize known operators and can be considered as a review of known results: for an infinite medium (Kröner, 1971; Willis, 1977, 1980, 1981) and for a periodic medium (Suquet, 1990; Moulinec and Suquet, 1994, 1998), and will be followed by a FFT-based numerical method proposed by Suquet (1990); Moulinec and Suquet (1998); Michel et al. (1999).

3.1.4.1.a Γ-Operator for an Infinite Medium

Let us consider a homogeneous infinite elastic medium characterized by the stiffness $\mathbf{L}^o$ and subjected to a pre-stress field $\boldsymbol{\tau}(\mathbf{x})$.

The equilibrium equation can be written as:

$$\boldsymbol{\sigma}(\mathbf{x}) \,.\, \boldsymbol{\nabla} = 0, \tag{3.21}$$

where the stress field may be split into an elastic part and a pre-stress part $\boldsymbol{\tau}(\mathbf{x})$ as:

$$\boldsymbol{\sigma}(\mathbf{x}) = \mathbf{L}^o\, \mathbf{e}(\mathbf{x}) + \boldsymbol{\tau}(\mathbf{x}), \tag{3.22}$$

where the strain field $\mathbf{e}(\mathbf{x})$ is linearly related to the displacement field $\mathbf{u}(\mathbf{x})$ by

$$\mathbf{e}(\mathbf{x}) = \mathbf{u}(\mathbf{x}) \otimes^s \boldsymbol{\nabla}, \tag{3.23}$$

where $\mathbf{u}(\mathbf{x})$ is the displacement field, $\mathbf{e}(\mathbf{x})$ the corresponding strain field (the symmetrical part $\mathbf{u}(\mathbf{x}) \otimes^s \boldsymbol{\nabla}$ of $\mathbf{u}(\mathbf{x}) \otimes \boldsymbol{\nabla}$), $\boldsymbol{\sigma}(\mathbf{x})$ the total stress field.

$\mathbf{L}^o$ is a uniform elasticity tensor given, in the case of an isotropic medium, by:

$$\mathbf{L}^o\, \mathbf{e}(\mathbf{x}) = \lambda\, tr(\mathbf{e}(\mathbf{x}))\, \mathbf{1} + 2\mu\, \mathbf{e}(\mathbf{x}).$$

The prestressed field or "polarization field" $\boldsymbol{\tau}(\mathbf{x})$, may come from an eigenstrain due to thermal expansion, plasticity or other physical phenomena (see e.g. Mura (1991); Bornert et al. (2001)). It is defined within all 3D space and vanishes at infinity so that the integral (3.25) below converges.

Substituting (3.22) into (3.21) leads to:

$$(\mathbf{L}^o\, \mathbf{e}(\mathbf{x})) \,.\, \boldsymbol{\nabla} + \boldsymbol{\tau}(\mathbf{x}) \,.\, \boldsymbol{\nabla} = 0. \tag{3.24}$$

For a given polarization stress field $\boldsymbol{\tau}(\mathbf{x})$, the solution of equation (3.24) can be expressed by using a non-local $\boldsymbol{\Gamma}$-operator of the linear homogeneous medium $\mathbf{L}^o$ as:

$$\mathbf{e}(\mathbf{x}) = -\int \boldsymbol{\Gamma}(\mathbf{x} - \mathbf{x}')\, \boldsymbol{\tau}(\mathbf{x}')\, d\mathbf{x}', \tag{3.25}$$

where the $\boldsymbol{\Gamma}$-operator is related to the Green's function of the infinite homogeneous body $\mathbf{G}$ (Kelvin's tensor for an isotropic medium for example) by:

$$\Gamma_{ijkl}(\mathbf{x} - \mathbf{x}') = -\mathbf{G}_{jk,il}(\mathbf{x} - \mathbf{x}'), \tag{3.26}$$

and it is noted that the fourth-order tensor possesses the symmetry on the indices (ij), (kl).

The Green's function of the infinite homogeneous $\mathbf{G}(\mathbf{x})$ is itself the solution of the following differential equation:

$$L^o_{ijkl}\, G_{mk,lj}(\mathbf{x}) + \delta_{mi}\, \delta(\mathbf{x}) = 0. \tag{3.27}$$

It is well known that the Green's function $\mathbf{G}(\mathbf{x})$ is characterized by a $1/r$ singularity for 3D and a logarithmic singularity $ln(r)$ for the 2D case, where $r = |\mathbf{x}-\mathbf{x}'|$. The $\mathbf{\Gamma}$-operator is therefore strongly singular. The convolution product in (3.25) is very difficult to estimate in the real space and it is therefore in many cases more suitable to use the Fourier transforms of $\mathbf{G}$ and $\mathbf{\Gamma}$.

The $\mathbf{\Gamma}$-operator and the corresponding strain defined in (3.26) and (3.25) will be therefore obtained by using Fourier transforms. The Fourier transform of $f(\mathbf{x})$ and its inverse are defined as:

$$\hat{f}(\mathbf{k}) = \int f(\mathbf{x})\, e^{-i\mathbf{k}.\mathbf{x}} d\mathbf{x}, \quad f(\mathbf{x}) = \frac{1}{8\pi^3} \int \hat{f}(\mathbf{k})\, e^{i\mathbf{k}.\mathbf{x}} d\mathbf{k}, \tag{3.28}$$

where all the integrals are taken on $\mathbf{R}^3$, the index i denotes the complex number ($i = \sqrt{-1}$), $\mathbf{k} = (k_1, k_2, k_3)$ is the wave-vector, $\mathbf{k}.\mathbf{x}$ is a scalar product. The 3-dimensional Fourier transforms of (3.26) and (3.27) lead to:

$$\hat{\Gamma}_{ijkl}(\mathbf{k}) = k_i k_l \hat{G}_{jk}(\mathbf{k}) \quad \text{and} \quad -L^o_{ijkl}\, \hat{G}_{mk}(\mathbf{k}) k_l k_j + \delta_{mi} = 0. \tag{3.29}$$

By setting $K^o_{ik}(\mathbf{k}) = L^o_{ijkl} k_l k_j$ which are components of the acoustic tensor of the homogeneous material and $N^o(\mathbf{k})$ denoting the inverse of $K^o(\mathbf{k})$, the operator $\mathbf{\Gamma}$ can be expressed in the Fourier domain as:

$$\hat{\Gamma}_{ijkl}(\mathbf{k}) = \frac{1}{4}\Big(N^o_{ik}(\mathbf{k}) k_j k_l + N^o_{il}(\mathbf{k}) k_j k_k + N^o_{jk}(\mathbf{k}) k_i k_l + N^o_{jl}(\mathbf{k}) k_i k_k\Big). \tag{3.30}$$

The Fourier components of the $\mathbf{\Gamma}$-operator are explicitly given for different types of anisotropy of the homogeneous medium (see e.g. Willis (1977, 1980, 1981); Mura (1991)). For an isotropic material with Lamé coefficients (λ, μ), it takes the form:

$$\hat{\Gamma}_{ijkl} = \frac{1}{4\mu|\mathbf{k}|^2}(\delta_{ik} k_j k_l + \delta_{jk} k_i k_l + \delta_{il} k_j k_k + \delta_{jl} k_i k_k) - \frac{\lambda+\mu}{\mu(\lambda+2\mu)} \frac{k_i k_j k_k k_l}{|\mathbf{k}|^4}. \tag{3.31}$$

3.1.4.1.b Case of Periodic Boundary Conditions

Let us now consider a periodic medium characterized by a basic cell Y. Any periodic function $f(\mathbf{x})$ can be expanded into the Fourier series:

$$f(\mathbf{x}) = \sum_{\mathbf{k}} \hat{f}(\mathbf{k})\, e^{i\mathbf{k}.\mathbf{x}}, \quad \hat{f}(\mathbf{k}) = \frac{1}{|Y|} \int_Y f(\mathbf{x})\, e^{-i\mathbf{k}.\mathbf{x}} d\mathbf{x}, \tag{3.32}$$

where the tips of discrete wave-vectors $\mathbf{k}$ are points of the reciprocal lattice.

If one considers now a periodic polarization tensor $\boldsymbol{\tau}$, it is possible to define the periodic $\boldsymbol{\Gamma}$-operator and the corresponding strains along the same lines as that used for the infinite medium. After transformation into the Fourier space of the equations (3.21, 3.22, 3.23) and elimination of $\hat{\sigma}_{ij}$ between the equations, the expression of operator $\boldsymbol{\Gamma}$ has finally the same form as (3.30). The periodic strain field of the problem can then be obtained in the real space $\mathbf{e}^p(\mathbf{x})$ and the Fourier space $\hat{\mathbf{e}}^p(\mathbf{k})$ by means of the periodic $\boldsymbol{\Gamma}$-operator associated with the homogeneous elastic medium with stiffness $\mathbf{L}^o$ (see Suquet (1990); Moulinec and Suquet (1994, 1998)),

$$\begin{aligned} &\text{In real space}: \qquad \mathbf{e}^p(\mathbf{x}) = -\boldsymbol{\Gamma} * \boldsymbol{\tau}(\mathbf{x}). \\ &\text{In Fourier space}: \quad \hat{\mathbf{e}}^p(\mathbf{k}) = -\hat{\boldsymbol{\Gamma}}(\mathbf{k})\,\hat{\boldsymbol{\tau}}(\mathbf{k}) \quad \forall \mathbf{k} \neq 0,\ \hat{\mathbf{e}}^p(0) = 0. \end{aligned} \tag{3.33}$$

In this case the strain field given by (3.33) complies obviously to boundary conditions along the periodic boundaries of Y.

3.1.4.2 FFT-based Method for Periodic Media

To solve the localization problem (3.15) with periodic boundary conditions, Suquet (1990); Moulinec and Suquet (1998); Michel et al. (1999) have recently proposed a numerical method based on Fast Fourier Transform (FFT). This method will be briefly recalled in this section. In fact, the local elastic problem (3.15) can be solved by introducing a homogeneous reference medium with elastic stiffness $\mathbf{L}^o$. A new problem created in the reference medium with the same boundary conditions is characterized by Eq. (3.21), Eq. (3.22), and Eq. (3.23) where the polarization field $\boldsymbol{\tau}(\mathbf{x})$ is given by:

$$\boldsymbol{\tau}(\mathbf{x}) = (\mathbf{L}(\mathbf{x}) - \mathbf{L}^o)\ (\mathbf{E} + \mathbf{e}^p(\mathbf{x})) + \mathbf{L}^o\,\mathbf{E} \tag{3.34}$$

The problem (3.21), (3.22), (3.23) and (3.34) with periodic boundary conditions has the same structure as the basic problem (3.15) in which the periodic strain field $\mathbf{e}^p(\mathbf{x})$ was given in (3.33). The total strain field is therefore obtained by:

$$\begin{aligned} &\boldsymbol{\epsilon}(\mathbf{x}) = -\boldsymbol{\Gamma} * \boldsymbol{\tau}(\mathbf{x}) + \mathbf{E}, \\ &\hat{\boldsymbol{\epsilon}}(\mathbf{k}) = -\hat{\boldsymbol{\Gamma}}(\mathbf{k})\,\hat{\boldsymbol{\tau}}(\mathbf{k}) \quad \forall \mathbf{k} \neq 0,\ \hat{\boldsymbol{\epsilon}}(0) = \mathbf{E}. \end{aligned} \tag{3.35}$$

3.1.4.2.a Iterative Algorithm

It can be seen that the polarization stress tensor is a function of the strain field. The solutions field of the problem is therefore solved by using an iterative procedure. At each iteration, the polarization field is calculated by (3.34). Note that the constant term $\mathbf{L}^o\,\mathbf{E}$ in (3.34) can be neglected, since it does not influent the convergence of solutions field. The basic iterative algorithm proposed by Moulinec and Suquet (1994, 1998) is:

$$
\begin{aligned}
&\text{Initialization:}\\
&\quad \boldsymbol{\epsilon}^0(\mathbf{x}) = \mathbf{E}, \quad \boldsymbol{\sigma}^0(\mathbf{x}) = \mathbf{L}(\mathbf{x})\,\boldsymbol{\epsilon}^0(\mathbf{x}),\\
&\text{Iterate i+1 :} \quad \boldsymbol{\epsilon}^i(\mathbf{x}) \quad \text{and} \quad \boldsymbol{\sigma}^i(\mathbf{x}) \quad \text{being known}\\
&\quad \text{a)} \quad \boldsymbol{\tau}^i(\mathbf{x}) = \boldsymbol{\sigma}^i(\mathbf{x}) - \mathbf{L}^o\,\boldsymbol{\epsilon}^i(\mathbf{x}),\\
&\quad \text{b)} \quad \hat{\boldsymbol{\tau}}^i(\mathbf{k}) = \mathscr{F}\left[\boldsymbol{\tau}^i(\mathbf{x})\right],\\
&\quad \text{c)} \quad \text{Convergence test,}\\
&\quad \text{d)} \quad \hat{\boldsymbol{\epsilon}}^{i+1}(\mathbf{k}) = -\hat{\boldsymbol{\Gamma}}(\mathbf{k})\,\hat{\boldsymbol{\tau}}^i(\mathbf{k}) \quad \forall \mathbf{k} \neq \mathbf{0}, \quad \hat{\boldsymbol{\epsilon}}^{i+1}(\mathbf{0}) = \mathbf{E},\\
&\quad \text{e)} \quad \boldsymbol{\epsilon}^{i+1}(\mathbf{x}) = \mathscr{F}^{-1}\left[\hat{\boldsymbol{\epsilon}}^{i+1}(\mathbf{k})\right],\\
&\quad \text{e)} \quad \boldsymbol{\sigma}^{i+1}(\mathbf{x}) = \mathbf{L}(\mathbf{x})\,\boldsymbol{\epsilon}^{i+1}(\mathbf{x}),
\end{aligned}
\tag{3.36}
$$

where $\mathscr{F}$ and $\mathscr{F}^{-1}$ denote the Fourier transform and its inverse. For the convergence test, Moulinec and Suquet (1998) proposed a convergence criterion which ensures that all local equations are accurately satisfied, more specifically the convergence is reached when $\boldsymbol{\sigma}^{i+1}$ is in equilibrium. The error serving to check convergence is:

$$
\text{error}^i = \frac{\left(< ||\boldsymbol{\sigma}^i \,.\, \boldsymbol{\nabla}||^2 >\right)^{1/2}}{|| < \boldsymbol{\sigma}^i > ||} = \frac{\left(< ||\mathbf{k} \,.\, \hat{\boldsymbol{\sigma}}^i(\mathbf{k})||^2 >\right)^{1/2}}{|| < \hat{\boldsymbol{\sigma}}^i(\mathbf{0}) > ||} \tag{3.37}
$$

The iterative procedure is stopped when the error is smaller than a prescribed value. The studies of the convergence of the iterative procedure using Fourier series solution can be found in Moulinec and Suquet (1994, 1998); Michel et al. (1999); Eyre and Milton (1999); Michel et al. (2001); Bonnet (2007).

3.1.4.2.b Digital Image

Based on the above iterative algorithm, it can be seen that the calculation of the effective elastic properties of heterogeneous composite requires a precise knowledge of the mechanical properties of the materials at any points of the unit cell. In practice, these material elastic properties can be determined if the geometry information of the microstructure is completely known. It is possible for a simple geometry form. Practically however, this approach will cost too much or not succeed for complex microstructures. To overcome this problem, the digital image method has been shown as an efficient technique. It allows to calculate the material elastic properties of a heterogeneous medium at any point of the space without difficulty. The original idea of the method used in the analysis of heterogeneous materials was proposed by Moulinec and Suquet (1994) for which a real microstructure is produced by a digital image obtained from a Scanner Electron Microscopy (SEM). In the same idea, the use of the digital image for the numerical

computations has also been studied by Garboczi and Day (1995). In recent years, this technique is widely used due to its conveniences.

The digital image is made of points or pixels arranged in rows and columns. The quality of images depends on the image resolution defined as the number of points used to compose the image. The use of digital image, as well as a technique of image processing (if necessary) have shown an effectiveness for composite materials and it has been widely applied in recent years (Moulinec and Suquet, 1994, 1998). Due to the fact that a digital image contains the points (pixels-2D, 3D-volxels) distributed uniformly, the mechanical properties of the material will be assigned at each point from a given image. For complicated microstructures with different colors characterizing the different constituents, a technique of image treatment must be taken to distinguish them and then apply the mechanical properties to each component.

3.2 Homogenization of Periodic Plates

The above section presented the homogenization of periodic media where the solving methods of the localization problem subject to periodic boundary conditions, including the FFT-based method, have been introduced. Practically however, many structures have periodic microstructures but they are simultaneously subjected to other constraints on their boundaries. For example, a given boundary condition due to the defect generated periodically in material media or a stress-free boundary condition in beam and plate problems. Such conditions have to be taken into account in the localization elastic problems, which will thus be a main discussion subject in the following paragraphs.

This section is devoted to present a resolution method of the local boundary value problem for periodic media with traction-free boundary conditions, and from which a new corresponding $\mathbf{\Gamma}$-operator is formulated. This operator will be used to calculate the effective elastic properties of periodic thin plates. To do so, it is first necessary to recall several homogenization methods for periodic heterogeneous plates as well as thin periodic plates homogenization.

3.2.1 Homogenization Methods for Periodic Plates

The homogenization of elastic periodic plates has been widely studied by many authors (Duvaut and Metellus, 1976; Caillerie, 1984; Kohn and Vogelius, 1984; Lewiński and Telega, 1999; Cecchi and Sab, 2002a,b, 2004). In fact, this problem is related to the coexistence of two characteristic length scales: L, the typical size of the plate and t, thickness of the plate. Moreover the in-plane periodicity of the structure introduces an additional characteristic length ϵ which describes the in-plane size of the unit cell that generates the plate by periodicity. For a fixed value of L, the homogenization problem consists in finding the asymptotic solution when t and ϵ tend to zero. As shown in Caillerie (1984) and Kohn and Vogelius (1984), the homogenization scheme depends on the rates of convergence of t and ϵ towards zero. It is generally assumed that ϵ is a function of t which behaves likes t^a with $a > 0$, near zero. Indeed, in the process of homogenization, the order

of passage to the limit of these two parameters does not commute. It leads to different overall results for constitutive equations of the equivalent homogeneous plate. Three following cases have been considered: $a < 1$, $a = 1$ and $a > 1$ (a detailed review on the asymptotic homogenization theory of periodic heterogeneous plates can be found in Bourgeois (1997); Lewiński and Telega (1999); Dallot (2007)).

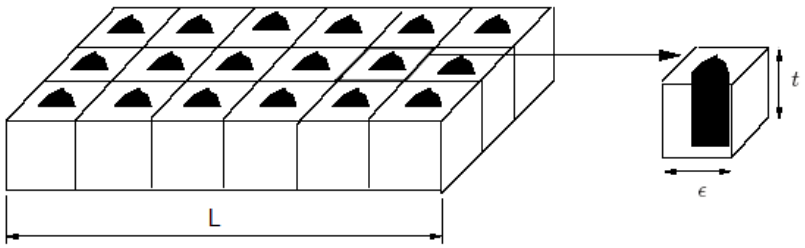

Figure 3.3: Heterogeneous 3D structure and its unit cell.

- In the first case ($a < 1$), the thickness of the plate is very much smaller than the size of the period. In this case, we make firstly the thickness tend zero, then the period of the heterogeneity. During the first stage, the 3D heterogeneous structure becomes a heterogeneous periodic plate and then the second passage to the limit leads to solving two-dimensional cellular localization problems, the elasticity operator being the fourth elasticity operator for the plate (Kohn and Vogelius (1984); Caillerie (1984) generalizing the early work of Duvaut and Metellus (1976) on the homogenization of periodic thin plates in bending). These authors started from the formulation of a two-dimensional heterogeneous problem based on a periodic Love-Kirchhoff model to achieve a homogenized model of the same type. It is also worthwhile to notice, in this framework, works on the perforated plates (Duvaut and Metellus, 1976) and the reinforced plates (Artola and Duvaut, 1977).

- In the second case ($a > 1$), the plate has a period very smaller than the thickness. This case performs the successive passages to the limit in an inverse order of that in the first case. When the period tends to zero, the 3D heterogeneous structure is first homogenized. Then, when the thickness of the plate tends to zero, the obtained homogeneous 3D-body is then substituted by a 2D plate model of Love-Kirchhoff (in bending in Kohn and Vogelius (1984) and in membrane and bending in Caillerie (1984)).

- In the third case ($a = 1$: $t \sim \epsilon \to 0$), the thickness of the plate is comparable with the period. In this situation, the two parameters become a single parameter and an asymptotic development technique leads to a formulation of three-dimensional cellular problems (Caillerie, 1982, 1984). The 3D heterogeneous body is directly substituted by a homogeneous Love-Kirchhoff plate whose stiffness constants are computed by solving an auxiliary boundary problem on the 3D unit cell. Lewiński and Telega (1999) also showed that the problems established in Kohn and Vogelius (1984) are equivalent to those of Caillerie (1984)

with regard to determining the homogenized behavior law. Lewiński and Telega (1999) also generalized, in the case $a = 1$, the works of Caillerie (1984) and Kohn and Vogelius (1984) for the non-symmetrical periodic, heterogeneous and variable thickness plates. They also obtain an equivalent homogeneous behavior of Love-Kirchhoff type.

The search of asymptotic solutions based on the limit studies of the scale parameters with the three above basic cases, especially the last case when studying the 3D unit cell, has been widely applied to different structures with numerous researches. Cecchi and Sab (2002a,b, 2004) have applied the Love-Kirchhoff plate model to study the behaviors of masonry structures. Bourgeois et al. (1998); Sab (2003); Dallot and Sab (2008a,b) generalized the Caillerie (1984) plate model for the limit analysis of periodic plates. A homogenized Reissner-Mindlin plate model was recently studied by Cecchi and Sab (2007) for orthotropic periodic plates and applied for brickwork panels. Based on the asymptotic expansion method, Buannic et al. (2003) presented a numerical method for computation of the effective properties of corrugated core sandwich panels where the shear effect of the Reissner-Mindlin plate was also mentioned. The studies on periodic heterogeneous beams based on the asymptotic expansion method can be found in Kolpakov (1995), and Buannic and Cartraud (2001).

Most of the approaches have used the asymptotic homogenization theory to determine the effective properties of the periodic plate. Because of the meshing difficulties, the finite element method was applied as a good first approach. Several studies used variational principles to derive bounds for the effective elastic properties of heterogeneous beams and plates (Kolpakov, 1999; Kolpakov and Sheremet, 1999; Kolpakov, 1998).

3.2.2 Thin Periodic Plates and Related Homogenized Problem

Consider an elastic plate which is periodic in the in-plane directions. Assume that the thickness of the plate, t, and the heterogeneity typical length, ϵ, are of the same order and that they are very small in comparison with the in-plane typical length of the plate, L ($\epsilon \sim t \ll L$). The purpose of this section is to substitute a homogeneous elastic 2D Love-Kirchhoff plate model to the heterogeneous 3D model.

To do so, the 3D elastic problem is first stated. Then, a Love-Kirchhoff model is described by introducing the homogenized plate stiffness tensors. Finally, one presents the determination of homogenized plate stiffness tensors in terms of the distribution of the 3D stiffness tensor in the unit cell Y which generates the plate by periodicity.

3.2.2.1 The 3D Problem

The heterogeneous plate under consideration occupies a domain $\Psi = \Omega \times]-\frac{t}{2}, \frac{t}{2}[$ where Ω is the middle surface of the plate and t is its thickness. The boundary of the plate, $\partial\Psi$, is decomposed

into three parts:

$$\partial\Psi = \partial\Psi_l \cup \partial\Psi_3^+ \cup \partial\Psi_3^-, \text{ with } \partial\Psi_l = \partial\Omega\times]-\frac{t}{2},\frac{t}{2}[\text{ and } \partial\Psi_3^\pm = \Omega \times \left\{\pm\frac{t}{2}\right\}.$$

The plate is fixed on its lateral boundary, $\partial\Psi_l$, and is submitted to distributed forces $\mathbf{h}^\pm$ on its upper and lower boundaries, $\partial\Psi_3^+$ and $\partial\Psi_3^-$.

The fourth-order stiffness tensor $\mathbf{L}(\mathbf{x})$ characterizing the elastic properties of the constituent material at every point $\mathbf{x} = (x_1, x_2, x_3)$ of Ψ is introduced:

$$\boldsymbol{\sigma}(\mathbf{x}) = \mathbf{L}(\mathbf{x})\,\boldsymbol{\epsilon}(\mathbf{x}) \tag{3.38}$$

where $\boldsymbol{\sigma}(\mathbf{x})$ is the second-order symmetric stress tensor and $\boldsymbol{\epsilon}(\mathbf{x})$ is the second-order symmetric strain tensor at point $\mathbf{x}$. The tensor $\mathbf{L}$ has the following symmetries:

$$L_{ijkl} = L_{klij} = L_{jikl} = L_{ijlk},$$

and is positive in the sense of the quadratic form:

$$\boldsymbol{\epsilon}\,\mathbf{L}\,\boldsymbol{\epsilon} = L_{ijkl}\epsilon_{ij}\epsilon_{kl} > 0$$

for all non zero symmetric second-order tensor $\boldsymbol{\epsilon}$. The following notations are used: Greek index $\alpha, \beta, \delta, \gamma = 1, 2$. Latin index $i, j, k, l = 1, 2, 3$.

The elastic problem is to find in Ψ a displacement vector field $\mathbf{u}$, a strain tensor field $\boldsymbol{\epsilon}$ and a stress tensor field $\boldsymbol{\sigma}$ such that the static conditions:

$$\begin{cases} \boldsymbol{\sigma}\,.\,\boldsymbol{\nabla} = 0, \\ \\ \boldsymbol{\sigma}\,.\,\boldsymbol{e}_3 = \mathbf{h}^\pm \quad \text{on } \partial\Psi_3^\pm, \end{cases} \tag{3.39}$$

the kinematic conditions:

$$\begin{cases} \boldsymbol{\epsilon} = \mathbf{u} \otimes^s \boldsymbol{\nabla} = \text{grad}^s(\mathbf{u}) \\ \\ \mathbf{u} = 0 \quad \text{on } \partial\Psi_l, \end{cases} \tag{3.40}$$

and the constitutive law (3.38) are satisfied. Here, $(\boldsymbol{e}_1, \boldsymbol{e}_2, \boldsymbol{e}_3)$ is the orthonormal basis associated with coordinates (x_1, x_2, x_3) and grad^s denotes the symmetric part of the gradient operator ($\text{grad}^s(\mathbf{u})$ will be used in this section in place of $\mathbf{u} \otimes^s \boldsymbol{\nabla}$).

3.2.2.2 The Homogenized Plate Problem

The considered plate is a periodic structure in direction 1 and 2 so that it is possible to extract an elementary cell which contains all information necessary to completely describe the plate. This

cell is denoted by:

$$Y = \omega \times]-\frac{t}{2}, \frac{t}{2}[$$

where $\omega \subset \mathbb{R}^2$; the boundary ∂Y of Y is decomposed into three parts:

$$\partial Y = \partial Y_l \cup \partial Y_3^+ \cup \partial Y_3^-, \text{ with } \partial Y_3^{\pm} = \omega \times \left\{ \pm \frac{t}{2} \right\}.$$

Assuming that t is of the same order of the typical size of ω and that t is very small as compared to the typical size of Ω, Caillerie (1984) showed that the 3D-body can be modelled as a homogeneous Love-Kirchhoff plate according to the homogenization procedure described hereafter.

The following notations are used. $\mathbf{N} = N_{\alpha\beta}(x_1, x_2)$ are the macroscopic in-plane (membrane) stress field resultants for the homogenized plate with $(x_1, x_2) \in \Omega$; $\mathbf{M} = M_{\alpha\beta}(x_1, x_2)$ are the macroscopic out-of-plane (flexural) stress field resultants; $\mathbf{E} = E_{\alpha\beta}(x_1, x_2)$ is the in-plane strain field; $\boldsymbol{\chi} = \chi_{\alpha\beta}(x_1, x_2)$ is the out-of-plane (curvature) strain field; $\mathbf{U} = U_i(x_1, x_2)$ is the plate displacement field.

The plate problem is to find a generalized stress field $(\mathbf{N}, \mathbf{M})$, an out-of-plane shear resultant field $\mathbf{Q} = Q_\alpha(x_1, x_2)$, a plate displacement field $\mathbf{U} = U_i(x_1, x_2)$ and a generalized strain field $(\mathbf{E}, \boldsymbol{\chi})$ on Ω satisfying the balance equations:

$$\begin{cases} N_{\alpha\beta,\beta} + h_\alpha^+ + h_\alpha^- = 0, \\ \\ M_{\alpha\beta,\beta} - Q_\alpha + \frac{t}{2}\left(h_\alpha^+ - h_\alpha^-\right) = 0, \\ \\ Q_{\alpha,\alpha} + h_3^+ + h_3^- = 0, \end{cases} \tag{3.41}$$

the kinematic compatibility conditions:

$$\begin{cases} E_{\alpha\beta} = \frac{1}{2}(U_{\alpha,\beta} + U_{\beta,\alpha}), \quad \chi_{\alpha\beta} = -U_{3,\alpha\beta}, \\ \\ \mathbf{U} = 0, \; U_{3,n} = 0, \qquad \forall (x_1, x_2) \in \partial\Omega, \end{cases} \tag{3.42}$$

and the plate constitutive law:

$$\begin{pmatrix} \mathbf{N} \\ \mathbf{M} \end{pmatrix} = \begin{pmatrix} \mathbf{A} & \mathbf{B} \\ \mathbf{B}^T & \mathbf{D} \end{pmatrix} \begin{pmatrix} \mathbf{E} \\ \boldsymbol{\chi} \end{pmatrix} \tag{3.43}$$

Here, $U_{3,n}$ is the derivative of U_3 with respect to the normal direction to $\partial\Omega$, the boundary of Ω. The overall fourth-order tensors $\mathbf{A}$, $\mathbf{B}$ and $\mathbf{D}$ can be determined by solving an auxiliary elastic problem over Y as described in the next section. They have the following symmetries:

$$\begin{cases} A_{\alpha\beta\gamma\delta} = A_{\gamma\delta\alpha\beta} = A_{\beta\alpha\gamma\delta} = A_{\alpha\beta\delta\gamma}, \\ \\ D_{\alpha\beta\gamma\delta} = D_{\gamma\delta\alpha\beta} = D_{\beta\alpha\gamma\delta} = D_{\alpha\beta\delta\gamma}, \\ \\ B_{\alpha\beta\gamma\delta} = B_{\beta\alpha\gamma\delta} = B_{\alpha\beta\delta\gamma}, \end{cases} \tag{3.44}$$

and

$$B^T_{\alpha\beta\gamma\delta} = B_{\gamma\delta\alpha\beta}.$$

3.2.2.3 Determination of $(\mathbf{A}, \mathbf{B}, \mathbf{D})$

The determination of $(\mathbf{A}, \mathbf{B}, \mathbf{D})$ is as follows: for every $(\mathbf{N}, \mathbf{M})$ the set of statically compatible 3D stress field $\boldsymbol{\sigma}$ of unit cell Y is defined by:

$$SA(\mathbf{N}, \mathbf{M}) = \left\{ \begin{array}{l} \boldsymbol{\sigma} \,\Big|\, N_{\alpha\beta} = t\langle\sigma_{\alpha\beta}\rangle, M_{\alpha\beta} = t\langle x_3\sigma_{\alpha\beta}\rangle, \ \boldsymbol{\sigma} \,.\, \boldsymbol{\nabla} = 0 \quad \text{in } Y, \\ \\ \quad \boldsymbol{\sigma}\cdot\mathbf{n} \ \text{ anti-periodic on } \partial Y_l; \ \ \boldsymbol{\sigma}\cdot\boldsymbol{e}_3 = 0 \ \text{ on } \partial Y_3^{\pm} \end{array} \right\} \tag{3.45}$$

where $\langle\cdot\rangle$ is the volume average operator on Y. For every $(\mathbf{E}, \boldsymbol{\chi})$, the set of kinematically compatible displacement fields of the unit cell, $\mathbf{v} = (v_i)$ is defined by:

$$KA(\mathbf{E}, \boldsymbol{\chi}) = \left\{ \mathbf{v} \,\Big|\, \text{grad}^s(\mathbf{v}) = \widetilde{\mathbf{E}} + x_3\widetilde{\boldsymbol{\chi}} + \text{grad}^s(\mathbf{u}^{per}), \ \mathbf{u}^{per} \text{ periodic on } \partial Y_l \right\} \tag{3.46}$$

where the following notations are used:

$$\widetilde{E}_{\alpha\beta} = E_{\alpha\beta}, \quad \widetilde{E}_{i3} = 0, \ \ \widetilde{\chi}_{\alpha\beta} = \chi_{\alpha\beta}, \quad \widetilde{\chi}_{i3} = 0.$$

For unit cell $Y = \omega\times]-\frac{t}{2}, \frac{t}{2}[$ with rectangular section $\omega =]-\frac{l_1}{2}, \frac{l_1}{2}[\times]-\frac{l_2}{2}, \frac{l_2}{2}[$, $\boldsymbol{\sigma}\cdot\mathbf{n}$ anti-periodic on ∂Y_l means:

$$\begin{cases} \sigma_{1j}\left(\frac{l_1}{2}, x_2, x_3\right) = \sigma_{1j}\left(-\frac{l_1}{2}, x_2, x_3\right) \ \forall (x_2, x_3) \in]-\frac{l_2}{2}, \frac{l_2}{2}[\times]-\frac{t}{2}, \frac{t}{2}[\\ \\ \sigma_{2j}\left(x_1, \frac{l_2}{2}, x_3\right) = \sigma_{2j}\left(x_1, -\frac{l_2}{2}, x_3\right) \ \forall (x_1, x_3) \in]-\frac{l_1}{2}, \frac{l_1}{2}[\times]-\frac{t}{2}, \frac{t}{2}[\end{cases},$$

and $\mathbf{u}^{per}$ periodic on ∂Y_l means:

$$\begin{cases} \mathbf{u}^{per}\left(\frac{l_1}{2}, x_2, x_3\right) = \mathbf{u}^{per}\left(-\frac{l_1}{2}, x_2, x_3\right) \ \forall (x_2, x_3) \in]-\frac{l_2}{2}, \frac{l_2}{2}[\times]-\frac{t}{2}, \frac{t}{2}[\\ \\ \mathbf{u}^{per}\left(x_1, \frac{l_2}{2}, x_3\right) = \mathbf{u}^{per}\left(x_1, -\frac{l_2}{2}, x_3\right) \ \forall (x_1, x_3) \in]-\frac{l_1}{2}, \frac{l_1}{2}[\times]-\frac{t}{2}, \frac{t}{2}[\end{cases}.$$

Actually, the displacement $\mathbf{v}$ in (3.46) is uniquely determined in terms of $(\mathbf{E}, \boldsymbol{\chi})$ and $\mathbf{u}^{per}$ up to a rigid body motion:

$$\mathbf{v}(\mathbf{x}) = \begin{pmatrix} (E_{11} + x_3\chi_{11})\, x_1 + (E_{12} + x_3\chi_{12})\, x_2 \\ (E_{12} + x_3\chi_{12})\, x_1 + (E_{22} + x_3\chi_{22})\, x_2 \\ -\left(\chi_{11}\frac{x_1^2}{2} + \chi_{12}x_1x_2 + \chi_{22}\frac{x_2^2}{2}\right) \end{pmatrix} + \mathbf{u}^{per}(\mathbf{x}).$$

The sets $SA(\mathbf{N}, \mathbf{M})$ and $KA(\mathbf{E}, \boldsymbol{\chi})$ are actually in duality in the sense of the virtual work on the unit cell:

$$\forall \boldsymbol{\sigma} \in SA(\mathbf{N}, \mathbf{M}), \quad \forall \mathbf{v} \in KA(\mathbf{E}, \boldsymbol{\chi}), \quad \mathbf{N}\,\mathbf{E} + \mathbf{M}\,\boldsymbol{\chi} = t\langle \boldsymbol{\sigma}\, \mathrm{grad}^s(\mathbf{v})\rangle. \tag{3.47}$$

Indeed, due to periodicity conditions, $\boldsymbol{\sigma}\,.\,\boldsymbol{\nabla} = 0$ and $\boldsymbol{\sigma}\cdot\mathbf{e}_3 = 0$ on $\partial Y_3^{\pm}$, we have:

$$\begin{aligned} t\langle \boldsymbol{\sigma}\, \mathrm{grad}^s(\mathbf{u}^{per})\rangle &= \frac{1}{|\omega|}\int_{\mathbf{x}\in Y} \boldsymbol{\sigma}\, \mathrm{grad}^s(\mathbf{u}^{per}) dY \\ &= -\frac{1}{|\omega|}\int_{\mathbf{x}\in Y} (\boldsymbol{\sigma}\,.\,\boldsymbol{\nabla})\,.\mathbf{u}^{per} dY + \frac{1}{|\omega|}\int_{\mathbf{x}\in\partial Y} (\boldsymbol{\sigma}.\mathbf{n})\,.\mathbf{u}^{per} dS \\ &= 0 \end{aligned}$$

For fixed $(\mathbf{E}, \boldsymbol{\chi})$, the auxiliary elastic boundary value problem to be solved on Y is to find:

$$\begin{aligned} &\mathbf{v} \in KA(\mathbf{E}, \boldsymbol{\chi}), \ \boldsymbol{\sigma} \in SA = \underset{(\mathbf{N}', \mathbf{M}')}{\cup} SA(\mathbf{N}', \mathbf{M}') \\ &\quad \text{such that} \\ &\boldsymbol{\sigma} = \mathbf{L}(\mathbf{x})\,\boldsymbol{\epsilon}(\mathbf{v}) \quad \text{in } Y \end{aligned} \tag{3.48}$$

This problem has a unique solution $\mathbf{v}^{(\mathbf{E},\boldsymbol{\chi})}$ (up to a rigid body motion), $\boldsymbol{\epsilon}^{(\mathbf{E},\boldsymbol{\chi})}$ and $\boldsymbol{\sigma}^{(\mathbf{E},\boldsymbol{\chi})}$ which linearly depends on $(\mathbf{E}, \boldsymbol{\chi})$. Hence, the corresponding generalized stresses defined by

$$N_{\alpha\beta}^{(\mathbf{E},\boldsymbol{\chi})} = t\langle \sigma_{\alpha\beta}^{(\mathbf{E},\boldsymbol{\chi})}\rangle, \ M_{\alpha\beta}^{(\mathbf{E},\boldsymbol{\chi})} = t\langle x_3\sigma_{\alpha\beta}^{(\mathbf{E},\boldsymbol{\chi})}\rangle,$$

are linear functions of $(\mathbf{E}, \boldsymbol{\chi})$. The linear operator $(\mathbf{E}, \boldsymbol{\chi}) \to (\mathbf{N}^{(\mathbf{E},\boldsymbol{\chi})}, \mathbf{M}^{(\mathbf{E},\boldsymbol{\chi})})$ is self-adjoint (or symmetric) in the following sense:

$$\mathbf{N}^{(\mathbf{E}^1,\boldsymbol{\chi}^1)}\,\mathbf{E}^2 + \mathbf{M}^{(\mathbf{E}^1,\boldsymbol{\chi}^1)}\,\boldsymbol{\chi}^2 = \mathbf{N}^{(\mathbf{E}^2,\boldsymbol{\chi}^2)}\,\mathbf{E}^1 + \mathbf{M}^{(\mathbf{E}^2,\boldsymbol{\chi}^2)}\,\boldsymbol{\chi}^1$$

for all $(\mathbf{E}^1, \boldsymbol{\chi}^1)$ and $(\mathbf{E}^2, \boldsymbol{\chi}^2)$. Indeed, using (3.47) and the symmetries of $\mathbf{L}(\mathbf{x})$, we have:

$$\begin{aligned}\mathbf{N}^{(\mathbf{E}^1,\boldsymbol{\chi}^1)}\,\mathbf{E}^2+\mathbf{M}^{(\mathbf{E}^1,\boldsymbol{\chi}^1)}\,\boldsymbol{\chi}^2 &= t\langle\boldsymbol{\sigma}^{(\mathbf{E}^1,\boldsymbol{\chi}^1)}\,\mathrm{grad}^s\left(\mathbf{v}^{(\mathbf{E}^2,\boldsymbol{\chi}^2)}\right)\rangle\\ &= t\langle\mathrm{grad}^s\left(\mathbf{v}^{(\mathbf{E}^1,\boldsymbol{\chi}^1)}\right)\,\mathbf{L}(\mathbf{x})\,\mathrm{grad}^s\left(\mathbf{v}^{(\mathbf{E}^2,\boldsymbol{\chi}^2)}\right)\rangle\\ &= t\langle\boldsymbol{\sigma}^{(\mathbf{E}^2,\boldsymbol{\chi}^2)}\,\mathrm{grad}^s\left(\mathbf{v}^{(\mathbf{E}^1,\boldsymbol{\chi}^1)}\right)\rangle\\ &= \mathbf{N}^{(\mathbf{E}^2,\boldsymbol{\chi}^2)}\,\mathbf{E}^1+\mathbf{M}^{(\mathbf{E}^2,\boldsymbol{\chi}^2)}\,\boldsymbol{\chi}^1\end{aligned}$$

It turns up that the linear operator $(\mathbf{E},\boldsymbol{\chi})\rightarrow\left(\mathbf{N}^{(\mathbf{E},\boldsymbol{\chi})},\mathbf{M}^{(\mathbf{E},\boldsymbol{\chi})}\right)$ can be uniquely expressed through three fourth-order tensors $(\mathbf{A},\mathbf{B},\mathbf{D})$ having the symmetries (3.44) as:

$$\begin{aligned}\mathbf{N}^{(\mathbf{E},\boldsymbol{\chi})} &= \mathbf{A}\,\mathbf{E}+\mathbf{B}\,\boldsymbol{\chi}\\ \mathbf{M}^{(\mathbf{E},\boldsymbol{\chi})} &= \mathbf{B}^T\,\mathbf{E}+\mathbf{D}\,\boldsymbol{\chi}\end{aligned}$$

Using kinematic variational formulation of the elastic problem on Y, an equivalent definition for $(\mathbf{A},\mathbf{B},\mathbf{D})$ is derived as: $\forall\,(\mathbf{E},\boldsymbol{\chi})$,

$$\mathbf{E}\,\mathbf{A}\,\mathbf{E}+2\mathbf{E}\,(\mathbf{B}\,\boldsymbol{\chi})+\boldsymbol{\chi}\,\mathbf{D}\,\boldsymbol{\chi}=\min_{\mathbf{v}\in KA(\mathbf{E},\boldsymbol{\chi})}t\langle\mathrm{grad}^s\,(\mathbf{v})\,\mathbf{L}(\mathbf{x})\,\mathrm{grad}^s\,(\mathbf{v})\rangle \tag{3.49}$$

Similarly, using static variational formulation of the elastic problem on Y, another equivalent definition for $(\mathbf{A},\mathbf{B},\mathbf{D})$ is derived as: $\forall\,(\mathbf{E},\boldsymbol{\chi})$,

$$\mathbf{E}\,\mathbf{A}\,\mathbf{E}+2\mathbf{E}\,(\mathbf{B}\,\boldsymbol{\chi})+\boldsymbol{\chi}\,\mathbf{D}\,\boldsymbol{\chi}=\max_{\boldsymbol{\sigma}\in SA}2t\langle\boldsymbol{\sigma}\,\left(\widetilde{\mathbf{E}}+x_3\tilde{\boldsymbol{\chi}}\right)\rangle-t\langle\boldsymbol{\sigma}\,\mathbf{S}\,(\mathbf{x})\,\boldsymbol{\sigma}\rangle. \tag{3.50}$$

Here $\mathbf{S}$ is the compliance tensor $\mathbf{S}=(\mathbf{L})^{-1}$.

3.2.3 Γ-Operator for Periodic Media with Traction-Free Boundary Conditions

Section 3.1.4 presented the explicit expression of the $\boldsymbol{\Gamma}$-operator necessary to solve the elastic problem with boundary condition at infinity (Willis, 1977, 1981; Drugan and Willis, 1996) or with periodic boundary conditions (Suquet, 1990; Moulinec and Suquet, 1994, 1998). The solution of the elasticity problem characterized by boundary conditions and by body forces can then be expressed from these $\boldsymbol{\Gamma}$-operators. Up to now such a strategy was restricted to the use of known $\boldsymbol{\Gamma}$-operators. In some cases, other specific boundary conditions must be considered: for example in the case of beams or plates, traction-free boundary conditions must be taken into account. In this case a new $\boldsymbol{\Gamma}$-operator is necessary.

Therefore, the purpose of this section is to formulate a new $\boldsymbol{\Gamma}$-operator for periodic media with traction-free boundary conditions. It will be used to obtain the effective elastic properties of periodic thin plates where it is assumed that the thickness of the plate and the heterogeneity

typical length are of the same order, and that they are very small in comparison with the in-plane typical length of the plate L (case $a = 1$). The Fast Fourier Transform method is used to solve the auxiliary elasticity problem. The solution is split into a classical periodic solution and a complementary solution to account for the traction-free boundary conditions. The effective elastic properties of the plate are finally obtained by the calculation of strain energy in which the strain and stress fields are obtained by a basic iterative algorithm. The numerical validation of the method will be performed on two numerical examples. The $\mathbf{\Gamma}$-operator formulated in this section can obviously be used for other applications, for example to study the field generated by defects in elastic solids with given boundary conditions.

Let us now consider a basic cell Y. Mixed conditions are defined along the boundaries of the cell as follows: periodic boundary conditions are assumed along the boundaries perpendicular to x_1 and x_2 while traction-free boundary conditions are assumed along the boundary perpendicular to x_3. The domain Y of the cell is defined by:

$$Y = \left\{ \mathbf{x} \in \mathbf{R}^3,\, \mathbf{x} = (x_1, x_2, x_3),\, x_1 \in \left]0, l_1\right[, x_2 \in \left]0, l_2\right[, x_3 \in \left]-\frac{t}{2}, \frac{t}{2}\right[\right\}. \tag{3.51}$$

The domain $\omega = \left]0, l_1\right[\times \left]0, l_2\right[$ is the middle surface of the cell with the boundary $\partial\omega$ and $\partial Y_l = \partial\omega \times \left]-\frac{t}{2}, \frac{t}{2}\right[$ is the lateral boundary of Y. The top and bottom surfaces of the cell are denoted by $\partial Y^{\pm} = \omega \times \{\pm\frac{t}{2}\}$. All formulations are performed under the assumption of a linear elastic behavior and small deformations of materials.

For a given periodic polarization $\boldsymbol{\tau}$, the problem to solve on Y is now defined in the following form:

$$\begin{cases} \boldsymbol{\sigma}(\mathbf{x}) \,.\, \boldsymbol{\nabla} = 0, \quad \boldsymbol{\sigma}(\mathbf{x}) = \mathbf{L}^o\, \mathbf{e}(\mathbf{x}) + \boldsymbol{\tau}(\mathbf{x}), \\ \\ \mathbf{e}(\mathbf{x}) = \mathbf{u}(\mathbf{x}) \otimes^s \boldsymbol{\nabla}, \\ \\ \mathbf{u}(\mathbf{x}) \text{ periodic on } \partial Y_l, \quad \boldsymbol{\sigma}(\mathbf{x}) \,.\, \mathbf{n} \text{ antiperiodic on } \partial Y_l, \end{cases} \tag{3.52}$$

and traction-free boundary conditions on $\partial Y^{\pm}$ are assumed,

$$\boldsymbol{\sigma} \,.\, \boldsymbol{e}_3 = 0 \quad \text{on} \quad \partial Y^{\pm}. \tag{3.53}$$

For $\boldsymbol{\tau}(\mathbf{x}) \in \mathbf{L}^2(Y)$, the boundary value problem (3.52, 3.53) can be solved by expanding the polarization stress into the Fourier series defined in (3.32),

$$\boldsymbol{\tau}(\mathbf{x}) = \sum_{\mathbf{k}} \hat{\boldsymbol{\tau}}(\mathbf{k})\, e^{i\mathbf{k}.\mathbf{x}}, \tag{3.54}$$

where the coefficients of the Fourier series $\hat{\boldsymbol{\tau}}(\mathbf{k})$ can be calculated by the Fast Fourier Transform (FFT) (see e.g. Soize (1993), Gasquet and Witomski (2000), Kaßbohm et al. (2005)).

The solution $\mathbf{u}(\mathbf{x})$ of the problem (3.52, 3.53) can be split into two terms: the first term can be obtained with the standard periodicity conditions in the direction x_3 (as in the previous section) and the second term is the complement which is necessary to comply to the traction-free boundary conditions:

$$\mathbf{u}(\mathbf{x}) = \mathbf{u}^p(\mathbf{x}) + \mathbf{u}^h(\mathbf{x}),$$

with,

$$\mathbf{u}^p(\mathbf{x}) = \sum_{\mathbf{k}} \hat{\mathbf{u}}^p(\mathbf{k})\, e^{i\mathbf{k}.\mathbf{x}}, \quad \mathbf{u}^h(\mathbf{x}) = \sum_{\tilde{\mathbf{k}}} \tilde{\mathbf{u}}^h(\tilde{\mathbf{k}}, x_3)\, e^{ik_\alpha x_\alpha}, \tag{3.55}$$

where $\tilde{\mathbf{k}} = (k_1, k_2)$, $\mathbf{k} = (k_1, k_2, k_3)$ are the discrete wave vectors arranged along a discrete lattice having a period $2\pi/l_i$ ($l_3 = t$) along the direction x_i.

$\mathbf{u}^p(\mathbf{x})$ is the solution of the problem (3.52) with full periodicity conditions for which the corresponding strain $\mathbf{e}^p(\mathbf{x})$ is defined in (3.33) and the stress field is then expressed in the Fourier space as follows:

$$\hat{\boldsymbol{\sigma}}^p(\mathbf{k}) = \lambda\, tr(\hat{\mathbf{e}}^p(\mathbf{k}))\, \mathbf{1} + 2\mu\, \hat{\mathbf{e}}^p(\mathbf{k}) + \hat{\boldsymbol{\tau}}(\mathbf{k}).$$

The complementary displacement field $\mathbf{u}^h(\mathbf{x})$ due to the traction-free boundary conditions complies to the following system of equations:

$$\begin{cases} \boldsymbol{\sigma}^h(\mathbf{x})\,.\,\boldsymbol{\nabla} = 0, \quad \boldsymbol{\sigma}^h(\mathbf{x}) = \mathbf{L}^o\, \mathbf{e}^h(\mathbf{x}), \\ \\ \mathbf{e}^h(\mathbf{x}) = \mathbf{u}^h(\mathbf{x}) \otimes^s \boldsymbol{\nabla}, \\ \\ \sigma^h_{j3}(x_1, x_2, x_3 = \pm\frac{t}{2}) = -\sigma^p_{j3}(x_1, x_2, x_3 = \pm\frac{t}{2}), \\ \\ \mathbf{u}^h(\mathbf{x}) \text{ periodic on } \partial Y_l, \quad \boldsymbol{\sigma}^h(\mathbf{x})\,.\,\mathbf{n} \text{ antiperiodic on } \partial Y_l. \end{cases} \tag{3.56}$$

The solution of problem (3.56), complying to periodic boundary condition along the boundaries perpendicular to x_1 and x_2 has been defined in the second term of (3.55) where $\tilde{\mathbf{u}}^h(\tilde{\mathbf{k}}, x_3)$ has to be obtained. The corresponding strains and stresses are, respectively:

$$\mathbf{e}^h(\mathbf{x}) = \sum_{\tilde{\mathbf{k}}} \tilde{\mathbf{e}}^h(\tilde{\mathbf{k}}, x_3)\, e^{ik_\alpha x_\alpha}, \quad \boldsymbol{\sigma}^h(\mathbf{x}) = \sum_{\tilde{\mathbf{k}}} \tilde{\boldsymbol{\sigma}}^h(\tilde{\mathbf{k}}, x_3)\, e^{ik_\alpha x_\alpha}. \tag{3.57}$$

The strain field is related to the displacement field by:

$$\tilde{\mathbf{e}}^h(\tilde{\mathbf{k}}, x_3) = \tilde{\mathbf{u}}^h(\tilde{\mathbf{k}}, x_3) \otimes^s \boldsymbol{\nabla}', \tag{3.58}$$

where the operator $\boldsymbol{\nabla'}$ is defined by $\boldsymbol{\nabla'} = [ik_1 \quad ik_2 \quad \partial_3]^T$. The operator ∂ indicates the partial differentiation with respect to the coordinate subscript that follows. The stress field is obtained from the constitutive equations:

$$\tilde{\boldsymbol{\sigma}}^h(\tilde{\mathbf{k}}, x_3) = \lambda\Big(\tilde{\mathbf{u}}^h(\tilde{\mathbf{k}}, x_3).\boldsymbol{\nabla'}\Big)\,\mathbf{1} + 2\mu\Big(\tilde{\mathbf{u}}^h(\tilde{\mathbf{k}}, x_3) \otimes^s \boldsymbol{\nabla'}\Big). \tag{3.59}$$

The equilibrium equation $\boldsymbol{\sigma}^h(\mathbf{x}).\boldsymbol{\nabla} = 0$ becomes $\tilde{\boldsymbol{\sigma}}^h(\tilde{\mathbf{k}}, x_3).\boldsymbol{\nabla'} = 0$ which leads to:

$$\Big[(\lambda+\mu)\boldsymbol{\nabla'} \otimes^s \boldsymbol{\nabla'} + \mu(\boldsymbol{\nabla'}.\boldsymbol{\nabla'})\,\mathbf{1}\Big].\,\tilde{\mathbf{u}}^h(\tilde{\mathbf{k}}, x_3) = 0, \tag{3.60}$$

where,

$$\boldsymbol{\nabla'} \otimes^s \boldsymbol{\nabla'} = \begin{bmatrix} -k_1^2 & -k_1k_2 & ik_1\partial_3 \\ -k_1k_2 & -k_2^2 & ik_2\partial_3 \\ ik_1\partial_3 & ik_2\partial_3 & \partial_{33}^2 \end{bmatrix}, \quad \boldsymbol{\nabla'}.\boldsymbol{\nabla'} = \partial_{33}^2 - (k_1^2+k_2^2). \tag{3.61}$$

The solution of equation (3.60) is (see appendix B.1):

$$\tilde{\mathbf{u}}^h(\tilde{\mathbf{k}}, x_3) = (\mathbf{a}^+ + x_3\mathbf{b}^+)\,e^{sx_3} + (\mathbf{a}^- + x_3\mathbf{b}^-)\,e^{-sx_3}, \tag{3.62}$$

where:

$$\mathbf{a}^\pm = \begin{Bmatrix} a_1^\pm \\ a_2^\pm \\ \pm\frac{1}{is}(a_1^\pm k_1 + a_2^\pm k_2 - i\frac{\lambda+3\mu}{\lambda+\mu}b_3^\pm) \end{Bmatrix}, \quad \mathbf{b}^\pm = \begin{Bmatrix} \pm\frac{ik_1}{s}b_3^\pm \\ \pm\frac{ik_2}{s}b_3^\pm \\ b_3^\pm \end{Bmatrix}, \quad s = \sqrt{k_1^2+k_2^2}. \tag{3.63}$$

The six complex coefficients $(a_1^\pm, a_2^\pm, b_3^\pm)$ are obtained from the six boundary conditions defined in (3.56) which are rewritten as follows:

$$\tilde{\sigma}_{j3}^h(\tilde{\mathbf{k}}, \pm\frac{t}{2}) = -\sum_{k_3} \hat{\sigma}_{j3}^p(\mathbf{k}) e^{\pm ik_3\frac{t}{2}}. \tag{3.64}$$

The previous relation leads to the explicit expressions of $(a_1^\pm, a_2^\pm, b_3^\pm)$ as follows:

$$
\begin{aligned}
b_3^{\pm} &= w^{\pm} g^{+} + w^{\mp} g^{-}, \\
a_2^{\pm} &= -\tfrac{ik_2}{2s^2\sinh(st)}\left(c_1 b_3^{\pm} + st b_3^{\mp}\right) \pm \tfrac{s^2+k_1^2}{4\mu s^3\sinh(st)}(q_2^{\pm} e^{\frac{st}{2}} - q_2^{\mp} e^{-\frac{st}{2}}) \mp \tfrac{k_1 k_2}{4\mu s^3\sinh(st)}(q_1^{\pm} e^{\frac{st}{2}} - q_1^{\mp} e^{-\frac{st}{2}}), \\
a_1^{\pm} &= -\tfrac{k_1 k_2}{s^2+k_1^2} a_2^{\pm} - \tfrac{ik_1}{(s^2+k_1^2)\sinh(st)}\left(c_1 b_3^{\pm} + st b_3^{\mp}\right) \pm \tfrac{s}{2\mu(s^2+k_1^2)\sinh(st)}(q_1^{\pm} e^{\frac{st}{2}} - q_1^{\mp} e^{-\frac{st}{2}}),
\end{aligned}
\tag{3.65}
$$

where:

$$
\begin{aligned}
q_1^{\pm} &= -\textstyle\sum_{k_3} e^{\pm ik_3\frac{t}{2}}\,\hat{\sigma}_{13}^{p}(\mathbf{k}), \\
q_2^{\pm} &= -\textstyle\sum_{k_3} e^{\pm ik_3\frac{t}{2}}\,\hat{\sigma}_{23}^{p}(\mathbf{k}), \\
q_3^{\pm} &= -\textstyle\sum_{k_3} e^{\pm ik_3\frac{t}{2}}\hat{\sigma}_{33}^{p}(\mathbf{k}), \\
w^{\pm} &= \mp\tfrac{e^{\pm\frac{st}{2}}\sinh(st)+ste^{\mp\frac{st}{2}}}{4\mu(\sinh^2(st)-s^2t^2)}, \quad c_1 = (\tfrac{st}{2} - \tfrac{\mu}{\lambda+\mu})e^{st} + (\tfrac{st}{2} + \tfrac{\mu}{\lambda+\mu})e^{-st}, \\
g^{\pm} &= q_3^{\pm} \pm \tfrac{i}{s\sinh(st)}\left[(k_1 q_1^{\pm} + k_2 q_2^{\pm})\cosh(st) - (k_1 q_1^{\mp} + k_2 q_2^{\mp})\right].
\end{aligned}
\tag{3.66}
$$

The derivation of the displacement field (equations (3.62) and (3.63)) and the calculation of the coefficients $(a_1^{\pm}, a_2^{\pm}, b_3^{\pm})$ from the boundary condition (3.64) are given in appendix B.1. The complementary strain field $\tilde{\mathbf{e}}^h(\tilde{\mathbf{k}}, x_3)$ is then obtained by (3.58).

The total strain field is a combination of the two components obtained from (3.33) and (3.58):

$$
\mathbf{e}(\mathbf{x}) = \mathbf{e}^p(\mathbf{x}) + \mathbf{e}^h(\mathbf{x}), \tag{3.67}
$$

where,

$$
\mathbf{e}^p(\mathbf{x}) = \sum_{\mathbf{k}} \hat{\mathbf{e}}^p(\mathbf{k})\, e^{i\mathbf{k}\cdot\mathbf{x}}, \quad \mathbf{e}^h(\mathbf{x}) = \sum_{\tilde{\mathbf{k}}} \tilde{\mathbf{e}}^h(\tilde{\mathbf{k}}, x_3)\, e^{ik_\alpha x_\alpha}. \tag{3.68}
$$

Expression (3.63) shows that the coefficients $(a_1^{\pm}, a_2^{\pm}, b_3^{\pm})$ and the complementary displacement field $\tilde{\mathbf{u}}^h(\tilde{\mathbf{k}}, x_3)$ must be obtained also for $s \neq 0$ or $|\tilde{\mathbf{k}}| \neq 0$. As a result, the corresponding strain field $\tilde{\mathbf{e}}^h(\tilde{\mathbf{k}}, x_3)$ is obtained. The complete expression of the strains $\tilde{\mathbf{e}}^h(\tilde{\mathbf{k}}, x_3)$ is given in appendix B.2.

Finally, the strain field is related to the polarization field via a $\boldsymbol{\Gamma}$-operator which can be considered as a projection of the polarizations onto the strains. The previous formulations enable to construct a new $\boldsymbol{\Gamma}$-operator for the mixed boundary conditions. In fact, for a given polarization field, the total strain field is obtained from equations (3.67) and (3.68) where the complementary strain field is calculated by expressions (3.58), (3.62) and (3.65), while the periodic strain field is defined classically by (3.33). This step will be used in the following part to obtain the effective

elastic properties of a thin plate.

3.2.4 Application to Thin Plate Homogenization

Let us consider a Love-Kirchhoff heterogeneous plate having a thickness t which is located within a domain $\Omega\times]-\frac{t}{2},\frac{t}{2}[$, $t\in R^+$. $\Omega\in\mathbf{R}^2$ is the middle surface of the plate. The plate exhibits a periodic structure in directions x_1 and x_2 so that it is possible to extract an elementary cell Y given by (3.51) which contains all the information necessary to completely describe the plate and more precisely the value of the elasticity tensor $\mathbf{L}(\mathbf{x})$ at each point. It is assumed that the thickness of the plate and the typical length of the cell are of the same order, and that they are very small in comparison with the in-plane typical length of the plate.

The "homogenization problem" on Y is defined as follows:

$$\begin{cases} \boldsymbol{\sigma}(\mathbf{x})\,.\,\boldsymbol{\nabla}=0, \quad \boldsymbol{\sigma}(\mathbf{x})=\mathbf{L}(\mathbf{x})\,\boldsymbol{\epsilon}(\mathbf{x}), \\ \\ \boldsymbol{\epsilon}(\mathbf{x})=\mathbf{E}+x_3\boldsymbol{\chi}+\mathbf{e}(\mathbf{u}(\mathbf{x})), \\ \\ \mathbf{u}(\mathbf{x}) \text{ periodic on } \partial Y_l, \quad \boldsymbol{\sigma}(\mathbf{x})\,.\,\mathbf{n} \text{ antiperiodic on } \partial Y_l, \end{cases} \tag{3.69}$$

and the free boundary conditions on $\partial Y^{\pm}$ are assumed,

$$\boldsymbol{\sigma}\,.\,\boldsymbol{e}_3=0 \quad \text{on} \quad \partial Y^{\pm}. \tag{3.70}$$

This problem allows to obtain the stiffness properties related to the macroscopic kinematics defined by the "in plane" membrane strain $\mathbf{E}$ and the curvature $\boldsymbol{\chi}$ of the middle surface of the plate. The problem (3.69, 3.70) is transformed into the boundary value problem (3.52, 3.53) defined in the previous section by introducing a homogeneous elastic reference medium $\mathbf{L}^o$, leading to the polarization field $\boldsymbol{\tau}(\mathbf{x})$ given by:

$$\boldsymbol{\tau}(\mathbf{x})=\mathbf{L}(\mathbf{x})\;[\mathbf{E}+x_3\boldsymbol{\chi}+\mathbf{e}(\mathbf{u}(\mathbf{x}))]-\mathbf{L}^o\,\mathbf{e}(\mathbf{u}(\mathbf{x})) \tag{3.71}$$

The strain field $\mathbf{e}(\mathbf{u}(\mathbf{x}))$, symmetrical part of $\mathbf{u}(\mathbf{x})\otimes\boldsymbol{\nabla}$, will be written simply as $\mathbf{e}(\mathbf{x})$ in the following. The "macroscopic" fields $\mathbf{E}$ and $\boldsymbol{\chi}$ have only the in-plane components: $E_{j3}=0$, $\chi_{j3}=0$ (see Caillerie (1984)).

The boundary value problem (3.69, 3.70, 3.71) has the same structure as the basic problem (3.52, 3.53). The polarization tensor is now a function of the unknown strain field. Equations (3.69), (3.70) are therefore solved by using a basic iterative procedure. At each iteration, the polarization field is given by (3.71).

3.2.4.1 Homogenization Procedure

The homogenized elastic properties of the plate are obtained from the elastic strain energy per unit area of the plate expressed by (see (3.49)):

$$\frac{1}{|\omega|}\int_Y \boldsymbol{\sigma}(\mathbf{x})\,\boldsymbol{\epsilon}(\mathbf{x})\,dY = \mathbf{EAE} + 2\mathbf{EB}\boldsymbol{\chi} + \boldsymbol{\chi}\mathbf{D}\boldsymbol{\chi}. \tag{3.72}$$

It can be seen that the homogenized stiffness properties $(\mathbf{A}, \mathbf{B}, \mathbf{D})$ of the plate will be obtained by using an appropriate choice of the macroscopic tensors $(\mathbf{E}, \boldsymbol{\chi})$ and by calculating the elastic strain energy.

The discrete Fourier transform is performed by discretization of the cell Y into a regular grid: $(N_1 \times N_2)$ points (pixels - 2D problems) or $(N_1 \times N_2 \times N_3)$ points (voxels - 3D problems). For three-dimensional problems in the space (x_1, x_2, x_3), the coordinates in the real space are defined by:

$$x_\alpha = (i_\alpha - 1)\frac{l_\alpha}{N_\alpha}, \quad i_\alpha = 1, ..., N_\alpha, \quad \text{and} \quad x_3 = i_3\frac{t}{N_3}, \quad i_3 = -\frac{N_3}{2}, ..., 0, ..., \frac{N_3}{2} - 1. \tag{3.73}$$

This discretization is appropriate for using the Fast Fourier Transform (FFT) as soon as N_i are powers of 2. The computation of the FFT corresponds to the wave-number orders $n_i = [0, ..., \frac{N_i}{2} - 1, -\frac{N_i}{2}, ..., -1]$. The components of the wave vectors are then defined as follows:

$$k_\alpha = \frac{2\pi n_\alpha}{l_\alpha}, \quad k_3 = \frac{2\pi n_3}{t}. \tag{3.74}$$

This discretization will be used for the analysis of the plane strain problems studied in the following section.

3.2.4.2 Iterative Algorithm

The boundary value problem (3.69, 3.70) is solved using the method proposed in section 3.2.3 with a given polarization field in (3.71). The iterative algorithm necessary to compute the strain and stress fields of the problem (3.69, 3.70) comprises the steps described as follows for the 3D case:

Initialization:

$$\mathbf{e}^0(\mathbf{x}) = 0, \quad \boldsymbol{\sigma}^0(\mathbf{x}) = \mathbf{L}(\mathbf{x}) \Big[\mathbf{E} + x_3\boldsymbol{\chi} + \mathbf{e}^0(\mathbf{x})\Big],$$

Iterate i+1 : $\mathbf{e}^i(\mathbf{x})$ and $\boldsymbol{\sigma}^i(\mathbf{x})$ being known

$$\begin{aligned}
&\text{a)} \quad \boldsymbol{\tau}^i(\mathbf{x}) = \boldsymbol{\sigma}^i(\mathbf{x}) - \mathbf{L}^o\,\mathbf{e}^i(\mathbf{x}),\\
&\text{b)} \quad \hat{\boldsymbol{\tau}}^i(\mathbf{k}) = \mathscr{F}_3\Big[\boldsymbol{\tau}^i(\mathbf{x})\Big],\\
&\text{c)} \quad \hat{\mathbf{e}}_p^{i+1}(\mathbf{k}) = -\hat{\boldsymbol{\Gamma}}(\mathbf{k})\,\hat{\boldsymbol{\tau}}^i(\mathbf{k}) \quad \forall \mathbf{k} \neq 0, \quad \hat{\mathbf{e}}_p^{i+1}(0) = 0 \quad \text{and} \quad \tilde{\mathbf{e}}_h^{i+1}(\tilde{\mathbf{k}}, x_3),\\
&\text{d)} \quad \mathbf{e}_p^{i+1}(\mathbf{x}) = \mathscr{F}_3^{-1}\Big[\hat{\mathbf{e}}_p^{i+1}(\mathbf{k})\Big] \quad \text{and} \quad \mathbf{e}_h^{i+1}(\mathbf{x}) = \mathscr{F}_2^{-1}\Big[\tilde{\mathbf{e}}_h^{i+1}(\tilde{\mathbf{k}}, x_3)\Big],\\
&\text{e)} \quad \mathbf{e}^{i+1}(\mathbf{x}) = \mathbf{e}_p^{i+1}(\mathbf{x}) + \mathbf{e}_h^{i+1}(\mathbf{x}),\\
&\text{f)} \quad \boldsymbol{\sigma}^{i+1}(\mathbf{x}) = \mathbf{L}(\mathbf{x}) \Big[\mathbf{E} + x_3\boldsymbol{\chi} + \mathbf{e}^{i+1}(\mathbf{x})\Big],\\
&\text{g)} \quad \text{Convergence test,}
\end{aligned} \tag{3.75}$$

where $\mathscr{F}_l$ and $\mathscr{F}_l^{-1}$ denote the Fourier transform and its inverse. Subscript l denotes the number of dimensions needed for the Fourier transform. Additionally, the periodic strain fields $(\mathbf{e}^p(\mathbf{x}), \hat{\mathbf{e}}^p(\mathbf{k}))$ are computed by the FFT algorithm in the 3 directions ($\mathscr{F}_3$) while the complementary fields $(\mathbf{e}^h(\mathbf{x}), \tilde{\mathbf{e}}^h(\tilde{\mathbf{k}}, x_3))$ need only the Fourier transformations along the 2 periodic directions of the plate ($\mathscr{F}_2$). The explicit calculation of the strains $\tilde{\mathbf{e}}^h(\tilde{\mathbf{k}}, x_3)$ is given in the appendix B.2.

For the convergence test, Moulinec and Suquet (1998) proposed a convergence criterion which ensures that all local equations (and more specifically the equilibrium equations) are accurately satisfied. In practice, this requirement is stronger than the convergence of the elastic energy. However, due to the fact that the effective elastic properties of the plate in this paper are directly obtained by the consideration of the elastic strain energy as described in section 3.2.4.1, it is logical to choose the energy criterion for the convergence of the algorithm (3.75). The iterative procedure is stopped at step $i+1$ when the relative increment between step i and step $i+1$ of strain energy is smaller than a prescribed value ς (typically $\varsigma = 10^{-4}$ in our calculations. This value ensures the convergence of the effective elastic properties of the plate).

3.3 Numerical Applications

Numerical applications of the previous theory are performed for two examples. The first example is the study of a laminate problem. The comparison is made with the closed-form solution. In the second example, we consider a plane problem related to an inclusion which is periodic along one direction of the horizontal plane of the plate. The homogenized stiffnesses obtained are compared

to those of a finite element model.

3.3.1 Laminate

Let us consider a symmetrical laminate which is made of four homogeneous layers having the same thickness. This laminate may be considered as having a periodic structure along direction x (problem 2D) so that it is possible to extract a unit cell presented in figure 3.4. The following parameters are used for numerical computations, $t = 0.1$, $l_1 = 0.1$ and $E_1 = 46\text{GPa}$, $\nu_1 = 0.3$, $E_2 = 10\text{GPa}$, $\nu_2 = 0.3$ (Young's modulus, Poisson's ratio of the phases 1 and 2 respectively).

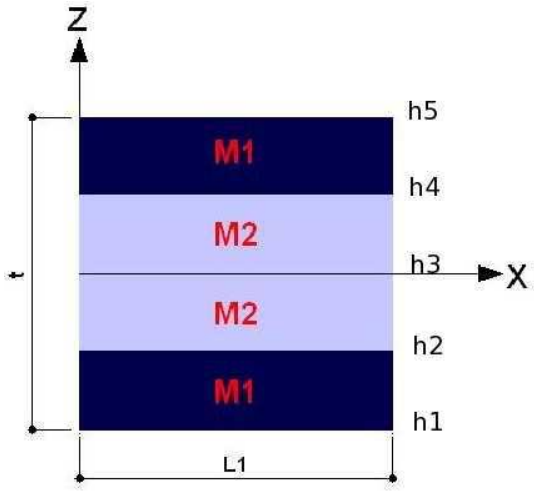

Figure 3.4: Elementary cell of 4-layer plate.

The effective properties of the plate are obtained by consideration of the strain energy defined in (3.72). It can be computed by an equivalent way in the Fourier space (see e.g. Soize (1993)). Due to the symmetry with respect to the middle surface, the coupling stiffness of the plate B is null. It is thus sufficient to identify the homogenized stiffnesses (A, D). The macroscopic fields used for the computation are: $(E = 1, \chi = 0)$, $(E = 0, \chi = 1)$. They allow to calculate the homogenized membrane and bending stiffnesses of the plate, respectively. The solution is compared to classical closed-form solutions of the effective stiffnesses of the Love-Kirchhoff plate given by the following relations:

$$A = \sum_{i=1}^{n}(h_i - h_{i-1})\frac{E_i}{1-\nu_i^2},\ B = \frac{1}{2}\sum_{i=1}^{n}(h_i^2 - h_{i-1}^2)\frac{E_i}{1-\nu_i^2},\ D = \frac{1}{3}\sum_{i=1}^{n}(h_i^3 - h_{i-1}^3)\frac{E_i}{1-\nu_i^2}, \quad (3.76)$$

where h_i (i=1,...,5) are the vertical positions of the bottom face, interfaces between the layers, and the top face of the plate respectively (see figure 3.4).

Table 3.1 presents the homogenized stiffnesses obtained from the present theory and from the closed-form solution. The values noted in parentheses represent the CPU times when using a

Table 3.1: Effective stiffnesses of the symmetrical 4-layer plate, $N_1 = 2^3$.

	Analytical solution	Present solution			
		$N_3 = 2^4$	$N_3 = 2^5$	$N_3 = 2^6$	No. itera.
A	3.0769	3.077 (0.4s)	3.077 (0.7s)	3.077 (1.2s)	10
D	0.0038	0.00382 (0.5s)	0.003805 (0.8s)	0.003802 (1.2s)	10

standard PC. The results obtained in table 3.1 are calculated by using a low number of discretized points along x-direction ($N_1 = 2^3$). That can be explained by the fact that the material properties are uniform in the horizontal plane of the plate. In addition, the results showed that the convergence of the solution toward the closed-form solution is fast so that a good approximation can be reached for a low number of discretization points along the z-direction ($N_3 = 2^6$). The iterative algorithm is stopped after 10 iterations for $\varsigma = 10^{-4}$. Figure 3.5 presents the variation profile of the average of elastic strain energy for the calculation of the membrane stiffness given in table 3.1. It can be observed that the strain energy converges rapidly after less than 10 iterations and that the value obtained for $\varsigma = 10^{-4}$ is stable when the iterative process is continued (up to 10^{-10}).

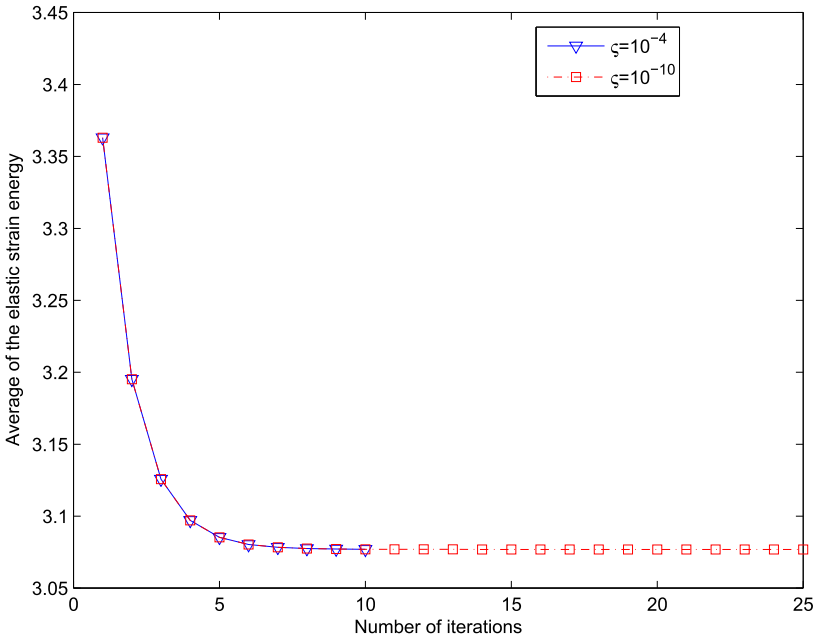

Figure 3.5: Convergence of the elastic strain energy.

The rate of convergence of the algorithm depends on the following parameters: the wave number N used in the Fourier transforms, the number of iterations during the iterative process,

the elastic properties of the reference medium and of the phases. The studies of the convergence of the basic iterative algorithm can be found in Moulinec and Suquet (1994, 1998); Michel et al. (1999). Improved algorithms for an arbitrary phase contrast are described by Michel et al. (2001) and Moulinec and Suquet (2003). These authors used a convergence criterium based on the vanishing of the local equilibrium equations. In the case of the plate, the local equilibrium does not suffice to insure the equilibrium, because it must be completed by the traction-free boundary condition on the faces of the plate. It is shown above that the energy computed with an accuracy of $1e-4$ remains stationary when the convergence process is continued and that the possible occurrence of a "plateau" is excluded. Bonnet (2007) considered also the convergence of the basic algorithm for the sum of the Neuman series. For a two-phase composite medium, the Lamé coefficients (λ, μ) of the homogeneous reference medium are related to the properties of the phases by:

$$\begin{aligned} \lambda &= \alpha\lambda_m + (1-\alpha)\lambda_i, \\ \mu &= \alpha\mu_m + (1-\alpha)\mu_i, \end{aligned} \tag{3.77}$$

where the subscripts m, i denote matrix and inclusion, respectively. For the properties of the previous reference medium, Michel et al. (1999), Moulinec and Suquet (1994, 1998) used $\alpha = 0.5$ to ensure the convergence of the local fields in the calculations of the basic algorithm. This value has been also used for the computations in the above laminate problem.

3.3.2 Plate with Periodic Inclusions

We consider in this section a panel with a periodic repartition of parallelipedic fibers. Figure 3.6 presents the 2D section of the panel structure and the corresponding unit cell. The following parameters are used for numerical calculations, $t_1 = 0.025$, $l_1 = 0.1$, $\nu_i = 0.3$, $t_2 = 0.025$, $t = 0.1$, $\nu_m = 0.3$.

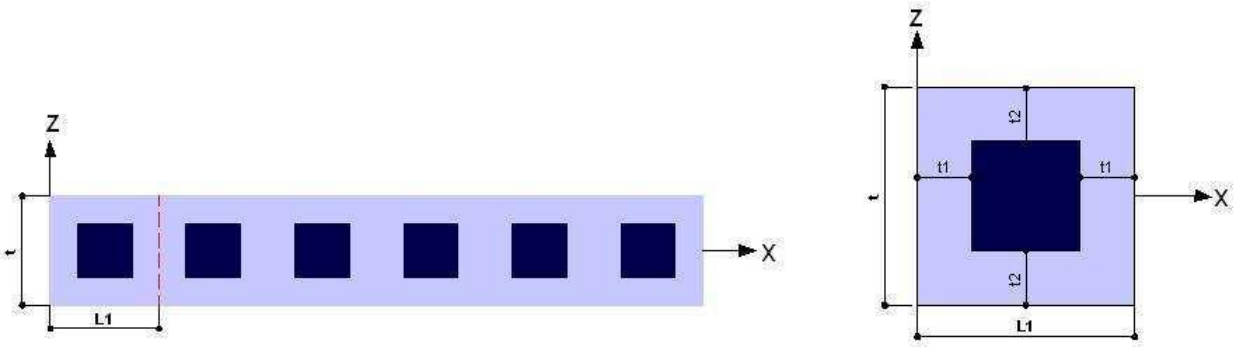

Figure 3.6: Panel with periodic inclusions and the related unit cell.

As for the case of the laminate, the calculation of the homogenized membrane stiffness of the plate is performed by using the uniform macroscopic strain condition ($E = 1$), while the computation of the effective bending stiffness is obtained by the condition ($\chi = 1$). The cell is

symmetrical in this example which leads obviously to null coupling stiffness. The approximate solution of the present model is validated by comparison with that of a finite element model. The finite element calculation is performed with a meshing which ensures the convergence of the elastic strain energy. The solution is obtained by using ABAQUS software and linear quadrilateral elements CPE4R (plane strain). Additionally, it can be seen that the periodic cell presents two axes of symmetry. As a consequence, it is sufficient to consider a quarter of the periodic cell (2D problem). Figures 3.7 and 3.8 present the displacement boundary conditions for the calculation of the homogenized stiffnesses A and D, respectively. The boundary conditions taking into account the symmetries of the period are obtained from the developments reported in the appendix. The measurement of a "relative error" is defined by the relationship:

$$\text{error}\,(\%) = \frac{M_c - M_m}{M_m} \times 100\% \tag{3.78}$$

where M_c is the solution obtained from the present model, and M_m is the one obtained from the FEM model.

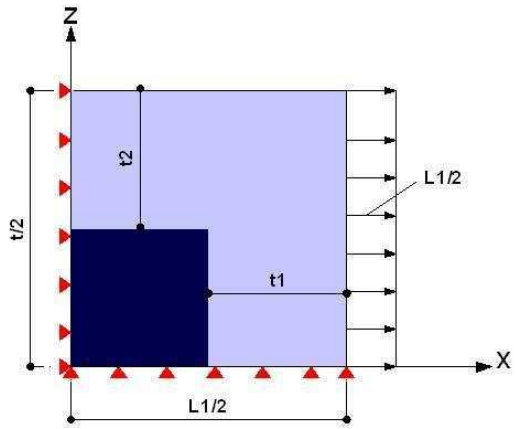

Figure 3.7: FEM model: displacement condition on a quarter of unit cell for calculation of A.

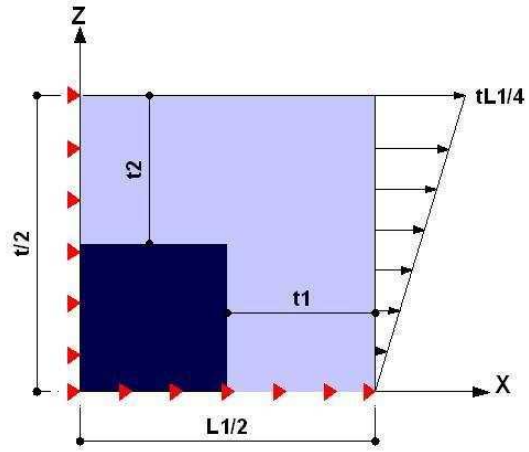

Figure 3.8: FEM model: displacement condition on a quarter of unit cell for calculation of D.

Table 3.2: Effective membrane stiffness of the panel plate, $E_i/E_m = 10, E_m = 1, \alpha = 0.5$.

N	FEM	Proposed solution		
		value (error %)	times (s)	No. itera.
2^4	0.16288	0.16209 (-0.485%)	0.9	15
2^5	0.16288	0.16257 (-0.19%)	3.4	16
2^6	0.16288	0.16279 (-0.055%)	12	16
2^7	0.16288	0.16287 (-0.006%)	50	16

Table 3.3: Effective bending stiffness of the panel plate, $E_i/E_m = 10, E_m = 1, \alpha = 0.5$.

N	FEM	Proposed solution		
		value (error %)	times (s)	No. itera.
2^4	1.0652e-4	1.0701e-4 (0.460%)	1	18
2^5	1.0652e-4	1.0659e-4 (0.066%)	4	18
2^6	1.0652e-4	1.0654e-4 (0.019%)	14	18
2^7	1.0652e-4	1.0654e-4 (0.019%)	57	18

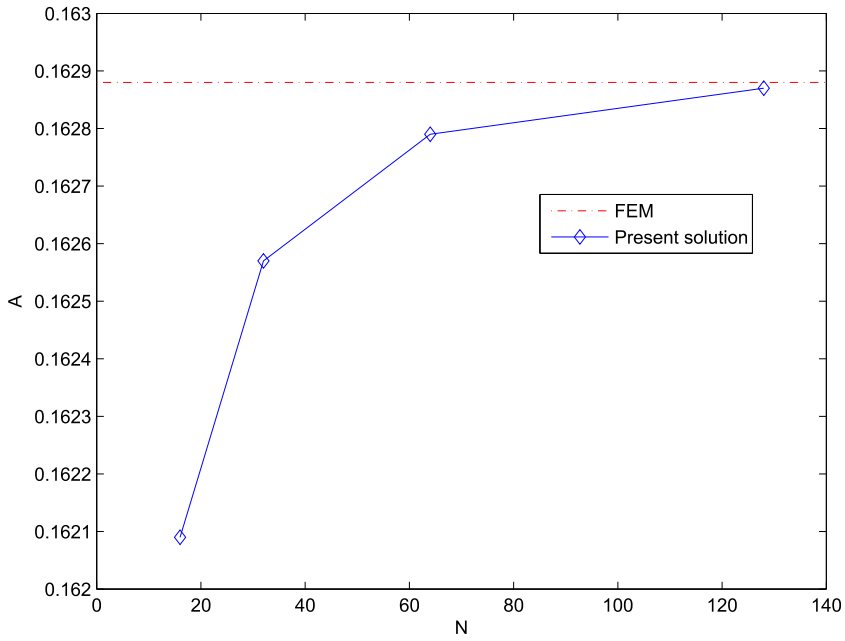

Figure 3.9: Comparison for A with the FEM solution.

Table 3.4: Effective membrane stiffness of the panel plate, $E_m/E_i = 1000, E_i = 1, \alpha = 0.65$.

N	FEM	Present solution		
		value (relative error %)	times (s)	No. itera.
2^4	58.495	58.363 (-0.226%)	0.6	8
2^5	58.495	58.472 (-0.039%)	2	9
2^6	58.495	58.502 (0.0120%)	7	9
2^7	58.495	58.506 (0.0188%)	28	9

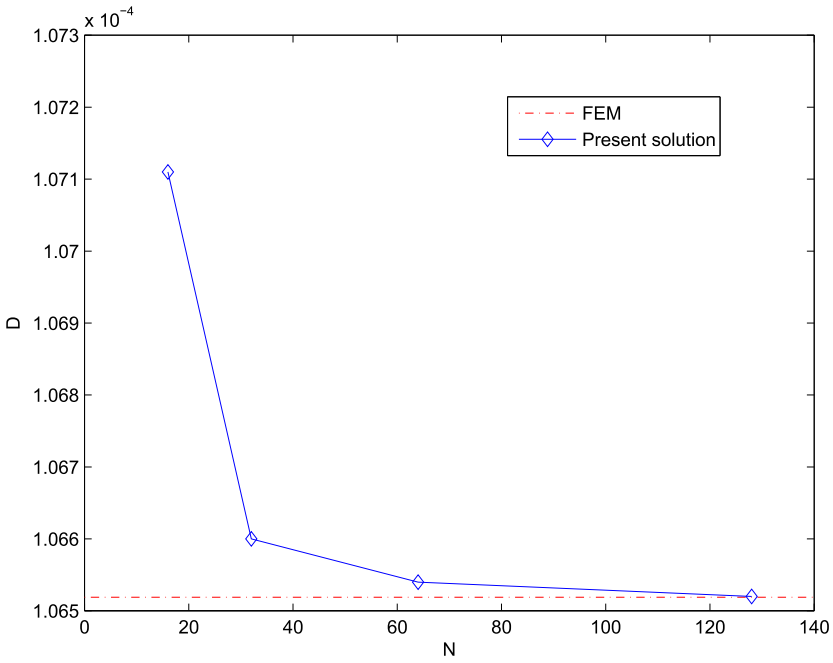

Figure 3.10: Comparison for D with the FEM solution.

Table 3.5: Homogenized bending stiffness of the panel plate, $E_m/E_i = 1000, E_i = 1, \alpha = 0.65$.

N	FEM	Present solution		
		value (relative error %)	times (s)	No. itera.
2^4	0.08225	0.08244 (0.231%)	0.5	8
2^5	0.08225	0.08230 (0.060%)	1.7	8
2^6	0.08225	0.08227 (0.024%)	6	8
2^7	0.08225	0.08226 (0.012%)	25	8

Tables 3.2 and 3.3 provide the comparison between the homogenized stiffnesses A and D obtained respectively by the present theory and by the finite element model. The space discretization defined in (3.73) is performed by using the same number of points along two directions, i.e. $N_1 = N_3 = N$. It can be seen that the homogenized properties are near to those obtained from the finite element model even for a low number of pixels. The variation profile of the solution in comparison with the FEM solution is presented in figures 3.9 and 3.10 where it can be seen that the bending stiffness and the membrane stiffness display an opposite variation with the spatial resolution of the image: the bending stiffness decreases with the spatial resolution while the membrane stiffness increases with the spatial resolution. Usually (Moulinec and Suquet, 1994, 1998), it is observed that the elastic energy decreases when increasing the spatial resolution in the case of a problem where a macroscopic strain is applied at the beginning of the iterative

process. Conversely (Bonnet, 2007), the dual method using an applied macroscopic stress leads to increasing values of the elastic energy. In the present case, a macroscopic strain is applied, but traction-free boundary conditions are taken into account along the boundaries of the plate. The mixed nature of the problem explains the different kinds of convergences observed in figures 3.9 and 3.10.

The reference medium is chosen according to Michel et al. (1999), Moulinec and Suquet (1994, 1998) with $\alpha = 0.5$. The CPU times and the number of iterations depend on the contrast between the phases and on the discretized number of points. As seen in tables 3.2 and 3.3 the calculation time for the problem with contrast $E_i/E_m = 10$ and stiffer inclusions increases with the number of discretization points. In practice, a difficulty of convergence was observed by other authors when using the present basic algorithm for composites with very stiff inclusions (Moulinec and Suquet, 1994, 1998; Michel et al., 1999; Bonnet, 2007). The accelerated scheme of Eyre and Milton (1999), the augmented Lagrangian method of Michel et al. (2001) or the dual solution (stress formulation) described in Bonnet (2007) could be considered to obtain a better convergence in this case.

Table 3.6: Homogenized membrane stiffness of the panel plate, $E_i = 0, E_m = 10$.

N	FEM	Present solution		
		value (relative error %)	times (s)	No. itera.
2^4	0.5840	0.5826 (-0.24%)	0.6	8
2^5	0.5840	0.5837 (-0.05%)	2	9
2^6	0.5840	0.5839 (-0.017%)	7	9
2^7	0.5840	0.5840 ($\sim$ 0.0%)	28	9

Table 3.7: Homogenized bending stiffness of the panel plate, $E_i = 0, E_m = 10$.

N	FEM	Present solution		
		value (relative error %)	times (s)	No. itera.
2^4	8.224e-4	8.242e-4 (0.219%)	0.6	8
2^5	8.224e-4	8.228e-4 (0.049%)	2	8
2^6	8.224e-4	8.225e-4 (0.012%)	6	8
2^7	8.224e-4	8.224e-4 ($\sim$ 0.0%)	25	8

Solutions for inclusions softer than the matrix or voids are also reported here, for which the parameter $\alpha = 0.65$ proposed by Bonnet (2007) has been used. Tables 3.4 and 3.5 present the comparison between the homogenized membrane and bending stiffnesses of the plate obtained from the present model and from the FEM model. The solutions are obtained for a contrast

$E_m/E_i = 1000$. It can be seen that the homogenized stiffnesses obtained from the present solution agree with those of the FEM even for a low resolution. The iterative procedure is stopped after about 8 iterations for a prescribed value of the relative error of 10^{-4}. Additionally, the CPU times obtained in tables 3.4 and 3.5 show the fastness of computation.

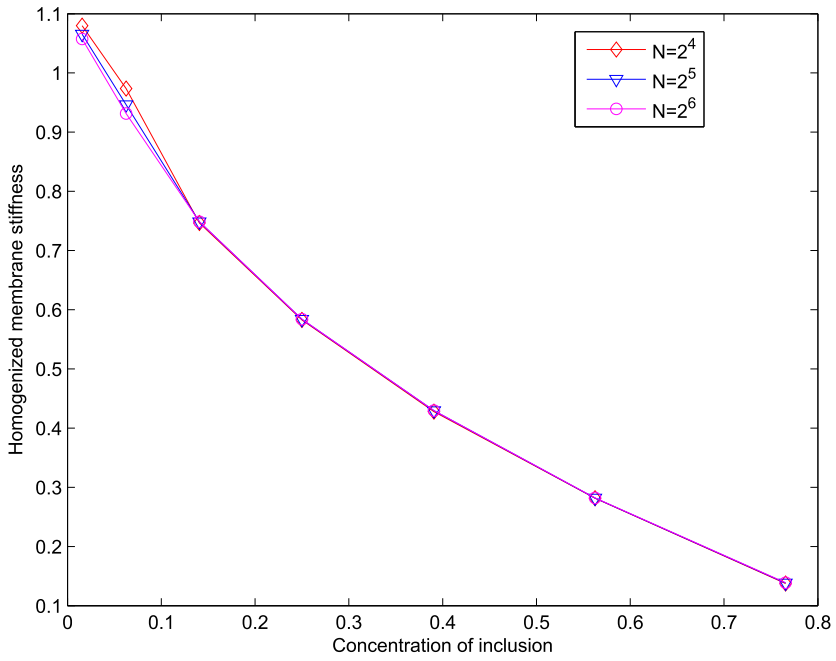

Figure 3.11: Variation of the membrane stiffness according to the volume fraction of inclusion.

For the plate with a periodic rectangular void, tables 3.6 and 3.7 present the comparison of the effective stiffnesses with those obtained by FEM. Elastic moduli $E_i = 0$, $E_m = 10$GPa are chosen for the computations. As previously, the results provide a good precision even for a low resolution. The CPU time increases with the number of discretization points, but it can be seen that in spite of the infinite contrast between voids and matrix, the iterations are stopped rapidly when the iterative scheme is stopped for a prescribed relative error of 10^{-4} (see tables 3.6 and 3.7).

To check the validity of the present solution for different volume fractions of voids , figures 3.11 and 3.12 present the homogenized stiffnesses of the plate in terms of the concentration of voids (the volume fraction of voids varies within $[1/64, 49/64]$) and of the number of discretized points in one direction N. As for the results obtained in tables 3.6 and 3.7 it can be seen that a number of wave-numbers of $N = 2^5$ in each direction is convenient to reach the convergence.

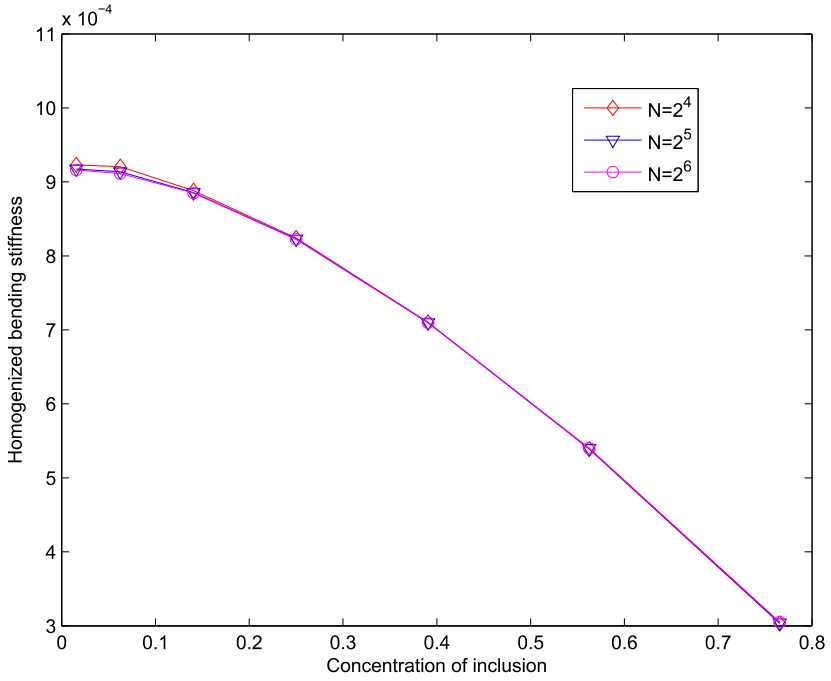

Figure 3.12: Variation of the bending stiffness according to the volume fraction of inclusion.

3.4 Conclusion of the Chapter

This chapter has presented a $\boldsymbol{\Gamma}$-operator for the media with mixed boundary conditions: periodicity conditions and traction-free boundary conditions. This operator computed from the properties of a "reference medium" has been used to obtain the solution on the cell period needed to obtain the effective properties of plates made of periodically distributed inhomogeneous cells. Applications were performed and the comparison of the results obtained here with those obtained from closed-form solutions and with finite element results have shown the accuracy and the speed of convergence of the series solution. The convergence is slow for very stiff inclusions. The solution could be improved by using the accelerated scheme of Eyre and Milton (1999), the augmented Lagrangian method of Michel et al. (2001) or the dual solution (stress formulation) described in Bonnet (2007). The numerical computations reported in this chapter have been performed for 2D-case. The application of the method described in this chapter to 3D problems increases the quantity of wave numbers by $N^{3/2}$. However, the high speed of the Fourier method can allow this increase of computational cost.

Chapter 4

Hashin-Shtrikman Variational Principle for Heterogeneous Plates

This chapter presents a Hashin-Shtrikman variational principle for heterogeneous plates which is similar to the well-known Hashin-Shtrikman variational principle. This variational principle is based on a self-adjoint $\boldsymbol{\Gamma}$-operator for a periodic medium with traction-free boundary conditions proposed by the authors (Nguyen et al., 2008b). This variational formulation enables to derive lower and upper bounds for the effective in-plane and out-of-plane elastic properties of the plate. Two applications of the general theory are considered: In-plane invariant polarization stresses are first used to derive the bounds proposed by Kolpakov (1999) for general heterogeneous plates. Next, n-phase plates whose constituents are statistically homogeneous in the in-plane directions are studied. The example of a two-phase material made of elastic isotropic materials is performed. The computed effective elastic properties of the plate are compared with those obtained from the classical Hashin-Shtrikman solutions (Hashin and Shtrikman, 1962a,b). The comparison of the relative differences yielded between both methods allows to evaluate the size effect of the heterogeneity.

4.1 Introduction

The prediction of the effective properties of heterogeneous media from the material properties and the geometrical arrangement of their constituting phases requires the solving of a boundary value problem on a representative volume. The characteristic size of this representative volume must be much greater than that of the microstructure to ensure that the material can accurately be treated as homogeneous with spatially constant averages. If the geometrical arrangement of the heterogeneities within the medium is perfectly described, the solving of any boundary value problem is possible. Practically however, only a few features of the geometry (typically the volume fraction of each phase and low-order correlation functions) are known. In such a case, effective properties can not be obtained exactly, but lower and upper bounds can be derived from

variational principles.

The application of variational methods to composite materials was initiated by Hill (1952) who recovered the so-called Voigt and Reuss bounds. A refined estimation of these bounds has been proposed by Kolpakov (1999); Kolpakov and Sheremet (1999); Kolpakov (1998) for the overall elastic properties of heterogeneous plates and beams. The classical variational principles usually require either compatible strain fields or self-balanced stress fields. The Hashin and Shtrikman (1962a,b) variational principles may be the most widely used since they lead to optimal bounds for the conductivity, bulk, and shear moduli of isotropic composites made of isotropic constituents. These principles are expressed in terms of polarization stress fields on which no constraint is imposed, contrarily to the case of classical variational formulations. Hashin and Shtrikman (1967) subsequently extended those principles to inhomogeneous elastic bodies subject to polarization fields and mixed boundary conditions. Willis (1977, 1981) summarized and generalized the Hashin-Shtrikman variational principles by using a $\mathbf{\Gamma}$-operator on an infinite medium.

In contrast, when the characteristic size of the macroscopic scale is not much greater than that of the heterogeneities, size effects require the use of a more sophisticated modelling, like higher-order and Cosserat media (see e.g. Sab (1991); Forest and Sab (1998); Forest et al. (2001); Yuan et al. (2008)), to capture the actual material response. Drugan and Willis (1996) and Drugan (2003) employed the Hashin-Shtrikman-Willis variational principles (Hashin and Shtrikman, 1962a,b; Willis, 1977, 1981) to derive nonlocal constitutive equations of infinite random linear elastic composite materials and the minimal size of the representative volume element (RVE). The size of the RVE has been extensively studied numerically (see e.g. Sab (1992); Gusev (1997); Terada et al. (1998); Kanit et al. (2003); Sab and Nedjar (2005)). This subject will also be considered in this work when analyzing random plates.

A new method for the computation of the effective elastic properties of a periodic plate was recently proposed by Nguyen et al. (2008b) and presented in the previous chapter. The theoretical derivations rely on a new $\mathbf{\Gamma}$-operator for periodic media with traction-free boundary conditions, on an iterative algorithm and on the use of the Fast Fourier Transform (FFT). This new method proves numerically efficient to estimate the effective elastic properties of plates.

Based on this previous work (Nguyen et al., 2008b), this chapter aims at formulating a Hashin-Shtrikman variational principle for heterogeneous plates that supplies bounds for the effective in-plane and out-of-plane elastic stiffnesses. The thickness and the period of the plate are assumed to be of the same order and much smaller than the in-plane typical characteristic size L of the plate (case $a = 1$). The stiffness constants of the plate can thus be computed by solving a boundary value problem on a unit cell. Two applications of the theory are considered. In-plane invariant polarization stresses are first used to refine the Voigt and Reuss bounds proposed by Kolpakov (1999) for general heterogeneous plates. Secondly, n-phase plates whose constituents are distributed randomly but in a statistically uniform manner in the in-plane directions are studied. The derived energy functional expressed in terms of the polarizations depends on the thickness-coordinate only and the computation of the effective elastic properties of the plate re-

quires the use of a two-point distribution function. The example of a two-phase plate made of isotropic materials is considered. The derived effective elastic properties of the plate are compared with those obtained with the classical Hashin-Shtrikman solutions (Hashin and Shtrikman, 1962a,b, 1965), and the comparison of the relative differences between two methods allows to predict the size effect of the heterogeneity.

This work is organized as follows. In section 2 a Hashin-Shtrikman variational principle for heterogeneous plates is derived. It is based on the $\mathbf{\Gamma}$-operator for periodic media with traction-free boundary conditions (Nguyen et al., 2008b) and on the classical Hashin-Shtrikman-Willis variational principles (Hashin and Shtrikman, 1962a,b; Willis, 1977, 1981; Drugan and Willis, 1996). This general variational formulation enables to derive lower and upper bounds for the effective elastic properties of heterogeneous plates. Section 3 presents an application of the results derived in section 2 to deterministic materials. In-plane polarization stress fields are assumed to be invariant, which allows for an explicitly solving of the localization elastic problem. In section 4, we apply the theory to random materials and derive the Hashin-Shtrikman variational formulation for plates whose constituents are distributed randomly but in a statistically uniform manner in the in-plane directions. The functional is expressed in terms of the in-plane invariant polarizations. Then a randomly distributed two-phase plate made of isotropic constituents is considered. An analysis of the effects of the size of heterogeneity is finally performed.

4.2 Theoretical Formulation

The unit cell Y that generates the plate by periodicity in the (x_1, x_2)-directions is the 3D domain:

$$Y = \left\{ \mathbf{x} \in \mathbf{R}^3,\, \mathbf{x} = (x_1, x_2, x_3),\, x_i \in \left]-\frac{l_i}{2}, \frac{l_i}{2}\right[,\, i = 1,2,3 \right\}. \tag{4.1}$$

The domain $\omega = \left]-\frac{l_1}{2}, \frac{l_1}{2}\right[\times \left]-\frac{l_2}{2}, \frac{l_2}{2}\right[$ is the middle surface of the cell. $\partial\omega$ is the boundary of ω and $\partial Y_l = \partial\omega \times \left]-\frac{t}{2}, \frac{t}{2}\right[(l_3 = t)$ is the lateral boundary of Y. The top and bottom surfaces of the cell are $\partial Y^{\pm} = \omega \times \{\pm\frac{t}{2}\}$. Mixed conditions are defined along the boundaries of the cell as follows: Periodic boundary conditions are assumed along ∂Y_l while traction-free boundary conditions are assumed along $\partial Y^{\pm}$. All formulations are performed under the assumption of a linear elastic behavior and small deformations of materials. The Greek indices belong to $\{1,2\}$ and the Latin indices to $\{1,2,3\}$.

The local elastic problem defined on Y is:

$$\begin{cases} \boldsymbol{\sigma}(\mathbf{x}) \,.\, \boldsymbol{\nabla} = 0,\ \boldsymbol{\sigma}(\mathbf{x}) = \mathbf{L}(\mathbf{x})\, \boldsymbol{\epsilon}(\mathbf{x}),\ \boldsymbol{\epsilon}(\mathbf{x}) = \mathbf{E} + x_3 \boldsymbol{\chi} + \mathbf{e}(\mathbf{v}^{per}(\mathbf{x})), \\ \mathbf{e}(\mathbf{v}^{per}(\mathbf{x})) = \mathbf{v}^{per}(\mathbf{x}) \otimes^s \boldsymbol{\nabla}, \\ \boldsymbol{\sigma}(\mathbf{x}) \,.\, \boldsymbol{e}_3 = 0 \quad \text{on } \partial Y^{\pm}, \\ \mathbf{v}^{per}(\mathbf{x}) \text{ periodic on } \partial Y_l, \quad \boldsymbol{\sigma}(\mathbf{x}) \,.\, \mathbf{n} \text{ anti-periodic on } \partial Y_l, \end{cases} \tag{4.2}$$

where the nabla operator $\boldsymbol{\nabla}$ is used to express the gradient and divergence operators ($\mathbf{v}^{per} \otimes \boldsymbol{\nabla} = v^{per}_{i,j}\, \boldsymbol{e}_i \otimes \boldsymbol{e}_j$, $\boldsymbol{\sigma} \,.\, \boldsymbol{\nabla} = \sigma_{ij,j}\, \boldsymbol{e}_i$). $\boldsymbol{e}_i$ are the vectors of an orthogonal basis of the space, $\mathbf{v}^{per}(\mathbf{x})$ is the (x_1, x_2)-periodic displacement field, $\mathbf{e}(\mathbf{v}^{per}(\mathbf{x}))$ the corresponding strain field (the symmetrical part of $\mathbf{v}^{per}(\mathbf{x}) \otimes \boldsymbol{\nabla}$), $\boldsymbol{\epsilon}(\mathbf{x})$ the total strain field, $\mathbf{L}(\mathbf{x})$ the elasticity tensor and $\boldsymbol{\sigma}(\mathbf{x})$ the total stress field. The macroscopic membrane strains, $\mathbf{E}$, and the macroscopic curvatures, $\boldsymbol{\chi}$, only have in-plane components ($E_{j3} = 0, \chi_{j3} = 0$).

Once the solution of the boundary value problem (4.2) is obtained, the homogenized elastic properties of the plate are derived from the elastic strain energy expressed by:

$$W = \frac{1}{2} < \boldsymbol{\sigma}(\mathbf{x})\, \boldsymbol{\epsilon}(\mathbf{x}) > = \frac{1}{2} \left(\mathbf{N}\, \mathbf{E} + \mathbf{M}\, \boldsymbol{\chi} \right), \tag{4.3}$$

where the brackets $< . >$ correspond to the following operator on the unit cell:

$$< f > = \frac{1}{|\omega|} \int_Y f(\mathbf{x})\, d\mathbf{x}. \tag{4.4}$$

$\mathbf{N}$ is the membrane stress tensor and $\mathbf{M}$ is the flexure moment tensor:

$$N_{\alpha\beta} = < \sigma_{\alpha\beta} >, \quad M_{\alpha\beta} = < x_3\, \sigma_{\alpha\beta} > . \tag{4.5}$$

Equation (4.3) can be interpreted as the macro-homogeneity condition of Hill-Mandel which ensures that the macroscopic elastic strain energy of a given representative volume element is equal to the integral of the microscopic elastic strain energy within this volume.

Hence, the strain energy per unit area becomes:

$$W = \frac{1}{2} < \boldsymbol{\sigma}(\mathbf{x})\, \boldsymbol{\epsilon}(\mathbf{x}) > = \frac{1}{2} \left(\mathbf{E}\mathbf{A}\mathbf{E} + 2\mathbf{E}\mathbf{B}\boldsymbol{\chi} + \boldsymbol{\chi}\mathbf{D}\boldsymbol{\chi} \right), \tag{4.6}$$

where the homogenized elastic tensors $(\mathbf{A}, \mathbf{B}, \mathbf{D})$ of the plate are:

$$\mathbf{N} = \mathbf{A}\, \mathbf{E} + \mathbf{B}\, \boldsymbol{\chi}, \quad \text{and} \quad \mathbf{M} = \mathbf{B}^T\, \mathbf{E} + \mathbf{D}\, \boldsymbol{\chi}, \tag{4.7}$$

where the superscript T is the transposition operator.

Moreover, the elastic problem (4.2) may be solved by introducing a homogeneous reference medium of stiffness $\mathbf{L}^o$ and a polarization field, $\boldsymbol{\tau}$:

$$\begin{cases} \boldsymbol{\sigma}(\mathbf{x}) \,.\, \boldsymbol{\nabla} = 0,\ \boldsymbol{\sigma}(\mathbf{x}) = \mathbf{L}^o\, \boldsymbol{\epsilon}(\mathbf{x}) + \boldsymbol{\tau}(\mathbf{x}),\ \boldsymbol{\epsilon}(\mathbf{x}) = \mathbf{E} + x_3 \boldsymbol{\chi} + \mathbf{e}(\mathbf{v}^{per}(\mathbf{x})), \\ \mathbf{e}(\mathbf{v}^{per}(\mathbf{x})) = \mathbf{v}^{per}(\mathbf{x}) \otimes^s \boldsymbol{\nabla}, \\ \boldsymbol{\sigma}(\mathbf{x}) \,.\, \boldsymbol{e}_3 = 0 \quad \text{on } \partial Y^{\pm}, \\ \mathbf{v}^{per}(\mathbf{x}) \text{ periodic on } \partial Y_l, \quad \boldsymbol{\sigma}(\mathbf{x}) \,.\, \mathbf{n} \text{ anti-periodic on } \partial Y_l, \end{cases} \tag{4.8}$$

where the polarization field $\boldsymbol{\tau}(\mathbf{x})$ is given by:

$$\boldsymbol{\tau}(\mathbf{x}) = \Delta\mathbf{L}(\mathbf{x})\, \boldsymbol{\epsilon}(\mathbf{x}) \quad \text{with} \quad \Delta\mathbf{L}(\mathbf{x}) = \mathbf{L}(\mathbf{x}) - \mathbf{L}^o. \tag{4.9}$$

We note that the elastic problem (4.8) with $(\mathbf{E}, \boldsymbol{\chi}, \boldsymbol{\tau})$ can be split into two auxiliary problems:

- An auxiliary problem identical to the elastic problem (4.8) but in which $\boldsymbol{\tau} = 0$. It coincides with the set of equations (4.2) for $\mathbf{L}(\mathbf{x}) = \mathbf{L}^o$ and admits the fields $(\boldsymbol{\sigma}^o, \boldsymbol{\epsilon}^o, \mathbf{v}_o^{per})$ as a solution.
- Another auxiliary problem identical to the elastic problem (4.8) but in which $\mathbf{E} = 0$ and $\boldsymbol{\chi} = 0$. This second auxiliary admits the fields $(\boldsymbol{\sigma}^{per}, \mathbf{e}(\mathbf{u}^{per}), \mathbf{u}^{per})$ as a solution.

As a result, the fields solution of the elastic problem (4.8) with $(\mathbf{E}, \boldsymbol{\chi}, \boldsymbol{\tau})$ are the superposition of $(\boldsymbol{\sigma}^o, \boldsymbol{\epsilon}^o, \mathbf{v}_o^{per})$ with $(\boldsymbol{\sigma}^{per}, \mathbf{e}(\mathbf{u}^{per}), \mathbf{u}^{per})$.

4.2.1 Homogeneous Solutions in the Reference Medium

This section is devoted to the first auxiliary problem introduced in the previous section. The fields $(\boldsymbol{\sigma}^o(\mathbf{x}), \boldsymbol{\epsilon}^o(\mathbf{x}), \mathbf{v}_o^{per}(\mathbf{x}))$ which are solutions of the local elastic problem (4.2) defined on the reference medium with stiffness $\mathbf{L}^o$ are derived from the following system of equations:

$$\begin{cases} \boldsymbol{\sigma}^o(\mathbf{x}) \,.\, \boldsymbol{\nabla} = 0,\ \boldsymbol{\sigma}^o(\mathbf{x}) = \mathbf{L}^o\, \boldsymbol{\epsilon}^o(\mathbf{x}),\ \boldsymbol{\epsilon}^o(\mathbf{x}) = \mathbf{E} + x_3 \boldsymbol{\chi} + \mathbf{e}^o(\mathbf{v}_o^{per}(\mathbf{x})), \\ \mathbf{e}^o(\mathbf{v}_o^{per}(\mathbf{x})) = \mathbf{v}_o^{per}(\mathbf{x}) \otimes^s \boldsymbol{\nabla}, \\ \boldsymbol{\sigma}^o(\mathbf{x}) \,.\, \boldsymbol{e}_3 = 0 \quad \text{on} \quad \partial Y^{\pm}, \\ \mathbf{v}_o^{per}(\mathbf{x}) \text{ periodic on } \partial Y_l, \quad \boldsymbol{\sigma}^o(\mathbf{x}) \,.\, \mathbf{n} \text{ anti-periodic on } \partial Y_l, \end{cases} \tag{4.10}$$

This problem has a trivial solution, $(\boldsymbol{\sigma}^o(x_3), \boldsymbol{\epsilon}^o(x_3), \mathbf{v}_o^{per}(x_3))$, that depends on x_3 only. This trivial solution can be derived directly by solving the ordinary differential equations in x_3 for

given boundary conditions. To do so, the stresses and strains are split into their in-plane and out-of-plane components:

$$\begin{cases} \boldsymbol{\sigma}^o_{(i)} = (\sigma^o_{11}, \sigma^o_{22}, \sigma^o_{12})^T, \quad \boldsymbol{\sigma}^o_{(o)} = (\sigma^o_{33}, \sigma^o_{23}, \sigma^o_{13})^T, \\ \boldsymbol{\epsilon}^o_{(i)} = (\epsilon^o_{11}, \epsilon^o_{22}, 2\epsilon^o_{12})^T, \quad \boldsymbol{\epsilon}^o_{(o)} = (\epsilon^o_{33}, 2\epsilon^o_{23}, 2\epsilon^o_{13})^T, \end{cases} \tag{4.11}$$

where the indices (i) and (o) indicate the in-plane and out-of-plane components, respectively. Similarly, the reference elastic tensor $\mathbf{L}^o$ is also split into four 3×3 matrices: The in-plane components $\mathbf{L}^o_{(i)(i)}$, the coupling components $\mathbf{L}^o_{(i)(o)}$ and $\mathbf{L}^o_{(o)(i)}$, and the out-of-plane components $\mathbf{L}^o_{(o)(o)}$. $\mathbf{L}^o_{(i)(i)}$ and $\mathbf{L}^o_{(o)(o)}$ are symmetrical while $\mathbf{L}^o_{(i)(o)}$ and $\mathbf{L}^o_{(o)(i)}$ verify $(\mathbf{L}^o_{(i)(o)})^T = \mathbf{L}^o_{(o)(i)}$.

The constitutive equation thus becomes:

$$\begin{cases} \boldsymbol{\sigma}^o_{(i)}(x_3) = \mathbf{L}^o_{(i)(i)} \boldsymbol{\epsilon}^o_{(i)}(x_3) + \mathbf{L}^o_{(i)(o)} \boldsymbol{\epsilon}^o_{(o)}(x_3), \\ \boldsymbol{\sigma}^o_{(o)}(x_3) = \mathbf{L}^o_{(o)(i)} \boldsymbol{\epsilon}^o_{(i)}(x_3) + \mathbf{L}^o_{(o)(o)} \boldsymbol{\epsilon}^o_{(o)}(x_3). \end{cases} \tag{4.12}$$

One observes that the in-plane strains are equal to the macroscopic strains, i.e., $\boldsymbol{\epsilon}^o_{(i)}(x_3) = \mathbf{E}_{(i)} + x_3 \boldsymbol{\chi}_{(i)}$, since the in-plane components of $\mathbf{e}^o(\mathbf{v}^{per}_o)$ are zero. Moreover, from the balance equations and the boundary conditions, one finds out that the out-of-plane stresses $\boldsymbol{\sigma}^o_{(o)}(x_3)$ are also zero. Hence, the out-of-plane strains can be expressed in terms of the in-plane strains:

$$\boldsymbol{\epsilon}^o_{(o)}(x_3) = -(\mathbf{L}^o_{(o)(o)})^{-1} \mathbf{L}^o_{(o)(i)} \boldsymbol{\epsilon}^o_{(i)}(x_3). \tag{4.13}$$

Substituting (4.13) into the first equation of (4.12), one links the in-plane stresses to the in-plane strains:

$$\boldsymbol{\sigma}^o_{(i)}(x_3) = \mathbf{L}^o_{(s)} \boldsymbol{\epsilon}^o_{(i)}(x_3), \tag{4.14}$$

where

$$\mathbf{L}^o_{(s)} = \mathbf{L}^o_{(i)(i)} - \mathbf{L}^o_{(i)(o)} (\mathbf{L}^o_{(o)(o)})^{-1} \mathbf{L}^o_{(o)(i)} = (\mathbf{L}^{o-1}_{(i)(i)})^{-1} \tag{4.15}$$

is the plane-stress elastic stiffness matrix of the reference medium.

4.2.2 The Γ-Operator

This section is devoted to the second auxiliary problem introduced in section 4.2. This second auxiliary problem corresponds to Eqs. (4.8) in which $\mathbf{E} = 0$ and $\boldsymbol{\chi} = 0$:

$$\begin{cases} \boldsymbol{\sigma}^{per}(\mathbf{x}) \,.\, \boldsymbol{\nabla} = 0,\ \boldsymbol{\sigma}^{per}(\mathbf{x}) = \mathbf{L}^o\, \mathbf{e}(\mathbf{u}^{per}(\mathbf{x})) + \boldsymbol{\tau}(\mathbf{x}), \\ \\ \mathbf{e}(\mathbf{u}^{per}(\mathbf{x})) = \mathbf{u}^{per}(\mathbf{x}) \otimes^s \boldsymbol{\nabla}, \\ \\ \boldsymbol{\sigma}^{per}(\mathbf{x}) \,.\, \boldsymbol{e}_3 = 0 \quad \text{on} \quad \partial Y^{\pm}, \\ \\ \mathbf{u}^{per}(\mathbf{x}) \text{ periodic on } \partial Y_l, \quad \boldsymbol{\sigma}^{per}(\mathbf{x}) \,.\, \mathbf{n} \text{ anti-periodic on } \partial Y_l, \end{cases} \tag{4.16}$$

where the polarization stress tensor is given by Eq. (4.9). Eqs. (4.16) defines a $\boldsymbol{\Gamma}$-operator which expresses the total strain $\mathbf{e}(\mathbf{x})$ in terms of $\boldsymbol{\tau}$:

$$\mathbf{e} = -\boldsymbol{\Gamma}\boldsymbol{\tau} \tag{4.17}$$

This work aims at obtaining an explicit expression for the $\boldsymbol{\Gamma}$-operator, in order to derive a Hashin-Shtrikman variational principle. Following the procedure of Nguyen et al. (2008b), the field $\mathbf{u}^{per}(\mathbf{x})$ solution of Eqs. (4.16) is split into two terms: $\mathbf{u}^{per}(\mathbf{x}) = \mathbf{u}^p(\mathbf{x}) + \mathbf{u}^h(\mathbf{x})$. $\mathbf{u}^p(\mathbf{x})$ is obtained with the standard periodicity conditions in the x_3-direction and the complementary term $\mathbf{u}^h(\mathbf{x})$ enables to recover the stress-free boundary condition. Likewise, the total strain and the $\boldsymbol{\Gamma}$-operator are expressed as $\mathbf{e} = \mathbf{e}^p + \mathbf{e}^h$ and $\boldsymbol{\Gamma} = \boldsymbol{\Gamma}_p + \boldsymbol{\Gamma}_h$ where $\mathbf{e}^p$ and $\boldsymbol{\Gamma}_p$ correspond to the standard periodic problem and $\mathbf{e}^h$ and $\boldsymbol{\Gamma}_h$ to the complementary problem.

The boundary value problem (4.16) can be solved by expanding the polarization stress $\boldsymbol{\tau}(\mathbf{x}) \in \mathbf{L}^2(Y)$ into three-dimensional Fourier series (see Eq. (3.32)). The periodic strain field $\mathbf{e}^p(\mathbf{x})$ solution of Eqs. (4.16) is derived from:

$$\begin{cases} \boldsymbol{\sigma}^p(\mathbf{x}) \,.\, \boldsymbol{\nabla} = 0,\ \boldsymbol{\sigma}^p(\mathbf{x}) = \mathbf{L}^o\, \mathbf{e}^p(\mathbf{x}) + \boldsymbol{\tau}(\mathbf{x}),\ \mathbf{e}^p(\mathbf{x}) = \mathbf{u}^p(\mathbf{x}) \otimes^s \boldsymbol{\nabla}, \\ \\ \mathbf{u}^p(\mathbf{x}) \text{ periodic on } \partial Y, \quad \boldsymbol{\sigma}^p(\mathbf{x}) \,.\, \mathbf{n} \text{ anti-periodic on } \partial Y. \end{cases} \tag{4.18}$$

$\mathbf{e}^p(\mathbf{x})$ can be explicitly derived in the Fourier space (see Suquet (1990); Moulinec and Suquet (1994) for details). It is then used to define the corresponding self-adjoint periodic $\boldsymbol{\Gamma}_p$-operator defined by:

$$\mathbf{e}^p(\mathbf{x}) = -\frac{1}{|Y|} \int_Y \boldsymbol{\Gamma}_p(\mathbf{x} - \mathbf{x}')\, \boldsymbol{\tau}(\mathbf{x}')\, d\mathbf{x}'. \tag{4.19}$$

In contrast, the strain field $\mathbf{e}^h(\mathbf{x})$ and the related operator $\mathbf{\Gamma}_h(\mathbf{x})$ are derived by solving:

$$\begin{cases} \boldsymbol{\sigma}^h(\mathbf{x}) \,.\, \boldsymbol{\nabla} = 0,\ \boldsymbol{\sigma}^h(\mathbf{x}) = \mathbf{L}^o\, \mathbf{e}^h(\mathbf{x}),\ \mathbf{e}^h(\mathbf{x}) = \mathbf{u}^h(\mathbf{x}) \otimes^s \boldsymbol{\nabla}, \\ \\ \sigma^h_{j3}(\mathbf{x}) = -\sigma^p_{j3}(\mathbf{x}) \quad \text{on} \quad \partial Y^{\pm}, \\ \\ \mathbf{u}^h(\mathbf{x}) \text{ periodic on } \partial Y_l, \quad \boldsymbol{\sigma}^h(\mathbf{x}) \,.\, \mathbf{n} \text{ anti-periodic on } \partial Y_l. \end{cases} \tag{4.20}$$

Eqs. (4.20) were solved by Nguyen et al. (2008b) by using Fourier transforms in the periodic (x_1, x_2)-directions. $\mathbf{e}^h$ and the corresponding operator $\mathbf{\Gamma}_h$ are linked by:

$$\mathbf{e}^h(\mathbf{x}) = -\frac{1}{|Y|} \int_Y \mathbf{\Gamma}_h(\tilde{\mathbf{x}} - \tilde{\mathbf{x}}', x_3, x_3')\, \boldsymbol{\tau}(\mathbf{x}')\, d\mathbf{x}', \tag{4.21}$$

where the $\mathbf{\Gamma}_h$-operator is periodic in the (x_1, x_2)-directions and $(\tilde{\mathbf{x}} - \tilde{\mathbf{x}}', x_3, x_3')$ holds for $(x_1 - x_1', x_2 - x_2', x_3, x_3')$ (see appendix B for details).

Since $\mathbf{\Gamma} = \mathbf{\Gamma}_p + \mathbf{\Gamma}_h$ and since $\mathbf{\Gamma}$ is a self-adjoint operator, $\mathbf{\Gamma}_h$ also is a self-adjoint operator. The self-adjoint character of $\mathbf{\Gamma}$ can be directly inferred from Eqs. (4.16). To do so, let us consider a kinematically admissible field, $\mathbf{e}(\mathbf{x}) \in \mathscr{U}$, and a statically admissible stress field, $\boldsymbol{\sigma}(\mathbf{x}) \in \mathscr{S}$, where:

$$\mathscr{U} = \Big\{ \mathbf{e}(\mathbf{x}) \Big/ \mathbf{e}(\mathbf{x}) = \mathbf{u}^{per}(\mathbf{x}) \otimes^s \boldsymbol{\nabla},\ \mathbf{u}^{per}(\mathbf{x}) \text{ periodic on } \partial Y_l \Big\}, \tag{4.22}$$

$$\mathscr{S} = \Big\{ \boldsymbol{\sigma}(\mathbf{x}) \Big/ \boldsymbol{\sigma}(\mathbf{x}) \,.\, \boldsymbol{\nabla} = 0,\ \boldsymbol{\sigma}(\mathbf{x}) \,.\, \boldsymbol{e}_3 = 0 \text{ on } \partial Y^{\pm},\ \boldsymbol{\sigma}(\mathbf{x}) \,.\, \mathbf{n} \text{ anti-periodic on } \partial Y_l \Big\}. \tag{4.23}$$

For any fields $(\boldsymbol{\sigma}_1, \mathbf{e}_1)$ and $(\boldsymbol{\sigma}_2, \mathbf{e}_2)$ solution of Eqs. (4.16) with polarization fields $\boldsymbol{\tau}_1$ and $\boldsymbol{\tau}_2$, respectively, $\boldsymbol{\sigma}_1$ and $\boldsymbol{\sigma}_2$ are statically admissible and $\mathbf{e}_1$ and $\mathbf{e}_2$ are kinematically admissible. From Green's theorem, they verify:

$$< \boldsymbol{\sigma}_1\, \mathbf{e}_2 >_Y = 0, \quad \text{and} \quad < \boldsymbol{\sigma}_2\, \mathbf{e}_1 >_Y = 0. \tag{4.24}$$

Substituting the stress field, $\boldsymbol{\sigma} = \mathbf{L}^o \mathbf{e} + \boldsymbol{\tau}$, into Eq. (4.24) yields:

$$< \boldsymbol{\tau}_1\, \mathbf{e}_2 >_Y = - < \mathbf{e}_1 \mathbf{L}^o \mathbf{e}_2 >_Y, \quad < \boldsymbol{\tau}_2\, \mathbf{e}_1 >_Y = - < \mathbf{e}_2 \mathbf{L}^o \mathbf{e}_1 >_Y . \tag{4.25}$$

From the symmetry of the elastic tensor $\mathbf{L}^o$, we thus have $< \boldsymbol{\tau}_1\, \mathbf{e}_2 >_Y = < \boldsymbol{\tau}_2\, \mathbf{e}_1 >_Y$. The $\mathbf{\Gamma}$-operator links strains to polarization stresses:

$$\mathbf{e}_1 = -\mathbf{\Gamma} \boldsymbol{\tau}_1 \quad \text{and} \quad \mathbf{e}_2 = -\mathbf{\Gamma} \boldsymbol{\tau}_2. \tag{4.26}$$

Therefore,

$$< \boldsymbol{\tau}_1 \, \boldsymbol{\Gamma} \boldsymbol{\tau}_2 >_Y = < \boldsymbol{\tau}_2 \, \boldsymbol{\Gamma} \boldsymbol{\tau}_1 >_Y = < \mathbf{e}_1 \mathbf{L}^o \mathbf{e}_2 >_Y \quad \forall \boldsymbol{\tau}_1, \boldsymbol{\tau}_2, \tag{4.27}$$

which proves that $\boldsymbol{\Gamma}$ is a self-adjoint operator. Setting $\boldsymbol{\tau}_1 = \boldsymbol{\tau}_2$ in Eq. (4.27) also shows that $\boldsymbol{\Gamma}$ is positive. Combining Eq. (4.27) with Eq. (4.26) yields: $\boldsymbol{\Gamma} = \boldsymbol{\Gamma} \, \mathbf{L}^o \, \boldsymbol{\Gamma}$. Finally, since $\boldsymbol{\Gamma}_p$ is a self-adjoint operator, $\boldsymbol{\Gamma}_h$ also is a self-adjoint operator and verifies:

$$< \boldsymbol{\tau}_1 \, \mathbf{e}_2^h >_Y = < \boldsymbol{\tau}_2 \, \mathbf{e}_1^h >_Y \quad \text{or} \quad < \boldsymbol{\tau}_1 \, \boldsymbol{\Gamma}_h \boldsymbol{\tau}_2 >_Y = < \boldsymbol{\tau}_2 \, \boldsymbol{\Gamma}_h \boldsymbol{\tau}_1 >_Y \, . \tag{4.28}$$

4.2.3 The Hashin-Shtrikman Functional

This section introduces a variational formulation for heterogeneous plates. This variational formulation is based on the well-known variational principle of Hashin and Shtrikman (1962a,b, 1967) and Willis (1981) as well as on the $\boldsymbol{\Gamma}$-operator introduced in section 4.2.2.

First, the expressions $\boldsymbol{\epsilon}(\mathbf{x}) = \boldsymbol{\epsilon}^o(\mathbf{x}) + \mathbf{e}(\mathbf{u}^{per}(\mathbf{x}))$ and $\boldsymbol{\sigma}(\mathbf{x}) = \boldsymbol{\sigma}^o(\mathbf{x}) + \boldsymbol{\sigma}^{per}(\mathbf{x})$ are substituted into expression of the average strain energy (4.6):

$$W = \frac{1}{2} < \boldsymbol{\sigma} \, \boldsymbol{\epsilon} > = \frac{1}{2} < \boldsymbol{\sigma} \, \boldsymbol{\epsilon}^o > \, . \tag{4.29}$$

The above equation was obtained by noting that $< \boldsymbol{\sigma} \, \mathbf{e} > = 0$ for any $\mathbf{e}(\mathbf{x}) \in \mathscr{U}$ and $\boldsymbol{\sigma}(\mathbf{x}) \in \mathscr{S}$. Moreover, since $\boldsymbol{\sigma}^{per}(\mathbf{x}) = \mathbf{L}^o \, \mathbf{e}(\mathbf{x}) + \boldsymbol{\tau}(\mathbf{x})$, $\boldsymbol{\epsilon} = \Delta \mathbf{L}^{-1} \, \boldsymbol{\tau}$ and $\mathbf{e} = -\boldsymbol{\Gamma} \boldsymbol{\tau}$, we have:

$$\begin{aligned} \boldsymbol{\epsilon}^o \, \boldsymbol{\sigma} &= \boldsymbol{\epsilon}^o \, (\boldsymbol{\sigma}^o + \mathbf{L}^o \mathbf{e} + \boldsymbol{\tau}) = \boldsymbol{\epsilon}^o \, \boldsymbol{\sigma}^o + \boldsymbol{\epsilon}^o \, \mathbf{L}^o \, \mathbf{e} + \boldsymbol{\epsilon}^o \boldsymbol{\tau} + \boldsymbol{\tau} \boldsymbol{\epsilon}^o - \boldsymbol{\tau} \boldsymbol{\epsilon}^o \\ &= \boldsymbol{\epsilon}^o \mathbf{L}^o \boldsymbol{\epsilon}^o + \boldsymbol{\epsilon}^o \mathbf{L}^o \mathbf{e} + 2 \boldsymbol{\tau} \boldsymbol{\epsilon}^o - \boldsymbol{\tau} (\boldsymbol{\epsilon} - \mathbf{e}) \\ &= \boldsymbol{\epsilon}^o \mathbf{L}^o \boldsymbol{\epsilon}^o + \boldsymbol{\epsilon}^o \mathbf{L}^o \mathbf{e} + 2 \boldsymbol{\tau} \boldsymbol{\epsilon}^o - \boldsymbol{\tau} \, \Delta \mathbf{L}^{-1} \, \boldsymbol{\tau} - \boldsymbol{\tau} \, \boldsymbol{\Gamma} \boldsymbol{\tau}. \end{aligned} \tag{4.30}$$

Since $< \boldsymbol{\sigma}^o \, \mathbf{e} > = 0$ for $\mathbf{e}(\mathbf{x}) \in \mathscr{U}$ and $\boldsymbol{\sigma}^o(\mathbf{x}) \in \mathscr{S}$, the term $\boldsymbol{\epsilon}^o \mathbf{L}^o \mathbf{e}$ vanishes from Eq. (4.30). The total potential energy can thus be expressed in terms of the polarization field under a quadratic form:

$$W(\boldsymbol{\tau}) = \frac{1}{2} < \boldsymbol{\epsilon}^o \mathbf{L}^o \boldsymbol{\epsilon}^o > + \frac{1}{2} < 2 \boldsymbol{\tau} \boldsymbol{\epsilon}^o - \boldsymbol{\tau} \, \Delta \mathbf{L}^{-1} \, \boldsymbol{\tau} - \boldsymbol{\tau} \, \boldsymbol{\Gamma} \boldsymbol{\tau} > \, . \tag{4.31}$$

The previous expression is a Hashin-Shtrikman functional (Hashin and Shtrikman, 1962a,b, 1967; Willis, 1977, 1981) in which the $\boldsymbol{\Gamma}$-operator corresponds to a periodic plate with traction-free boundary conditions. This expression will be used in the next section to supply lower and upper bounds for the effective elastic properties of the plate.

4.2.4 Extreme Conditions on the Functional

The extreme conditions on the energy are derived as follows: A small variation of the polarization field $\boldsymbol{\tau}$ is performed and the corresponding difference in energy (4.31), $\Delta W(\boldsymbol{\tau}) = W(\boldsymbol{\tau} + \delta\boldsymbol{\tau}) - W(\boldsymbol{\tau})$, is calculated. The second-order variation of the functional is found to be:

$$\delta^2 W(\boldsymbol{\tau}) = -\frac{1}{2} < \delta\boldsymbol{\tau}\,(\Delta\mathbf{L}^{-1} + \boldsymbol{\Gamma})\,\delta\boldsymbol{\tau} > . \tag{4.32}$$

Since $\boldsymbol{\Gamma}$ is positive, if $\Delta\mathbf{L} > 0$, then $\delta^2 W < 0$ and $W(\boldsymbol{\tau})$ reaches a global maximum. Moreover, noticing that $\boldsymbol{\Gamma}\,\mathbf{L}^o\,\boldsymbol{\Gamma} = \boldsymbol{\Gamma}$, $\mathbf{L}_o^{1/2}\,\boldsymbol{\Gamma}\,\mathbf{L}_o^{1/2}$ is a projection and:

$$\mathbf{L}_o^{1/2}\,\boldsymbol{\Gamma}\,\mathbf{L}_o^{1/2} \leq \mathbf{I} \quad \text{implying} \quad \boldsymbol{\Gamma} \leq \mathbf{L}_o^{-1} \quad \text{and} \quad \Delta\mathbf{L}^{-1} + \boldsymbol{\Gamma} \leq \Delta\mathbf{L}^{-1} + \mathbf{L}_o^{-1}. \tag{4.33}$$

Finally, since:

$$\Delta\mathbf{L}^{-1} + \mathbf{L}_o^{-1} = \Delta\mathbf{L}^{-1} + \mathbf{L}_o^{-1}\,\Delta\mathbf{L}\,\Delta\mathbf{L}^{-1} = \mathbf{L}_o^{-1}\,\mathbf{L}\,\Delta\mathbf{L}^{-1}, \tag{4.34}$$

the second order variation of the functional can be rewritten as:

$$\delta^2 W(\boldsymbol{\tau}) \geq -\frac{1}{2} < \delta\boldsymbol{\tau}\,(\mathbf{L}_o^{-1}\,\mathbf{L}\,\Delta\mathbf{L}^{-1})\,\delta\boldsymbol{\tau} > . \tag{4.35}$$

If $\Delta\mathbf{L} < 0$, then $\delta^2 W > 0$ and W has a global minimum value (see e.g. Willis (1977, 1981); Milton (2002) for details). The extreme values of the elastic energy can be obtained by finding the stationary value of this energy, and the conditions imposed on $\Delta\mathbf{L}$ enable to compute lower and upper bounds. To use this remark, the functional (4.31) is rewritten as: $W(\boldsymbol{\tau}) = W_o + W_1(\boldsymbol{\tau})$, where:

$$W_o = \frac{1}{2} < \boldsymbol{\epsilon}^o\,\mathbf{L}^o\,\boldsymbol{\epsilon}^o > = \frac{1}{2}\int_{-t/2}^{t/2} \boldsymbol{\epsilon}^o_{(i)}(x_3)\,\mathbf{L}^o_{(s)}\,\boldsymbol{\epsilon}^o_{(i)}(x_3)\,dx_3, \tag{4.36}$$

and:

$$W_1(\boldsymbol{\tau}) = \frac{1}{2} < 2\boldsymbol{\tau}\,\boldsymbol{\epsilon}^o - \boldsymbol{\tau}\,\Delta\mathbf{L}^{-1}\,\boldsymbol{\tau} - \boldsymbol{\tau}\,\boldsymbol{\Gamma}\,\boldsymbol{\tau} > . \tag{4.37}$$

Eq. (4.36) shows that W_o can be explicitly calculated and does not depend on $\boldsymbol{\tau}$. Therefore, the extrema of W are given by:

$$\begin{cases} \mathrm{Max}_{\boldsymbol{\tau}} W = W_o + \mathrm{Max}_{\boldsymbol{\tau}}\, W_1(\boldsymbol{\tau}) \quad \Delta\mathbf{L} > 0, \\ \\ \mathrm{Min}_{\boldsymbol{\tau}} W = W_o + \mathrm{Min}_{\boldsymbol{\tau}}\, W_1(\boldsymbol{\tau}) \quad \Delta\mathbf{L} < 0, \end{cases} \tag{4.38}$$

where the average of the elastic strain energy is related to the macroscopic strain energy which contains the stiffness constants of the plate. Hence Eqs. (4.38) supply lower and upper bounds for the effective elastic properties of the plate. The functional $W_1(\boldsymbol{\tau})$ will be considered in more

details in the following sections. Eqs. (4.38) show also that the lower and upper bounds depend on the properties of the reference medium. An optimization on the reference medium will thus yield optimal bounds.

4.3 Bound Estimates for (x_1, x_2)-Invariant Polarization Fields

In this section we introduce (x_1, x_2)-invariant polarization stress fields (i.e., $\boldsymbol{\tau}(\mathbf{x}) = \boldsymbol{\tau}(x_3)$) in the variational formulation. A laminated plate with elastic properties that are (x_1, x_2)-independent (i.e., $\mathbf{L}(\mathbf{x}) = \mathbf{L}(x_3)$) is first considered. In such a case, the fields solution of Eqs. (4.2) are invariant in the (x_1, x_2)-directions: $(\boldsymbol{\sigma}(\mathbf{x}), \boldsymbol{\epsilon}(\mathbf{x}), \mathbf{v}(\mathbf{x})) = (\boldsymbol{\sigma}(x_3), \boldsymbol{\epsilon}(x_3), \mathbf{v}(x_3))$. Hence, as is the case with homogeneous plates, the solution can be obtained analytically and the overall elastic properties of the plate are given by:

$$(\mathbf{A}, \mathbf{B}, \mathbf{D}) = \int_{-t/2}^{t/2} (1, x_3, x_3^2)\, \mathbf{L}_{(s)}(x_3)\, dx_3, \tag{4.39}$$

where $\mathbf{L}_{(s)}(x_3)$ is the plane-stress elastic matrix at x_3 which verifies Eq. (4.15). Moreover, for any $\mathbf{L}'(x_3) \geq \mathbf{L}(x_3)$ we have:

$$\left(\mathbf{A}', \mathbf{B}', \mathbf{D}'\right) \geq \left(\mathbf{A}, \mathbf{B}, \mathbf{D}\right), \tag{4.40}$$

in the sense of the corresponding strain energy. Let us consider the more general case $\mathbf{L}(\mathbf{x}) = \mathbf{L}(x_1, x_2, x_3)$. In such a case the functional W_1 (4.37) is given by:

$$W_1(\boldsymbol{\tau}) = \frac{1}{2} \int_{-t/2}^{t/2} \left[2\boldsymbol{\tau}(x_3)\boldsymbol{\epsilon}^o(x_3) - \boldsymbol{\tau}(x_3)\, \overline{\Delta \mathbf{L}^{-1}}(x_3)\boldsymbol{\tau}(x_3) - \boldsymbol{\tau}(x_3)\boldsymbol{\Gamma}\boldsymbol{\tau}(x_3) \right] dx_3, \tag{4.41}$$

where $\overline{\mathbf{f}}(x_3)$ is the (x_1, x_2)-average of $\mathbf{f}(x_1, x_2, x_3)$:

$$\overline{\mathbf{f}}(x_3) = \frac{1}{|\omega|} \int \mathbf{f}(x_1, x_2, x_3)\, dx_1 dx_2. \tag{4.42}$$

In the present case, the material is layered in the thickness of the plate and $W_1(\boldsymbol{\tau})$ is expressed depends on x_3 only. In contrast to the laminated plate, Eqs. (4.38) show that there exists an elastic tensor $\mathbf{L}^*(x_3)$ that depends on x_3:

$$\mathbf{L}^*(x_3) = \left(\overline{\Delta \mathbf{L}^{-1}}(x_3) \right)^{-1} + \mathbf{L}^o, \tag{4.43}$$

from which the homogenized stiffnesses of the plate $(\mathbf{A}^*, \mathbf{B}^*, \mathbf{D}^*)$ are derived:

$$(\mathbf{A}^*, \mathbf{B}^*, \mathbf{D}^*) = \int_{-t/2}^{t/2} (1, x_3, x_3^2)\, \mathbf{L}^*_{(s)}(x_3)\, dx_3. \tag{4.44}$$

Equation (4.38) yields:

$$\begin{cases} (\mathbf{A},\mathbf{B},\mathbf{D}) \geq (\mathbf{A}^*,\mathbf{B}^*,\mathbf{D}^*) & \forall \mathbf{L}^o,\ \Delta\mathbf{L} > 0, \\ \\ (\mathbf{A},\mathbf{B},\mathbf{D}) \leq (\mathbf{A}^*,\mathbf{B}^*,\mathbf{D}^*) & \forall \mathbf{L}^o,\ \Delta\mathbf{L} < 0. \end{cases} \tag{4.45}$$

The bounds for the homogenized elastic properties of the plate vary with the reference medium and can therefore be optimized by an appropriate choice of the reference medium. To do so, one considers the following two limit problems: $\mathbf{L}^o$ tends to zero and $\mathbf{L}^o$ tends to to infinity.

For the case $\mathbf{L}^o \to \infty$ and $\Delta\mathbf{L} < 0$, with no loss of generality, one can write $\mathbf{L}^o = \beta\mathbf{I}$ where $\mathbf{I}$ is the unit matrix and β is a positive coefficient which tends to infinity. One performs the following transformations:

$$\overline{\Delta\mathbf{L}^{-1}}(x_3) = \overline{[\mathbf{L}(\mathbf{x}) - \mathbf{L}^o]^{-1}} = -\beta^{-1}\overline{[\mathbf{I} - \beta^{-1}\mathbf{L}(\mathbf{x})]^{-1}}. \tag{4.46}$$

By using the development:

$$(\mathbf{I} - \mathbf{X})^{-1} = \mathbf{I} + \mathbf{X} + \mathbf{X}^2 + \ldots \quad \forall \mathbf{X}, ||\mathbf{X}|| < \mathbf{1}, \tag{4.47}$$

equation (4.46) becomes:

$$\overline{\Delta\mathbf{L}^{-1}}(x_3) = -\beta^{-1}[\mathbf{I} + \beta^{-1}\overline{\mathbf{L}}(x_3) + \beta^{-2}\overline{\mathbf{L}^2}(x_3) + \ldots]. \tag{4.48}$$

The high-order terms in Eq. (4.48) can be neglected when $\beta \to \infty$. Hence, by making use of Eq. (4.47) again for $\left(\overline{\Delta\mathbf{L}^{-1}}(x_3)\right)^{-1}$, one obtains:

$$\mathbf{L}^*(x_3) \to \overline{\mathbf{L}}(x_3) \quad \text{when} \quad \beta \to \infty. \tag{4.49}$$

We prove next that the above limit value, $\overline{\mathbf{L}}(x_3)$, is the minimum value of $\mathbf{L}^*(x_3)$, i.e., $\mathbf{L}^*(x_3) \geq \overline{\mathbf{L}}(x_3)$ with $\Delta\mathbf{L} < 0$. This proof requires the following inequality to be verified:

$$\left(\overline{\Delta\mathbf{L}^{-1}}(x_3)\right)^{-1} \geq \overline{\mathbf{L}}(x_3) - \mathbf{L}^o = \overline{\Delta\mathbf{L}}(x_3). \tag{4.50}$$

By substituting $\mathbf{M} = -\Delta\mathbf{L} > 0$ into Eq. (4.50), one recovers the inequality between the Voigt and Reuss bounds: $\overline{\mathbf{M}} \geq \left(\overline{\mathbf{M}^{-1}}\right)^{-1}$. Therefore Eq. (4.50) is satisfied for any $\Delta\mathbf{L} < 0$ and the limit value $\overline{\mathbf{L}}(x_3)$ yields the optimal upper bound for the effective in-plane and out-of-plane elastic properties of the plate:

$$(\mathbf{A}^*,\mathbf{B}^*,\mathbf{D}^*)^+ = \int_{-t/2}^{t/2} (1, x_3, x_3^2)\, \overline{\mathbf{L}}_{(s)}(x_3)\, dx_3 = \int_{-t/2}^{t/2} (1, x_3, x_3^2)\, (\overline{\mathbf{L}}^{-1}_{(i)(i)})^{-1}(x_3)\, dx_3. \tag{4.51}$$

Furthermore, for the case $\mathbf{L}^o \to 0$ and $\Delta\mathbf{L} > 0$, from Eq. (4.43) follows $\mathbf{L}^*(x_3) \to \left(\overline{\mathbf{L}^{-1}}\right)^{-1}$. We prove next that $\left(\overline{\mathbf{L}^{-1}}\right)^{-1}$ is the maximum value of $\mathbf{L}^*(x_3)$. To do so, the inequality $\mathbf{L}^*(x_3) \leq \left(\overline{\mathbf{L}^{-1}}\right)^{-1}$ with $\Delta\mathbf{L} > 0$ has to be verified.

Since for any $\mathbf{G} \geq 0$, $\left(\overline{\mathbf{G}^{-1}}\right)^{-1}$ is concave, the following relation holds for any $\mathbf{G}_1 \geq 0$ and $\mathbf{G}_2 \geq 0$ and $\lambda \in [0,1]$:

$$\left(\overline{(\lambda\mathbf{G}_1 + (1-\lambda)\mathbf{G}_2)^{-1}}\right)^{-1} \geq \lambda\left(\overline{\mathbf{G}_1^{-1}}\right)^{-1} + (1-\lambda)\left(\overline{\mathbf{G}_2^{-1}}\right)^{-1}. \tag{4.52}$$

Substituting $\mathbf{G}_1 = \Delta\mathbf{L}$, $\mathbf{G}_2 = \mathbf{L}^o$ and $\lambda = 1/2$ in the above equation yields:

$$\left(\overline{(\Delta\mathbf{L} + \mathbf{L}^o)^{-1}}\right)^{-1} \geq \left(\overline{\Delta\mathbf{L}^{-1}}\right)^{-1} + \left(\overline{\mathbf{L}^{o-1}}\right)^{-1}. \tag{4.53}$$

Therefore, the limit value, $\left(\overline{\mathbf{L}^{-1}}\right)^{-1}$, is the maximum value of $\mathbf{L}^*(x_3)$ and the optimal lower bound for the effective elastic properties of the plate is:

$$(\mathbf{A}^*, \mathbf{B}^*, \mathbf{D}^*)^- = \int_{-t/2}^{t/2} (1, x_3, x_3^2)\left(\overline{\mathbf{L}^{-1}}_{(i)(i)}\right)^{-1}(x_3)\, dx_3. \tag{4.54}$$

The optimal bounds obtained in Eq. (4.54) and Eq. (4.51) with the use of the Hashin-Shtrikman functional are those proposed by Kolpakov (1999). Kolpakov used the Castigliano functional with a statically admissible in-plane stress field depending on x_3 and the Lagrange functional with a kinematically admissible out-of-plane displacement field depending on x_3.

But, the Voigt and Reuss bounds may be far from each other, especially if the plate is made of materials which exhibit a significant mechanical contrast. By focusing on the polarizations in the phases however, those bounds can be improved. We will do so in the next section to analyze random heterogeneous plates.

4.4 Bound Estimates for Random Plates

Many materials are randomly distributed. When the characteristic size of the structural material elements is much greater than that of the microstructure, the material can accurately be treated as locally homogeneous with spatially constant average properties. Many studies have been performed on such materials and used variational principles to derive lower and upper bounds for their overall properties (see e.g. Hashin and Shtrikman (1962a,b); Willis (1977, 1981)). For many materials however, these conditions are not met and more efficient methods are required to compute the actual material response. The minimum size of the representative volume element (RVE) has been studied by Drugan and Willis (1996) and then Drugan (2003) based on nonlocal constitutive equations. They considered random linear elastic composite materials of infinite

extent. The size of the RVE has been the subject of numerous numerical studies also (see e.g. Sab (1992); Gusev (1997); Terada et al. (1998); Kanit et al. (2003); Sab and Nedjar (2005); Lachihab and Sab (2005, 2008)).

Moreover, for some materials the assumption of statistical homogeneity does not apply. Functionally graded materials (FGM) are examples of such materials. The continuous spatial variation of properties in those materials prevents the use of the methods developed for statistically uniform heterogeneous materials. We can cite the work of Luciano and Willis (2004) who applied the theory presented in Drugan and Willis (1996) to derive nonlocal constitutive equations for functionally graded materials. Several other micromechanical models have been proposed for the analysis of the overall thermomechanical properties of FGM (see e.g. Reiter and Dvorak (1997, 1998); Suresh and Mortensen (1998)).

Homogenization methods for plates have been presented in the first section. For randomly distributed materials, the use of variational principles to derive bounds for the effective elastic properties of the plates has actually been rarely studied. This section aims at estimating bounds for the effective elastic properties of random plates. It is based on the Hashin-Shtrikman functional formulated in section 2. We assume that the constituent materials are statistically homogeneous along directions which are parallel to the plane (x_1, x_2) of the plate, that the in-plane dimensions of the plate are much greater that its thickness.

4.4.1 n-Phase Random Plates

Let us now consider a composite with a random microstructure made of n phases whose geometrical distribution is characterized by α. Let ψ be the space of all samples of microstructure and $p(\alpha)$ the probability density of α in ψ. Thus, any property, f, of the material is a function of α and its ensemble average is defined as:

$$\mathbb{E}f(\alpha) = \int_{\psi} f(\alpha)\, p(\alpha)\, d\alpha. \tag{4.55}$$

Thus, the probability $P_r(\mathbf{x})$ of finding the phase r at the location $\mathbf{x}$ is:

$$P_r(\mathbf{x}) = \mathbb{E}I_r(\mathbf{x}, \alpha) = \int_{\psi} I_r(\mathbf{x}, \alpha)\, p(\alpha)\, d\alpha, \tag{4.56}$$

where $I_r(\mathbf{x}, \alpha)$ is the indicator function of the region occupied by the phase r, $I_r(\mathbf{x}, \alpha) = 1$ when $\mathbf{x} \in Y_r$ and $I_r(\mathbf{x}, \alpha) = 0$ otherwise. Likewise, the two-point probability $P_{rs}(\mathbf{x}, \mathbf{x}')$ of finding simultaneously the phase r at the location $\mathbf{x}$ and the phase s at the location $\mathbf{x}'$ is:

$$P_{rs}(\mathbf{x}, \mathbf{x}') = \mathbb{E}(I_r(\mathbf{x}, \alpha) I_s(\mathbf{x}', \alpha)) = \int_{\psi} I_r(\mathbf{x}, \alpha)\, I_s(\mathbf{x}', \alpha)\, p(\alpha)\, d\alpha. \tag{4.57}$$

If phase r (where $r = 1, 2, \ldots, n$) is homogeneous and has a modulus $\mathbf{L}_r$, the elastic tensor $\mathbf{L}(\mathbf{x})$ in sample α and its ensemble average are:

$$\mathbf{L}(\mathbf{x},\alpha) = \sum_r L_r I_r(\mathbf{x},\alpha), \quad \mathbb{E}\mathbf{L}(\mathbf{x},\alpha) = \sum_r L_r P_r(\mathbf{x}). \tag{4.58}$$

Furthermore, we assume that the materials are statistically homogeneous in the (x_1, x_2)-directions. The characteristic properties are thus insensitive to translations in those directions:

$$P_r(\mathbf{x}) = P_r(x_3), \quad P_{rs}(\mathbf{x},\mathbf{x}') = P_{rs}(\tilde{\mathbf{x}} - \tilde{\mathbf{x}}', x_3, x_3'). \tag{4.59}$$

Moreover, the polarization field in each phase is assumed not to depend on x_1 and x_2, i.e., $\boldsymbol{\tau}_r(\mathbf{x}) = \boldsymbol{\tau}_r(x_3)$. In the following, the polarization field is assumed to be a linear combination of the indicator functions and can therefore be expressed as:

$$\boldsymbol{\tau}(\mathbf{x},\alpha) = \sum_r \boldsymbol{\tau}_r(x_3) I_r(\mathbf{x},\alpha). \tag{4.60}$$

It is usual to use $\boldsymbol{\Gamma}$-operator for a periodic medium in the case of statistically homogeneous random media, as soon as the period is large enough compared to the correlation length (see e.g. Sab and Nedjar (2005)). This process will be used thereafter.

The previous definitions are introduced to enable the analysis of the ensemble average of the functional (4.31). Since W_o does not depend on $\boldsymbol{\tau}$, the total energy $W(\boldsymbol{\tau})$ and $W_1(\boldsymbol{\tau})$ have the same stationary point. Averaging the functional (4.37) now yields:

$$\begin{aligned}
\mathbb{E}W_1(\boldsymbol{\tau}) = \frac{1}{2} < 2\sum_r \boldsymbol{\tau}_r(x_3)\boldsymbol{\epsilon}^o(x_3)\, P_r(x_3) - \sum_r \boldsymbol{\tau}_r(x_3)\Delta\mathbf{L}_r^{-1} P_r(x_3)\boldsymbol{\tau}_r(x_3) \\
- \sum_r \sum_s \boldsymbol{\tau}_r(x_3)|Y|^{-1} \int_Y \boldsymbol{\Gamma}_p(\tilde{\mathbf{x}} - \tilde{\mathbf{x}}', x_3 - x_3') P_{rs}(\tilde{\mathbf{x}} - \tilde{\mathbf{x}}', x_3, x_3')\boldsymbol{\tau}_s(x_3')\, d\mathbf{x}' \\
- \sum_r \sum_s \boldsymbol{\tau}_r(x_3)|Y|^{-1} \int_Y \boldsymbol{\Gamma}_h(\tilde{\mathbf{x}} - \tilde{\mathbf{x}}', x_3, x_3') P_{rs}(\tilde{\mathbf{x}} - \tilde{\mathbf{x}}', x_3, x_3')\boldsymbol{\tau}_s(x_3')\, d\mathbf{x}' > .
\end{aligned} \tag{4.61}$$

where $\boldsymbol{\epsilon}^o(x_3)$ is the total strain field estimated in the reference medium. It is a deterministic function of x_3 (see section 4.2.1).

4.4.2 Discretization

We remind that the search for lower and upper bounds for the effective elastic properties of the plate can be performed by estimating the stationary value of the functional (4.61) (see section 4.2.4). To do so, one discretizes the plate in the x_3 and x_3' directions with N_3 points each. The polarization field in the phase is approximated by a piecewise function:

$$\boldsymbol{\tau}_r(x_3) = \sum_m \boldsymbol{\tau}_r^m\, I_m(x_3), \tag{4.62}$$

where I_m is the indicator function of the finite intervals whose union yields the x_3-axis. Therefore, the functional (4.61) can be rewritten as follows:

$$\mathbb{E}W_1 \simeq \frac{t}{2N_3} \sum_m \left[\sum_r 2\boldsymbol{\tau}_r^m \boldsymbol{\epsilon}_m^o P_r^m - \sum_r \boldsymbol{\tau}_r^m \Delta \mathbf{L}_r^{-1} P_r^m \boldsymbol{\tau}_r^m \right.$$
$$\left. - \sum_{m'} \sum_r \sum_s \boldsymbol{\tau}_r^m \frac{1}{N_3|\omega|} \int_\omega \left(\boldsymbol{\Gamma}_p^{mm'}(\tilde{\mathbf{x}}') + \boldsymbol{\Gamma}_h^{mm'}(\tilde{\mathbf{x}}') \right) P_{rs}^{mm'}(\tilde{\mathbf{x}}') \boldsymbol{\tau}_s^{m'} \, d\tilde{\mathbf{x}}' \right], \tag{4.63}$$

where $\boldsymbol{\Gamma}_p^{mm'}(\tilde{\mathbf{x}}') = \boldsymbol{\Gamma}_p(\tilde{\mathbf{x}}', x_3(m) - x_3'(m'))$, $\boldsymbol{\Gamma}_h^{mm'}(\tilde{\mathbf{x}}') = \boldsymbol{\Gamma}_h(\tilde{\mathbf{x}}', x_3(m), x_3'(m'))$, $P_{rs}^{mm'}(\tilde{\mathbf{x}}') = P_{rs}(\tilde{\mathbf{x}}', x_3(m), x_3'(m'))$, $\boldsymbol{\epsilon}_m^o = \boldsymbol{\epsilon}^o(x_3(m))$, $P_r^m = P_r(x_3(m))$. To derive Eq. (4.63), we used the following property, based on the periodicity of the functions in the x_1 and x_2 directions:

$$\int_Y \boldsymbol{\Gamma}_p(\mathbf{x} - \mathbf{x}') P_{rs}(\tilde{\mathbf{x}} - \tilde{\mathbf{x}}', x_3, x_3') d\mathbf{x}' = \int_Y \boldsymbol{\Gamma}_p(\tilde{\mathbf{x}}', x_3 - x_3') P_{rs}(\tilde{\mathbf{x}}', x_3, x_3') d\mathbf{x}'. \tag{4.64}$$

We note that the integral expressions in (4.64) and (4.63) can be computed in the Fourier space with the wave vectors (k_1, k_2) using Parseval's theorem. For $m, m' = 1, \ldots, N_3$ points, Eq. (4.63) yields:

$$\mathbb{E}W_1 = \frac{t}{2N_3} \left(2\mathbf{T}^T \mathbf{F} - \mathbf{T}^T \mathbf{M}_l \mathbf{T} - \mathbf{T}^T \mathbf{M}_p \mathbf{T} - \mathbf{T}^T \mathbf{M}_h \mathbf{T} \right), \tag{4.65}$$

where $\mathbf{F}$, $\mathbf{M}_l$, $\mathbf{M}_p$ and $\mathbf{M}_h$ are linear and quadratic operators of the functional (4.63) and where the vector $\mathbf{T}$ is made of the discretized values of the polarization fields whose values are uniform in each discretized interval (see Eq. (4.62)):

$$\mathbf{T} = (\boldsymbol{\tau}_1^1, \ldots, \boldsymbol{\tau}_n^1, \ldots, \boldsymbol{\tau}_1^{N_3}, \ldots, \boldsymbol{\tau}_n^{N_3}) \quad \text{with} \quad \boldsymbol{\tau}_r^m = \boldsymbol{\tau}_r(x_3(m)), \tag{4.66}$$

where the polarization field in each phase is written under the form of a six-component vector (3D-problem): $(\tau_{11}, \tau_{22}, \tau_{33}, \tau_{23}, \tau_{13}, \tau_{12})^T$.

The vector $\mathbf{F}$ is computed from the 1-point probability function and from the strain field produced in the reference medium $\boldsymbol{\epsilon}^o(x_3)$. $\boldsymbol{\epsilon}^o(x_3)$ also is represented by a six component vector, $(\epsilon_{11}^o, \epsilon_{22}^o, \epsilon_{33}^o, 2\epsilon_{23}^o, 2\epsilon_{13}^o, 2\epsilon_{12}^o)^T$. The symmetrical square matrix $\mathbf{M}_l$ is determined from the 1-point probability function, the mechanical properties of the constituent materials and the mechanical properties of the reference medium. The square matrices $\mathbf{M}_p$ and $\mathbf{M}_h$ are computed from the operators $\boldsymbol{\Gamma}_p$ and $\boldsymbol{\Gamma}_h$ and from the two-point probability function P_{rs}. Moreover, we note that $\mathbf{M}_p$ and $\mathbf{M}_h$ are symmetrical matrices, since $\boldsymbol{\Gamma}_p$ and $\boldsymbol{\Gamma}_h$ are self-adjoint operators which verify: $\Gamma_{ijkl}^p(\mathbf{x} - \mathbf{x}') = \Gamma_{klij}^p(\mathbf{x}' - \mathbf{x})$ and $\Gamma_{ijkl}^h(\tilde{\mathbf{x}} - \tilde{\mathbf{x}}', x_3, x_3') = \Gamma_{klij}^h(\tilde{\mathbf{x}}' - \tilde{\mathbf{x}}, x_3', x_3)$.

The functional (4.65) is stationary when the following stationary condition is verified:

$$\mathbf{T}_s = (\mathbf{M}_l + \mathbf{M}_p + \mathbf{M}_h)^{-1} \mathbf{F}. \tag{4.67}$$

Hence, the stationary value of the average of the energy functional is obtained as:

$$\mathbb{E}W_1^s = \frac{t}{2N_3}\,\mathbf{T}_s^T\,\mathbf{F}. \tag{4.68}$$

The above value, used with Eq. (4.36), allows for the computation of bounds for the effective elastic properties of the random plate. Those bounds vary with the choice of the reference medium and an appropriate choice of the elastic tensor $\mathbf{L}^o$ enables the optimization of those bounds. The present theory was derived in the general case of periodic random plates whose constituent materials are statistically homogeneous in the (x_1, x_2)-directions. To validate the steps described above, the simple case of an isotropic material is considered next. The estimated bounds for the homogenized elastic stiffnesses of a Love-Kirchhoff plate will enable to study the effects of the size of the heterogeneity in homogenization problems.

4.4.3 Plates with Randomly Distributed Inclusions

Consider now a Love-Kirchhoff plate made of two isotropic material phases. The 1-point probability function $P_r(\mathbf{x})$ is the volume fraction c_r and the 2-point probability function is invariant by translations and rotations. Expressions derived analytically as well as numerically to estimate the two-point probability function exist for numerous random material distributions (see e.g. Torquato (2001)). In this section, we consider a microstructure with a matrix containing a random distribution of non-overlapping spherical particles, for which the two-point probability function can be derived analytically. In fact, it can be computed from a correlation function as follows (see e.g. Drugan and Willis (1996)):

$$P_{rs}(|\mathbf{x}-\mathbf{x}'|) = c_r c_s + c_r(\delta_{rs} - c_s)\,h(|\mathbf{x}-\mathbf{x}'|), \tag{4.69}$$

where c_r, c_s are the volume fractions of the phases r and s, respectively. This probability function is expressed in terms of the relative distance of two sampled points, namely $r = |\mathbf{x}-\mathbf{x}'|$. The 2-point correlation function of such a material can be expressed under an exponential form (Drugan, 2003):

$$h(r) = e^{-\frac{r}{a}}, \tag{4.70}$$

where the coefficient a is a function of the radius R and of the volume fraction c_1 of the spherical inclusions (phase 1):

$$a^2 = R^2\frac{5A_1c_1(1+2\tilde{c}_1) + 2B_1[(1+2\tilde{c}_1)(2+c_1) - c_1(\tilde{c}_1/c_1)^{2/3}(10-2\tilde{c}_1+\tilde{c}_1^2)]}{10B_1(1-c_1)(1+2\tilde{c}_1)}, \tag{4.71}$$

where

$$\tilde{c}_1 = c_1 - \frac{1}{16}c_1^2,\; A_1 = \frac{3}{2}\frac{\tilde{c}_1^2(1-0.7117\tilde{c}_1-0.114\tilde{c}_1^2)}{(1-\tilde{c}_1)^4},\; B_1 = 12A_1\frac{(1-\tilde{c}_1)^2}{\tilde{c}_1(2+\tilde{c}_1)}. \tag{4.72}$$

This analytical expression is consistent with the numerical results obtained by Torquato and Stell (1985) who used the Percus and Yevick (1958) model of the statistic problem with random hard sphere distributions corrected by Verlet and Weis (1972) (see Drugan (2003) for details). Figures 4.1 and 4.2 display the profiles of the two-point matrix probability function along the in-plane direction in which the in-plane coordinate is normalized with respect to the diameter of the spherical inclusions. Moreover, since the inclusions cannot overlap, their concentration has an upper bound. This value is considered to be 0.64 (Torquato, 2001). One observes that the probability functions decrease and are then stationary. Figure 4.2 shows that the minimum in-plane correlation length is $10R$, above which a plateau appears.

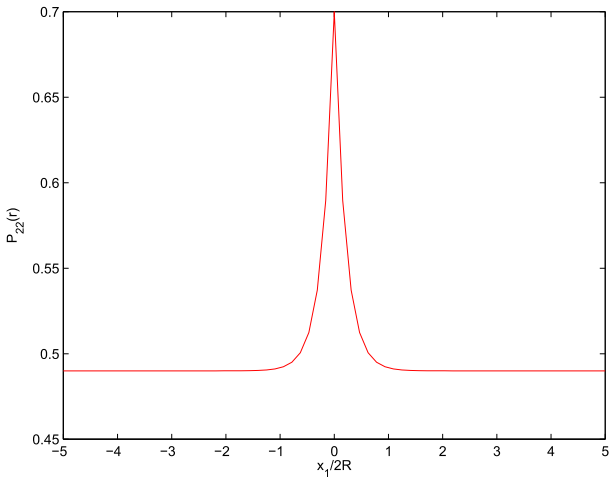

Figure 4.1: The two-point matrix probability function, $P_{22}(r)$, $c_1 = 0.3$.

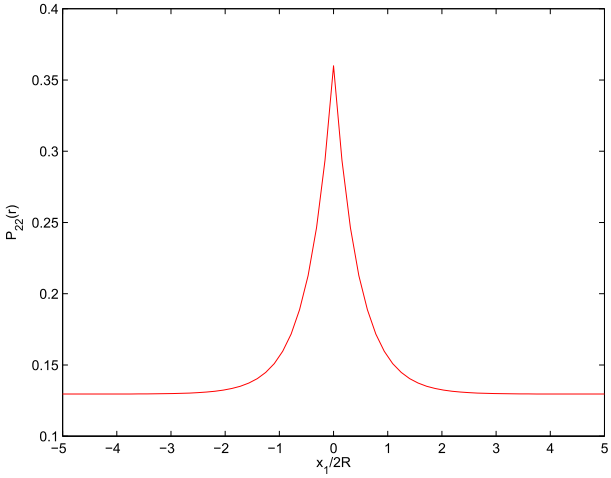

Figure 4.2: The two-point matrix probability function, $P_{22}(r)$, $c_1 = 0.64$.

To apply numerically the theory here presented, the computations are performed in the limit of a plane deformation problem in the x_2-direction. A discretization of the space in the (x_1, x_3)-directions is necessary. The coordinates of the discretized points are defined as follows:

$$x_j = j\frac{l_j}{N_j}, \quad \text{with} \quad j = -\frac{N_j}{2}, \ldots, 0, \ldots, \frac{N_j}{2} - 1 \quad (j = 1, 3). \tag{4.73}$$

This discretization also is appropriate to use the Fast Fourier Transform (FFT), hence $N_j = 2^p$, $p \in \mathbb{N}^+$. The computation of the FFT corresponds to the wave-number order $n_j = [0, ..., \frac{N_j}{2} - 1, -\frac{N_j}{2}, ..., -1]$. The components of the wave vectors are then defined as follows: $k_j = 2\pi n_j / l_j$.

The homogenized elastic stiffnesses of the plate will be obtained by an appropriate choice of the macroscopic strains $(\mathbf{E}, \boldsymbol{\chi})$ and by the computation of the extreme values of the energy functional W_o and $\mathbb{E}W_1^s$. For the purpose of comparison, this approximation will be compared with the stiffness properties computed from the classic Hashin-Shtrikman estimates (UHS for the upper bound and LHS for the lower bound): The effective compressibility and shear moduli will be calculated first. Then the elastic stiffnesses of the plate will then be obtained from the

homogeneous plate theory. Values between the bounds also are introduced for the purpose of comparison by taking into account the choice of the reference medium: $\mathbf{L}^o = \alpha\mathbf{L}_1 + (1-\alpha)\mathbf{L}_2$ with $\alpha \in (0,1)$.

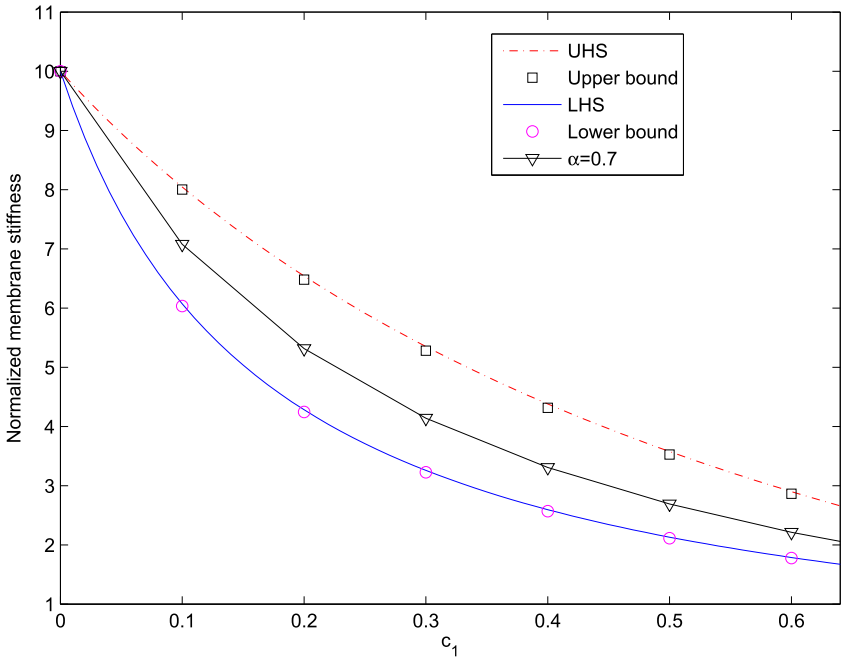

Figure 4.3: Comparison of the normalized membrane stiffness, $E_2/E_1 = 10$, $t/2R = 20$, $l_1/2R = 20$.

Figures 4.3 and 4.4 display comparisons of the homogenized membrane and bending stiffnesses obtained with the theory developed in this work with the stiffnesses derived from the classic solution of Hashin-Shtrikman. One notes that our best choices for lower and upper bounds are similar to those of Hashin and Shtrikman (1962a,b), i.e., $\mathbf{L}^o = \mathbf{L}_1$ and $\mathbf{L}^o = \mathbf{L}_2$ ($\mathbf{L}_1 < \mathbf{L}_2$), respectively. The values are expressed in terms of the concentration of the phase 1 and normalized with the stiffnesses produced in a homogeneous medium with properties of the phase 1. A discretization with $N_1 = N_3 = 2^7$ which ensured the convergence of the solution, was used for the computations. Figures 4.3 and 4.4 showed that the lower and upper bounds are identical for the two methods. This can be explained by the fact that the result is calculated for a large ratio $l_1/2R = 20$ (very large in-plane period) and $t/2R = 20$ for which there is no size effect of the heterogeneity.

To consider the convergence of the stiffnesses of the plate in terms of the normalized in-plane period $l_1/2R$, the case $l_1/2R = 20$ is chosen as a reference case. The measurement of a "relative error" is defined by the relationship:

$$\text{error}\,(\%) = \frac{M_c - M_m}{M_m} \times 100\%, \tag{4.74}$$

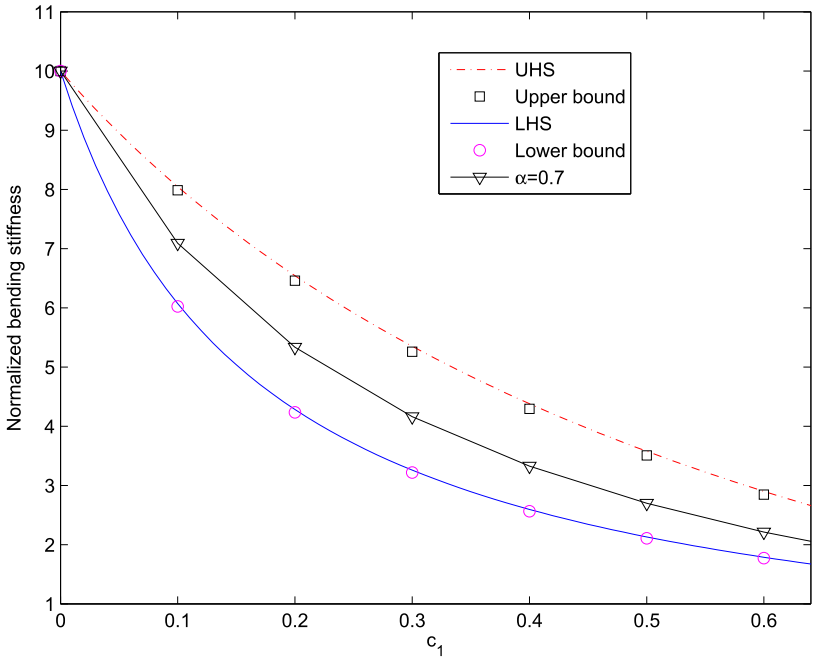

Figure 4.4: Comparison of the normalized bending stiffness, $E_2/E_1 = 10$, $t/2R = 20$, $l_1/2R = 20$.

where M_m is the stiffness of the present theory obtained from the reference case, and M_c is the one obtained from the other cases. The obtained results are presented in table 4.1 for the case $c_1 = 0.64$. It can be seen that $l_1/2R = 10$ ensures the convergence of the membrane and bending stiffnesses with a relative error smaller than 0.5%. So, this value will be used in the sequel to study the effect of the size of the heterogeneity with respect to the ratio $t/2R$.

Table 4.1: Normalized stiffnesses of a random plate, $E_1/E_2 = 1/10$, $t/2R = 5$, $c_1 = 0.64$.

$l_1/2R$	A/A_1 (relative error %)		D/D_1 (relative error %)	
	lower bound	upper bound	lower bound	upper bound
5	1.6963 (1.82%)	2.7459 (4.17%)	1.6980 (2.51 %)	2.7458 (5.26%)
7.5	1.6750 (0.54%)	2.6707 (1.32%)	1.6727 (0.98 %)	2.6560 (1.82%)
10	1.6680 (0.12%)	2.6449 (0.34%)	1.6628 (0.38%)	2.6177 (0.35%)
15	1.6650 (-0.06%)	2.6321 (-0.15%)	1.6563 (-0.01%)	2.6073 (-0.05%)
20	1.6660	2.6360	1.6565	2.6085

Moreover, to illustrate the size effect of the heterogeneity in terms of $l_1/2R$, the effective elastic stiffnesses here derived are compared to those obtained from the classic Hashin-Shtrikman bounds. This comparison allows to display the relative differences between both homogenization methods. For a fixed value of $t/2R = 5$, figure 4.5 displays the relative differences related to the

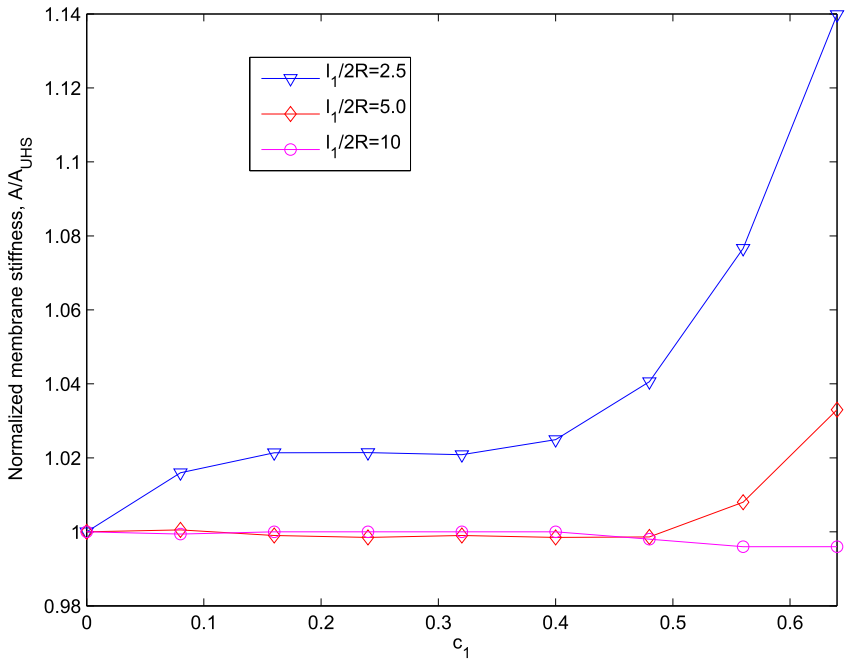

Figure 4.5: Normalized upper bound of the membrane stiffness, $E_2/E_1 = 10$, $t/2R = 5$.

membrane stiffness for the upper bound for three cases: $l_1/2R = 2.5$, $l_1/2R = 5$ and $l_1/2R = 10$. Obviously, the difference between the two approaches decreases when $l_1/2R$ increases. The effect of the size of the heterogeneities can be neglected above $l_1/2R = 5$ with a relative error smaller than 4%. This means that the minimum in-plane correlation length is $10R$. This value is larger than the RVE size proposed by Drugan and Willis (1996); Drugan (2003) for an infinite material medium.

The study of the boundary effect of the plate is displayed in figures 4.6 and 4.7 in which the relative differences of both homogenization methods in terms of $t/2R$ are computed for $l_1/2R = 10$. It can be seen that the relative differences converge for $t/2R = 6$, above which a plateau appears and the boundary effect can be neglected above $t/2R = 3$ with a relative difference smaller than 4%.

The above obtained results also show that the effect on the bending stiffness is similar to that on the membrane stiffness. We can therefore reasonably assert that homogenization methods would yield the same relative difference for the real material. The results presented above were derived for a small mechanical contrast between the constituent materials. When this contrast becomes large, the difference between the lower and upper bounds becomes larger and therefore the prediction of the overall behavior is not accurate anymore. Main topics of future research should be the quantitative estimation of the size effect of the heterogeneity as well as of the size of the representative volume element for plates made of materials with a significant contrast in their mechanical properties.

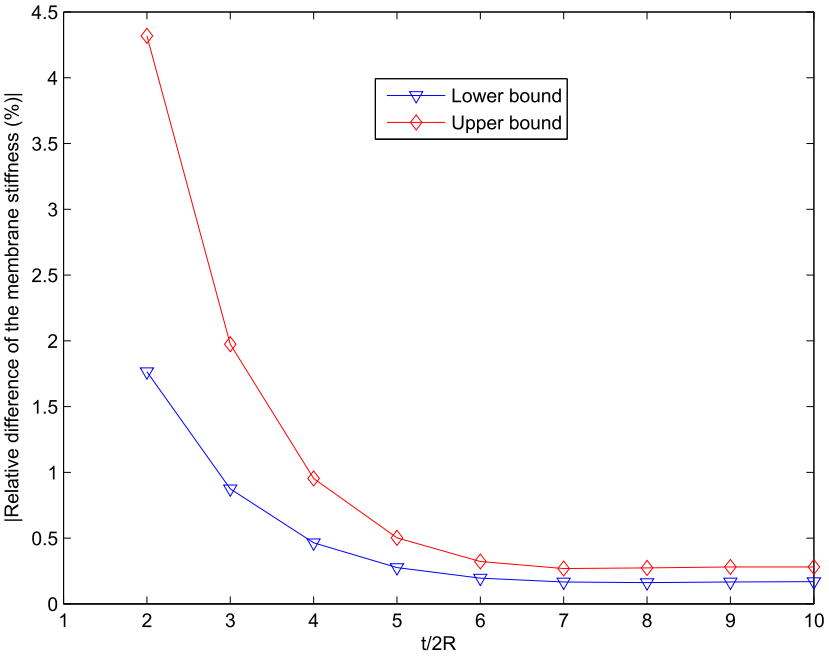

Figure 4.6: Relative difference of the membrane stiffness, $E_2/E_1 = 10$, $l_1/2R = 10$.

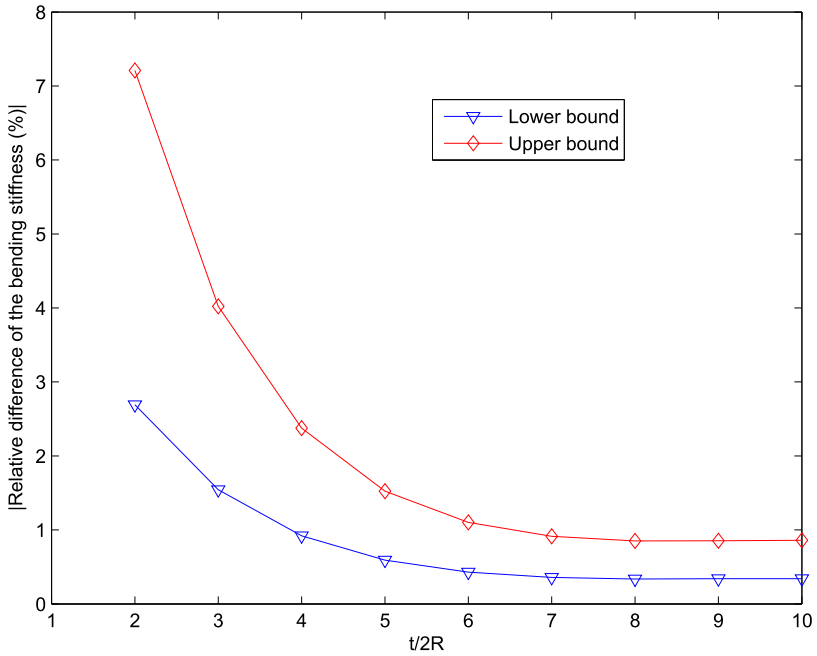

Figure 4.7: Relative difference of the bending stiffness, $E_2/E_1 = 10$, $l_1/2R = 10$.

4.5 Conclusion of the Chapter

This chapter presented a Hashin-Shtrikman variational principle for heterogeneous plates based on a $\mathbf{\Gamma}$-operator for periodic media with stress-free boundary conditions. Two applications were considered. First, we considered materials having deterministic properties for which the invariance of the polarization stresses in the in-plane directions led to an explicit solving of the localization elastic problem. When the materials are stratified through the thickness of the plate, we obtain a functional expressed in terms of the components depending on the thickness coordinate using the in-plane average. We also proved that the optimal lower and upper bounds for any anisotropy of the reference medium coincide with the refined estimates of the Voigt and Reuss bounds proposed by Kolpakov (1999) for heterogeneous plates.

In the second application, a Hashin-Shtrikman variational formulation was derived for random heterogeneous plates. The assumption of a statistically uniform distribution of the materials in the in-plane directions of the plate yielded a simplified expression of the functional in terms of the in-plane invariant polarizations. A simple example with isotropic materials was considered and allowed to predict the effect of the size of the heterogeneities. For this example, the homogenized elastic properties of the plate were compared with those obtained from the classic Hashin-Shtrikman solutions (Hashin and Shtrikman, 1962a,b, 1965). The relative differences between the results of both methods were small.

Furthermore, it is known that the use of variational principles to estimate the bounds for the effective elastic properties is not accurate anymore when the contrast in constituent material properties is large. To overcome this problem, a general numerical solution based on the Fast Fourier Transform proposed by Nguyen et al. (2008b) can be used in a Monte-Carlo simulation to predict the minimum size of the representative volume element for random plates.

Chapter 5

Representative Volume Element for Plates with Random Microstructures

This chapter applies the homogenization theory proposed in the third chapter for estimating the minimum size of the Representative Volume Element (RVE) for a random plate. To do so, the microstructure of the plate is randomly generated first with identical hexagons. The Monte-Carlo method is then introduced to estimate the ensemble average of the effective properties of the plate for many independent realizations on each volume size. The minimum size of the representative volume element will finally be derived from a required precision on the mean value and variance of the effective properties of the plate.

5.1 Introduction

The numerical estimate of the effective properties of random heterogeneous materials from the constitutive law and the spatial distribution of different components of the microstructure is a main subject in the mechanics of random materials. It is related to the determination of the size of the RVE which has been recently studied widely with the numerical and statistical tools (Sab, 1992; Gusev, 1997; Terada et al., 1998; Ostoja-Starzewski, 1993, 1996, 1998; Kanit et al., 2003; Sab and Nedjar, 2005; Lachihab and Sab, 2005, 2008).

The RVE is usually seen as a volume containing heterogeneous materials. It is sufficiently large to be statistically representative of the composite, i.e., to effectively include a sampling of all microstructural heterogeneities that occur in the composite. The RVE must thus include a large number of micro-heterogeneities (grains, fibers,...). It must however remain small enough to be considered as a volume element of continuum mechanics. Several types of boundary conditions can be prescribed on this volume to impose a given mean strain or a given mean stress to the material element.
Another definition of the RVE was recently proposed by Drugan and Willis (1996): "It is the smallest material volume element of the composite for which the usual spatially constant (overall

modulus) macroscopic constitutive representation is a sufficiently accurate model to represent mean constitutive response". This approach does not consider statistical fluctuations of the effective properties over finite domains. Hence, the obtained RVE size is smaller than that of the previous studies. An analytical estimation for the RVE is derived by these authors from this definition and the Hashin-Shtrikan variational principle for infinite media. Several expansions of this theory can be found in Drugan (2003); Luciano and Willis (2004). It should be emphasized that this theory may be not accurate for microstructures with a high contrast in material properties. For this reason, the numerical techniques showed the advantages in comparison with the variational approaches.
The numerical computation of the RVE size of a random medium is based on the solution of the boundary value problem on the RVE for many realizations of the random medium. Up to now, such a strategy was limited to boundary value problems with homogenous or periodic boundary conditions. However, mixed boundary conditions must be used for periodic plates as shown in the third chapter: In-plane periodic conditions for the lateral boundaries of the unit cell and traction-free boundary conditions for the other boundaries of the unit cell. For random microstructures, there are three length scales: the thickness of the plate, the heterogeneity typical size (the mean radius of the inclusions in a two-phase material, for instance) and the in-plane size of the RVE which has to be determined. The size effect of the heterogeneity has been indeed studied in the previous chapter using the Hashin-Shtrikman variational principle for heterogeneous plates. However, when the contrast in material properties is high, the use of the numerical methods is more appropriate.

The purpose of this chapter is therefore to numerically estimate the size of the RVE of a random heterogeneous plate. The approach is based on the numerical method presented in the chapter 3 for computing the effective elastic properties of periodic heterogeneous plates. This chapter is organized as follows: The geometrical modelling of the microstructure of the plate is first presented. Then, the well-known Monte-Carlo method for computing ensemble average is recalled. Finally, we will present the numerical results.

5.2 Generation of the Microstructure

The microstructure of real materials is often very complicated and the analysis on such real geometries is too difficult. Hence, the real microstructure is usually idealized with a virtual microstructure which can be easily generated. The virtual microstructure considered here is a two-phase material consisting of a random 2D network of hexagonal particles having the same shape as shown in figure 5.1. The elastic properties are randomly and independently assigned to each particle: The particle belongs to phase 1 with probability c_1 and to phase 2 with probability $1 - c_1$. Phases 1 and 2 are both isotropic with the same Poisson's ratio (ν=0.3). The contrast in the Young's modulus will be considered. Actually, this 2D microstructure corresponds to a fiber-matrix microstructure.

The random microstructure of a unit cell generating the plate is illustrated in the figure

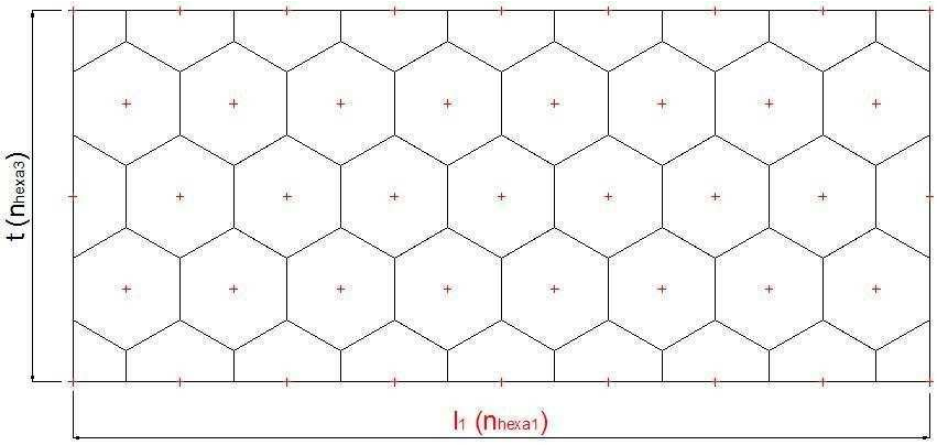

Figure 5.1: Illustration of the geometry of a hexagonal network.

Figure 5.2: Illustration of a unit cell with 8x4 hexagons and $c_1 = 0.5$.

5.2. White color is assigned to phase 1 (inclusion) and black color to phase 2 (matrix). The number of white particles in the cell can be controlled in order to satisfy a required density. Moreover, the generated microstructure must be compatible with periodicity condition on the vertical boundaries of the unit cell. This means that two half-hexagons situated on the two vertical opposite faces are occupied by the same phase.

5.3 Mean Effective Properties

A numerical method for the computation of the effective elastic properties of periodic plates has been presented in the chapter 3. It is based on a new $\mathbf{\Gamma}$-operator for periodic media with traction-free boundary conditions, the Fast Fourier Transform and an iterative procedure. The convergence of this procedure is actually fast for soft inclusions, including voids. Thus, it will use to compute the effective elastic properties of each realization of the above described random

plate.

For a given unit cell geometry Y as defined in (3.51), and for N independent realizations of the microstructure in the cell Y, let $(Z_1, \ldots, Z_N)$ represent the N computed effective properties corresponding to these realizations. The mean effective property is the ensemble average $\mathbb{E}(Z)$ of the random variable Z. It can be computed by using the Monte-Carlo method. The mean value of Z and its standard deviation are respectively estimated by:

$$\overline{Z}_N = \frac{1}{N}(Z_1 + \cdots + Z_N), \tag{5.1}$$

and,

$$\sigma_N^2 = \frac{1}{N-1}\sum_{i=1}^{N}(Z_i - \overline{Z}_N)^2. \tag{5.2}$$

The absolute and relative errors on the mean value obtained with N independent realizations of the volume Y are respectively estimated by:

$$\epsilon_{abs} = 1.96\frac{\sigma_N}{\sqrt{N}}, \tag{5.3}$$

and,

$$\epsilon_{rela} = 1.96\frac{\sigma_N}{\overline{Z}_N\sqrt{N}}. \tag{5.4}$$

For sufficiently large N, there is a 95%-probability for $E(Z)$ to be in the confidence interval $[\overline{Z}_N - \epsilon_{rela}\overline{Z}_N, \overline{Z}_N + \epsilon_{rela}\overline{Z}_N]$. The number of realizations N is chosen so that the obtained errors are smaller to a given precision for each volume size.

5.4 Parametric Study

The computed effective properties depend on the following parameters: n_{hexa3}, the number of hexagons in the x_3-direction (thickness), n_{hexa1}, the number of hexagons in the x_1-direction (length), E_1/E_2, the contrast in the Young's modulus and c_1, the volume fraction of phase 1. For fixed n_{hexa3}, E_1/E_2 and c_1, the minimum size for the RVE is the number n_{hexa1} for which the mean effective elastic properties reach their asymptotic values up to a given precision. However, according to similar studies of the literature, this should occur before the vanishing of the dispersion. Moreover, in the case of voids, a percolated microstructure can be generated for a critical volume fraction.

Figure 5.3 displays the effective membrane stiffness computed in terms of the number of hexagons in the x_1-direction (n_{hexa1}). The effective stiffness is normalized with that produced in a homogeneous medium with properties of the phase 1. The results are calculated with the

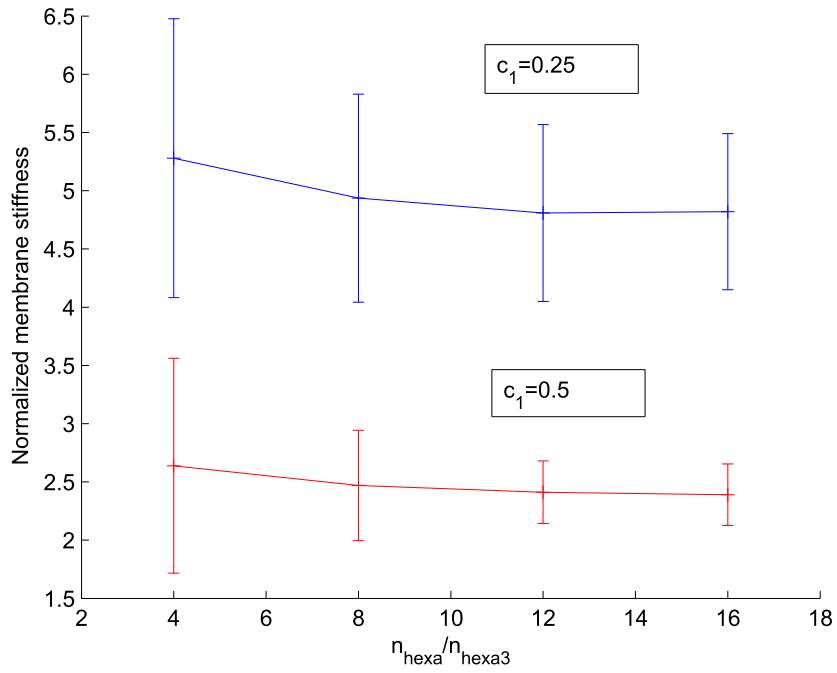

Figure 5.3: Mean value and intervals of confidence for $E_2/E_1 = 10$, $\epsilon_{rela} \leq 1\%$

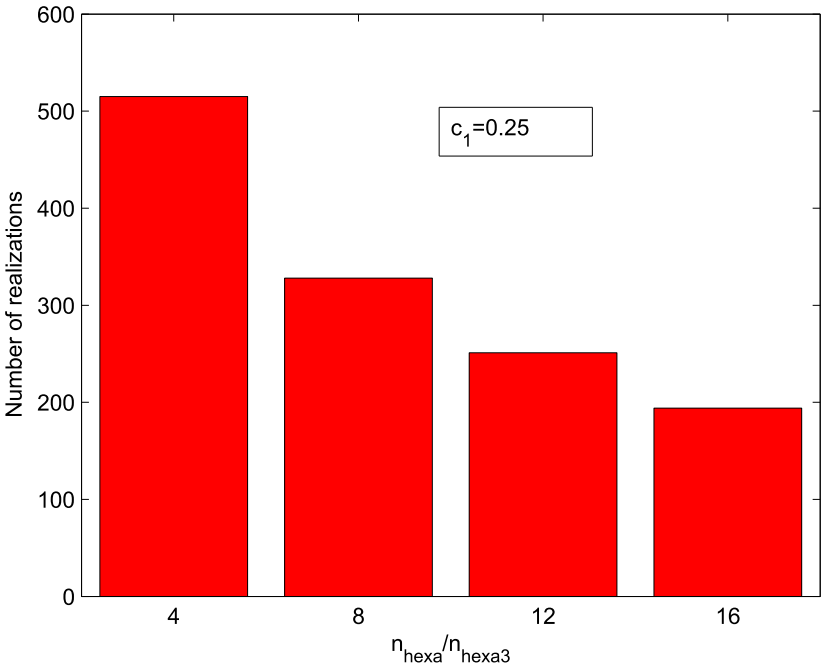

Figure 5.4: Number of realizations in terms of n_{hexa1} for $E_2/E_1 = 10$, $\epsilon_{rela} \leq 1\%$

concentration of the phase 1, $c_1 = 0.25$ and $c_1 = 0.5$. The ensemble average values are displayed with their corresponding intervals of confidence: $[\overline{Z}_N - 1.96\sigma_N, \overline{Z}_N + 1.96\sigma_N]$. Moreover, to compare with the result obtained in the chapter 4, a contrast in material properties, $E_2/E_1 = 10$, is selected.
Figure 5.3 showed that for a fixed n_{hexa3} ($n_{hexa3} = 4$ in this example), the mean values of the effective membrane stiffness of the plate decreases when n_{hexa1} increases and that these values are stationary starting from $n_{hexa1} = 12$ from which a "plateau" appears. Additionally, it is noted that since the results presented in the figure 5.3 are computed with a small number of hexagons in the thickness, the vanishing of the dispersion of the mean membrane stiffness will require a great number of hexagons in the plane.
Figure 5.4 presents the number of realizations in terms of the number of hexagons in the x_1-direction. Obviously, the number of realizations decreases when the number of hexagons increases. Finally, in comparison with the result obtained from the Hashin-Shtrikman variational principle presented in the chapter 4, one observes that, for this example, there is no the significant difference between the present simulation and the variational calculation. So, a study of the minimal size of the RVE for a high contrast needs to be considered.

5.5 Conclusion of the chapter

This chapter presented a simulation for estimating the minimum size of the Representative Volume Element (RVE) for a random plate. It is based on a new numerical method proposed in the chapter 3 for calculating the effective elastic properties of periodic plates. The microstructure of a two-phase plate was randomly generated with identical hexagons and the ensemble average of the effective properties of the plate for many independent realizations on each volume size was calculated by using the Monte-Carlo method.
The obtained result for a small contrast in material properties is similar with that obtained by using the Hashin-Shtrikman variational principle presented in the chapter 4. The effect of the morphology of the microstructure in this case is small.
So, main topics of future research should be the quantitative estimation of the size of the representative volume element for present plates made of materials with a significant contrast in their mechanical properties.

General Conclusions and Perspectives

The issues discussed in this thesis focus on the identification of the transverse shear effects for functionally graded plates and the proposition of a new $\boldsymbol{\Gamma}$-operator for periodic media with traction-free boundary conditions. This operator has been first used to compute numerically the effective elastic properties of periodic plates. It has been then used to study the size effect of the heterogeneity of random plates.

The first chapter presented functionally graded materials as an advanced composite material with gradual spatial variations of the material properties to improve the thermomechanical performance of classical multilayered materials. In this chapter, we reminded several plate models used for the analysis of thermomechanical behaviour of these materials, as well as homogenization methods for determining the effective properties of functionally graded materials. The conclusions derived from this chapter led to the proposition of a plate model for functionally graded materials with improved shear stiffness and a new homogenization method for heterogeneous plates.

In the second chapter, we proposed a plate model based on the first-order shear deformation plate theory (FSDT) for functionally graded materials where the improved shear stiffness and shear correction coefficients were identified. The obtained results from the closed-form solutions showed that the shear correction factor is not the same as the one of the homogeneous FSDT models, and is a function of the ratio between elastic moduli of constituents and of the distribution of materials through the models. Its effect is the most significant for the sandwich plate. For a classical, non-symmetrical FGM plate, the maximum tensile stress is located within the plate, contrarily to the case of a homogenous plate. The variation of the shear stress through the thickness of the FG plate given by the FSDT model is identical to the one given by the finite element model, while this is not the case for the higher-order plate models.

In the third chapter, the homogenization methods for periodic media and for heterogeneous plates were first reminded, including the resolution methods of the localization elastic problems. We then proposed a new method for solving of the boundary value problem on a 3D unit cell with both periodic and traction-free boundary conditions. This approach allowed formulating a new corresponding $\boldsymbol{\Gamma}$-operator. This operator has been then used to compute the effective

elastic properties of plates made of periodically distributed inhomogeneous cells where a basic iterative algorithm has been used. Numerical applications were performed and the comparison of the obtained results with closed-form solutions and finite-element results have shown the accuracy and the speed of convergence of the series solution. The convergence is slow for very stiff inclusions.

Based on the $\mathbf{\Gamma}$-operator established in Chapter 3, we proposed a Hashin-Shtrikman variational principle for heterogeneous plates in Chapter 4. For deterministic microstructures, the assumption of invariant in-plane polarization stresses led to an equivalent laminated plate by using in-plane average of materials in the thickness. We proved that the optimal lower and upper bounds for the effective elastic properties of the plate were the refined estimates on the Voigt and Reuss bounds proposed by Kolpakov (1999) for heterogeneous plates.
A Hashin-Shtrikman variational formulation was also derived for random heterogeneous plates whose constituents were supposed to be statistically uniform in the in-plane directions. A two-phase plate made of isotropic materials was analyzed for a microstructure with impenetrable inclusions. To predict the size effect of the heterogeneity, the obtained effective elastic properties of the plate were compared with those derived from the classic Hashin-Shtrikman estimates. The obtained relative differences between two methods showed that the scale effect due to the traction-free boundaries is small.

In the chapter 5, we applied the numerical method proposed in Chapter 3 to estimate the minimal size of the Representative Volume Element (RVE) of a two-phase random plate. The microstructure of the plate was randomly generated with identical hexagons. The calculation of the effective properties of the plate was performed by the Monte-Carlo method. A small contrast in material properties was considered and the obtained results showed that there is no the significant differences, in the prediction of the in-plane minimal size of RVE of the plate, in comparison with the obtained results in the chapter 4. However, this numerical estimation will be efficient when studying with a high contrast of materials since the use of the variational principle in this situation is not accurate anymore due to a large difference of the bounds.

The publications related to this thesis are: Nguyen et al. (2007), Nguyen et al. (2008a), Nguyen et al. (2008b), Nguyen et al. (2008c).

Finally, let us discuss some possible future works.
In fact, the gradual spatial variation in material properties of the functionally graded materials has been widely developed for aeronautic applications. The use of this concept for civil engineering applications is a promising field for future researches. An optimal arrangement of materials can indeed create innovative structures having the required resistant, thermal and acoustic capacities (for example, light concrete structures). The first-order plate model presented in Chapter 2 and the homogenization plate models of Chapters 3 and 4 can be used as the basic tools for deriving the optimal distribution of phases. Moreover, an experimental strategy has to be considered in order to fabricate the optimally graded structure.

From the theoretical point of view, the homogenization method proposed in Chapter 3 has

been applied for computing the effective in-plane and out-of-plane elastic properties of periodic plates. It is therefore necessary to develop the theory for identifying the transverse shear stiffness of periodic plates (see the work of Cecchi and Sab (2007)). Moreover, the computations reported in Chapter 3 were based on a basic iterative algorithm where the convergence was slow for very stiff inclusions. The improvement of this algorithm could be considered by using the accelerated scheme of Eyre and Milton (1999), the augmented Lagrangian method of Michel et al. (2001) or the dual solution described in Bonnet (2007). The expansion of the proposed homogenization theory for nonlinear media also is an interesting study.

Concerning Chapter 4, we have the following observations. The improvement of the refined estimates on the Voigt and Reuss bounds can be considered by using directly the solution field proposed in Chapter 3. Moreover, an identification of the variation of the polarization stress field needs to be analyzed for the quality of the bounds for the effective properties of the plate.
Finally, based on the procedure established in Chapter 5, a quantitative estimate of the minimal size of the representative volume element of random plates for a high contrast in material properties can be performed.

Appendix A

Closed-Form Solutions for Functionally Graded Plates

A.1 Navier's Solution for the Functionally Graded Reissner-Mindlin Plate

The boundary conditions for the simply supported rectangular plates are of the form,

$$\begin{aligned}
&u_o(x,0)=0, \quad w_o(x,0)=0, \quad \theta_x(x,0)=0,\\
&u_o(x,b)=0, \quad w_o(x,b)=0, \quad \theta_x(x,b)=0,\\
&v_o(0,y)=0, \quad w_o(0,y)=0, \quad \theta_y(0,y)=0,\\
&v_o(a,y)=0, \quad w_o(a,y)=0, \quad \theta_y(a,y)=0,\\
&N_{xx}(0,y)=0, \quad N_{xx}(a,y)=0,\\
&N_{yy}(x,0)=0, \quad N_{yy}(x,b)=0,\\
&M_{xx}(0,y)=0, \quad M_{xx}(a,y)=0,\\
&M_{yy}(x,0)=0, \quad M_{yy}(x,b)=0.
\end{aligned} \tag{A.1}$$

The external force is expressed as a double trigonometric series,

$$q(x,y)=\sum_{n=1}^{\infty}\sum_{m=1}^{\infty} q_{mn} sin\lambda x\, sin\mu y, \tag{A.2}$$

where $\lambda = m\pi/a$ and $\mu = n\pi/b$. The coefficients q_{mn} for the uniformly distributed load are defined as follows:

$$q_{mn}=\begin{cases} \frac{16q_o}{mn\pi^2} & \text{for m,n odd}\\ 0 & \text{for m,n even}\end{cases} \tag{A.3}$$

where q_o represents the load intensity on the plate surface. The Navier's solution for simply supported plates under the uniform distributed load is given by:

$$u_o(x,y) = \sum_{n=1}^{\infty}\sum_{m=1}^{\infty} u_{mn} cos\lambda x\, sin\mu y, \tag{A.4}$$

$$v_o(x,y) = \sum_{n=1}^{\infty}\sum_{m=1}^{\infty} v_{mn} sin\lambda x\, cos\mu y, \tag{A.5}$$

$$w_o(x,y) = \sum_{n=1}^{\infty}\sum_{m=1}^{\infty} w_{mn} sin\lambda x\, sin\mu y, \tag{A.6}$$

$$\theta_x(x,y) = \sum_{n=1}^{\infty}\sum_{m=1}^{\infty} x_{mn} cos\lambda x\, sin\mu y, \tag{A.7}$$

$$\theta_y(x,y) = \sum_{n=1}^{\infty}\sum_{m=1}^{\infty} y_{mn} sin\lambda x\, cos\mu y. \tag{A.8}$$

The equilibrium equations of plates are given by,

$$N_{\alpha\beta,\beta} = 0, \quad M_{\alpha\beta,\beta} = Q_\alpha, \quad Q_{\alpha,\alpha} + q = 0. \tag{A.9}$$

The constitutive relations can be written as:

$$\begin{aligned} N_{\alpha\beta}(x,y) &= A_{\alpha\beta\gamma\delta}\epsilon^o_{\gamma\delta}(x,y) + B_{\alpha\beta\gamma\delta}\chi_{\gamma\delta}(x,y), \\ M_{\alpha\beta}(x,y) &= B_{\alpha\beta\gamma\delta}\epsilon^o_{\gamma\delta}(x,y) + D_{\alpha\beta\gamma\delta}\chi_{\gamma\delta}(x,y), \\ Q_\alpha(x,y) &= H_{\alpha\beta}\,\gamma_{\beta 3}(x,y) \quad \text{given in (2.14)}, \end{aligned} \tag{A.10}$$

where $\epsilon^o_{\gamma\delta}$ and $\chi_{\gamma\delta}$ are given in (2.2), and $H_{\alpha\beta}$ are the improved shear stiffnesses given in (2.17). Substituting equations (A.4 - A.8), (A.2, A.3) into (A.9), the following equation system is obtained,

$$\begin{bmatrix} s_{11} & s_{12} & 0 & s_{14} & s_{15} \\ s_{12} & s_{22} & 0 & s_{24} & s_{25} \\ 0 & 0 & s_{33} & s_{34} & s_{35} \\ s_{14} & s_{24} & s_{34} & s_{44} & s_{45} \\ s_{15} & s_{25} & s_{35} & s_{45} & s_{55} \end{bmatrix} \begin{Bmatrix} u_{mn} \\ v_{mn} \\ w_{mn} \\ x_{mn} \\ y_{mn} \end{Bmatrix} = \begin{Bmatrix} 0 \\ 0 \\ q_{mn} \\ 0 \\ 0 \end{Bmatrix}, \tag{A.11}$$

where the coefficients of the matrix s are given by,

$$\begin{aligned}
&s_{11} = A_{1111}\lambda^2 + A_{1212}\mu^2,\ s_{12} = (A_{1122} + A_{1212})\lambda\mu,\\
&s_{14} = B_{1111}\lambda^2 + B_{1212}\mu^2, s_{15} = (B_{1122} + B_{1212})\lambda\mu,\\
&s_{22} = A_{1212}\lambda^2 + A_{2222}\mu^2,\ s_{24} = s_{15},\\
&s_{25} = B_{1212}\lambda^2 + B_{2222}\mu^2,\ s_{33} = H_{55}\lambda^2 + H_{44}\mu^2,\\
&s_{34} = H_{55}\lambda,\ s_{35} = H_{44}\mu,\\
&s_{44} = H_{55} + D_{1111}\lambda^2 + D_{1212}\mu^2,\\
&s_{45} = (D_{1122} + D_{1212})\lambda\mu,\\
&s_{55} = H_{44} + D_{2222}\mu^2 + D_{1212}\lambda^2.
\end{aligned} \tag{A.12}$$

The in-plane stress fields are defined as follows,

$$\sigma_{xx} = -\frac{E(z)}{1-\nu(z)^2}\sum_{n=1}^{\infty}\sum_{m=1}^{\infty}\left[(u_{mn}\lambda + \nu(z)\mu v_{mn}) + z(x_{mn}\lambda + \nu(z)\mu y_{mn})\right] sin\lambda x\, sin\mu y, \tag{A.13}$$

$$\sigma_{yy} = -\frac{E(z)}{1-\nu(z)^2}\sum_{n=1}^{\infty}\sum_{m=1}^{\infty}\left[(v_{mn}\mu + \nu(z)\lambda u_{mn}) + z(y_{mn}\mu + \nu(z)\lambda x_{mn})\right] sin\lambda x\, sin\mu y, \tag{A.14}$$

$$\sigma_{xy} = \frac{E(z)}{2(1+\nu(z))}\sum_{n=1}^{\infty}\sum_{m=1}^{\infty}\left[(u_{mn}\mu + \lambda v_{mn}) + z(x_{mn}\mu + \lambda y_{mn})\right] cos\lambda x\, cos\mu y. \tag{A.15}$$

Transverse shear stresses are determined by expression (2.13) as follows,

$$\sigma_{xz} = \tilde{m}_{1111}(z)\, H_{55}\sum_{n=1}^{\infty}\sum_{m=1}^{\infty}\left[x_{mn} + \lambda w_{mn}\right] cos\lambda x\, sin\mu y, \tag{A.16}$$

$$\sigma_{yz} = \tilde{m}_{1212}(z)\, H_{44}\sum_{n=1}^{\infty}\sum_{m=1}^{\infty}\left[y_{mn} + \mu w_{mn}\right] sin\lambda x\, cos\mu y. \tag{A.17}$$

A.2 Closed-Form Solution for the Functionally Graded Sandwich Panel in Cylindrical Bending

Assuming that for cylindrical bending $\theta_y = 0$ everywhere, the boundary conditions for the clamped sandwich panel are of the form,

$$\begin{aligned}
&v_o(x=0) = 0,\ u_o(x=0),\ w(x=0) = 0,\\
&\theta_x(x=0) = 0,\\
&\\
&v_o(x=a) = 0,\ u_o(x=a) = 0,\ w(x=a) = 0,\\
&\theta_x(x=a) = 0.
\end{aligned} \tag{A.18}$$

The equilibrium equations (A.9) for the cylindrical bending plate can be written simplify as follows,

$$M_{xx,x} - Q_x = 0,\ Q_{x,x} + q = 0,\ N_{xx,x} = 0. \tag{A.19}$$

The generalized constitutive relations (A.10) for the isotropic materials are expressed explicitly,

$$\begin{cases} N_{xx} = A_{1111} u_{o,x} + B_{1111} \theta_{x,x}, \\ N_{yy} = A_{1122} u_{o,x} + B_{1122} \theta_{x,x}, \\ N_{xy} = A_{1212} v_{o,x}. \end{cases} \tag{A.20}$$

$$\begin{cases} M_{xx} = B_{1111} u_{o,x} + D_{1111} \theta_{x,x}, \\ M_{yy} = B_{1122} u_{o,x} + D_{1122} \theta_{x,x}, \\ M_{xy} = B_{1212} v_{o,x}, \end{cases} \tag{A.21}$$

and

$$Q_x = H_{55} \left(\theta_x + w_{,x} \right). \tag{A.22}$$

Similarly, substituting the expressions (A.20, A.21, A.22) into the equilibrium equations (A.19), leads to the following relations

$$D \theta_{x,xx} - H_{55} \left(\theta_x + w_{,x} \right) = 0, \tag{A.23}$$

$$H_{55} \left(w_{o,xx} + \theta_{x,x} \right) + q = 0, \tag{A.24}$$

where $D = D_{1111} - B_{1111}^2 / A_{1111}$ is the stiffness of the sandwich panel. For $q(x) = q_o = const$ and by applying the boundary conditions (A.18), the equations (A.23) and (A.24) lead to:

$$\theta_x(x) = -\frac{q_o a^3}{12D} \left[2 \left(\frac{x}{a} \right)^3 - 3 \left(\frac{x}{a} \right)^2 + \left(\frac{x}{a} \right) \right], \tag{A.25}$$

$$w_o(x) = \frac{q_o a^4}{24D} \left[\left(\frac{x}{a} \right)^2 - \left(\frac{x}{a} \right) \right]^2 + \frac{q_o a^2}{2H_{55}} \left[\left(\frac{x}{a} \right) - \left(\frac{x}{a} \right)^2 \right]. \tag{A.26}$$

The maximal deflection obtained at the middle of the plate ($x = a/2$) is of the form :

$$w_{omax} = \frac{q_o a^4}{384D} \left(1 + \frac{48D}{H_{55} a^2} \right). \tag{A.27}$$

Appendix B

Solution of the Complementary Auxiliary Problem and Calculation of Related Operators

B.1 Displacement Field

The complementary solution $\tilde{\mathbf{u}}^h(\tilde{\mathbf{k}}, x_3)$ is obtained from a second order differential equation system with 3 degrees of freedom which was described in (3.60) and (3.61). To solve this problem, the solution field is chosen firstly as of the form,

$$\tilde{\mathbf{u}}^h(\tilde{\mathbf{k}}, x_3) = \mathbf{d}\, e^{r x_3}, \quad \mathbf{d} \neq 0. \tag{B.1}$$

Substituting this field into the system (3.60) leads to the following condition, deduced from the null value of the determinant of the system of equations :

$$(r^2 - s^2)^3 = 0 \quad \text{where} \quad s = \sqrt{k_1^2 + k_2^2}. \tag{B.2}$$

Generally, this relation leads a priori to the fact that $\mathbf{d}$ is a second-order polynomial of x_3 and that the solution is of the form,

$$\tilde{\mathbf{u}}^h(\tilde{\mathbf{k}}, x_3) = (\mathbf{a}^+ + \mathbf{b}^+ x_3 + \mathbf{c}^+ x_3^2)\, e^{s x_3} + (\mathbf{a}^- + \mathbf{b}^- x_3 + \mathbf{c}^- x_3^2)\, e^{-s x_3}. \tag{B.3}$$

However, the values of $(\mathbf{a}^\pm, \mathbf{b}^\pm, \mathbf{c}^\pm)$ are not independent, because the solution of the system of equations (3.60) must be described by using only 6 independent constants. Introducing expression (A.3) into equation (3.60) allows to express $\tilde{\mathbf{u}}^h$ by using 6 independent constants $a_1^+, a_1^-, a_2^+, a_2^-, b_3^+, b_3^-$ and to show that $\mathbf{c}^+ = \mathbf{c}^- = 0$.

More precisely, the 3 boundary conditions at the top face ($x_3 = t/2$) and 3 boundary conditions at the bottom face ($x_3 = -t/2$) of the unit cell enable to construct a system of 6 equations for determining 6 coefficients of the vector $\boldsymbol{\xi} = (a_1^+, a_1^-, a_2^+, a_2^-, b_3^+, b_3^-)$,

$$\mathbf{K}\boldsymbol{\xi} = \mathbf{q}, \tag{B.4}$$

where

$$\mathbf{K} = \begin{bmatrix} \frac{\mu}{s}(s^2+k_1^2)e^{s\frac{t}{2}} & -\frac{\mu}{s}(s^2+k_1^2)e^{-s\frac{t}{2}} & \frac{\mu}{s}k_1k_2e^{s\frac{t}{2}} & -\frac{\mu}{s}k_1k_2e^{-s\frac{t}{2}} & 2\frac{\mu}{s}ik_1\gamma^-e^{s\frac{t}{2}} & 2\frac{\mu}{s}ik_1\gamma^+e^{-s\frac{t}{2}} \\ \frac{\mu}{s}(s^2+k_1^2)e^{-s\frac{t}{2}} & -\frac{\mu}{s}(s^2+k_1^2)e^{s\frac{t}{2}} & \frac{\mu}{s}k_1k_2e^{-s\frac{t}{2}} & -\frac{\mu}{s}k_1k_2e^{s\frac{t}{2}} & -2\frac{\mu}{s}ik_1\gamma^+e^{-s\frac{t}{2}} & -2\frac{\mu}{s}ik_1\gamma^-e^{s\frac{t}{2}} \\ \frac{\mu}{s}k_1k_2e^{s\frac{t}{2}} & -\frac{\mu}{s}k_1k_2e^{-s\frac{t}{2}} & \frac{\mu}{s}(s^2+k_2^2)e^{s\frac{t}{2}} & -\frac{\mu}{s}(s^2+k_2^2)e^{-s\frac{t}{2}} & 2\frac{\mu}{s}ik_2\gamma^-e^{s\frac{t}{2}} & 2\frac{\mu}{s}ik_2\gamma^+e^{-s\frac{t}{2}} \\ \frac{\mu}{s}k_1k_2e^{-s\frac{t}{2}} & -\frac{\mu}{s}k_1k_2e^{s\frac{t}{2}} & \frac{\mu}{s}(s^2+k_2^2)e^{-s\frac{t}{2}} & -\frac{\mu}{s}(s^2+k_2^2)e^{s\frac{t}{2}} & -2\frac{\mu}{s}ik_2\gamma^+e^{-s\frac{t}{2}} & -2\frac{\mu}{s}ik_2\gamma^-e^{s\frac{t}{2}} \\ -2\mu ik_1e^{s\frac{t}{2}} & -2\mu ik_1e^{-s\frac{t}{2}} & -2\mu ik_2e^{s\frac{t}{2}} & -2\mu ik_2e^{-s\frac{t}{2}} & 2\mu\eta^-e^{s\frac{t}{2}} & -2\mu\eta^+e^{-s\frac{t}{2}} \\ -2\mu ik_1e^{-s\frac{t}{2}} & -2\mu ik_1e^{s\frac{t}{2}} & -2\mu ik_2e^{-s\frac{t}{2}} & -2\mu ik_2e^{s\frac{t}{2}} & -2\mu\eta^+e^{-s\frac{t}{2}} & 2\mu\eta^-e^{s\frac{t}{2}} \end{bmatrix}, \tag{B.5}$$

with $\gamma^\pm = s\frac{t}{2} \pm \frac{\mu}{\lambda+\mu}$, $\eta^\pm = s\frac{t}{2} \pm \frac{\lambda+2\mu}{\lambda+\mu}$, and the components of the vector $\mathbf{q} = (q_1^+, q_1^-, q_2^+, q_2^-, q_3^+, q_3^-)$ are defined in (B.8). The closed-form solution of (B.4) has been presented in the third chapter.

B.2 Strain Field

The calculation of the strain field $\tilde{\mathbf{e}}^h(\tilde{\mathbf{k}}, x_3)$ for $|\tilde{\mathbf{k}}| \neq 0$ ($s \neq 0$) is performed owing to the compatibility condition which may be expressed as follows:

$$\tilde{\mathbf{e}}^h(\tilde{\mathbf{k}}, x_3) = \mathbf{P}(\tilde{\mathbf{k}}, x_3)\,.\,\boldsymbol{\xi}(\tilde{\mathbf{k}}) = \mathbf{P}(\tilde{\mathbf{k}}, x_3)\,\mathbf{K}^{-1}(\tilde{\mathbf{k}})\,\mathbf{q}(\tilde{\mathbf{k}}) \quad \forall |\tilde{\mathbf{k}}| \neq 0, \tag{B.6}$$

where

$$\mathbf{P} = \begin{bmatrix} ik_1e^{sx_3} & ik_1e^{-sx_3} & 0 & 0 & -\frac{k_1^2}{s}x_3e^{sx_3} & \frac{k_1^2}{s}x_3e^{-sx_3} \\ 0 & 0 & ik_2e^{sx_3} & ik_2e^{-sx_3} & -\frac{k_2^2}{s}x_3e^{sx_3} & \frac{k_2^2}{s}x_3e^{-sx_3} \\ -ik_1e^{sx_3} & -ik_1e^{-sx_3} & -ik_2e^{sx_3} & -ik_2e^{-sx_3} & (x_3s - \frac{2\mu}{\lambda+\mu})e^{sx_3} & -(x_3s + \frac{2\mu}{\lambda+\mu})e^{-sx_3} \\ \frac{k_1k_2}{2s}e^{sx_3} & -\frac{k_1k_2}{2s}e^{-sx_3} & \frac{s^2+k_2^2}{2s}e^{sx_3} & -\frac{s^2+k_2^2}{2s}e^{-sx_3} & \frac{ik_2}{s}(x_3s - \frac{\mu}{\lambda+\mu})e^{sx_3} & \frac{ik_2}{s}(x_3s + \frac{\mu}{\lambda+\mu})e^{-sx_3} \\ \frac{s^2+k_1^2}{2s}e^{sx_3} & -\frac{s^2+k_1^2}{2s}e^{-sx_3} & \frac{k_1k_2}{2s}e^{sx_3} & -\frac{k_1k_2}{2s}e^{-sx_3} & \frac{ik_1}{s}(x_3s - \frac{\mu}{\lambda+\mu})e^{sx_3} & \frac{ik_1}{s}(x_3s + \frac{\mu}{\lambda+\mu})e^{-sx_3} \\ \frac{ik_2}{2}e^{sx_3} & \frac{ik_2}{2}e^{-sx_3} & \frac{ik_1}{2}e^{sx_3} & \frac{ik_1}{2}e^{-sx_3} & -\frac{k_1k_2}{s}x_3e^{sx_3} & \frac{k_1k_2}{s}x_3e^{-sx_3} \end{bmatrix}, \tag{B.7}$$

and the components of the vector $\mathbf{q}(\tilde{\mathbf{k}}) = (q_1^+, q_1^-, q_2^+, q_2^-, q_3^+, q_3^-)$ are derived from the boundary conditions (3.64). They are expressed in terms of the periodic stresses, $\hat{\boldsymbol{\sigma}}^p(\mathbf{k})$, in the Fourier space:

$$q_j^{\pm} = -\sum_{k_3} e^{\pm ik_3 \frac{t}{2}}\, \hat{\sigma}^p_{j3}(\mathbf{k}) = -\sum_{k_3} e^{\pm ik_3 \frac{t}{2}}\, \hat{\Delta}_{j3mn}(\mathbf{k})\, \hat{\tau}_{mn}(\mathbf{k}), \tag{B.8}$$

where $\hat{\boldsymbol{\Delta}}(\mathbf{k}) = \mathbf{I} - \mathbf{L}^o\, \hat{\boldsymbol{\Gamma}}_p(\mathbf{k})$ and noticing that $\hat{\boldsymbol{\Delta}}(\mathbf{k})$ is calculated with $\mathbf{k} \neq 0$ and it is reduced to the unity matrix $\mathbf{I}$ for $\mathbf{k} = 0$. Therefore, the relation (B.8) allows to construct a matrix $\mathbf{S}(\mathbf{k})$ constituted from the product $e^{\pm ik_3 \frac{t}{2}}\, \hat{\Delta}_{j3mn}(\mathbf{k})$ according to the vector $\mathbf{q}(\tilde{\mathbf{k}})$ corresponding, hence

$$\mathbf{q}(\tilde{\mathbf{k}}) = -\sum_{k_3} \mathbf{S}(\mathbf{k})\, \hat{\boldsymbol{\tau}}(\mathbf{k}). \tag{B.9}$$

Substituting the previous expression into (B.6) and taking into account the Fourier transformation in x_3' of the polarizations leads to

$$\tilde{\mathbf{e}}^h(\tilde{\mathbf{k}}, x_3) = -\frac{1}{t} \int_{-t/2}^{t/2} \tilde{\boldsymbol{\Gamma}}_h(\tilde{\mathbf{k}}, x_3, x_3')\, \tilde{\boldsymbol{\tau}}(\tilde{\mathbf{k}}, x_3')\, dx_3', \tag{B.10}$$

where operator $\tilde{\boldsymbol{\Gamma}}_h(\tilde{\mathbf{k}}, x_3, x_3')$ at the given points (x_3, x_3') is defined by

$$\tilde{\boldsymbol{\Gamma}}_h(\tilde{\mathbf{k}}, x_3, x_3') = \mathbf{P}(\tilde{\mathbf{k}}, x_3)\, \mathbf{K}^{-1}(\tilde{\mathbf{k}}) \sum_{k_3} \mathbf{S}(\mathbf{k})\, e^{-ik_3 x_3'}. \tag{B.11}$$

It should be noted that this expression is calculated with $\tilde{\mathbf{k}} \neq 0$, its value at $\tilde{\mathbf{k}} = 0$ is also considered from the strains corresponding. Taking into account the definition (3.32), the complementary strains can be written in the real space as (4.21).

For $|\tilde{\mathbf{k}}| = 0$, the membrane strains $\tilde{e}^h_{\alpha\beta}$ are null due to the periodicity on ∂Y_l of the displacement field, i.e. $\tilde{e}^h_{\alpha\beta}(\tilde{\mathbf{k}} = 0, x_3) = 0$. The calculation of $\tilde{e}^h_{j3}(\tilde{\mathbf{k}} = 0, x_3)$ is also performed by using the boundary condition (3.64) and the differential equation system (3.60). This gives the expressions of the out-of-plane strain field as follows,

$$\begin{aligned} \tilde{e}^h_{33}(\tilde{\mathbf{k}} = 0, x_3) &= -\tfrac{1}{\lambda+2\mu} \textstyle\sum_{k_3} \hat{\sigma}^p_{33}(\tilde{\mathbf{k}} = 0, k_3)\, e^{ik_3 \frac{t}{2}} \\ \tilde{e}^h_{\alpha 3}(\tilde{\mathbf{k}} = 0, x_3) &= -\tfrac{1}{2\mu} \textstyle\sum_{k_3} \hat{\sigma}^p_{\alpha 3}(\tilde{\mathbf{k}} = 0, k_3)\, e^{ik_3 \frac{t}{2}}. \end{aligned} \tag{B.12}$$

For estimating the values of $\hat{\sigma}^p_{j3}$ at $\tilde{\mathbf{k}} = 0$, it is noted that the out-of-plane stresses, $\hat{\sigma}^p_{j3}$, are null for the case of $\tilde{\mathbf{k}} = 0$ and $k_3 \neq 0$. As a consequence, the calculation of the out-of-plane complementary strains in (B.12) is reduced to the case of $\mathbf{k} = 0$ where $\hat{\sigma}^p_{j3}(\mathbf{k} = 0) = \hat{\tau}_{j3}(\mathbf{k} = 0)$,

$$\tilde{e}^h_{33}(\tilde{\mathbf{k}} = 0, x_3) = -\frac{\hat{\tau}_{33}(\mathbf{k} = 0)}{\lambda + 2\mu}, \quad \tilde{e}^h_{\alpha 3}(\tilde{\mathbf{k}} = 0, x_3) = -\frac{\hat{\tau}_{\alpha 3}(\mathbf{k} = 0)}{2\mu}. \tag{B.13}$$

It allows to determine the non-null components of the $\tilde{\mathbf{\Gamma}}_h$ at $\tilde{\mathbf{k}} = 0$ as follows: $\tilde{\Gamma}^h_{3333}(\tilde{\mathbf{k}} = 0, x_3) = 1/(\lambda + 2\mu)$ and $\tilde{\Gamma}^h_{\alpha 3 \alpha 3}(\tilde{\mathbf{k}} = 0, x_3) = 1/2\mu$.

Appendix C

Modelling a Periodic Symmetrical Cell

The symmetries enable us to obtain simplifications, more specifically concerning the boundary conditions. The symmetries lead indeed to the use of "Dirichlet" boundary conditions instead of "periodicity" conditions, the former ones being easier to account for within finite element computations (see Cecchi and Sab (2002b)). Consider a symmetrical periodic cell Y which is subjected to the boundary conditions (3.70). The symmetrical domain Y is defined as follows,

$$Y = \left]-\frac{l_1}{2},\frac{l_1}{2}\right[\times \left]-\frac{l_2}{2},\frac{l_2}{2}\right[\times \left]-\frac{t}{2},\frac{t}{2}\right[.$$

In a general way, if $\mathbf{x} \rightarrow \mathbf{u}^*(\mathbf{x})$ is the image of the displacement field $\mathbf{x} \rightarrow \mathbf{u}(\mathbf{x})$ by a symmetry $\mathbf{S}$, we have

$$\mathbf{u}^*(\mathbf{x}) = \mathbf{S} \,.\, \mathbf{u}({}^t\mathbf{S}.\mathbf{x}),$$

while the image of a second order tensor by the symmetry $\mathbf{S}$ is expressed in general as follows,

$$\mathbf{M}^*(\mathbf{x}) = \mathbf{S} \,.\, \mathbf{M}({}^t\mathbf{S}.\mathbf{x}) \,.\, {}^t\mathbf{S}.$$

These calculations imply that the image by $\mathbf{S}$ of the solution $(\boldsymbol{\sigma}, \boldsymbol{\epsilon}, \mathbf{u})$ of the problem (3.69,

3.70) complies to the following system,

$$\begin{cases} \boldsymbol{\sigma}^* \,.\, \boldsymbol{\nabla} = 0, \quad \boldsymbol{\sigma}^*(\mathbf{x}) = \mathbf{L}(\mathbf{x})\, \boldsymbol{\epsilon}^*(\mathbf{x}), \\ \\ \boldsymbol{\epsilon}^*(\mathbf{x}) = \mathbf{S} \,.\, \mathbf{E}({}^t\mathbf{S}.\mathbf{x}) \,.\, {}^t\mathbf{S} + (\mathbf{S} \,.\, \mathbf{x})_3\, \mathbf{S} \,.\, \boldsymbol{\chi}({}^t\mathbf{S}.\mathbf{x}) \,.\, {}^t\mathbf{S} + \mathbf{S} \,.\, \mathbf{e}({}^t\mathbf{S}.\mathbf{x}) \,.\, {}^t\mathbf{S}, \\ \\ \sigma^*_{j3} = 0 \quad \text{on} \quad \partial Y^{\pm}, \\ \\ \mathbf{u}^*(\mathbf{x}) \text{ periodic on } \partial Y_l, \quad \boldsymbol{\sigma}^*(\mathbf{x}) \text{ antiperiodic on } \partial Y_l, \end{cases} \tag{C.1}$$

where the elastic coefficients of $\mathbf{L}(\mathbf{x})$ are assumed to be left invariant by the symmetry $\mathbf{S}$. It can be seen that if a symmetry $\mathbf{S}$ and macroscopic tensors $(\mathbf{E}, \boldsymbol{\chi})$ are chosen so that,

$$\begin{cases} \mathbf{E}(\mathbf{x}) = \mathbf{S} \,.\, \mathbf{E}({}^t\mathbf{S}.\mathbf{x}) \,.\, {}^t\mathbf{S}, \\ \\ x_3 \boldsymbol{\chi}(\mathbf{x}) = (\mathbf{S} \,.\, \mathbf{x})_3\, \mathbf{S} \,.\, \boldsymbol{\chi}({}^t\mathbf{S}.\mathbf{x}) \,.\, {}^t\mathbf{S}, \end{cases} \tag{C.2}$$

the star and non-star variables will comply to the same system of equations. It remains to check that these variables are subjected to the same boundary conditions. In this appendix, it will be shown how to take into account the symmetry for two cases of the plane problem: ($\mathbf{E} = 1$, $\boldsymbol{\chi} = 0$) and ($\mathbf{E} = 0$, $\boldsymbol{\chi} = 1$).

For the first case ($\mathbf{E} = 1$, $\boldsymbol{\chi} = 0$), the matrix $\mathbf{S}$ corresponding to the symmetry with respect to the z-axis is of the form,

$$\mathbf{S} = \begin{pmatrix} -1 & 0 \\ 0 & 1 \end{pmatrix}. \tag{C.3}$$

By using the symmetry properties, the images of the fields $(\boldsymbol{\sigma}, \boldsymbol{\epsilon}, \mathbf{u})$ by the symmetry $\mathbf{S}$ are obtained by the following expressions,

$$\mathbf{u}^*(x,z) = \begin{Bmatrix} -u_x(-x,z) \\ \\ u_z(-x,z) \end{Bmatrix}, \quad \mathbf{e}^*(x,z) = \begin{pmatrix} e_{xx} & -e_{xz} \\ \\ -e_{xz} & e_{zz} \end{pmatrix}(-x,z), \tag{C.4}$$

$$\boldsymbol{\sigma}^*(x,z) = \begin{pmatrix} \sigma_{xx} & -\sigma_{xz} \\ \\ -\sigma_{xz} & \sigma_{zz} \end{pmatrix}(-x,z). \tag{C.5}$$

It can be seen in this case that the symmetry relative to the z-axis complies to the relationship (C.2). It means that $\mathbf{u}^*$ and $\mathbf{u}$ comply to the same field equations and to the same boundary conditions. The images $\mathbf{u}^*$ and $\boldsymbol{\sigma}^*$ are therefore also a solution of the problem. Taking into account the periodicity conditions of the displacement field and the antiperiodicity conditions of

the stress field on ∂Y_l leads to:

$$\begin{aligned} &u_x(0,z) = u_x(\tfrac{l_1}{2},z) = u_x(-\tfrac{l_1}{2},z) = 0, \\ &\sigma_{xz}(0,z) = \sigma_{xz}(\tfrac{l_1}{2},z) = \sigma_{xz}(-\tfrac{l_1}{2},z) = 0. \end{aligned} \tag{C.6}$$

If the symmetry with respect to the x-axis is considered, the symmetrical matrix $\mathbf{S}$ is given by

$$\mathbf{S} = \begin{pmatrix} 1 & 0 \\ 0 & -1 \end{pmatrix}. \tag{C.7}$$

The images of the fields $(\boldsymbol{\sigma}, \boldsymbol{\epsilon}, \mathbf{u})$ are then obtained,

$$\mathbf{u}^*(x,z) = \begin{Bmatrix} u_x(x,-z) \\ \\ -u_z(x,-z) \end{Bmatrix}, \quad \mathbf{e}^*(x,z) = \begin{pmatrix} e_{xx} & -e_{xz} \\ \\ -e_{xz} & e_{zz} \end{pmatrix}(x,-z), \tag{C.8}$$

$$\sigma^*(x,z) = \begin{pmatrix} \sigma_{xx} & -\sigma_{xz} \\ \\ -\sigma_{xz} & \sigma_{zz} \end{pmatrix}(x,-z). \tag{C.9}$$

It can be observed that the relation (C.2) is always verified, leading to the following boundary conditions,

$$\begin{aligned} &\sigma_{xz}(x,0) = \sigma_{xz}(x,-\tfrac{t}{2}) = \sigma_{xz}(x,\tfrac{t}{2}) = 0, \\ &u_z(x,0) = \sigma_{zz}(x,-\tfrac{t}{2}) = \sigma_{zz}(x,\tfrac{t}{2}) = 0. \end{aligned} \tag{C.10}$$

If the quarter $Y_{1/4}$ of the domain Y is considered, with $Y_{1/4} = \left]0,\frac{l_1}{2}\right[\times \left]0,\frac{t}{2}\right[$, the local boundary value problem for the first case can be solved under the following boundary conditions,

$$\begin{cases} u_x^{total}(0,z) = \sigma_{xz}(0,z) = \sigma_{xz}(\tfrac{l_1}{2},z) = 0, \quad u_x^{total}(\tfrac{l_1}{2},z) = \tfrac{l_1}{2}, \\ \\ u_z^{total}(x,0) = \sigma_{xz}(x,0) = \sigma_{xz}(x,\tfrac{t}{2}) = \sigma_{zz}(x,\tfrac{t}{2}) = 0. \end{cases} \tag{C.11}$$

For the second case ($\mathbf{E} = 0, \boldsymbol{\chi} = 1$), if we consider the symmetry relative to the z-axis, the expression (C.2) is verified. As a result, the boundary conditions defined in (C.6) are hence used. On the contrary, if we analyze the symmetry relative to the x-axis, the image of the out-of-plane macroscopic strain is defined by $\boldsymbol{\chi}^* = -\mathbf{S}\,\boldsymbol{\chi}\,\mathbf{S}$. As a consequence, it can be observed that the fields $-\mathbf{u}^*$ and $-\boldsymbol{\sigma}^*$ are also the solution fields of the problem. It can therefore be deduced that:

$$\begin{aligned} &u_x(x,0) = \sigma_{xz}(x,-\tfrac{t}{2}) = \sigma_{xz}(x,\tfrac{t}{2}) = 0, \\ &\sigma_{zz}(x,0) = \sigma_{zz}(x,-\tfrac{t}{2}) = \sigma_{zz}(x,\tfrac{t}{2}) = 0. \end{aligned} \tag{C.12}$$

Using (C.6) and (C.12), the boundary conditions on the $Y_{1/4}$ can be written by the following expressions,

$$\begin{cases} u_x^{total}(0,z) = \sigma_{xz}(0,z) = \sigma_{xz}(\frac{l_1}{2},z) = 0, \quad u_x^{total}(\frac{l_1}{2},z) = \frac{l_1}{2}\,z, \\ \\ u_x^{total}(x,0) = \sigma_{zz}(x,0) = \sigma_{xz}(x,\frac{t}{2}) = \sigma_{zz}(x,\frac{t}{2}) = 0. \end{cases} \tag{C.13}$$

By applying the boundary conditions on the total displacement field $\mathbf{u}^{total}$ defined in (C.11, C.13) (for the plane problems), the boundary value problem (3.69, 3.70) can be solved by using a standard finite element package, because it involves now only Dirichlet boundary conditions and no more periodicity conditions. The homogenized properties of the plate can therefore be determined from the strain energy as described in section 3.2.4.1.

Bibliography

A. Bensoussan, J. L., Papanicolaou, G., 1978. Asymptotic analysis for periodic structures. North-Holland, Amsterdam.

Aboudi, J., Pindera, M. J., Arnold, S. M., 1999. Higher-order theory for functionally graded materials. Composites, Part B: Engineering 30, 777–832.

Artola, M., Duvaut, G., 1977. Homogénéisation d'une plaque renforcée. C. R. A. S., Paris, Série A 284, 707–710.

Auriault, J. L., Bonnet, G., 1985. Dynamique des composites élastiques périodiques. Arch. Mech. 37, 269–284.

Bakhvalov, N. S., 1974. Averaged characteristics of bodies with periodic structure (Russian). Dokl. Akad. Nauk. SSSR. 218, 1046–1048.

Bakhvalov, N. S., Panasenko, G. P., 1989. Homogenization: Averaging Processes in Periodic Media. Kluwer Academic Publishers, Dordrecht-Boston-London.

Becker, J., Cannon, R. M., Ritchie, R. O., 2002. Statistical fracture modelling: Crack path and fracture criteria with application to homogeneous and functionally graded materials. Eng. Fract. Mech. 69, 1521–1555.

Berthelot, J., 1992. Matériaux Composites: Comportement Mécanique et Analyse des Structures. Masson, Paris.

Bever, M. B., Duwez, P. F., 1972. Gradients in composite materials. Mater. Sci. Eng. 10, 1–8.

Böhm, H. J., Rammerstorfer, F. G., Weissenbek, E., 1993. Some simple models for micromechanical investigations of fiber arrangement effects in MMCs. Comput. Mater. Sci. 1, 177–194.

Bonnet, G., 2007. Effectives properties of elastic periodic composite media with fibers. J. Mech. Phys. Solids 55, 881–899.

Bornert, M., Bretheau, T., Gilormini, P., 2001. Homogénéisation en mécanique des matériaux 1: Matériaux aléatoires élastiques et milieux périodiques. Hermes Science Publications, Paris.

Bourgeois, S., 1997. Modélisation numérique des panneaux structuraux légers. Ph.D. Thesis, University Aix-Marseille.

Bourgeois, S., Débordes, O., Patou, P., 1998. Homogénéisation et plasticité des plaques minces. Rev. Eur. Elem. Finis 7, 39–54.

Brockenbrough, J. R., Suresh, S., Wienecke, H. A., 1991. Deformation of metal-matrix composites with continuous fibers: Geometrical effects of fiber distribution and shape. Acta Metall. Mater. 39, 735–752.

Buannic, N., Cartraud, P., 2001. Higher-order effective modeling of periodic heterogeneous beams. I. Asymptotic expansion method. Int. J. Solids Struct. 38, 7139–7161.

Buannic, N., Cartraud, P., Quesnel, T., 2003. Homogenization of corrugated core sandwich panels. Compos. Struct. 59, 299–312.

Buryachenko, V. A., 2001. Multiparticle effective field and related methods in micromechanics of composite materials. Appl. Mech. Rev. 54, 1–47.

Buryachenko, V. A., Rammerstorfer, F., 1998. Micromechanics and nonlocal effects in graded random structure matrix composites. Proceedings IUTAM-symposium on transformation problems in composite and active materials, 197–206.

Caillerie, D., 1982. Plaques élastiques minces à structure périodique de période et d'épaisseur comparables. C. R. A. S. Série II 294, 159–162.

Caillerie, D., 1984. Thin elastic and periodic plates. Math. Meth. in the Appl. Sci. 6, 159–191.

Caron, J., Sab, K., 2001. Un nouveau modèle de plaque multicouche épaisse. Acad. Sci. 329, 595–600.

Castaneda, P., 1991. The effective mechanical properties of non-linear isotropic composites. J. Mech. Phys. Solids. 39, 45–71.

Cecchi, A., Sab, K., 2002a. A multi-parameter homogenization study for modelling elastic masonry. Euro. J. Mech. A/Solids 21, 249–268.

Cecchi, A., Sab, K., 2002b. Out of plane model for heterogenous periodic materials: the case of masonry. Euro. J. Mech. A/Solids 21, 715–746.

Cecchi, A., Sab, K., 2004. A comparison between a 3d discrete model and two homogenized plate models for periodic elastic brickword. Int. J. Solids Struc. 41, 2259–2276.

Cecchi, A., Sab, K., 2007. A homogenized reissner-mindlin model for orthotropic periodic plates. application to brickwork panels. Int. J. Solids Struc. 44, 6055–6079.

Cheng, Z. Q., Batra, R. C., 2000a. Exact correspondence between eigenvalues of membranes and functionally graded simply supported polygonal plates. J. Sound Vibr. 229, 879–895.

Cheng, Z. Q., Batra, R. C., 2000b. Three-dimensional thermoelastic deformations of functionally graded elliptic plates. J. Sound Vibr. 31, 97–106.

Chi, S. H., Chung, Y. L., 2002. Cracking in sigmoid functionally graded coating. J. Mech. 18, 41–53.

Chi, S. H., Chung, Y. L., 2006a. Mechanical behavior of functionally graded material plates under transverse load - Part I: Analysis. Int. J. Solids Struct. 43, 3657–3674.

Chi, S. H., Chung, Y. L., 2006b. Mechanical behavior of functionally graded material plates under transverse load - Part II: Numerical results. Int. J. Solids Struct. 43, 3675–3691.

Cho, J. R., Ha, D. Y., 2001. Averaging and finite-element discretization approches in the numerical analysis of functionally graded materials. Mater. Sci. Eng. A A302, 187–196.

Cho, J. R., Ha, D. Y., 2002. Volume fraction optimization for minimizing thermal stress in ni-al2o3 functionally graded materials. Mater. Sci. Eng. A A334, 147–155.

Ciarlet, P. M., 1997. Mathematical Elasticity, Vol. II: Theory of Plates. North-Holland, Amsterdam.

Cohen, I., Bergman, D. J., 2003. Effective elastic properties of periodic composite medium. J. Mech. Phys. Solids 51, 1433–1457.

Croce, L. D., Venini, P., 2004. Finite elements for functionally graded Reissner-Mindlin plates. Comput. Methods Appl. Mech. Eng. 193, 705–725.

Dallot, J., 2007. Modélisation des structures multicouches en analyse limite. Application au renforcement de matériau "quasi-fragile-acier". Ph.D. thesis, Ecole Nationale des Ponts et Chaussées.

Dallot, J., Sab, K., 2008a. Limit analysis of multi-layered plates. Part I: The homogenized Love-Kirchhoff model. J. Mech. Phys. Solids. 56, 561–580.

Dallot, J., Sab, K., 2008b. Limit analysis of multi-layered plates. Part II: Shear effects. J. Mech. Phys. Solids. 56, 581–612.

Dao, M., Gu, P., Maewal, A., Asaro, R. J., 1997. A micromechanical study of residual stresses in functionally graded materials. Acta Mater. 45, 3265–3276.

Delale, F., Erdogan, F., 1983. The crack problem for a nonhomogeneous plane. J. Appl. Mech. Trans. ASME 50, 609–614.

Drugan, W. J., 2003. Two exact micromechanics-based nonlocal constitutive equations for random linear elastic composite materials. J. Mech. Phys. Solids 51, 1745–1772.

Drugan, W. J., Willis, J. R., 1996. A micromechanics-based nonlocal constitutive equation and estimates of representative volume element size for elastic composites. J. Mech. Phys. Solids 44, 497–524.

Duvaut, G., Metellus, A. M., 1976. Homogénéisation d'une plaque mince en flexion des structures périodique et symmétrique. C.R. Acad. Sci. Sér. A. 283, 947–950.

Elishakoff, I., Raton, B., Florida, Gentilini, C., Viloa, E., 2005. Three-dimensional analysis of an all-round clamped plate made of functionally graded materials. Acta Mech. 180, 21–36.

Eyre, D. J., Milton, G. W., 1999. A fast numerical scheme for computing the response of composites using grid refinement. Eur. Phys. J. AP. 6, 41–47.

Ferreira, A. J. M., Batra, R. C., Roque, C. M. C., Qian, Martins, P. A. L. S., 2004. Static analysis of functionally graded plates using third-order shear deformation theory and a meshless method. Compos. Struct. 193, 705–725.

Finot, M., Suresh, S., 1996. Small and large deformation of thick and thin-film multilayers: Effect of layer geometry, plasticity and compositional gradients. J. Mech. Phys. Solids 44, 683–721.

Forest, S., Pradel, F., Sab, K., 2001. Asymptotic analysis of heterogeneous cosserat media. Int. J. Solids Struct. 38, 4585–4608.

Forest, S., Sab, K., 1998. Cosserat overall modeling of heterogeneous materials. Mech. Res. Commun. 25, 449–454.

Garboczi, E. J., Day, A. R., 1995. An algorithm for computing the effective linear properties of heterogeneous materials: three dimensional results for composites with equal phase poisson ratios. J. Mech. Phys. Solids 43, 1349–1362.

Gasik, M. M., 1998. Micromechanical modelling of functionally graded materials. Comput. Mater. Sci. 13, 42–55.

Gasquet, C., Witomski, P., 2000. Analyse de Fourier et Applications. Masson, Paris.

Ghosh, S., Lee, K., Moorthy, S., 1995. Multiple scale analysis of heterogeneous elastic structures using homogenenization theory and Voronoi cell finite element method. Int. J. Solids Struct. 32, 27–62.

Ghugal, Y. M., Shimpi, R. P., 2002. A review of refined shear deformation theories of isotropic and anisotropic laminated plates. J. Reinf. Plast. Compos. 21, 775–813.

Gilormini, P., 2001. Realizable compressibility and conductivity in isotropic two-phase composites. C. R. Acad. Sci. Paris, Série IIb 329, 851–855.

Goetzel, C. G., Lavendel, H. W., 1964. Multiple scale analysis of heterogeneous elastic structures using homogenenization theory and Voronoi cell finite element method. Int. J. Solids Struct. 32, 149–162.

Grujicic, M., Zhang, Y., 1998a. Derivation of effective elastic properties of two-phase materials using Voronoi cell finite element method. Mater. Sci. Eng. A 251, 64–76.

Grujicic, M., Zhang, Y., 1998b. Determination of effective elastic properties of functionally graded materials using Voronoi cell finite element method. Mater. Sci. Eng. A A251, 64–76.

Gruttmann, F., Wagner, W., 2001. Shear correction factors in Timoshenko's beam theory for arbitrary shaped cross-sections. Comput. Mech. 27, 199–207.

Gusev, A. A., 1997. Representative volume element size for elastic composites: A numerical study. J. Mech. Phys. Solids 45, 1449–1459.

Hashin, Z., Shtrikman, S., 1962a. On some variational principles in anisotropic and nonhomogeneous elasticity. J. Mech. Phys. Solids 10, 335–342.

Hashin, Z., Shtrikman, S., 1962b. A variational approach to the theory of elastic behavior of polycrystals. J. Mech. Phys. Solids 10, 343–352.

Hashin, Z., Shtrikman, S., 1963. A variational approach to the theory of elastic behavior of multiphase materials. J. Mech. Phys. Solids 11, 127–140.

Hashin, Z., Shtrikman, S., 1965. On elastic behavior of fibre reinforced materials of arbitrary transverse phase geometry. J. Mech. Phys. Solids 13, 119–134.

Hashin, Z., Shtrikman, S., 1967. Variational priciples of elasticity in terms of the polarization. Int. J. Engng. Sci. 5, 213–223.

He, X. Q., Ng, T. Y., Sivashankera, S., Liew, K. M., 2001. Active control of FGM plates with integrated piezoelectric sensors and actuators. Int. J. Solids Struct. 38, 1641–1655.

Hildebrand, F. B., Reissner, E., Thomas, G. B., 1949. Notes on the foundations of the theory of small displacements of orthotropic shells. NACA T. N. No. 1833.

Hill, R., 1952. The elastic behavior of a crystalline aggregate. Proceeding of the Physical Society 65, 349–354.

Hill, R., 1965. A self-consistent mechanics of composite materials. J. Mech. Phys. Solids 13, 213–222.

Huang, J., Fadel, G. M., Blouin, V. Y., Grujicic, M., 2002. Bi-objecive optimization design of functionally gradient materials. Mater. Des. 23, 657–666.

Hutchinson, J. R., 2001. Shear coefficients for Timoshenko beam theory. J. Appl. Mech. 68, 87–92.

Iwakuma, T., Nemat-Nasser, S., 1983. Composites with periodic microstructure. Int. J. Solids Struct. 16, 13–19.

Jin, Z. H., Batra, R. C., 1996. Stress intensity relaxation at the tip of an edge crack in a functionally graded material subjected to a thermal shock. J. Therm. Stresses 19, 317–339.

Jin, Z. H., Paulino, G. H., 2001. Transient thermal stress analysis of an edge crack in a functionally graded material. J. Fract. 107, 73–98.

Kanit, T., Forest, S., Galliet, I., Mounoury, V., Jeulin, D., 2003. Determination of the size of the representative volume element for random composites: statistical and numerical approach. Int. J. Solids Struct. 40, 3647–3679.

Kant, T., Swaminathan, K., 2002. Anatical solutions for the static analysis of laminated composite and sandwich plates based on a higher order refined theory. Compos. Struct. 56, 329–344.

Kaßbohm, S., Müller, W. H., Feßler, R., 2006. Improved approximations of fourier coefficients for computing the response of periodic structures with arbitrary stiffness distribution. Comput. Mater. Sci. 37, 90–93.

Kaßbohm, S., Müller, W. H., Feßller, R., 2005. Fourier series for computing the response of periodic structures with arbitrary stiffness distribution. Comput. Mater. Sci. 32, 387–391.

Kohn, R. V., Vogelius, M., 1984. A new model for thin plates with rapidly varying thickness. Int. J. Solids Struct. 20, 333–350.

Koizumi, M., 1997. FGM Activities in Japan. Composites 28, 1–4.

Kolpakov, A. G., 1995. The asymptotic theory of thermoelastic beams. J. Appl. Mech. Tech. Phys. 36, 756–763.

Kolpakov, A. G., 1998. Variational principles for stiffnesses of a non-homogeneous beams. J. Mech. Phys. Solids 46, 1039–1053.

Kolpakov, A. G., 1999. Variational principles for stiffnesses of a non-homogeneous plate. J. Mech. Phys. Solids 47, 2075–2092.

Kolpakov, A. G., Sheremet, I. G., 1999. The stiffnesses of non-homogeneous plates. J. Appl. Maths. Mechs. 63, 633–640.

Kröner, E., 1971. Statistical continuum mechanics. Springer Verlag, Wien.

Lachihab, A., Sab, K., 2005. Aggregate composite materials: a contact based modeling. Comput. Mater. Sci. 33, 467–490.

Lachihab, A., Sab, K., 2008. Does a representative volume element exists for fatigue life prediction? the case of aggregate composites. Int. J. Numer. Anal. Methods Geomech. 32, 1005–1021.

Lee, K., Lee, S. W., 2003. A postprocessing approach to determine transverse stresses in geometrically nonlinear composite and sandwich structures. J. Compos. Mater. 37, 2207–2224.

Lewiński, T., Telega, J. J., 1999. Plates, Laminates and Shells: Asymptotic Analysis and Homogenization. World Scientific Publishing.

Liberscu, L., 1967. On the theory of anisotropic elastic shell and plates. Int. J. Solids Struct. 3, 53–68.

Lo, K. H., Christensen, R. M., Wu, E. M., 1977a. A high-order theory of plate deformation, Part I: Homogenous plates. J. Appl. Mech., 663–668.

Lo, K. H., Christensen, R. M., Wu, E. M., 1977b. A high-order theory of plate deformation, Part II : Laminated plates. J. Appl. Mech., 669–676.

Long, X., Delale, F., 2005. The mixed mode crack problem in an FGM layer bonded to a homogeneous half-plane. Int. J. Solids Struct. 42, 3897–3917.

Luciano, R., Barbero, E. J., 1994. Formulas for the stiffness of composites with periodic microstructure. Int. J. Solids Struct. 31, 2933–2944.

Luciano, R., Willis, J. R., 2004. Non-local constitutive equations for functionally graded materials. Mech. Mater. 36, 1195–1206.

Markworth, A. J., Ramesh, K. S., Jr, W. P. P., 1995. Review modelling studies applied to functionally graded materials. J. Mater. Sci. 30, 2183–2193.

Miara, B., Podio-Guidugli, P., 2006. Une approche formelle unifiée des théories de plaques et poutres linéairement élastique. C. R. Acad. Sci. Paris, Ser. I 343, 375–678.

Michel, J. C., Moulinec, H., Suquet, P., 1999. Effective properties of composite materials with periodic microstructure: a computational approach. Compu. Meth. Appl. Mech. Eng. 172, 109–143.

Michel, J. C., Moulinec, H., Suquet, P., 2001. A computational scheme for linear and non-linear composites with arbitrary phase contrast. Int. J. Numer. Meth. Eng. 52, 139–160.

Milton, G. W., 2002. The theory of composites. Cambridge Univ. Press, Cambridge.

Mindlin, R. D., 1951. Influence of rotary inertia and shear on flexural motion of isotropic elastic plates. J. Appl. Mech. 18, 31–38.

Mishnaevsky, L. L., 2005. Functionally gradient metal matrix composites: Numerical analysis of the microstructure-strength relationships. Compos. Sci. Technol. 66, 1873–1887.

Moës, M., Cloirec, M., Cartraud, P., Remacle, J. F., 2003. A computational approach to handle complex microstructure geometries. Compu. Meth. Appl. Mech. Eng. 192, 3163–3177.

Mori, T., Tanaka, T., 1973. Average stress in matrix and average elastic energy of materials with misfitting inclusions. Acta Mater. 21, 571–574.

Moulinec, H., Suquet, P., 1994. A fast numerical method for computing the linear and nonlinear properties of composites. C.R. Acad. Sci. 318, 1417–1423.

Moulinec, H., Suquet, P., 1998. A numerical method for computing the overall response of nonlinear composites with complex microstructure. Compu. Meth. Appl. Mech. Eng. 157, 69–94.

Moulinec, H., Suquet, P., 2003. Comparison of FFT-based methods for computing the response of composites with highly contrasted mechanical properties. Physica B. 338, 58–60.

Mura, T., 1991. Micromechanics of deflects in solids. Kluwer Academic Publisers.

Nadeau, J., Ferrari, M., 1999. Microstructural optimization of functionally graded transversely isotropic layer. Mech. Mater. 31, 637–651.

Naghdi, P. M., 1957. On the theory of thin elastic shells. Quarterly Appl. Math. 14, 369–380.

Nebozhyn, M. V., Gilormini, P., Castaneda, P. P., 2001. Variational self-consistent estimates for cubic viscoplastic polycrystals: the effects of grain anisotropy and shape. J. Mech. Phys. Solids 49, 313–340.

Nelson, R. B., Lorch, D. R., 1974. A refined theory for laminated orthotropic plates. J. Appl. Mech. 41, 177–183.

Neumann, S., Herrmann, K. P., Müller, W. H., 2002. Stress/strain computation in heterogenous bodies with discrete fourier transforms - different approaches. Compu. Mater. Sci. 25, 151–158.

Neumann, S., Herrmann, K. P., Paderborn, Germany, Müller, 2001. Fourier transforms - an alternative to finite elements for elastic-plastic stress-strain analyses of heterogeneous materials. Acta Mech. 149, 149–160.

Nguyen, T. K., Sab, K., Bonnet, G., 2007. Shear correction factors for functionally graded plates. Mech. Advanced Mater. Struct. 14, 567–575.

Nguyen, T. K., Sab, K., Bonnet, G., 2008a. First-order shear deformation plate models for functionally graded materials. Compos. Struct. 83, 25–36.

Nguyen, T. K., Sab, K., Bonnet, G., 2008b. Green's operator for a periodic medium with traction-free boundary conditions and computation of the effective properties of thin plates. Int. J. Solids Struct. doi: 10.1016/j.ijsolstr.2008.08.015.

Nguyen, T. K., Sab, K., Bonnet, G., 2008c. Hashin-Shtrikman variational principle for heterogeneous plates. J. Mech. Phys. Solids Submitted.

Nguyen, V. T., Caron, J. F., Sab, K., 2005. A model for thick laminates and sandwich plates. Compos. Sci. Technol. 65, 475–489.

Obata, Y., Noda, N., 1996. Optimum material design for functionally gradient material plate. Archive Appl. Mech. 66, 581–589.

Ostoja-Starzewski, M., 1993. Micromechanics as a basic of random continuum approximations. Proba. Eng. Mech. 8, 107–114.

Ostoja-Starzewski, M., 1996. Bounding of effective thermal conductivities of multiscale materials by essential and natural boundary conditions. Phys. Rev. B54, 278–285.

Ostoja-Starzewski, M., 1998. Random field models of heterogeneous materials. Int. J. Solids Struct. 35, 2429–2455.

Percus, J. K., Yevick, G. J., 1958. Analysis of classical statistical mechanics by means of collective coordinates. Phys. Rev. 110, 1–13.

Pindera, M. J., Dunn, P., 1997. Evaluation of the higher-order theory for functionally graded materials via the finite-element method. Compos. Part B: Engineering 28, 109–119.

Praveen, G. N., Reddy, J. N., 1998. Nonlinear transient thermoelastic analysis of functionally graded ceramic-metal plates. Int. J. Solids Struct. 35, 4457–4476.

Ramirez, F., Heyliger, P. R., Pan, E., 2006. Static analysis of functionally graded elastic anisotropic plates using a discrete layer approach. Composites, Part B: Engineering 37, 10–20.

Reddy, J. N., 1997. Mechanics of Laminated Composites Plates: Theory and Analysis. CRC Press, Boca Raton.

Reddy, J. N., 1999. Theory and Analysis of Elastic Plates. Taylor Francis, Philadelphia.

Reddy, J. N., 2000. Analysis of functionally graded materials. Int. J. Numer. Methods Eng. 47, 663–684.

Reddy, J. N., 2003. A new beam finite element for the analysis of functionally graded materials. Int. J. Mech. Sci. 45, 519–539.

Reissner, E., 1945. The effect of transverse shear deformation on the bending of elastic plates. J. Appl. Mech. 13, 69–77.

Reissner, E., 1975. On transverse bending of plates, including the effects of transverse shear deformation. Int. J. Solids Struct. 11, 569–573.

Reiter, T., Dvorak, G. J., 1997. Micromechanical models for graded composite materials. J. Mech. Phys. Solids 45, 1281–1302.

Reiter, T., Dvorak, G. J., 1998. Micromechanical models for graded composite materials: II. thermomechanical loading. J. Mech. Phys. Solids 46, 1655–1673.

Reuss, A., 1929. Calculation of the yield point of mixed crystals from plasticity conditions for single crystals. Zeitschrift für Angewandte Mathematik und Mechanik 9, 49–58.

Rolfes, R., Rohwer, K., 1997. Improved transverse shear stresses in composite finite elements based on first order shear deformation theory. Int. J. Numer. Methods Eng. 40, 51–60.

Rolfes, R., Rohwer, K., Ballerstaedt, M., 1998. Efficient linear transverse normal stress analysis of layered composite plates. Comput. Struct. 68, 643–652.

Sab, K., 1991. Principle de hill et homogénéisation des matériaux aléatoires. C. R. Acad. Sci. Paris, Sér. II 312, 1–5.

Sab, K., 1992. On the homogenization and the simulation of random materials. Euro. J. Mech. A/Solids 11, 585–607.

Sab, K., 2003. Yield design of thin periodic plates by a homogenization technique and an application to masonry wall. C. R. Mécanique 331, 641–646.

Sab, K., Nedjar, B., 2005. Periodization of random media and representative volume element size for linear composites. C. R. Mécanique 333, 187–195.

Sanchez-Palencia, E., 1974. Comportement local et macroscopique d'un type de milieux physiques hétérogènes. Int. J. Eng. Sci. 12, 331–351.

Satchi, V., Bhavani, V., 2001. Analysis of sandwich beams with functionally graded core. AIAA 1, 752–759.

Seremet, V. D., 1991. Handbook of Green's functions and matrices. Wit Press, Southampton.

Sill, L., Eliasi, R., Berlin, Y., 2002. Modelling of functionally graded materials in dynamic analyses. Compos., Part B 33, 7–15.

Soize, C., 1993. Méthodes mathématiques en analyse du signal. Masson, Paris.

Suquet, P., 1990. Une méthode simplifiée pour le calcul des propriétés élastiques de matériaux hétérogènes à structure périodique. C.R. Acad. Sci. 311, 769–774.

Suresh, S., Mortensen, A., 1998. Fundamentals of functionally graded materials: Processing and Thermomechanical Behaviour of Graded Metals and Metal-Ceramic Composites. Press, Cambridge.

Sze, K. Y., 2000. Predictor-corrector procedures for analysis of laminated plates using standard mindlin finite element models. Compos. Struct. 50, 171–182.

Tabot, D. R. S., Willis, J. R., 1985. Variational principles for inhomogeneous nonlinear media. J. Appl. Math. 35, 39–54.

Terada, K., Ito, T., Kikuchi, N., 1998. Characterization of the mechanical behaviors of solid-fluid mixture by the homogenization method. Comput. Methods Appl. Mech. Eng. 153, 223–257.

Timoshenko, S. P., Woinowsky-Krieger, S., 1959. Theory of Plates and Shells. McGraw-Hill, New York.

Tohgo, K., Masunari, A., Yoshida, M., 2006. Two-phase composite model taking into account the matricity of microstructure and its application to functionally graded materials. Compos., Part A: Appl. Sci. manuf. 37, 1688–1695.

Torquato, S., 2001. Random Heterogeneous Materials - Microstructure and Macroscopic properties. Springer, New York.

Torquato, S., Stell, G., 1985. Microstructure of two-phase random media. V. The n-point matrix probability functions for impenetrable spheres. J. Chem. Phys. 82, 980–987.

Tung, N. V., 2004. Modélisation globale et locale des structures multicouches par éléments finis de plaque. Ph.D. thesis, Ecole Nationale des Ponts et Chaussées.

Vel, S. S., Batra, R. C., 2002. Exact solution for thermoelastic deformations of functionally graded thick rectangular plates. AIAA 40, 1421–1433.

Vemaganti, K., Deshmukh, P., 2006. An adapty global-local approach to modeling functionally graded materials. Comput. Methods Appl. Mech. Eng. 195, 4230–4243.

Verlet, L., Weis, J. J., 1972. Equilibrium theory of simple liquids. Phys. Rev. A 5, 939–952.

Vlachoutsis, S., 1992. Shear correction factors for plates and shells. Int. J. Numer. Methods Eng. 33, 1537–1552.

Voigt, W., 1889. On the relation between the two elasticity constants of isotropic bodies. Wiedemanns Annalen der Physik und Chemie (Leipzig) 38, 573–587.

Weissenbek, E., Pettermann, H. E., Suresh, S., 1997. Elasto-plastic deformation of compositionally graded metal-ceramic composites. Acta Mater. 45, 3401–3417.

Willis, J. R., 1977. Bounds and self-consistent estimates for the overall properties of anisotropic composites. J. Mech. Phys. Solids. 25, 185–202.

Willis, J. R., 1980. A polarization approach to the scattering of elastic waves. I. scattering by a single inclusion. J. Mech. Phys. Solids 28, 287–305.

Willis, J. R., 1981. Variational and related methods for the overall properties of composites. Advances Appl. Mech. 21, 1–78.

Yin, H. M., Sun, L. Z., Paulino, G. H., 2004. Micromechanics-based elastic model for functionally graded materials with particle interactions. Acta Mater. 52, 3535–3543.

Yuan, X., Tomita, Y., Andou, T., 2008. A micromechanical approach of nonlocal modelling for media with periodic microstructures. Mech. Res. Commun. 35, 126–133.

Yung, Y. Y., Munz, D., 1996. Stress analysis in a two materials joint with a functionally graded material. In: Shiota, T., Miyamoto, M.Y (Eds), 41–46.

Zenkour, A. M., 2003. Analytical solution for bending of cross-ply laminated plates under thermo-mechanical loading. Compos. Struct. 65, 367–379.

Zenkour, A. M., 2004a. Buckling of fiber-reinforced viscoelastic composite plates using various plate theories. J. Eng. Math. 50, 75–93.

Zenkour, A. M., 2004b. Thermal effects on bending reponse of fiber-reinforced viscoelastic composite plates using a sinusoidal shear deformation theory. Acta Mech. 171, 171–187.

Zenkour, A. M., 2005a. A comprehensive analysis of functionally graded sandwich plates: Part 2 - buckling and free vibration. Int. J. Solids Struct. 42, 5243–5258.

Zenkour, A. M., 2005b. A comprehensive analysis of functionally graded sandwich plates: Part 1 - Deflection and stresses. Int. J. Solids Struct. 42, 5224–5242.

Zenkour, A. M., 2006. Generalized shear deformation theory for bending analysis of functionally graded materials. Appl. Math. Modelling 30, 67–84.

Zienkiewicz, O. C., Zhu, J. Z., 1992. The superconvergent patch recovery and a posteriori error estimates. Part 1: The recovery technique. Int. J. Numer. Methods Eng. 33, 1331–1364.

Zuiker, J. R., Dvorak, G. J., 1994. On the effective properties of functionally gradient materials. Compos. Eng. 4, 19–35.